Linking a Fluidized Bed Combustion Reactor

with an

Externally Fired Micro Gas Turbine

Dissertation

to attain the academic title

PhD

from the Faculty of Mechanical Engineering and Marine Technology

University of Rostock

Submitted by

Graduate Engineer Tristan Vincent

Rostock 2008
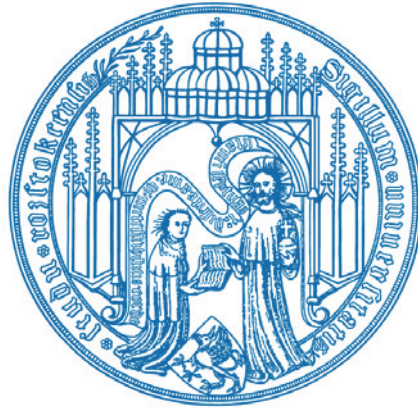
Kopplung einer Wirbelschichtfeuerung

mit einer

extern gefeuerten Mikrogasturbine

Dissertation

zur

Erlangung des akademischen Grades

Doktor-Ingenieur (Dr.-Ing.)

der Fakultät für Maschinenbau und Schiffstechnik

der Universität Rostock

vorgelegt von

Dipl.-Ing. Tristan Vincent

Rostock 2008

Preface

This doctoral thesis was written during my occupation as scientific colleague at the University of Rostock, Faculty of Mechanical Engineering and Marine Technology, Chair of Energy Systems and Turbo Machinery in Germany.

I would like to thank my mentor Prof. Dr.-Ing. habil. Dieter Steinbrecht and the other expert reviewers Prof. Dr.-Ing. habil. Jürgen Karl and Prof. Dr.-Ing. Klaus Dielmann for the valuable advice and helpful support essential for the accomplishment of this research work.

I owe particular thanks to Dr.-Ing. Rolf Strenziok and Dipl.-Ing. Eldor Backhaus and all my other colleagues at the Faculty of Mechanical Engineering and Marine Technology for their dedication and constructive support.

I would also like to thank my wife Maren and family, both near and far, for their patience and support, without which this dissertation would not have been possible.

Rostock, 10.12.08   Tristan Vincent

Tristan Vincent

Linking a Fluidized Bed Combustion Reactor with an Externally Fired Micro Gas Turbine

Contents

List of Figures

III List of Tables

IV Nomenclature

A	[m²]	area
a	[m²/s]	thermal diffusivity
$\dot{C}$	[kW/K]	heat capacity flux
c_p	[kJ/kg K]	specific heat at constant pressure
c_v	[kJ/kg K]	specific heat at constant volume
d	[mm]	diameter
h	[kJ/kg]	enthalpy
$\tilde{k}$, k	[W/m²K]	average heat transfer coefficient
L	[m, mm]	length
l	[mm]	characteristic length
LMTD	[K]	logarithmic mean temperature difference
$\dot{m}$	[kg/h, kg/s]	mass flow
NTU	[-]	number of transfer units
Nu	[-]	Nusselt number
P	[kW]	power
p	[kPa, bar]	pressure
Pr	[-]	Prandtl number
$\dot{Q}$	[kW]	heat flux
$\dot{q}_{in}$	[kW]	specific heat input
$\dot{q}_{out}$	[kW]	specific rejected heat
Re	[-]	Reynolds number
s	[kJ/kg K]	entropy
T	[°C, K]	temperature
$\dot{V}$	[m³ /h]	volume flow
w	[m/s]	velocity
x	[-]	isentropic exponent
Z_T	[-]	number of parallel heat exchanger tubes

Greek letters

α	[W/m²K]	heat transfer coefficient
Δ	[-]	difference
δ	[mm]	thickness
ζ	[-]	friction coefficient
η	[-], [10^{-6} Pa]	efficiency; dynamic viscosity
ϑ	[K, °C]	temperature
κ	[-]	kappa
λ	[W/mK], [-]	thermal conductivity; combustion air ratio
ν	[m²/s]	kinematic viscosity
π	[-]	pressure ratio
ρ	[kg/m³]	density
Σ	[-]	summation
Φ	[-]	heat transfer effectiveness

Subscripts

amb	ambient
C	compressor
comb	combustion
dyn	dynamic
e, el	electric
FB	fluidized bed
FG	flue gas
Fl Air	fluidisation air
Hx	heat exchanger
i	inner
L	lower
Lat	lateral
m	middle; mechanical
o	outer; standard state
r	reference
T	turbine
th	thermal
U	upper
w	wall

Abbreviations

CC	combined cycle
CEP	compressor exit pressure
CerHx	ceramic heat exchanger
CET	compressor exit Temperature
CHP	combined heat and power
CIT	compressor inlet temperature
CMC	ceramic matrix composites
CT	combustion temperature
EFCC	externally fired combined cycle
EFHAT	externally fired humid air turbine
EFMGT	externally fired micro gas turbine
Eq.	equation
FCC	face centred cubic
HTHx	high temperature heat exchanger
mf	moisture free
MGT	micro gas turbine
MMC	metal matrix composites
NG	natural gas
ODS	oxide dispersion strengthened
PEC	performance evaluation criterion
Rec	recuperator
s.	see
SFBC	stationary fluidized bed combustion
SRF	short rotation forestry
SS	stainless steel
STIG	steam injected gas turbine
Tab.	table
TEP	turbine exit pressure
TET	turbine exit temperature
TIT	turbine inlet temperature
wt	weight

1   Introduction

With the emerging world wide political consensus on the man made origin of the present climate change and the ever increasing horror scenarios of its consequences, the urgency of finding ecologically sustainable alternatives to the present fossil fuel fired economy has greatly increased.

Since the publishing of the latest reports from the Intergovernmental Panel of Climate Change (IPCC 2007), the reduction of greenhouse gases has clearly become the most important global environmental issue. To meet this enormous challenge, which means no less than a complete revolution in the worlds energy supply, a huge increase in energy efficiency and a substitution of fossil fuels by renewable energy resources will be necessary.

The European Union, which can be generally seen as the environmental world leader, has taken decided action in this concern and issued directives requiring an increase in the share of renewable energy in primary energy consumption to 20% by the year 2020.

With a proportion of over 40% (BMWi 2007) solid biomass is the most important renewable energy resource in Germany today and is expected to continue to grow very strongly. Biomass also represents one of the largest available renewable energy resources worldwide, it is permanently available irrespective of season of the year and weather and, in contrast to other renewable energy carriers like wind power or solar energy, biomass can easily be stored in large quantities for a long time.

Furthermore the carbon dioxide (CO_2) released during biomass combustion belongs to the "short carbon cycle"[1]. Therefore, in contrast to CO_2 from fossil fuel combustion, which belong to the "long carbon cycle"[2], biomass combustion is not considered to contribute to the greenhouse effect[3]. Therefore biomass combustion, as a substitute for fossil fuels, helps fulfil Germany's obligations under the Kyoto Protocol (1997) to reduce the release of greenhouse gases by 21%, in comparison to 1990 levels.

In Germany the introduction of the renewable energy law, and it's amendment in 2004 (EEG 2004), which guarantees a premium price for small scale renewable electricity generation has led to a boom in renewable electricity generation from wind, biogas and biomass (Gomez 2005). The economic compensation is designed to promote small scale distributed electricity generation and cogeneration. This is achieved by guaranteeing small scale producers a higher kilowatt price for their electricity. The implementation of this bonus system for environmentally sound and innovative technologies is an instrument which allows the German government to promote the further development and reward the utilisation of environmentally sustainable technologies (BMU 2007).

This has led to the establishment of a strong market for renewable electricity in Germany, which in turn has increased the research and development of new and innovative small scale biomass electricity generation systems which has led to an export boom of environmental technologies from Germany.

The potential of biomass to help solve the climate protection issue is undisputable, however although biomass is regenerative, it is not an inexhaustible resource, and so totally replacing

---

[1] The short carbon cycle refers to a short term carbon loop in which plants take up and bind carbon during photosynthesis, and release it again when they rot or are burnt. The short carbon cycle does not lead to a net increase in atmospheric CO_2 concentrations.

[2] The long carbon cycle refers to a long term carbon loop in which the plants, mostly from the carboniferous age (354 to 290 million years ago), took up carbon, died and were preserved in sediments and transformed by geological and petrochemical processes to coal and oil. These ancient organic residues contain stored carbon, which when burnt leads to a net increase in concentrations of CO_2 in the present day atmosphere.

[3] The greenhouse effect refers to an increase in greenhouse gases such as CO_2 in the atmosphere which, like glass, allow sunlight through, but prevent the reflected heat from escaping.

fossil fuels with biomass is not technically feasible.

Furthermore the criteria climate effectiveness, energy efficiency and economics must remain the deciding factors for the cultivation and utilisation of biomass.

The goal of 27% renewable electricity generation in Germany by 2020 (SRU 2007) means that with nearly 12% in 2006 (s. Fig. 1.1) an increase in renewable energy generation of 1% per year until 2020 is required, which apart from increased energy efficiency, must come from replacement of fossil fuels by renewables.
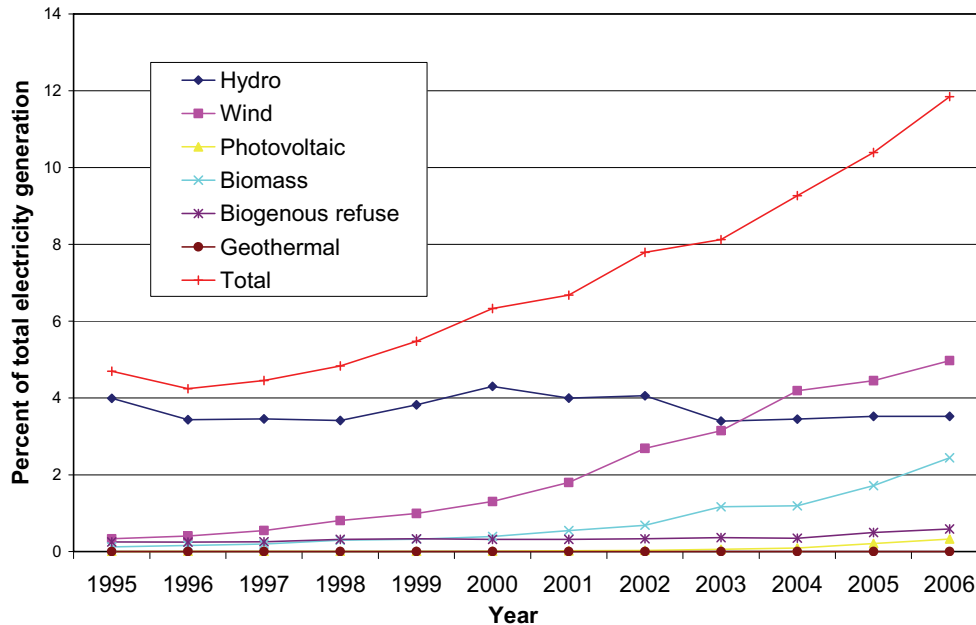
Data source: BMWi Statistic energy data, table 20 last update 02.10.2007

Fig. 1.1: Renewable electricity generation in Germany between 1995 and 2006 (BMWi 2007)

The main carriers of this development are wind and biomass[4]. Hydroelectric generation in Germany is largely stable due to the fact that most viable locations for hydropower in Germany are already in use, and that the EEG primarily supports small scale electricity generation[5], which makes it above all attractive for distributed electricity generation such as wind turbines or biogas plants.

Geothermal electricity generation has the potential to supply all our electricity needs, but problems with the high specific costs and risk related to the necessary deep well drilling, have led to a very low level of implementation.

Photovoltaic electricity generation has increased significantly but is still plagued by high costs, and although it has a huge potential it may be many years until it can play a substantial role in electricity supply.

As seen in Figure 1.2, with a share of 42% biomass is the most important renewable energy carrier with regard to the supply of heat and electricity in Germany today (SRU 2007). A major problem regarding electricity generation from biomass is that biomass is a highly distributed resource and has a low energy density in comparison to traditional fossil fuels. This makes it expensive to collect, transport and store, which in turn limits the "economy of scale"[6] for most biomass power plants.

High quality (woody) biomass which can readily be utilized in "state of the art" biomass fired power plants has become increasingly expensive in Germany in recent years as the domestic

---

[4] In Fig 1.1 biogas utilization is included under the rubric "Biomass".

[5] In the case of hydro power up to 20 MW.

[6] The "economy of scale" refers to the specific decrease in investment costs with respect to installed generation capacity (€/kW$_e$).

use of pellet boilers has steadily increased (BIZ 2002). The utilization of demolition and waste wood has also reached its capacity limits. This has led to the search for alternative sources of biomass supply. Figure 1.2 shows the distribution of total energy generation (heat and electricity) from renewables in Germany in 2006.

Other renewables (2) 3 %
Biogas incl. sewage gas 9 %
Hydro 10 %
Sewage sludge, RDF (1), landfillgas 7 %
Wind 14 %
Biodiesel a.o. liquid fuels 14 %
Photovoltaic 1 %
Wood, straw a.o. solids 42 %

(1) refuse derived fuels
(2) solarthermal, geothermal and heat pumps
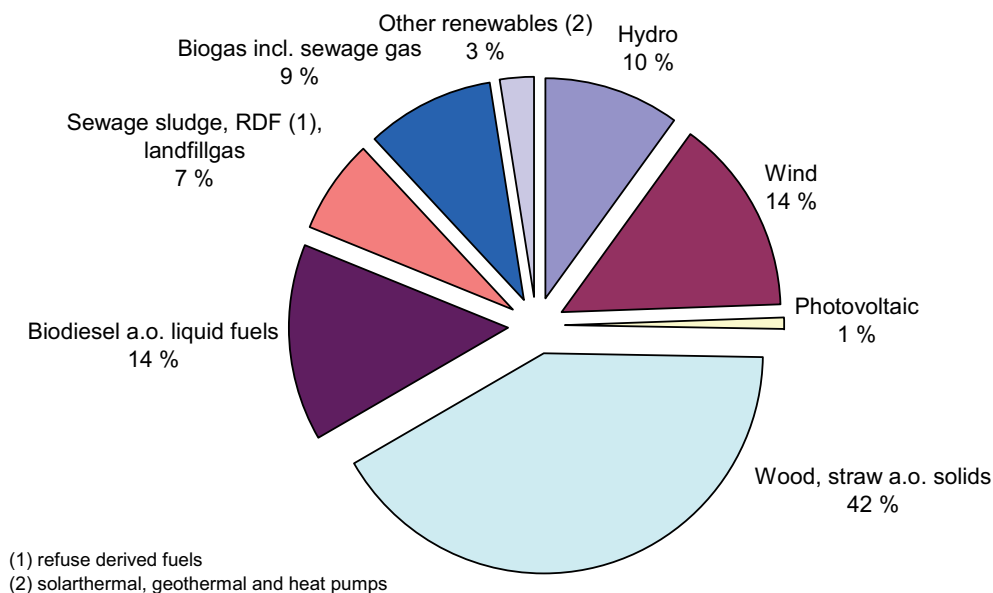
Fig. 1.2: Distribution of renewable energy generation in Germany 2006 (BMWi 2007)

Firstly biomass can be grown for energetic purposes, so called energy crops, as practiced in large scale[7] in the biodiesel and bioethanol industries. But it must be anticipated that this development will lead to a direct competition with the primary agricultural market and contribute to increasing food prices[8].

The energetic utilization of crop residues from primary agricultural and forestry production, on the other hand compliments primary agricultural production as there is already often a surplus of crop residues such as straw on the market which could be utilized for this purpose.

However low grade biomass such as agricultural crop residues exhibit problematic combustion characteristics due to their high ash and alkali metal contents which can cause fouling and slagging in the combustion chamber. There are at present no commercial power plants in Germany which directly utilize straw or other non-woody crop residues for electricity generation. This is primarily due to the lack of a suitable conversion technology.

The purpose of this research work is to develop a small-scale system based on a stationary fluidized bed combustion reactor linked with an externally fired micro gas turbine (SFBC-EFMGT) to meet the technological demand for efficient distributed generation of electricity from low quality biogenous solid fuels.

The linking of a stationary fluidized bed combustion reactor with an externally fired micro gas turbine presents an innovative new approach for efficient small scale distributed electricity generation from readily available problematic biomass fuels such as agricultural and forestry residues.

---

[7] In Germany the use of agricultural land for non-food crop production reached over 2 million hectares in 2007, 1.5 million of which were used for rap-seed cultivation (Berliner Zeitung 2008). This is equates to a 40 fold increased between 2004 and 2007.

[8] Grain prices in Germany rose respectively i.e. the wheat prices rose by over 40% in 2006 alone (BMU 2007).

1.1   Research Motivation and Goals

The main challenges with an externally fired micro gas turbine (EFMGT) system using biofuels are related to the development of a high temperature heat exchanger (HTHx) which replaces the traditional direct combustion in the cycle. The SFBC-EFMGT cycle employs an innovative metallic heat exchanger (Hx) placed within the fluidization zone of the stationary fluidized bed combustion (SFBC) reactor.
The heat exchange rate within the fluidization zone is up to a factor 10 higher than in conventional flue gas heat exchangers due to the direct contact between the hot sand and the heat exchanger tubes. This heat exchanger concept allows maximum air temperatures while minimizing heat exchanger size and cost.
The moderate combustion temperatures (750-900°C) within the SFBC reactor permit the utilization of cost-effective heat resistant metal alloys for the heat exchanger construction and make the SFBC reactor ideal for low quality biomass fuels, such as agricultural crop residues.

To test the technical feasibility of linking an EFMGT and SFBC reactor with an in-bed heat exchanger, a SFBC-EFMGT test-bed has been developed at the University of Rostock Chair of Environmental Technology as shown in Figure 1.3.
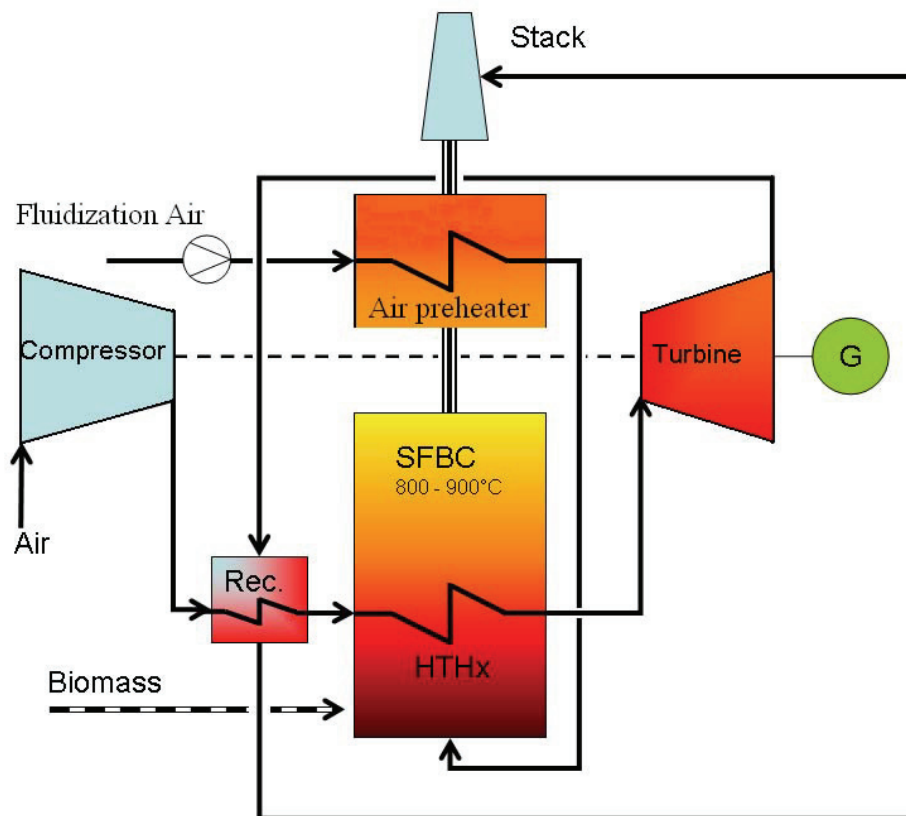
Fig. 1.3: SFBC-EFMGT test configuration at the University of Rostock

The SFBC-EFMGT cycle has the essential advantage that only clean hot air enters the turbine, which allows the combustion of solid fuels such as biomass (i.e. straw, forestry residues or other residual biomass) in a gas turbine cycle without the problems associated with erosion, slagging, fouling, and corrosion of the turbine blades.

The low grade biomass is combusted in the existing small scale (200 kW$_{th}$) atmospheric SFBC reactor, which is renowned for its excellent combustion of problematic biomass fuels. The fluidisation zone of the SFBC reactor contains a metallic heat exchanger, which transfers the heat of combustion to the compressed air stream coming from the EFMGT. The hot compressed air is expanded through the gas turbine driving the compressor and permanent magnet generator. The hot turbine exhaust air then enters the recuperator where it preheats the incoming compressed air stream before being released to the stack.

The SFBC-EFMGT prototype was constructed within the context of this dissertation by a research team consisting of the University of Rostock, Chair of Environmental Technology and Chair of Energy Systems and Turbo Machinery in conjunction with the Aachen University of Applied Sciences, Institute Nowum Energy.

The main objective of this research work is the development and testing of a SFBC-EFMGT prototype to demonstrate the concept feasibility. This task has three main components:

1   Design development and testing of a metallic in-bed heat exchanger for the stationary fluidized bed reactor:

- Selection of construction materials,

- Thermodynamic analysis and determination of the Hx design parameters,

- Geometric design,

- Construction testing and optimization of the heat exchanger.

This task was completed under the leadership of the University of Rostock and is described in detail in this dissertation.

2   Adaptation of a recuperated micro gas turbine to an externally fired micro gas turbine:

- Removal of the internal combustion chamber and fuel gas lines,

- Construction of air lines, outlet, inlet and delivery systems,

- Modification of the MGT software.

This task was completed under the leadership of the Aachen University of Applied Sciences, Institute Nowum Energy and is not described in detail in this dissertation.

3   The development of the SFBC-EFMGT prototype:

- Construction, testing and optimization of the SFBC-EFMGT prototype.

This task was completed under the leadership of the University of Rostock and Aachen University of Applied Sciences and is described in detail in this dissertation.

1.2   Small Scale Biomass Electricity Generation

Most of the existing biomass electrical generation capacity is based on combustion, raising steam and expansion through a steam turbine. Due to its relative complexity and cost this process is not usually commercially feasible for unit sizes below an electrical generation capacity of about 2 MW.

Biomass gasification and combustion in a gas turbine is a further option under development, but this system is also relatively complex and therefore only likely to be economically feasible on a larger scale than that envisioned for bio-fuelled microturbines.

It has been established in many feasibility studies, that there is a high potential for distributed rural electricity generation from solid biomass in a capacity range below 2 MW (Pajusalo 2005, Lymberopoulos 2004), or more specifically between 100 and 500 kWe (Cocco et al. 2006). In Germany the generation range below 500 kW is also economically advantageous because of the higher return on electricity sold to the grid.

Presently commercially available small size (100-500 kWe) technologies suitable for distributed generation of electricity from biomass are restricted to Stirling engines, Spilling steam expansion engines, biogas internal combustion motors and to a lesser extent the Organic Rankine Cycle (ORC).

However, such power units are characterized by high capital costs (2-4 k€/kW) and low conversion efficiencies (Duvia and Gaia 2002, Cocco et al. 2006). For this market the externally fired micro gas turbine (EFMGT) offers the advantage of higher electrical efficiencies in the right power range for distributed electricity generation and, in combination with a stationary fluidized bed, allows the utilization of readily available low cost solid biomass fuels such as agricultural and forestry residues.

1.2.1   Stirling Engines

Stirling engines are heat machines in which the working fluid (often helium) is moved back and forth between hot and cold heat exchangers (s. Fig. 1.4). The Stirling engine cycles through four main processes: cooling, compression, heating and expansion. The gas is expanded with an external heat source over the hot heat exchanger, and cooled with an external heat sink over the cold heat exchanger. A change in gas temperature will cause a corresponding change in gas pressure, while the motion of the piston causes the gas to be alternately expanded and compressed. When the gas is heated the pressure rises and causes the power piston to produce a power stroke. When the gas is cooled the pressure drops and less work is done to compress the gas on the return stroke, thus yielding a net power output.
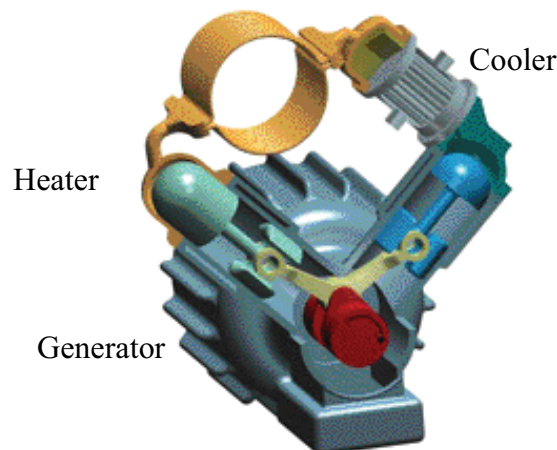
Fig. 1.4: Principle of the two cylinder SOLO Stirling 161 engine (Stirling 2007)

Small natural gas fired combined heat and power generation systems based on the Stirling technology have recently been commercialized at sizes suitable for single homes (0.5-9 kWe) by manufacturers such as Whispergen, Solo, STM-Power, Enatech, Sunpower and Stirling. Larger biomass fired Stirling CHP systems are in the research and development stage at the Technical University of Denmark. A 35 kW prototype, with an overall electrical efficiency of around 9% has been tested, and a 75 kW plant is the subject of ongoing research[1] (Obernberger et al. 2003).

1.2.2   Steam Expansion Engines (Spilling)
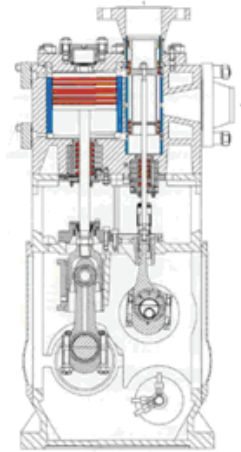
Fig. 1.5: Spilling steam expansion engine

The main advantage of steam expansion engines is their high flexibility for steam requirements and excellent part load performance. Their main drawback is their low electrical efficiency.

The electrical efficiency of the Spilling CHP steam expansion engine is around 10 to 12% with an electrical generation capacity of 25 to1500 kW (Spilling 2008, Lymberopoulos 2004).

Commercially available steam expansion engines are manufactured by the German company Spilling (Spilling 2008). Spilling steam expansion engines (s. Fig 1.5) are well suited for biomass combined heat and power systems firing wood and wood wastes in a steam raising boiler.

1.2.3   Organic Rankine Cycle (ORC)
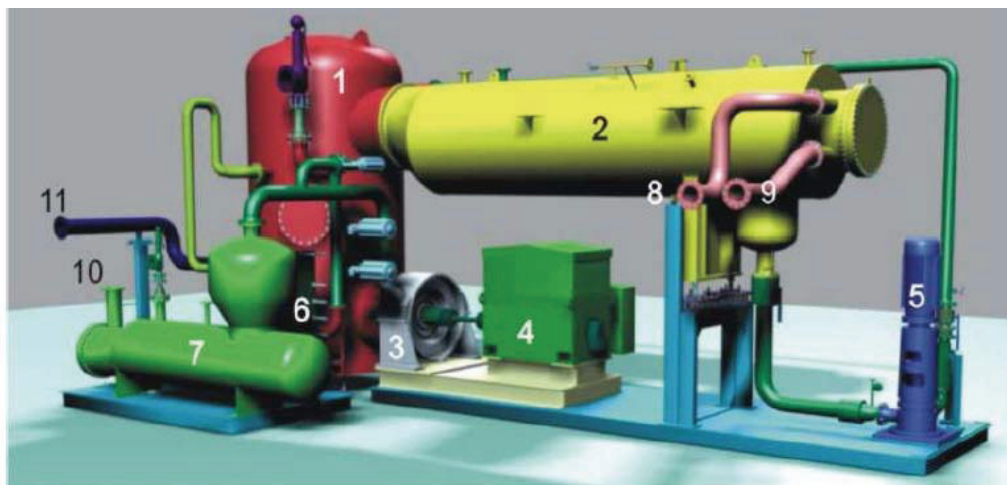
1 Regenerator	5 Circulation pump	9 Hot water outlet
2 Condenser	6 Pre-heater	10 Thermal oil inlet
3 Turbine	7 Evaporator	11 Thermal oil outlet
4 Electric generator	8 Hot water inlet	

Fig. 1.6: Organic Rankine Cycle (Turboden 2008)

---

[1] EU project BIOSTIRLING NNE5-1999-00097

The Organic Rankine Cycle (s. Fig. 1.6) is an indirectly heated closed cycle in which the turbine is driven by a high molecular mass organic fluid selected to exploit low temperature heat sources i.e. a fluid with sufficiently low boiling point. The organic working fluid is vaporized by application of a heat source in the evaporator after which it is expanded over the turbine and condensed back to a liquid before being pumped back to the evaporator, thus closing the thermodynamic cycle. The ORC cycle is suitable for low temperature heat sources such as geothermal energy and waste heat recovery, but also for higher temperature applications such as solar collector and biomass combustion power plants in which case high temperature thermal oil is used as a heat carrier and a regenerator is added, to further improve the cycle performance. ORC plants have electrical efficiencies between 12% and 18% and range from 400 kWe to 1500 kWe (Duvia and Gaia 2002, Turboden 2008, ZES 2004).

1.2.4 Biogas Plants

Most of the present distributed electricity generation systems utilizing biomass in Germany are based on fermenter biogas being fired in gas motors[2], while some research has been performed into biogas combustion in micro gas turbines (Janssen 2004, Peters 2004, FNR 2005, Vincent and Strenziok 2007, Greenvironment 2007).
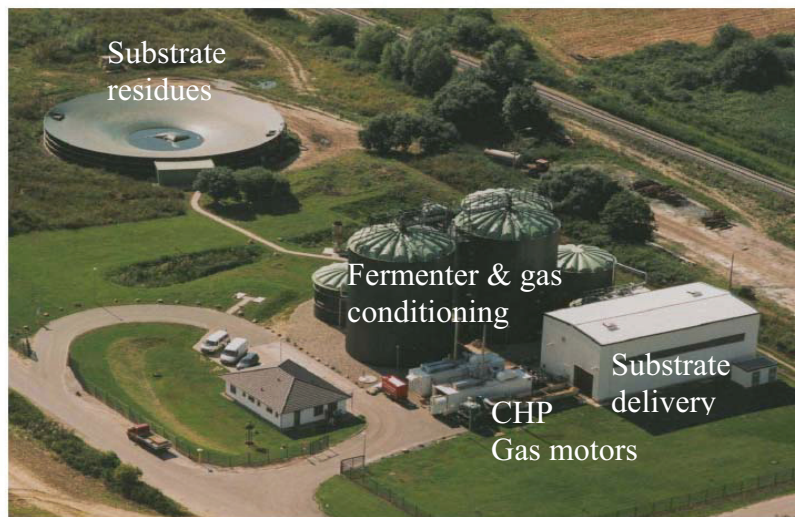
Fig. 1.7: Typical biogas plant in Germany

Biogas plants of this scale (s. Fig 1.7) present a large investment, require well organized material supply chains, and must employ at least two permanent staff to keep the plant operating. Biogas plants utilize liquid manure and organic conferment substrates such as maize silage, food scraps and waste vegetable oil. The delivered substrates are mixed and pumped into the fermenter where under an anaerobic environment it is partially converted to biogas by methanogenic bacteria. The biogas is then combusted in a gas motor (s. Fig. 1.8). The gas engines from Jenbacher are available in the power range from 250 kWe to 3000 kWe. The trend for biogas power plants with a generation capacity of 1 to 3 MW is to utilize several smaller motors to achieve better part load efficiencies, and also maximize the feed-in tariff, which is higher for smaller scale electricity generation.
Gas engines reach an electrical efficiency of around 35% but this does not include losses during the conversion of the raw biomass to biogas.

---

[2] Diesel and petrol motors

Fig. 1.8: Jenbacher type 2 gas engines (GE-Energy 2008)

The conversion efficiency of biomass to biogas depends largely on the biomass composition and reactor type, but can be averaged at around 45% based on the lower heating value of the wet biomass feedstock (Elmegaard and Qvale 2002). This corresponds to a net electrical efficiency of around 16%.

1.2.5   Externally Fired Gas Turbines

The only commercially available EFMGT (Talbott's BG 100) has an electrical generation capacity of 100 kW with an efficiency of around 20% (Talbott 2006).
Talbott's BG 100 (s. Fig. 1.9) requires good quality biomass with low ash content and high ash melting temperatures suitable for combustion temperatures over 1000°C. The BG 100 is therefore unsuitable for straw and other similar agricultural residues. If fired at much lower temperatures the efficiency of the system will drop to under 16% and the carbon monoxide (CO) emissions will increase dramatically (Pritchard 2002).
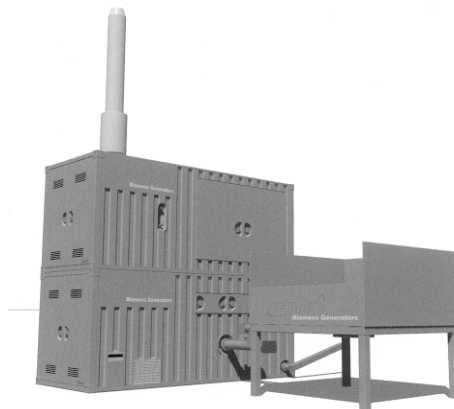
Fig. 1.9: Talbott's BG 100 externally fired micro gas turbine

The BG 100 is on the market for around 450 000 € (Lymberopoulos 2004, Pehn 2006).
Two reference plants exist at universities in the UK and one commercial plant has recently been installed at Zurich Airport in Switzerland.
The principle advantage of the EFGT process is that it avoids any contact between the turbine blades and the combustion gases, thus preventing damage by corrosive or particle loaded combustion gases and avoiding the critical issue of severe gas cleaning (Crosa et al.1998, Bram et al. 2005, Yan 1998). This in turn allows the utilization of solid fuels such as low grade biomass.
The critical component of the externally fired cycle is the high temperature heat exchanger, which also plays the key role for the plant efficiency (Farina and Avanzini 1993, Kautz 2005).

The high temperature heat exchanger is also the primary obstacle for the development of externally fired gas turbines (Yan and Eidensten 2000, Savola et al. 2005, Yan 1998).
Figure 1.10 gives an overview of typical electrical efficiencies for the commercially available plants for small scale biomass electricity generation.
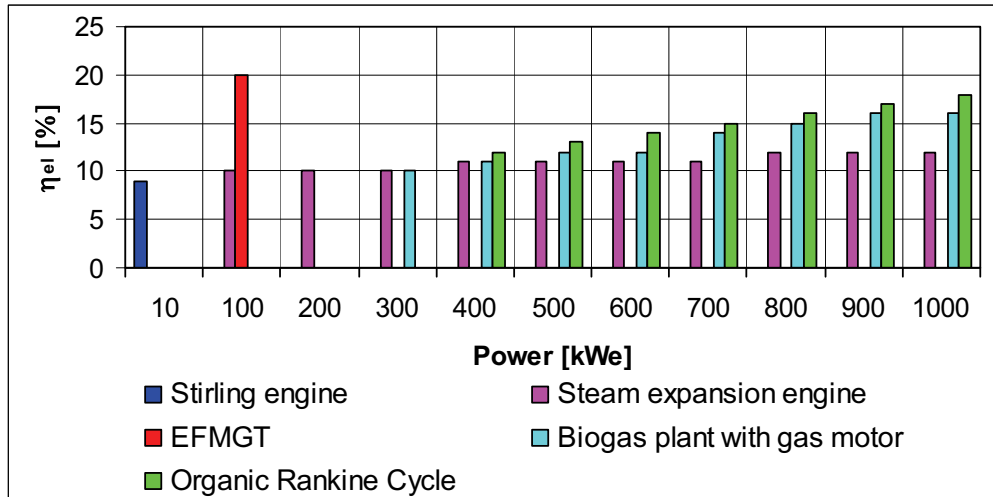
Fig. 1.10: Typical efficiencies of small scale biomass electricity generation

Figure 1.10 shows that there is a lack of commercially available technologies for the efficient generation of electricity from solid biomass feedstocks in the 100-300 kWe power range suitable for distributed generation. For applications of less than 100 kWe only the Stirling engine is theoretically capable of utilizing solid biomass, but practical application has proved not to be feasible due to the extreme level of fouling of the Stirling engine heat exchanger. The Spilling steam expansion engine is suitable for biomass and covers the required power range but, due to very low electrical efficiencies, will only be suitable in CHP mode when large amounts of heat are required, which is usually not the case for small scale distributed generation. The ORC cycle and biogas plants have somewhat higher electrical efficiencies, but are better suited for larger scale operations.
Theoretically the EFMGT has a factor of 2 to 5 higher electrical efficiency than the competing technologies in the relevant generation range. With an integrated biomass dryer electrical efficiencies of up to 33% are anticipated (Cocco et al 2006) for residual biomass, and over 50% (LCV basis) when utilizing liquid effluents with 80% water content (Elmegaard et al. 2001). Previous research at the University of Rostock, Chair of Energy Systems and Turbo Machinery, has revealed that a 100 kW EFMGT cycle should reach electrical efficiencies of over 27% (Kautz 2005). Figure 1.11 gives an overview of theoretical electrical efficiencies for some of the proposed biomass fuelled EFMGT systems.
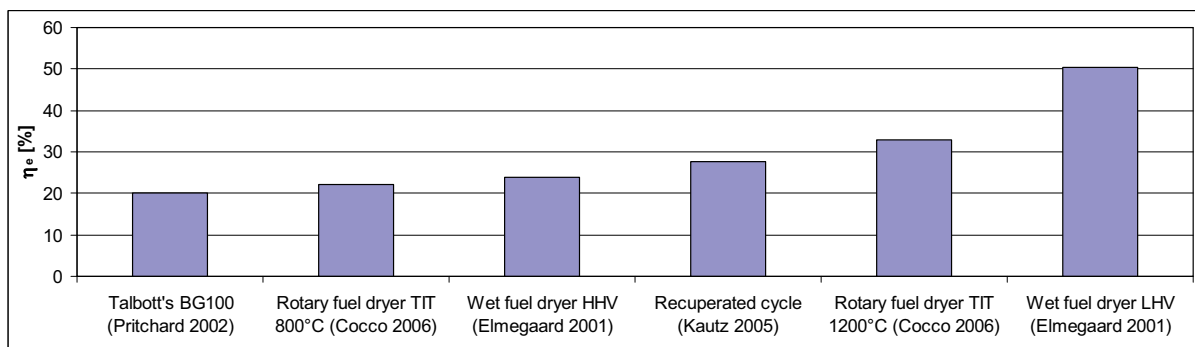
Fig. 1.11: Theoretical electrical efficiency of proposed biomass fuelled EFMGT cycles

Systems in the research and demonstration (R&D) phase which may be suitable for distributed generation include the direct combustion of pulverized biomass in a gas turbine with electrical efficiencies of up to 30% (ZES 2004, Wingelhofer 2006), various EFMGT systems, and biomass gasification in combination with gas turbines or fuel cells (Karl and Hein 2002, Karl et al. 2004, Karl 2006).

The directly fired biomass turbine has severe problems related to the flue gas cleaning. Although gasification can avoid the problems with the ash deposition, erosion and corrosion encountered during direct combustion of solid fuel, a significant proportion of the fuels energy content is lost in the gasification process, and the stringent requirements of gas turbines regarding particulates and alkali levels necessitates complicated and costly gas cleanup equipment (Anheden et al. 1999). Another limiting factor is the low calorific value of produced gas (Ferreira et al. 2002).

One notable exception is the application of allothermal steam gasification as practised in the Bio-HPR developed by Karl (Karl et al. 2000, Karl and Hein 2002, Karl et al. 2004, Metz et al. 2004). Some engineers believe that the internal combustion gas turbine coupled to a gasifier will give a higher efficiency than the externally fired gas turbine using solid biomass (Ferreira and Pilidis 2001). On the other hand the EFMGT is a simple robust system which may well have a competitive advantage over gasification for small scale systems.

Due to the still very serious problems with direct dust firing, the low efficiency of the ORC process, and the commercialization difficulties of gasification technologies, the most favourable candidate for small scale distributed electricity generation is the externally fired gas turbine (ZES 2004).

1.2.6   Summary and Recommendations

From both the European Union and German Government there is a strong level of financial support for further research and development of distributed energy generation from biomass.

There is notable lack of commercially available technologies utilizing solid biomass feedstocks in the range 100-400 kWe, which is the ideal generation capacity for distributed generation.

The only commercially available EFMGT is twice as efficient as the best competing technology, but is very expensive and the combustion system and temperatures are not suitable for low grade residual biomass such as straw.

The stationary fluidized bed reactor linked with an externally fired micro gas turbine has several major advantages over the existing Talbott's BG100 EFMGT system:

- Firstly, a metallic in-bed heat exchanger can be utilized which reduces the size and cost of the heat exchanger by up to a factor of 10.

- Secondly, due to the excellent combustion characteristics and low temperatures in the SFBC reactor, cost-effective low grade biomass fuels such as agricultural and forestry residues can be utilized.

The main challenge for the proposed SFBC-EFMGT remains the development of a suitable robust heat exchanger for the SFBC reactor.

2   Gas Turbines

A gas turbine is a heat engine which transforms the chemical energy of combustible gases or highly volatile liquids into thermal and finally into the rotational mechanical energy of the shaft which for stationary[1] applications is used to drive a generator to produce electricity.

The micro gas turbine (MGT) is an extremely small[2] compact gas turbine with recuperative air heating. The MGT consists of a radial compressor, a combustion chamber and radial power turbine. The compressor and the power turbine are connected by a shaft. The recuperator is located between the compressor and turbine (s. Fig. 2.1).
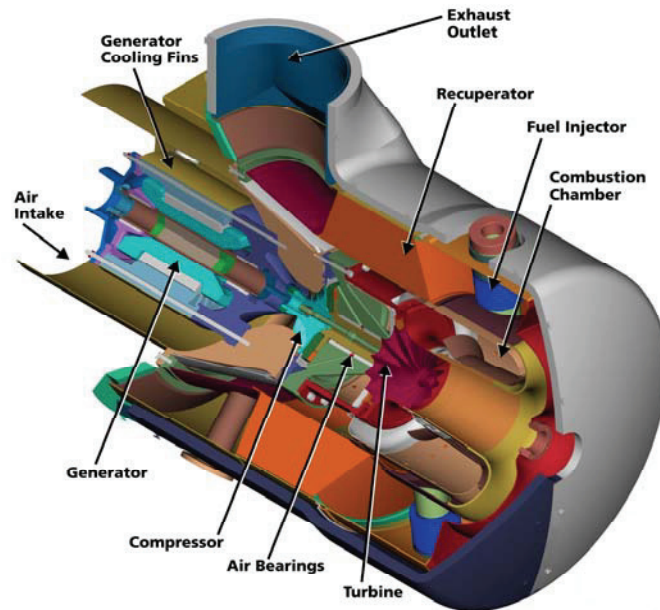
Fig. 2.1: Cross section of a micro gas turbine (www.microturbine.de)

The fresh intake air cools the generator and is drawn into the compressor. In the recuperator the compressed air is preheated by the turbine exhaust air before entering the combustion chamber where fuel is injected and the air/fuel mixture is combusted, further increasing the temperature of the working fluid.

Typical turbine fuels are natural gas, kerosene or diesel. The temperature in the combustion zone can reach up to 1500°C which is too hot for the metallic turbine blades. Therefore the hot gases are mixed with the - in the combustion uninvolved - excess air which cools the working fluid, in the case of microturbines to around 950°C, before it enters the power turbine. Microturbines work with an excess air ratio (λ) of around 6.5.

The working fluid is expanded through the turbine thereby transforming thermal energy into the mechanical, rotational energy of the turbine. The relaxed fluid then leaves the turbine as hot flue gas, which in the case of MGTs is utilized in the recuperator to heat the incoming compressed air stream.

In gas turbine power plants a large proportion of the turbine mechanical output is necessary to drive the compressor. The difference is then used by the generator to generate electricity. The thermodynamic principles of the gas turbine can best be explained on hand of the ideal Brayton (Joule) cycle as presented in Figure 2.2.

---

[1] Gas turbines are also the integral component in jet engines.
[2] Micro gas turbines produce between 30 and about 250 kWe.

2.1   Ideal Brayton (Joule) Cycle
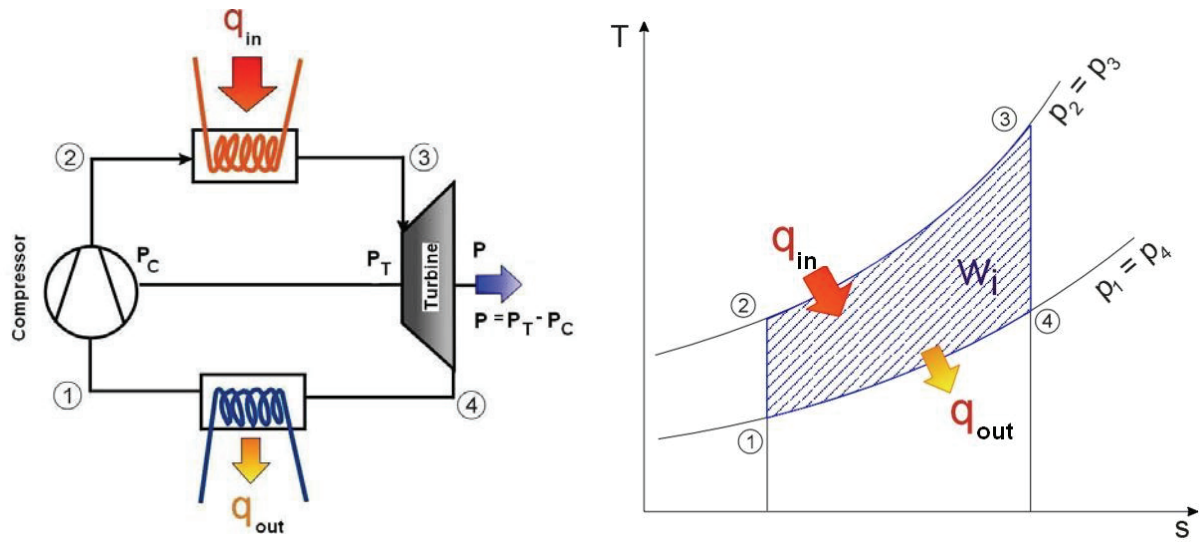
Fig. 2.2: Closed cycle ideal Brayton gas turbine flowchart and T-s diagram

The gas turbine ideal Brayton cycle consists of four thermodynamic changes of state:

- $1 \rightarrow 2$ isentropic compression

- $2 \rightarrow 3$ isobaric heating

- $3 \rightarrow 4$ isentropic expansion

- $4 \rightarrow 1$ isobaric cooling

The mechanical power (P_m) won by the process is the sum of the power produced by the turbine (P_T) and the power consumed by the compressor (P_C) as shown in equation [2-1].

$$P_m = P_T - P_C \qquad [2\text{-}1]$$

The efficiency (η_{th})[3] is the ratio of mechanical power to the system energy input [2-2], which can be expressed as an enthalpy difference (Δh).

$$\eta_{th} = \frac{P_T - P_C}{\dot{Q}_{in}} = \frac{(h_3 - h_4) - (h_2 - h_1)}{(h_3 - h_2)} \qquad [2\text{-}2]$$

For isentropic changes of state the association [2-3] is valid.

$$\frac{T_2}{T_1} = \left(\frac{p_2}{p_1}\right)^{\frac{x-1}{x}} \quad and \quad \frac{T_3}{T_4} = \left(\frac{p_3}{p_4}\right)^{\frac{x-1}{x}} \quad with \ x = \frac{c_p}{c_v} \qquad [2\text{-}3]$$

Thus, assuming a constant specific heat capacity (c_p, c_v), the thermal efficiency can be expressed as a function of the pressure ratio ($p_2/p_1 = \pi$) or the temperature ratio (T_1/T_2) [2-4].

---

[3] for stationary operation with constant air mass flow

$$\eta_{th} = 1 - \frac{1}{\pi^{\frac{x-1}{x}}} = 1 - \frac{T_1}{T_2}$$ [2-4]

The theoretical thermal efficiency of the ideal Brayton cycle increases with increasing pressure ratio as shown in Figure 2.3.
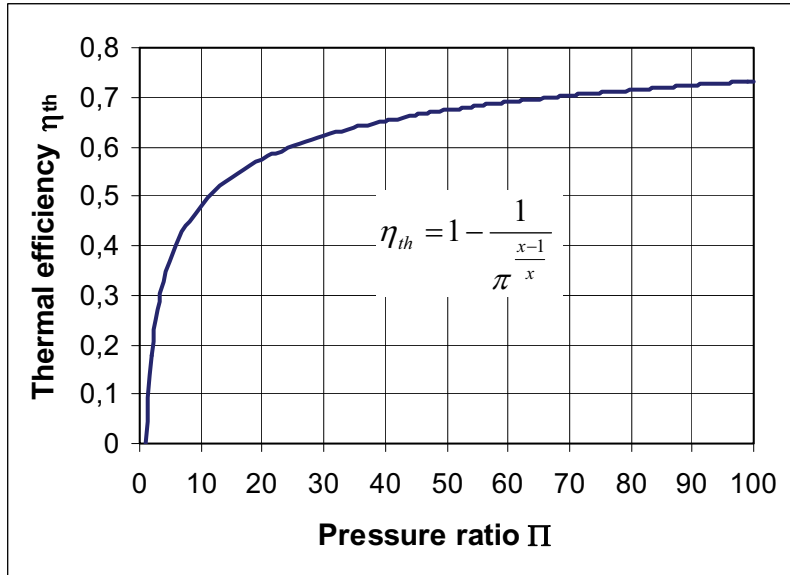
Fig. 2.3: Ideal thermal efficiency as a function of pressure ratio (Sörgel 1996)

2.2   Real Gas Turbine Cycle
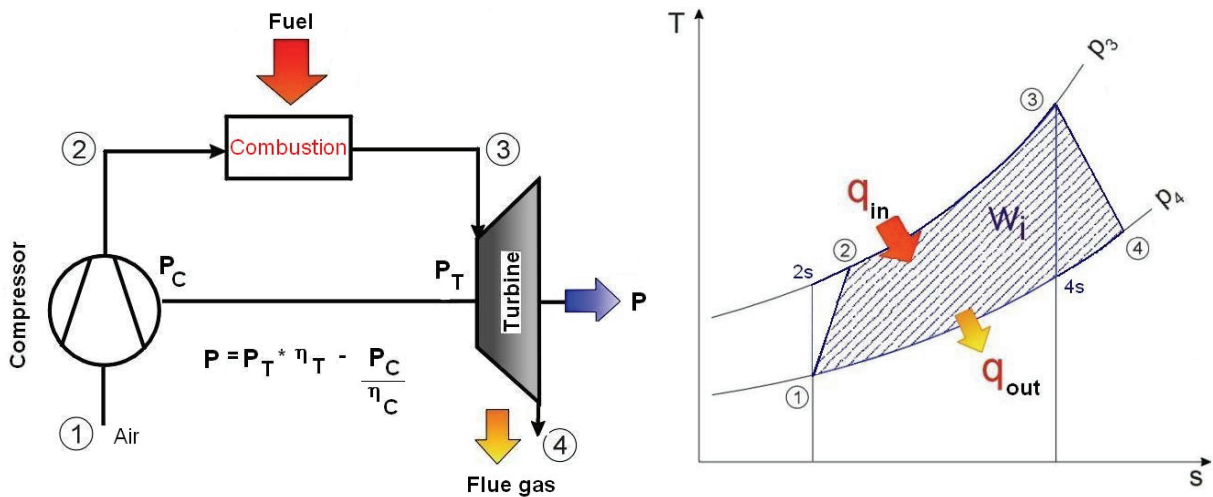
Fig. 2.4: Real open gas turbine cycle and T-s diagram

The ideal Brayton cycle is a highly simplified model of the real gas turbine cycle, which allows the derivation of fundamental relations leading to an estimation of thermal efficiency based on the process temperatures.

However the design and optimization of gas turbine cycles requires the consideration of the real gas turbine process which takes into account losses resulting from the irreversible changes of state with respect to the second law of thermodynamics.

- Friction: Dissipation work caused by friction losses during compression, transport and expansion lead to an increase in entropy; the real gas turbine process is not isentropic.

- Pressure: The combustion process results in pressure loss; the real gas turbine process is not isobaric.

- Heat: During real combustion processes heat is lost to the environment.

In the real gas turbine process T-s diagram (s. Fig. 2.4) the state conditions 1 and 3 are equated with the ideal process, however the temperature 2, after the compressor and 4, after the turbine, are higher than the respective isentropic process temperatures 2*s* and 4*s*.

This heat increase is an irreversible change of state, and thus according to the second law of thermodynamics ($\Delta s > 0$ for irreversible state changes) is bound with an increase in entropy (s) (Baehr 2002). On hand of the comparison between the ideal and real state changes the internal efficiency (η_i) of the turbo machinery (compressor and turbine) can be obtained as shown in equations [2-5] and [2-6].

For the compressor:
$$\eta_{iC} = \frac{h_{2s} - h_1}{h_2 - h_1} \qquad [2\text{-}5]$$

For the turbine:
$$\eta_{iT} = \frac{h_3 - h_4}{h_3 - h_{4s}} \qquad [2\text{-}6]$$

Thus with equations [2-2], [2-5] the thermal efficiency of the real gas turbine can be determined as shown in equation [2-7].

$$\eta_{th} = \frac{\eta_{iT}(h_3 - h_{4s}) - \dfrac{1}{\eta_{iC}}(h_{2s} - h_1)}{(h_3 - h_2)} \qquad [2\text{-}7]$$

The efficiency of the real gas turbine cycle depends on the pressure ratio (π), and on the turbine inlet temperature (TIT).
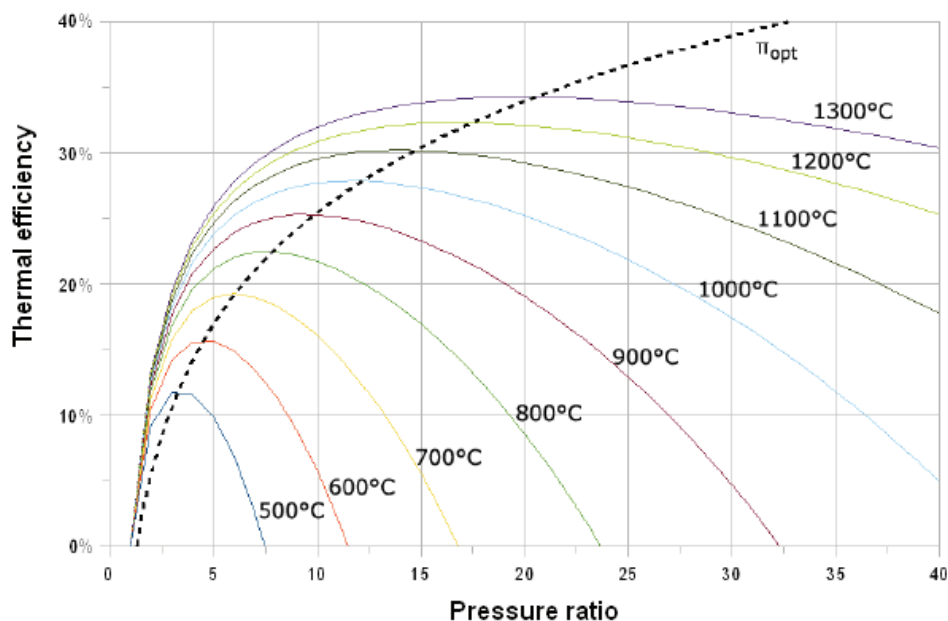
Fig. 2.5: Open gas turbine efficiency with respect to temperature and pressure ratio

The analysis of equation [2-7] reveals that every turbine inlet temperature (T_3) has an optimal pressure ratio (π_{opt}) for a maximal thermal efficiency (η_{th}) as shown in Figure 2.5 for a typical gas turbine.

2.3   Gas Turbine Cycles

The open cycle gas turbine process has a relatively low efficiency due to the high turbine outlet temperatures of around 500-600°C which represents a large enthalpy loss. On the other hand the flue gas enthalpy can be utilized downstream of the turbine to raise steam for a steam turbine, such as in gas and steam combined cycle power plants (s. Fig 2.6).

2.3.1   Gas and Steam Combined Cycle

Modern gas fired combined cycle (CC) power plants combine the Brayton and Rankine cycles (s. Fig. 2.6) to achieve electrical efficiencies of over 50%, which is the state of the art in high efficiency power plants.
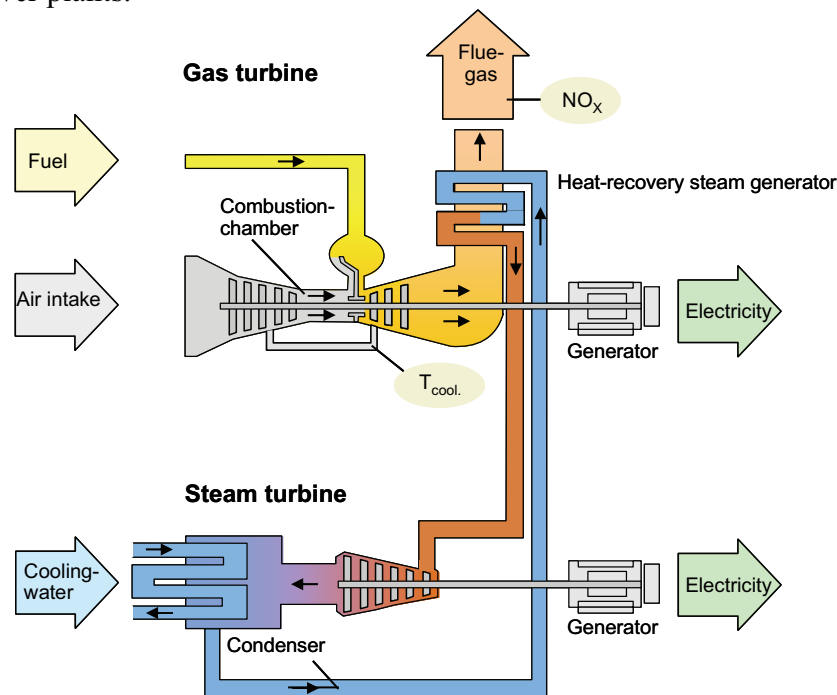
Fig. 2.6: Simplified gas and steam combined cycle power plant schema (Lenk 2006)

2.3.2   Recuperated Gas Turbine Cycle

For low temperature and pressure ratios the efficiency of the simple open gas turbine cycle quickly falls under 20% as can be seen in Figure 2.5.
However the recuperated gas turbine cycle (s. Fig. 2.7) allows micro gas turbines to realize efficiencies of 30% with turbine inlet temperatures of only around 950°C and a pressure ratio of 3.5.
This is achieved by recuperation of the turbine exhaust gas enthalpy to the compressed air stream after the compressor.
The main advantage of recuperated gas turbine cycle is the reduced fuel consumption, and

therefore higher efficiency in comparison to the simple open cycle as can be seen from the thermodynamic examination in equation [2-8] for stationary operation with constant air mass flow.

$$\eta_{th} = \frac{P_T - P_C}{\dot{Q}_{in} - \dot{Q}_{rec}} = \frac{(h_3 - h_4) - (h_2 - h_1)}{(h_3 - h_2) - (h_{2a} - h_2)}$$ [2-8]

The preheated air stream increases the enthalpy in the combustion chamber, thus reducing the required fuel mass flow and increasing the plant efficiency.
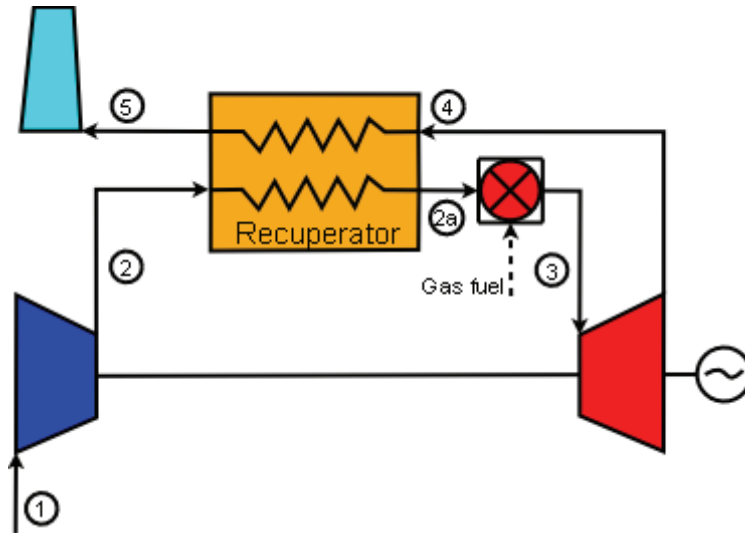
Fig. 2.7: Recuperated micro gas turbine cycle

The recuperation of the exhaust gas enthalpy to the compressed air stream is accentuated in the T-s diagram in Figure 2.8, where ΔT_U and ΔT_L are the upper and lower temperature difference between the flue gas and compressed air stream respectively and 2a is the air temperature after the recuperator.
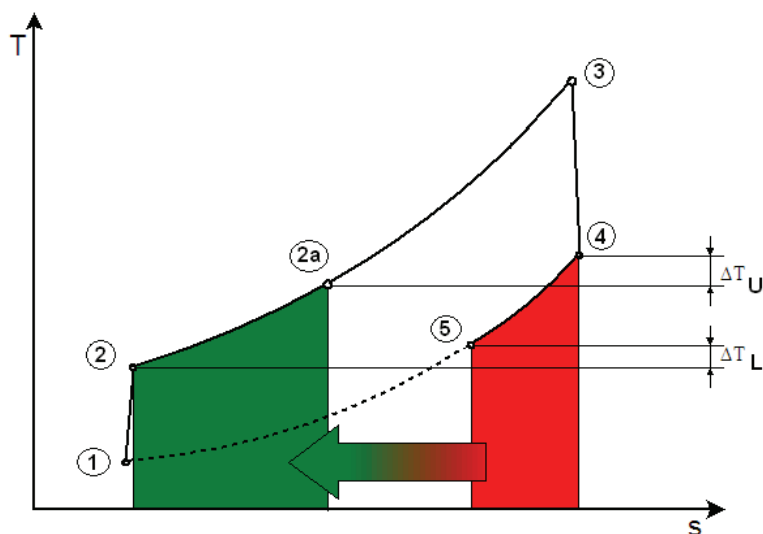
Fig. 2.8: Recuperated gas turbine T-s diagram (adapted from Kautz et al. 2004)

One of the requirements for a recuperated gas turbine is that the air temperature after the compressor is not already higher than the turbine exhaust gas temperature (otherwise the heat transfer direction in the recuperator reverses). This makes a recuperator unsuitable for large gas turbines with high pressure ratios because the air temperature increases proportional to the degree of compression as seen by solving equation [2-9] for T_2:

$$T_2 = T_1 \cdot \pi^{\frac{x-1}{x}}$$
[2-9]

Therefore recuperation is limited to smaller gas turbines with low pressure ratios such as micro gas turbines (MGTs) which are characterized by low pressure ratios.
The MGT technology would appear to be ideally suited to small scale distributed renewable electricity generation, except for one serious limitation:

Micro gas turbines require high quality gaseous (natural gas, treated biogas) or liquid (diesel, kerosene) fuels.

For distributed renewable electricity generation however the energetic utilization of readily available low quality solid biomass fuels is essential.
This limitation can be overcome by combining the advantages of the closed cycle gas turbine, (s. Fig. 2.2), – i.e. utilizing a heat exchanger between the heat source and working fluid – with the advantages of the recuperated micro gas turbine cycle (s. Fig. 2.7). This cycle is known as the externally fired micro gas turbine (EFMGT) and is shown in Figure 2.9.

2.3.3 Externally Fired Micro Gas Turbine Cycle

The externally fired micro gas turbine (EFMGT), as shown in Figure 2.9 is a further development of a recuperated gas turbine cycle (s. Fig. 2.7).
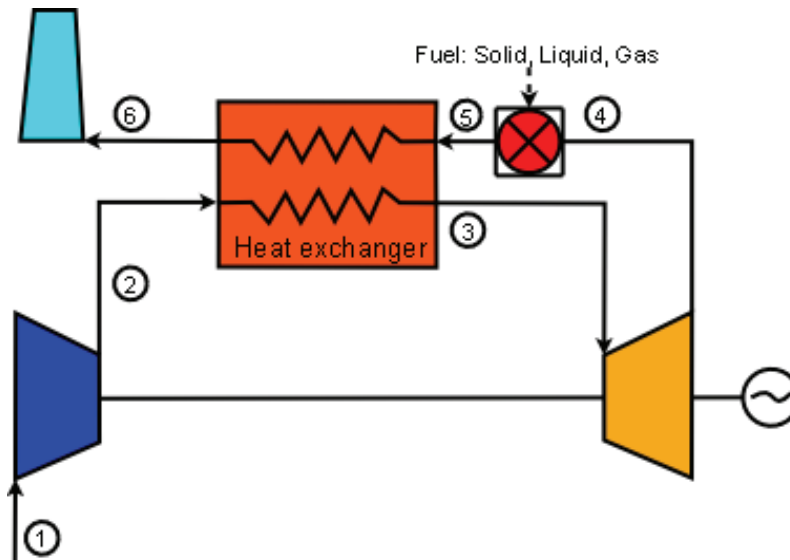
Fig. 2.9: Externally fired micro gas turbine cycle

The EFMGT cycle relies on a heat exchanger (2-3) to transfer the heat of combustion to a clean compressed air stream which is then expanded (3-4) over the gas turbine. The hot exhaust air (4) after the gas turbine is combusted in the furnace with the solid fuel producing

hot flue gases (5) which are cooled in the heat exchanger (5-6), heating the compressed air stream. The cooled exhaust gas is released to the stack (6).

As shown in equation [2-10] the heat exchanger efficiency is the quotient between the temperature difference in the heat exchanger (T_3-T_2) and the maximal temperature difference between the heat exchanger inlet and combustion temperature (T_5-T_2).

$$\eta_{Hx} = \frac{T_3 - T_2}{T_5 - T_2} = \frac{T_5 - \Delta T_U - T_2}{T_5 - T_2} = 1 - \frac{\Delta T_U}{T_5 - T_2} \qquad [2\text{-}10]$$

Thus the efficiency of the heat exchanger increases with decreasing difference (ΔT_U) between the upper air temperature and combustion temperature (s. Fig 2.10).
.
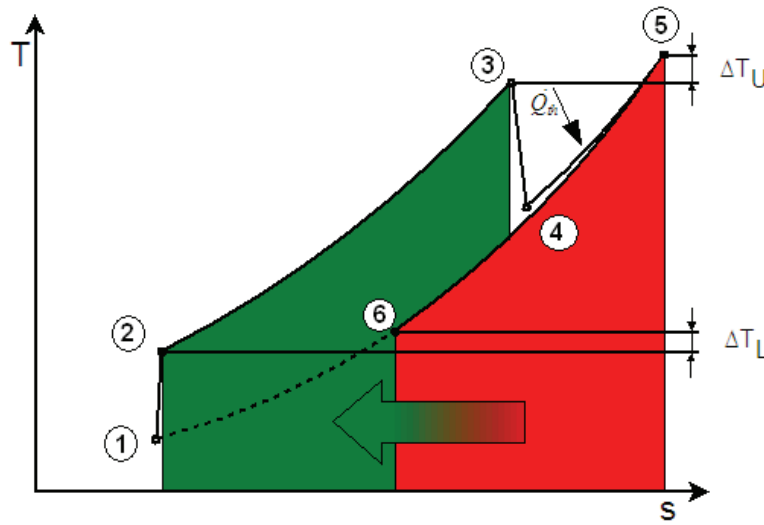
Fig. 2.10: Externally fired gas turbine T-s diagram (Kautz and Hansen 2004, 2007)

In the case of an external heat exchanger in which the air mass flow within the heat exchanger differs from that of the combustion gases, this association is known as the heat transfer effectiveness (Φ).
The heat exchanger efficiency on the other hand is given by the quotient out of heat exchanged to fuel input as shown in equation [2-11].

$$\eta_{Hx} = \frac{\dot{Q}_{Hx}}{\dot{Q}_{Fuel}} \qquad [2\text{-}11]$$

The thermal efficiency of the simple EFMGT cycle depends on the heat exchanger efficiency as shown in equation [2-12].

$$\eta_{th} = \frac{\eta_{Hx}(P_T - P_C)}{\dot{Q}_{in}} \qquad [2\text{-}12]$$

The EFMGT cycle efficiency can also benefit from the fuel saving influence of a recuperator as shown in equation [2-13].

$$\eta_{th} = \frac{\eta_{Hx}(P_T - P_C)}{\dot{Q}_{in} - \dot{Q}_{Recu}}$$

[2-13]

Due to the low pressure ratio of the EFMGT cycle, pressure drop in the heat exchanger has a large influence on the cycle efficiency.

The pressure drop in the heat exchanger decreases the pressure difference available for expansion over the turbine and thus reduces the power output. Based on their simulation results Hansen and Kautz (2004) recommended that an air side pressure drop of less than 100 mbar is necessary to avoid excessive loss in efficiency.

To take full advantage of the EFMGT technology its application for micro scale distributed generation from solid biomass fuels in conjunction with stationary fluidized bed combustion (SFBC) and in-bed heat exchanger is anticipated. The strengths of the proposed SFBC-EFMGT cycle rely on the following considerations:

- The working fluid is clean air instead of combustion gases so no particle cleanup of the gas turbine path is necessary.

- Essentially the EFMGT cycle can be operated with almost any fuel, including solid biomass or other difficult fuels because the sensitive turbo-machinery runs on clean hot air, not combustion gases as in internally fired gas turbines.

- A robust atmospheric stationary fluidised bed external combustion (SFBC) system can be utilised, which is suitable for a wide range of biomass fuels such as agricultural and forestry residues.

- This combustion system is compatible with a cost effective metallic fluidized bed heat exchanger. A heat exchanger immersed in the fluidized bed is able to achieve heat transfer rates up to 10 times higher than comparable flue gas/air heat exchangers, and attain air temperatures very close to the fluidized bed combustion temperature.

Nevertheless the fuel quality and type is still a major issue for the operation of the high temperature heat exchanger and the fluidized bed combustion reactor.

Many authors (Farina and Avanzini 1993, Yan et al 1998, Yan and Eidensten 2000, Crosa et al.1998) suggest that the problems relating to the combustion of solid fuel in a gas turbine have been shifted to the heat exchanger, but not yet solved. Thus the main area of research with respect to the EFMGT process remains the construction of an efficient cost-effective high temperature heat exchanger.

3   Externally Fired Gas Turbines: Research & Development

The first externally fired gas turbine plants were based on a closed cycle gas turbine configuration. They were introduced by Escher Wyss in Zurich as early as 1939 with some 20 plants being built, mainly using coal or coal gas as fuel (Bram et al. 2005).
With the increase in turbine inlet temperatures in modern gas turbines however, the closed cycle configuration was replaced by an open cycle configuration which eliminated the need to cool the working fluid after the turbine[1].
In the 1950's an open cycle EFGT test rig generating 500 kWe using peat fuel was constructed in Scotland (Savola et al. 2005). This demonstration experience led to the first industrial scale EFGT test plant being constructed in Ravensburg, Germany. The 2.3 MWe pulverised coal EFGT in Ravensburg operated reliably with metallic heat exchangers, but the achieved turbine inlet temperatures were too low to allow economic operation (Savola 2005).

The large scale externally fired cycles which have been tested over the last 30 years rely mostly on coal combustion as standard fuel, and utilize ceramic high temperature heat exchangers or natural gas topping combustion to achieve the required high turbine inlet temperatures.
However, large scale externally fired cycles have not yet been commercially successful, mostly due to technical problems associated with the high temperature heat exchangers and the lack of competitive advantage in comparison to modern coal and gas fired combined cycle power plants.
Advanced externally fired system configurations include the externally fired combined cycle (EFCC) and the externally fired humid air turbine (EFHAT)[2], which can be combined with a topping[3] or bottoming[4] cycle.
The EFGT is well suited as combined heat and power (CHP) or combined cycle (CC) plant with a heat recovery system, due to the fact that the air after the turbine still has a high temperature.
A bottoming steam cycle can increase the efficiency for larger plants but is too costly for small scale applications. For small scale applications the hot flue gases could be used for heating purposes while the clean hot turbine exhaust air is available for high quality processes such as grain or timber drying.
While the advanced EFCC and EFHAT systems are still being developed for medium to large scale coal fired power plants, simple micro-scale systems for solid biomass have recently become commercially available. The emphasis of this dissertation is on the development and testing of an externally fired micro gas turbine (EFMGT) linked with a SFBC reactor capable of utilizing readily available agricultural and forestry biomass residues.

3.1   Externally Fired Combined Cycle

The EFCC system is an externally fired gas turbine integrated with a bottoming steam turbine as shown in Figure 3.1a) and b).

---

[1] A hot turbine working fluid before the compressor in a closed cycle system leads to a low compressor efficiency due to the increased volume of the hot fluid.
[2] The EFHAT is also known as the externally fired evaporative gas turbine (EF-EvGT)
[3] Topping refers to supplementary firing, i.e. with natural gas, after the heat exchanger to achieve higher turbine inlet temperatures.
[4] Bottoming refers to the implementation of a steam cycle after the gas turbine such as in an EFCC plant.
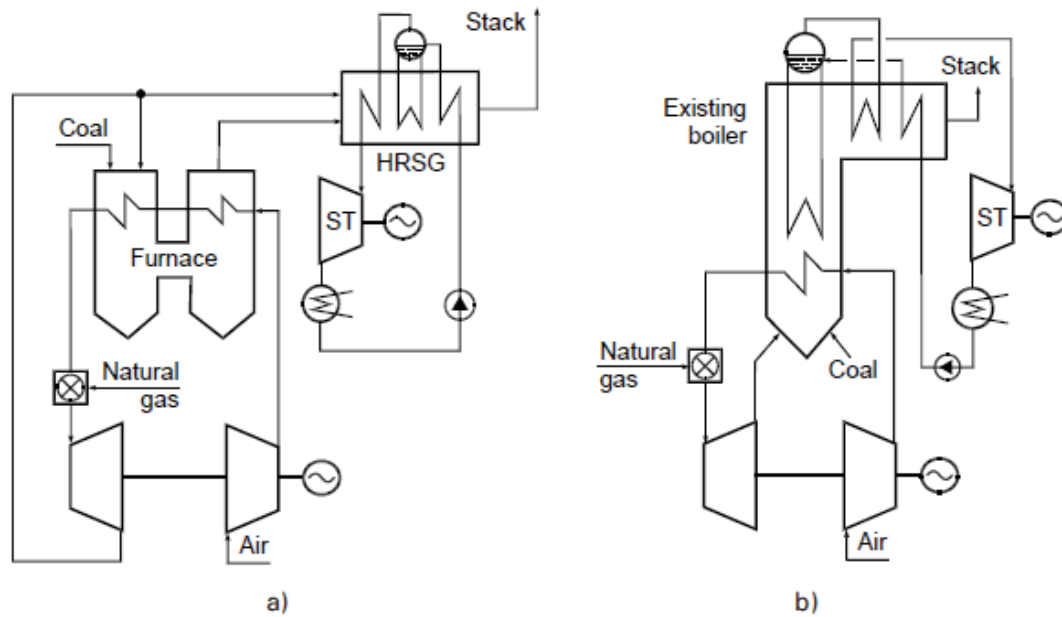
Fig. 3.1: a) Externally fired combined cycle power plant   b) Externally fired repowering

Figure 3.1 shows the typical large scale coal fired EFCC configuration for a new plant a) and a repowering project b) (Korobitsyn 1998). Low turbine inlet temperatures (TIT's), due to heat exchanger temperature restrictions, can be improved through the use of topping combustion with natural gas (Marroyen et al.1999). Topping combustion can increase the TIT to those appropriate for modern gas turbines and can also assist the plant start up and temperature control.

Topping combustion can also be performed with gas generated by biomass gasification or pyrolysis. The use of biomass gasification to generate the fuel gas for the topping cycle, as shown in Figure 3.2, decreases fuel costs, but increases the investment costs and plant complexity.
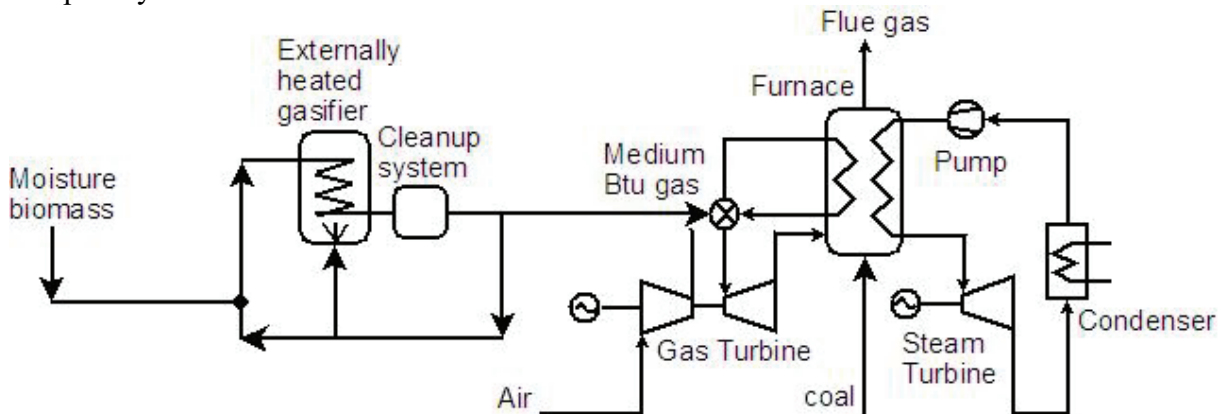
Fig. 3.2: EFCC with allothermal biomass steam gasification for topping combustion

Most of the recent externally fired gas turbine research work has been performed in America by Hague International, Foster Wheeler, United Technologies, Babcock and Wilcox and Westinghouse with funding from the US Department of Energy (DOE) within the framework of the "Clean Coal" programme.

Further information on large scale EFCCs (Huang and Naumowicz 1992, Foster-Pegg 1993 Agarwal and Frey 1995, Jahraus and Dieckmann 1995, Klara et al. 1996, Frey and Agarwal 1996, Agarwal 1997, Ferreira and Pilidis 2001, Ferreira et al. 2003, Hurley et. al. 2003 and Savola 2005) and the externally fired humid air turbine (Yan et al. 1994, Yan 1998,

Marroyen et al.1999, Yan and Eidensten 2000, Maunsbach et al. 2001, Wolf et al. 2002) is available in the respective literature.

The HIPPS, HITAF and REACH systems described in the literature represent the cutting edge research for large scale coal fired EFGTs. For small scale plants fluidized bed combustion is more appropriate as described by Foster-Pegg (1990). The research and demonstration emphasis has moved away from the dependency on high temperature ceramic heat exchangers and towards utilization of high temperature metallic alloys with topping combustion or a combination of metallic heat exchangers with more simple and robust convective ceramic air heaters.

For small scale lower temperature EFMGTs, such as proposed in this dissertation, it is therefore feasible to rely on metallic heat exchangers.

Pyrolysis gas topping combustion, such as in Foster Wheeler's HIPPS concept, is complicated due to the necessary particle cleanup, and may cause turbine blade damage or fouling and is thus unsuitable for small scale applications.

The utilization of a ceramic radiant air heater and convective flue gas air heater such as in United Technology's HITAF concept may also have merit for biomass furnaces, but for micro gas turbines the air preheating is accomplished much more elegantly by recuperation of the hot exhaust air from the turbine, which also rules out any problems with slagging or fouling.

Externally fired combined cycles and humidified gas turbines are not considered techno-economically relevant for micro gas turbine applications due to the high investment and operation costs.

Up until recently the driving force for the development of the externally fired gas turbine cycle has almost exclusively been its utilization in coal fired power plants. However, despite dedicated long-term research and development programmes a successful design has not yet materialized. This is due to the high costs and limited durability of the heat exchanger material in the presence of corrosive gases and the problems caused by heat exchanger fouling (Elmegaard et al. 2003).

3.2   Summary and Recommendations

The large majority of research work has been performed on large scale coal fuelled EFCC and EFHAT cycles, but due mainly to problems with the high temperature heat exchanger, commercial plants have not yet been developed.

Historically the only successful EFGT plants have utilized high temperature metallic heat exchangers, but due to low turbine inlet temperatures the efficiency of these plants was too low to be competitive.

Higher efficiencies are achievable with complex combined cycles utilizing ceramic heat exchangers and supplementary firing, but due to high construction and operation costs, and low reliability of the heat exchangers, this is at present not economically feasible.

The utilization of solid biomass in large scale externally fired cycles is largely unknown; it can be assumed that the necessary low combustion temperatures and the susceptibility of biomass to slagging and fouling make solid biomass unsuitable.

The externally fired micro gas turbine cycle is better suited for employment of biomass fuels due to the lower turbine inlet temperatures, which makes the utilization of reliable metallic heat exchangers possible.

4   Biomass Externally Fired Gas Turbines

Up until recently little work had been done on solid biofuelled externally fired gas turbine cycles. A theoretical assessment of large scale biomass EFGTs (20 to 100 MW) by Eidensten et al. (1996) came to the conclusion that utilizing a circulating fluidized bed (CFB) boiler results in a higher total efficiency and electrical efficiency than systems with grate fired boilers, however a top-fired[1] gas turbine was necessary because of the limitation of the bed temperature.

Possibilities for improving the efficiency of a biomass externally fired gas turbine (BEFGT) have also been assessed by Elmegaard et al. (2003).

4.1   Biomass Combustion Problematic

The physical composition of biomass fuels necessitates low combustion temperatures to avoid the ash softening and causing excessive slagging and fouling of heat exchangers (s. Fig. 4.1).
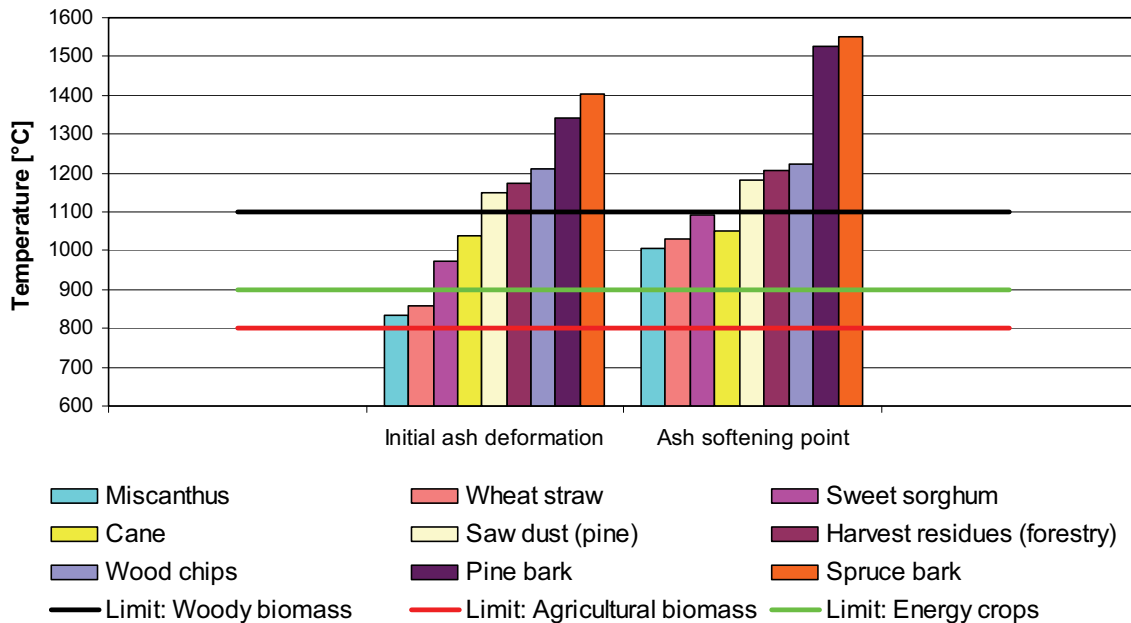
Fig. 4.1: Combustion temperature limits for selected biomass fuels

Figure 4.1 presents the experimental results of ash fusion behaviour of 10 biomass fuels under standard[2] laboratory conditions reported by Wilen et al. (1996).

The observed detrimental ash behaviour (slagging and fouling) during gasification tests in a fluidized bed commenced at a substantially lower temperature than the ash fusion temperature (sintering) measured under standard laboratory conditions (Wilen et al.1996). On the other hand a good correlation between detrimental ash behaviour and the sintering temperatures in a laboratory scale fluidized bed was observed.

This has been confirmed by stationary fluidized bed combustion tests at the University of Rostock, Chair of Environmental Technology, where sintering was observed for temperatures as low as 800°C for difficult agricultural biomass such as cereal straw (Steinbrecht 2006 b).

An explanation for this anomaly is that interactions between the silicon sand (SiO_2) of the fluidized bed and the alkali content (especially potassium) in the biomass fuel, lead to the

---

[1] Topping combustion increases the turbine inlet temperature (TIT).
[2] ASTM, ISO, oxidizing atmosphere

formation of eutectic[3] mixtures, which become sticky at temperatures well below the melting temperature of the biomass fuel, and cause the bed material to agglomerate with the ash at lower temperatures.

It is recommended here that the maximal bed temperature for the SFBC combustion of biomass fuels should not exceed the initial ash deformation temperature measured under standard laboratory conditions (s. Fig. 4.1).

The biomass fuels presented in Figure 4.1 can be divided into three main grades based on their initial ash deformation temperature. Essentially this classification reflects the biomass origins.

1   Woody biomass, suitable for combustion temperatures up to 1100°C:
        wood chips, sawdust, forest residues

2   Energy crops suitable for combustion temperatures up to 900°C:
        sweet sorghum and cane

3   Agricultural biomass suitable for combustion temperatures under 800°C:
        barley straw, wheat straw and Miscanthus

This is a generalised subdivision, for orientation only. Until a sufficient databank of combustion characteristics of biomass fuels in the SFBC reactor is available the ash fusion behaviour of each new fuel stock will be indispensable to determine the maximum allowable combustion temperature.

Due to the tightening market situation for woody biomass and the socio-economical difficulties associated with the wide scale cultivation of dedicated biomass crops, the emphasis of this research work is placed on the utilization of agricultural harvest residues such as straw.

- **For straw combustion temperatures of under 800°C are required.**

The difficulties caused by ash fusion and sintering during straw combustion are well known. These difficulties are generally associated with the high alkali content of the fuel. However no direct interdependence between biomass ash fusion temperature and the alkali content was found by the Technical Research Centre of Finland (VTT) in a study of 16 biomass feedstocks. Conversely a correlation between increasing silicon content and decreasing initial ash fusion temperature was observed (Wilen et al. 1996).

Table: 4.1 Chemical analyses of selected biomass properties in wt% (moisture free)

	Wt% (mf)			Trace components ppm-wt (mf)								
	N	Cl	S	Al	Ca	Fe	K	Mg	Na	P	Si	Ti
Demolition wood	1.1	0.10	0.09	469	3479	340	728	399	650	141	1135	985
Willow	0.2	0.01	0.03	19	3899	30	1421	378	127	651	69	14
Straw	0.9	1.28	0.29	5883	8531	3351	21561	3674	3230	1177	29857	199

(Data source ECN 2004)

The striking difference in the composition of straw in comparison to other biomass fuels (s. Tab. 4.1) is the very high silicon (Si) and alkali (Na, Mg, Ca, K) content. The alkali metals, especially potassium (K), become sticky at low temperatures causing the silicon to clump and

---

[3] low melting temperature mixtures

induce slagging and fouling at low temperatures. This suggests that the main difficulty is associated with the combination of high silicon (Si) and potassium (K) content in straw. Straw is also problematic due to its low calorific value, high chlorine and high sulphur content. The high chlorine and sulphur content increases the risk of high temperature heat exchanger corrosion.

This makes residual agricultural biomass difficult to utilize for energetic purposes with conventional boiler technology. Small scale fluidized bed technology on the other hand is ideally suited for problematic biomass fuels such as straw due to the low combustion temperature which decreases the danger of slagging, and the abrasive action of the fluidized bed which inhibits fouling.

The low temperature fluidized bed combustion also has the advantage that it allows primary "in-situ" emissions reductions measures to be exploited. Through the addition of calcium carbonate ($CaCO_3$), usually in the form of limestone, to the fluidized bed, sulphur dioxide (SO_2) can be bound in the form of gypsum (calcium sulphate $CaSO_4$) as shown in Equation [4-1]. This reaction is temperature dependant and runs retrograde re-releasing SO_2 at temperatures of over 900°C.

$$CaCO_3 + SO_2 + \tfrac{1}{2}\,O_2 \Leftrightarrow CaSO_4 + CO_2 \qquad\qquad [4\text{-}1]$$

The high chloride content in the straw fuel can also be bound by the addition of limestone to the fluidized bed as shown in equation [4-2].

$$CaCO_3 + Cl_2 \Leftrightarrow CaCl_2 + CO_2 + \tfrac{1}{2}\,O_2 \qquad\qquad [4\text{-}2]$$
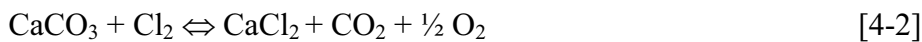
Similarly at temperatures of over 890°C this reaction runs retrograde, re-releasing the chloride (Steinbrecht 2006b). The situation is complicated by the presence of both sulphur and chloride in the fluidized bed because the sulphur dioxide can react with the already formed calcium chloride ($CaCl_2$) to form calcium sulphate ($CaSO_4$) and re-release the chloride (Cl_2). Chloride binding in the fluidized bed reactor is the topic of ongoing research work by professor Steinbrecht at the University of Rostock, Chair of Environmental Technology.

4.2   Supplementary Firing

Small scale EFMGTs must rely on simple means to improve overall efficiency, so that investment costs are kept to a minimum.

Theoretically efficiency can be increased by humidification or steam injection before the turbine, as in the humid air turbine (HAT) and steam injected gas turbine (STIGT) cycles (Lazzaretto and Segato 2001a, b, Agren et al. 2002, Wolf et al. 2002, Janson and Yan 2005), but these processes all increase the complexity and costs of the EFGT plant and are therefore not appropriate for microturbine based applications of under 1 MW and will not be discussed here in detail.

Supplementary firing is the simplest method to obtain higher turbine inlet temperatures and increase thermal efficiency without causing slagging or fouling of the heat exchanger. Biomass externally fired gas turbines can employ supplementary firing[4] after the heat exchanger as shown in Figure 4.2. The advantage of supplementary firing is the possibility to utilize low grade biomass fuel for low temperature combustion and gas for high temperature supplementary firing to increase the turbine inlet temperature and thus the cycle efficiency.

---

[4] also known as topping combustion
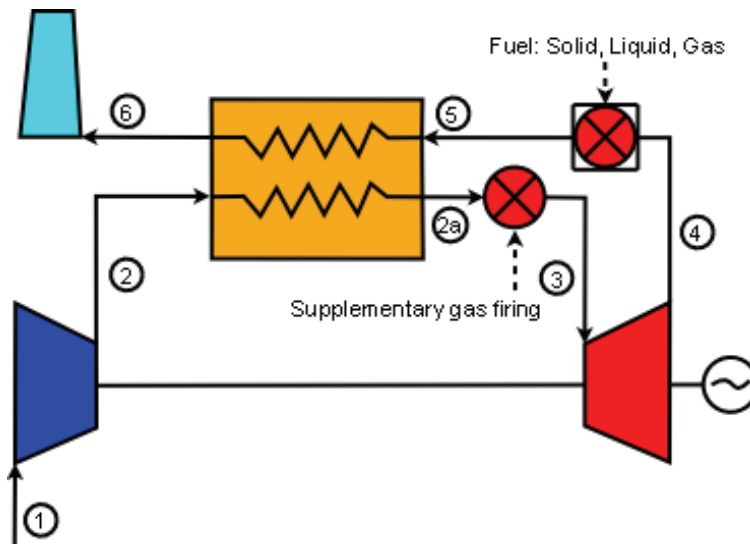
Fig. 4.2: Flow sheet of a biomass EFGT with supplementary firing

The EFGT cycle with supplementary firing, as shown in Figure 4.2, relies on a heat exchanger to transfer the combustion enthalpy (5-6) to a clean compressed air stream (2-2a) which is then further heated by supplementary gas firing (2a-3) before being expanded (3-4) over the gas turbine. The hot exhaust gases (4) from the gas turbine still contain enough oxygen[5] to allow utilization as combustion air in the solid fuel boiler. The hot flue gases (5) are cooled in the heat exchanger (5-6), heating the compressed air stream. The cooled exhaust gases (6) are released over the stack.

Supplementary firing can be based on natural gas, biogas or pyrolysis gas. The use of pyrolysis gas coming from two stage biomass conversion plants, allows the plant to run on 100% biomass, but its technical feasibility is questionable. Particularly technical problems with the pyrolysis reactor, condensation of the pyrolysis gases[6], and fouling of the heat exchanger with the high ash char[7] can be expected.

Supplementary firing with natural gas or biogas is technically much simpler, but causes higher operation costs due to the more expensive fuel. Supplementary natural gas firing is implemented in most large scale EFGT plants not utilizing ceramic heat exchangers. Some smaller scale plants such as the 500 kWe Vrije University Brussels (VUB) (s. Ch. 4.3.5), and also the VUB EFMGT (s. Ch. 5.1.1) also utilize natural gas for supplementary firing.

4.3   Research and Demonstration Projects

4.3.1   Biomass EFGT with Circulating Fluidized Bed

A theoretical investigation of medium scale heat and power production (8 MW fuel input) based on an externally fired gas turbine in combination with a biomass fuelled, atmospheric circulating fluidized bed (ACFB) furnace was performed by Anheden et al. (1999) from the Swedish Royal Institute of Technology in Stockholm.

---

[5] The combustion air ratio λ is typically around 6.5.

[6] Pyrolysis gases consist of condensable and permanent gas components. To avoid condensation of pyrolysis oil the pyrolysis gas must be kept at high temperature.

[7] The pyrolysis reaction reduces the volatiles content and respectively increases the inert (ash) and carbon contents of the fuel. For example a straw char can contain up to 50 wt% ash.

This conception foresees a conventional flue gas heat exchanger, in which the working fluid is heated to 550°C, followed by a metallic external bed heat exchanger (EBHX), designed to heat the working fluid to 800°C, with heat exchanger tubes immersed horizontally[8] in the bubbling bed to attain maximum hot-side heat transfer coefficients of up to 500 W/m²K. A maximum electrical efficiency of 33-38% is predicted when utilizing a cycle with two stage compression and inter-cooling[9] as presented in Figure 4.3.

1. Flue gas condenser
2. District heat
3. External bed heat exchanger (EBHX)
4. Flue gas heat exchanger (FGHX)

5. First-level intercooler (IC1)
6. Second-level intercooler (IC2)
7. Cooling water
8. First-level postcooler (PC1)
9. Second-level postcooler (PC2)
10. Flue gas condensate
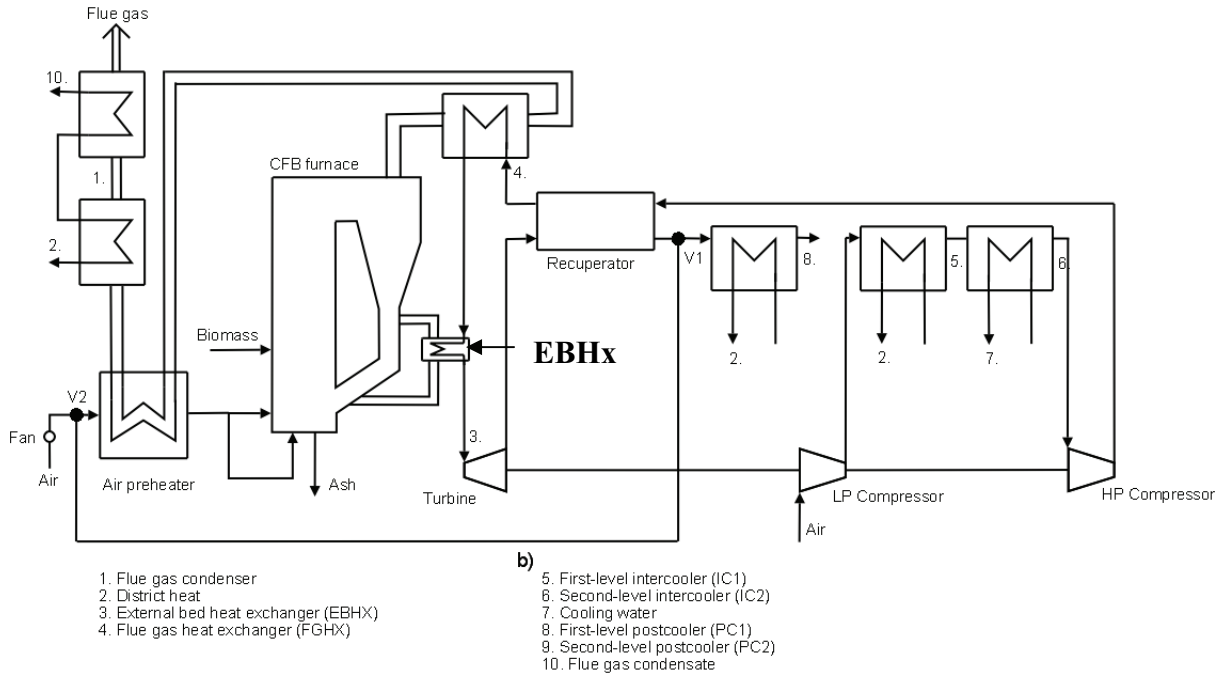
Fig. 4.3: Biomass fuelled atmospheric CFB with external bed heat exchanger (Anheden1999)

The main advantage of the system concept with EBHx is that it benefits from the high heat transfer coefficients in the fluidized bed to achieve high air temperatures despite relatively low combustion temperatures. The utilization of a fluidized bed heat exchanger ensures relatively high air temperatures (800°C) even with low combustion temperatures (850°C) due to the excellent heat transfer through particle convection within the fluidized bed.

This also allows the utilization of biomass fuels, which are characterized by low ash fusion temperatures. The biggest obstruction to the commercialization of EFGT cycles in this size range are the high specific investment costs caused by the plant complexity, and relatively low electrical efficiency. This technology will also be in competition with steam or ORC cycles which are technically and economically proven technologies for this generation capacity. It is suggested that the ideal size range for biomass fired EFGT technology lies under 1 MW_{th}.

4.3.2   Biomass EFGT with Fuel Dryer

Elmegaard et al. (2001, 2002) postulated that turbine inlet temperatures (TIT) as low as 700°C may still be interesting for externally fired micro gas turbines with a fuel dryer operating on wet biomass fuels as shown in Figure 4.4.

---

[8] This ensures the greatest particle impact, and therefore higher heat transfer coefficient.
[9] Intercooling increases the system efficiency by lowering the specific air volume seen by the compressor
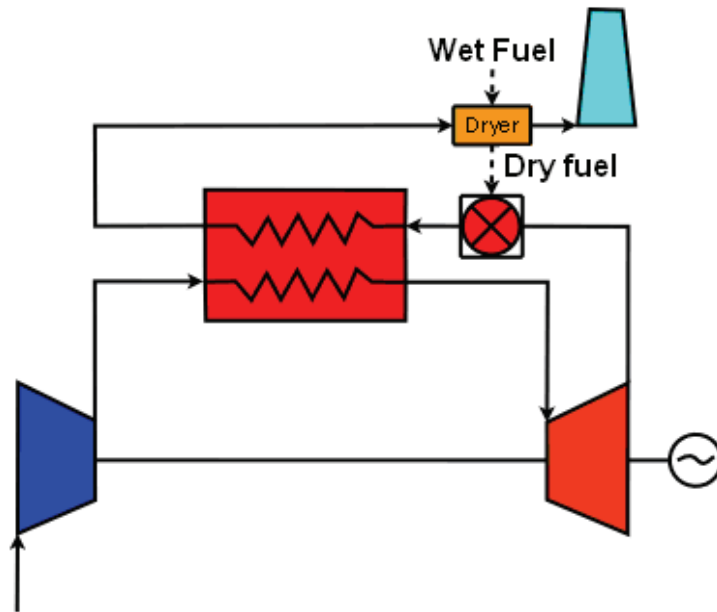
Fig. 4.4: Flow sheet of the wet EFGT cycle

By utilizing the turbine exhaust air to dry wet biomass fuels conversion efficiencies of over 60% can be reached by this plant configuration (Elmegaard and Qvale 2002). This is four times as high as the best competing technology in this size range. It is important to state that these Figures are based on the lower calorific values (LCV) of the fuel which in the case of very wet fuel are very low.

The higher the water content of the fuel the greater the advantage of the integrated dryer. The limitation on the moisture content of the fuel is reached when the temperature of the gas in the stack reaches the dew point, which occurred for fuels with > 83% water content (Elmegaard and Qvale 2002). In this case electrical efficiencies of 62.6% and 24.9% based on lower and higher heating values respectively were calculated (Elmegaard and Qvale 2002).

For biomass feedstocks with less than 55% water content such as most solid agricultural and forestry biomass residues, this system does not offer any great advantage. This is because the volumes of hot exhaust gases generated by the turbine are much higher than necessary to dry the biomass fuel.

Cocco et al. (2006) investigated a variation of this concept for residual agricultural and short rotation forestry (SRF) feedstocks. One of the primary drawbacks of biomass utilization, both residual or from SRF is their strong seasonal availability and low heating value when harvested. This is chiefly due to their high water content.

It is proposed that large amounts of biomass can be dried in summer when it is harvested, and in winter the turbine exhaust gases can be utilized for domestic heating purposes, while the previously dried biomass is combusted.

The integration of a biomass dryer has the potential to substantially increase the overall EFMGT plant efficiency, and help solve the excess heat utilization problematic.

4.3.3   Siebenlehn 2-2.3 MWe Biomass EFCC

The 10 MWth Siebenlehn plant owned and operated by the Department of Environment and Energy Technology (UET)[10] Technical University Freiberg in Germany utilizes a biomass fixed bed downdraft gasifier, a conventional metallic air heater, externally fired gas turbine

---

[10] Umwelt und Energietechnik

and a bottoming steam cycle. This plant is capable of generating 2-2.3 MWe with an efficiency of 23-27% (Bram 2005). There is very little published plant operation data available and the economic prospects of this combination of technology (gasification, combustion, metallic heat exchanger and steam turbine bottoming cycle) are not good.
It is questionable if the gasification of biomass and combustion of the gas is thermodynamically or economically rational unless performed as a topping cycle in large scale systems as proposed by Westinghouse and Foster-Wheeler (Yan 2000), or as allothermal biomass Heatpipe Reformer as demonstrated by Karl (Karl et al. 2004).

4.3.4   AFBC Externally Fired Humid Air Turbine Cycle

In 1994 the Energy and Environmental Research Corporation (EER) presented a consortium project which developed and completed pilot plant tests on a 1.5 MWe atmospheric fluidized bed combustion (AFBC) system combined with a humid air turbine. The AFBC-EFHAT plant was intended to run on a mix of agricultural and forestry residues and coal or waste oil. This system was designed to utilize an air humidifier and external flue gas heat exchanger. The hot turbine exhaust gas is utilized as fluidization and combustion air for the AFBC. Limestone can be added to the fluidized bed to capture sulphur. Based on the plant description, a theoretical efficiency of 25% was calculated by Ashworth et al. (1994). AFBC systems designed to generate from 25 kWe to 75 kWe are also discussed. These small plants would utilize a simpler AFBC system with annular heat exchanger around the fluidized bed combustion zone. Data on the AFBC combustion is reported, but no data concerning the flue gas heat exchanger or gas turbine operation is supplied. It is probable that the low air temperatures achieved in the flue gas heat exchanger resulted in very low turbine efficiencies.

4.3.5   Vrije University Brussels 500 kWe Biomass EFHAT

The Vrije University of Brussels (VUB) constructed and operated a 500 kWe demonstration[11] EFHAT plant (s. Fig. 4.5) in the period 1994-2001 (Bram et al. 2005, Savola et al. 2005).
The plant was based on a 600 kWe Volvo VT600 gas turbine with a design air mass flow rate of 3.5 kg/s at a pressure ratio of 8.5 bar and included an atmospheric bubbling fluidized bed gasifier, natural gas combustor and a metallic heat exchanger followed by water/steam injection and a hot water generation systems.

To increase the cycle efficiency both water injection after the compressor and topping combustion were foreseen, but due to budget restrictions the topping combustion was not implemented (Bram et al. 2005). Combustion of at least 20% natural gas together with the producer gas was included for control purposes and to ensure flame stability. The costs of the large metallic HTHx were kept under 10% of the total plant costs[12] by using commercially available metallic components. The metallic HTHx[13] had a maximum temperature of 850°C. The theoretical electrical efficiency of this plant was 24% (Bram et al. 2005).
The high operation costs caused by the natural gas fuel and water preparation have led to low economic perspectives for this plant, and operation was discontinued in 2001. The Vrije University Brussels initiated a new project with better economic perspectives based on an externally fired micro gas turbine (EFMGT) in 2003.

---

[11] Thermie project BM/00367/92/BE
[12] The total project costs were 2.7 M€. The costs for a 2.5MWe plant are estimated at 5 M€.
[13] The leading tubes were constructed from Haynes steel 120 alloy Ni-3Co-33Fe-25Cr-2.5Mo-2.5W, followed by finned tubes made of Hastelloy 800 HT and Avesta 253MA.
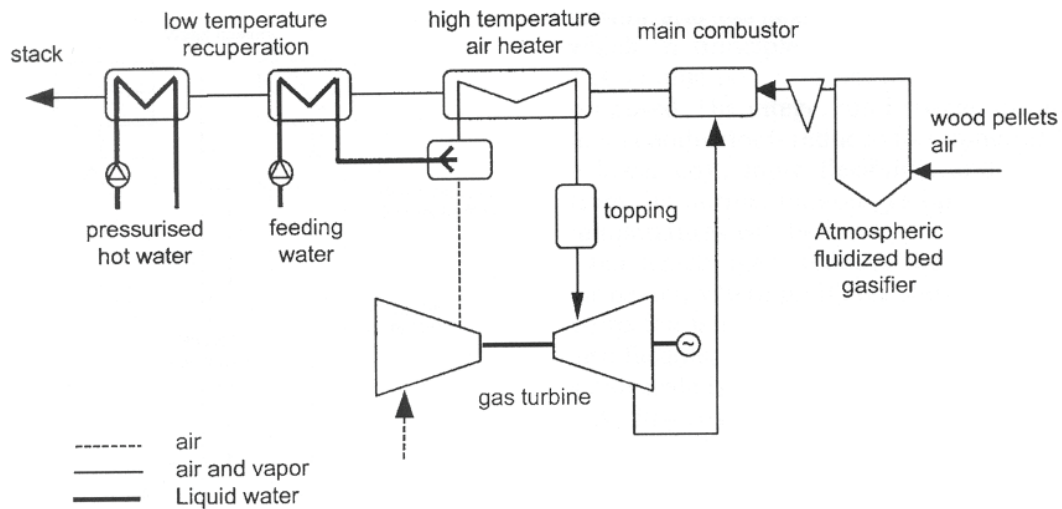
Fig. 4.5: EFHAT plant layout Vrije University Brussels (Bram et al. 2005)

Once again the low economic prospects of complex externally fired systems with gasification and/or supplementary firing are demonstrated. The dilemma is that the more complex the plant becomes, the larger it must to be to reduce the specific investment costs (€/kWe), and the more efficient it must be to be competitive with other available technologies. Downscaling on the other hand, as recognized by the VUB, allows the application of cost-effective simple robust plant designs based on MGT technology.

4.4   Summary and Recommendations

Biomass combustion temperatures are strongly dependent on the biomass quality: for agricultural biomass residues, temperatures of 750-850°C are relevant while for forestry residues temperatures between 1100-1400°C are possible.

Fluidized bed combustion is the best available technology for the utilization of problematic biomass feedstocks such as agricultural residues.

A recuperated gas turbine combined with a SFBC in-bed heat exchanger offers an elegant optimization between high TIT and low biomass combustion temperatures.

Supplementary firing with natural gas leads to high operation cost and should, in light of increasing gas costs, be avoided.

Complex gas turbine cycles such as combined cycles (CC) steam injected or humidified gas turbine (STIG, HAT) or integrated biomass gasification have not proven to be cost effective for biomass externally fired gas turbines.

The combination of a wet biomass fuel with fluidized bed combustion, biomass dryer and in-bed heat exchanger for the operation of an externally fired micro gas turbine has outstanding economic and ecological prospects for small scale distributed electricity generation.

Externally fired micro gas turbines represent the ideal technology for the development of a cost-effective distributed electricity generation plant for residual biomass.

5   Externally Fired Micro Gas Turbines: State of the Art

In recent years the interest in utilizing micro gas turbine technology for biomass externally fired processes has increased. This has resulted in several research and demonstration projects and one commercially available EFMGT plant.

5.1   EFMGT Research and Demonstration Projects

5.1.1   Vrije University of Brussels EFMGT

With the support of the Belgian utility company Electrabel and the Flemish Government Vrije University of Brussels initiated a new EFMGT project in 2003. The aim of this project was to reduce equipment and operating costs, by use of a simple solid biomass combustion rather than gasification as in their previous research plant, and by applying available low cost MGT turbo machinery. The plant configuration is shown in Figure 5.1.
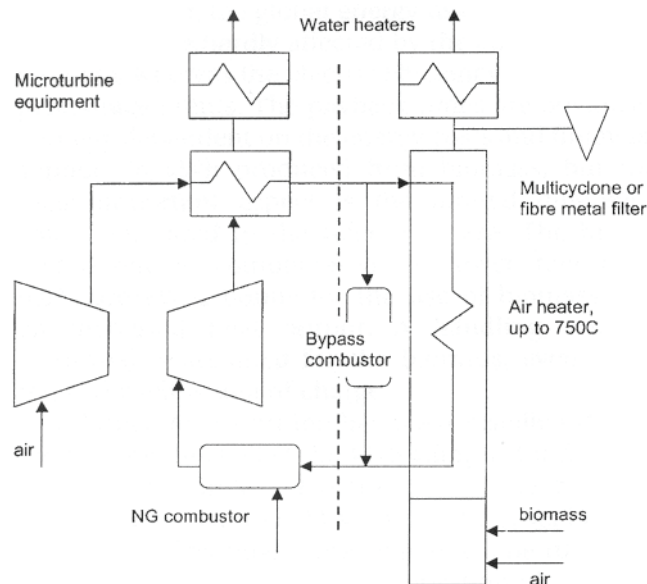
Fig. 5.1: Plant layout VUB EFMGT (Bram et al. 2005)

The EFMGT as shown above is planned to work on a combination of biomass (60%) with natural gas (40%) topping combustion to increase the TIT. Low temperature biomass combustion was necessary to avoid slagging and fouling of the metallic heat exchanger.
The integration of the natural gas topping combustion increases control flexibility and ensures high turbine inlet temperatures (TITs) in combination with a low cost metallic heat exchanger, but also incurs high operation costs, especially with increasing gas prices.
Another disadvantage of this arrangement is that the system is heavily reliant on heat (hot water) production but this also allows the integration between the turbine and biomass combustor to be reduced to a minimum, which increases operation flexibility.
The metallic heat exchanger is designed for flue gas temperatures of around 750°C and so can be constructed from available metallic materials. A Turbec (T100) MGT has been installed at the VUB campus for the purposes of the planned project, but will be run in its standard configuration on natural gas (NG) for the duration of the warranty before incorporation of a biomass combustor (Bram et al. 2005).

5.1.2   University of Genoa EFMGT with Two Stage Heat Exchanger

The University of Genoa, Thermochemical Power Group and Ansaldo Ricerche (ARI) have developed an EFMGT test rig based on the Elliot Energy Systems TA-80R micro gas turbine[1] (Traverso et al. 2003). The test rig which produces 50 kWe with a theoretical electrical efficiency of 16% has been installed at the ARI laboratories in 2003 (s. Fig. 5.2).
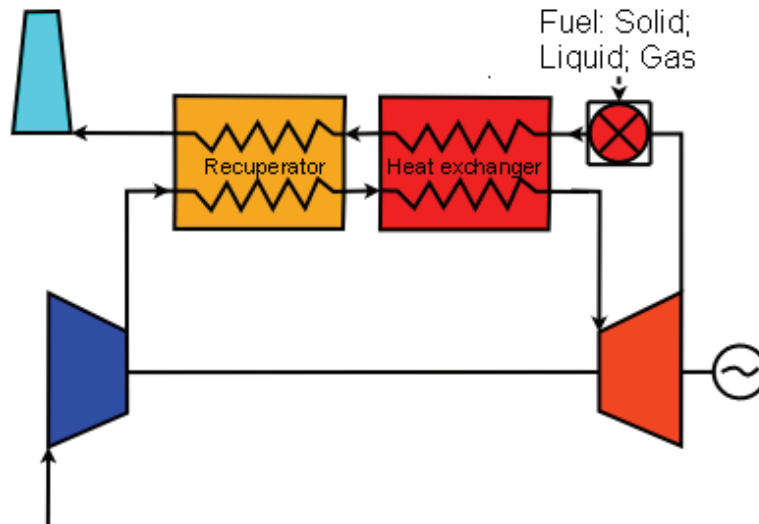
Fig. 5.2: University of Genoa EFMGT plant layout

The heat exchanger is divided into a high temperature metallic plate-box heat exchanger of large dimensions (1500 kg) and high cost (provided by fbmICOSS srl, Italy) for a maximum flue gas temperature of 800°C and a much smaller (120 kg) conventional MGT recuperator designed for flue gas temperatures lower than 650°C (Traverso et al. 2006).
This resulted in a turbine inlet temperature (TIT) of around 750°C which is 200°C lower than the optimum temperature for the MGT. It is planned to exchange the metallic HTHx for a ceramic HTHx – which will enable the optimal TIT of 900-950°C – when this technology becomes commercially available. At present the internal MGT combustion chamber (not shown in Fig. 5.2) is utilized as a topping combustor.
The main advantage of this system is the parallel utilization of a low temperature recuperator and a high temperature heat exchanger. This allows the existing MGT recuperator to be employed for lower temperatures, which makes a decrease in the size of the expensive high temperature heat exchanger possible.
The basic limitations and problems with this demo plant are related to thermal stresses and fouling in the HTHx (Savola et al. 2005).

The principle of this plant with the MGT recuperator and high temperature heat exchanger is similar to the proposed configuration at the University of Rostock, except that the fluidized bed combustion system with integrated heat exchanger is more than a factor 10 smaller (<100 kg) and in combination with the MGT recuperator is expected to deliver higher turbine inlet temperatures (≈800°C) due to the excellent heat transfer capacity in the fluidized bed reactor.

---

[1] The natural gas fired Elliot TA 80R recuperated MGT normally generates 80 kWe with 28% efficiency.

5.1.3   Technical University Munich and ZAE Bayern[2] EFMGT

The development of a high temperature heat exchanger for an indirectly biomass fired gas turbine process was the subject of a collaborated research project by the Bavarian Center for Applied Energy Research (ZAE Bayern) and the Technical University of Munich, supported by the state government of Bavaria[3].

The project goal was to assess tube bundles with structured surfaces, such as described by Kautz (2005), to increase the internal heat transfer coefficient of a furnace integrated high temperature heat exchanger on the basis of a fluidized bed combustor as shown in Figure 5.3.
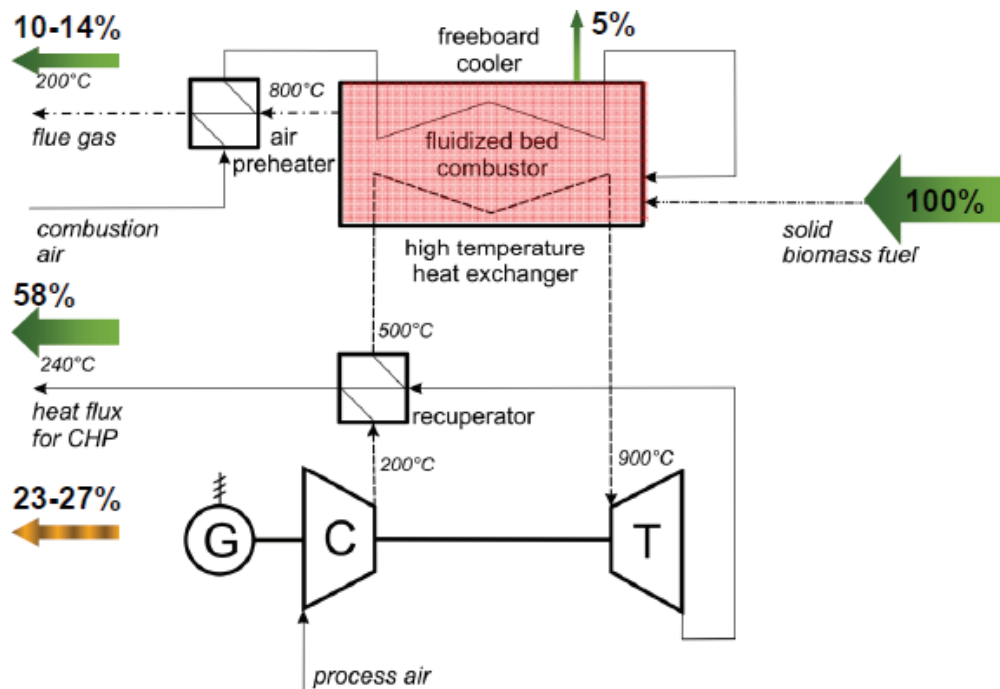
Fig. 5.3: Technical University Munich and ZAE Bayern EFMGT (Gallmetzer et al. 2008)

The first results of this research work from May 2008[4] verified that enhanced heat transfer coefficients can be obtained with structured tube surfaces in the immersed fluidized bed heat exchanger.

The increase in the heat conductance of indented tubes is a well known phenomenon resulting from the increased heat exchanger area and increased convection intensity through unstable eddy induction. The dimple geometry and the fluid Reynolds number determine the eddy form, which is the critical factor for heat transfer, but also for the pressure drop. The efficiency of spherical or tear-shaped indentations (dents or dimples) for this purpose has been described in the literature by many authors (Hassel et al. 2008).

However an increase in the heat transfer capacity also leads to an increase in pressure loss, which poses an elementary problem for the externally fired gas turbine cycle.

Although empirical equations for technical calculation of heat transfer on indented surfaces are available (Garvin 2001), theoretically the process is not yet fully understood.

Experimental results have revealed that the heat transfer in indented tubes can be increased by up to a factor 2.4 for the narrowest tubes with the ratios H/D[5] = 0.3 and T/D[6] = 0.2 for low Reynolds numbers (Hassel et al. 2008).

---

[2] Barvarian Center for Applied Energy Research
[3] Project Nr. 300-3400.00/05 IBG-HTW from July 2005 to December 2007
[4] 9th International Conference on Circulating Fluidized Beds 13-16th May 2008, Hamburg, Germany
[5] Tube diameter (H) / Dent diameter (D)
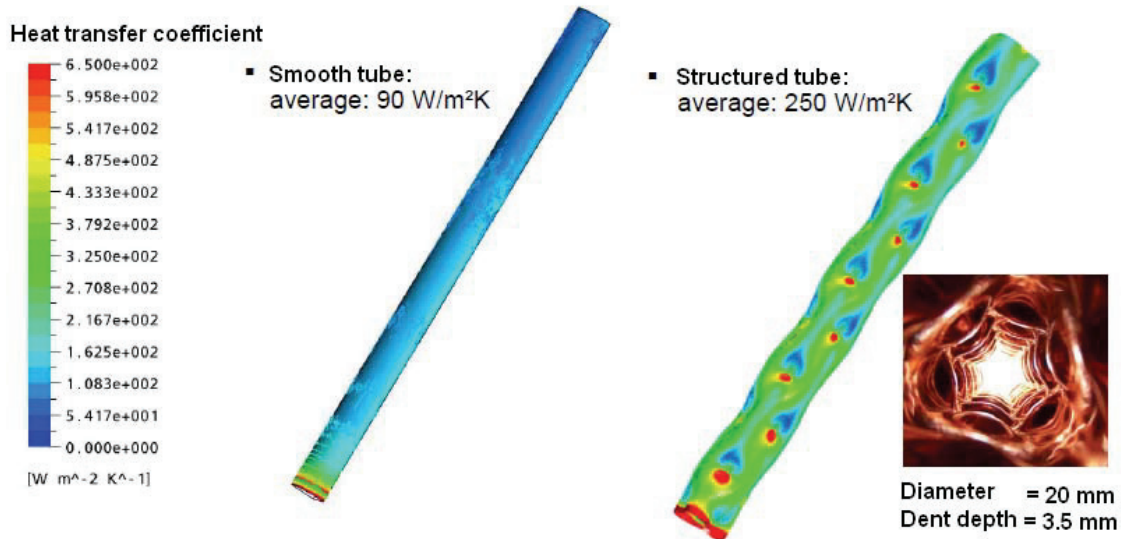
Fig. 5.4: Heat transfer coefficients for smooth and indented tubes (Gallmetzer et al. 2008)

In a comparison between smooth tubes, indented tubes and rilled tubes, the best results were obtained for indented tubes with an increase in the average heat transfer coefficient from 90 W/m²K (smooth tubes) to 250 W/m²K (indented tubes) as shown in Figure 5.4.

In the practical experiments by Gallmetzer et al. (2008) it was found that an indentation depth of at least 3.5 mm was necessary to significantly increase the performance of the tubes.

The performance evaluation takes the fundamental problem of increased pressure drop in the heat exchanger into account by assessing the relative increase in the pressure loss coefficient (ζ) with respect to the increase in Stanton number (ST). This can be calculated with the performance evaluation criterion (PEC) as described in equation [5-1] by Webb (Gallmetzer et al. 2008).

$$PEC = \frac{\left(\dfrac{ST_{structured\ tube}}{ST_{smooth\ tube}}\right)^3}{\dfrac{\zeta_{structured\ tube}}{\zeta_{smooth\ tube}}}\ [-]\quad ST = Nu\ /\ (\mathrm{Re} \times \mathrm{Pr}) \qquad [5\text{-}1]$$

Experimental results from Kautz (2005) on indented heat exchanger tubes registered a factor 6 increase in pressure drop in comparison to smooth tubes.

In the case of the SFBC-EFMGT this means that a structured surface may be unsuitable because one of the most critical criteria is to keep the pressure drop to a minimum.

5.1.4   Talbott's EFMGT Biomass Generator BG 100

In Europe Talbott's Heating Ltd. have developed the 80-100 kWe, 200 kWth Biomass Generator (BG 100), which is the only commercially available EFMGT on the market. Talbott's BG 100 plant was granted a patent[7] by the European Patent Office in 2004 (s. Fig. 5.5). The BG 100 plant, developed by Stafford (UK) based Talbott's Heating Ltd, utilizes a modified Bowman Power MGT[8].

---

[6] dent depth (T) / dent diameter (D)

[7] Patent EP 1 350 016 B1 granted on 03.11.2004, also available in German from Deutsches Patent- und Markenamt DE 601 06 976 T2 2005.12.01 (Talbott et al. 2004)

[8] The Bowman Power TG 50 MGT is based on the Elliot MGT.
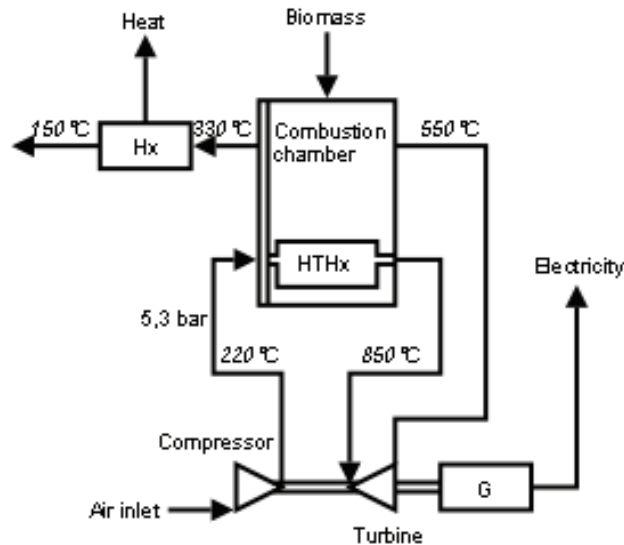
Fig. 5.5: Talbott's BG 100 EFMGT patent diagram

The BG 100, which was developed within the context of the New and Renewable Energy Programme of the Department of Trade and Industry (UK), is in the market release phase. In 2008 two reference BG 100 plants exist in England and one BG 100 ORC combined cycle plant is being constructed at Zurich Airport in Switzerland (Schmid and Gaegauf 2008).

The theoretical total electrical efficiency of the Talbott's test plant was calculated by Pritchard (2002) to be 17%, but to achieve this result a larger combustor and heat exchanger had to be constructed. Further improvement of this system design has led to the development of Talbott's commercially available Biomass Generator, BG 100, shown in Figure 5.6.
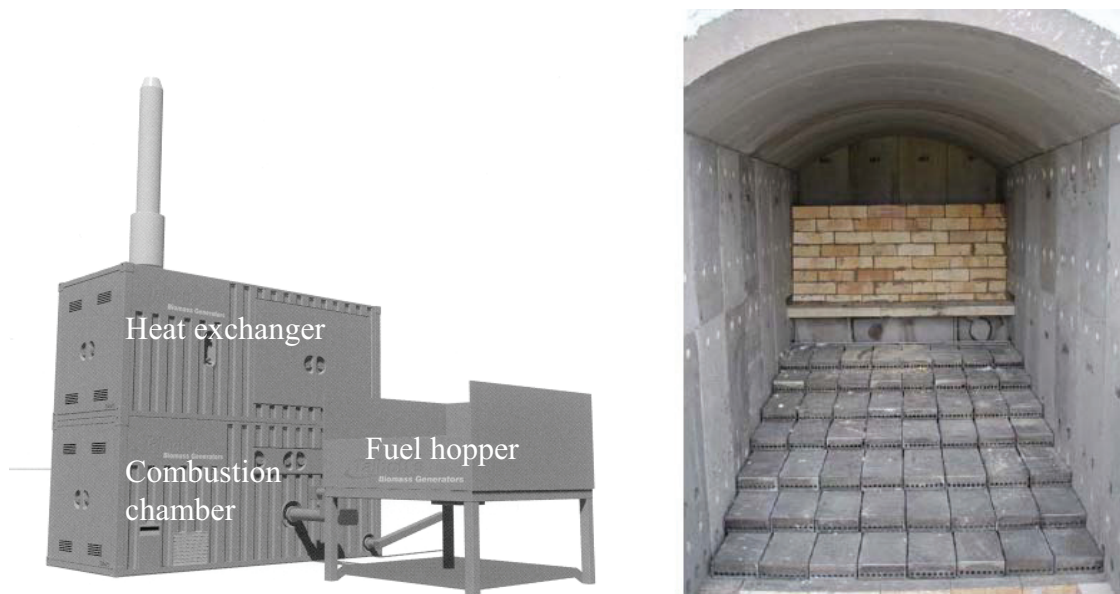
Fig. 5.6: Talbott's BG 100 EFMGT and combustion chamber (Talbott's brochure 2006)

The high temperature combustion chamber shown in Figure 5.6 is lined with ceramic refractory material.
The combustor fuel feed system consists of an agitator, rotary valve and transfer screw. The rotary valve regulates the fuel feed rate and must be manually adjusted depending on density and calorific value of the fuel.

Before the fuel enters the combustion chamber it is dried and preheated by slowly passing under the semi-conductive refractory ceramic step-grate.
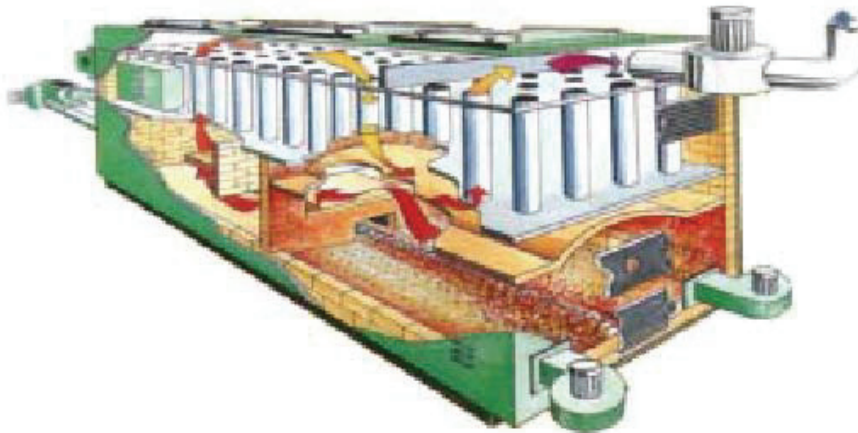
Fig. 5.7: Combustion chamber with heat exchanger (Pritchard 2002)

After the combustion chamber the flue gases are drawn under and over walls to reduce particulate carry over, and then around the outside of the multiple stainless steel alloy[9] tubes of the heat exchanger as shown in Figure 5.7. The air from the turbine compressor flows through the heat exchanger tubes. The heat exchanger with ceramic lined walls is designed for flue gas temperatures of around 1000°C. The compressed air enters the heat exchanger with about 200°C and 5.3 bar and leaves the heat exchanger with air temperatures of around 850°C.
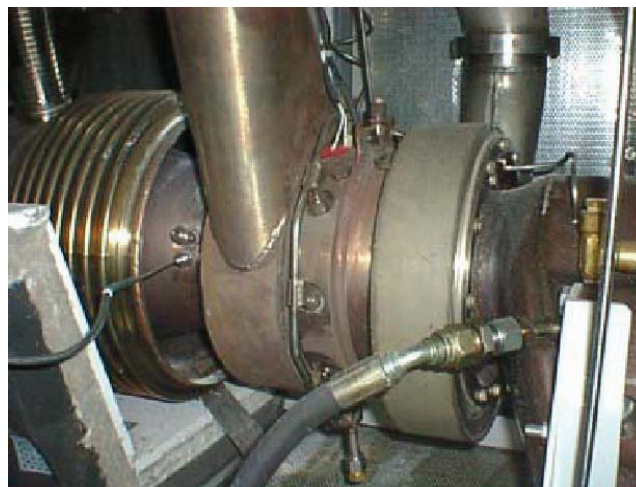
Fig. 5.8: Talbott's externally fired micro gas turbine (modified Bowman Power TG 50 MGT)

A Bowman Power TG 50 micro gas turbine was modified to function as an externally fired micro gas turbine as shown in Figure 5.8. The necessary modifications include:

- Compressor housing and ductwork
- Turbine housing and ductwork
- Removal and sealing of combustor liners and gas lines
- Turbine exhaust ductwork
- High temperature quick response temperature dump valve for over-speed protection
- New software for start-up and speed control

---

[9] The alloy is not further defined, but must operate at temperatures of up to 1000°C.

An assessment of Talbott's BG 100 illustrates the difficulties which need to be resolved for a solid biomass fuelled EFMGT:

1. The combustion temperature needs to be as high as possible to obtain sufficiently high turbine inlet temperatures but low enough to maintain fuel flexibility without danger of slagging and fouling.

2. High temperature flue gas heat exchangers are large and expensive.

3. To increase the cycle electrical efficiency to over 20% an integrated fuel drying system and recuperation of the turbine exhaust air to the combustion chamber as combustion air is necessary.

Talbott's have made a compromise between combustion temperature and fuel flexibility leading to a relatively good electrical efficiency (around 20%), and relatively high biomass feedstock quality requirements and very high heat exchanger costs to give a unit price of over 450 000 € (Pehn 2006b). The high cost of Talbott's BG 100 is the major hurdle to its widespread utilization for distributed electricity generation.

5.2   SFBC-EFMGT Plant Operation and Control

When a micro gas turbine cycle is modified into an externally fired micro gas turbine the large thermal inertia of the external combustion chamber and heat exchanger becomes the most influential parameter acting on the transient behaviour of the plant (Traverso et al. 2003, 2005). Problems arise with respect to the coupling of the long term response of the heat exchanger and the quick response of the turbine rotor with a suitable control system to protect the gas turbine from unstable behaviour.

At present it is difficult to obtain data on the main parameter settings in the control systems of micro gas turbines because this data is not published and the micro gas turbine manufacturers have tried to keep this data confidential (Traverso et al. 2003, Peters 2004).
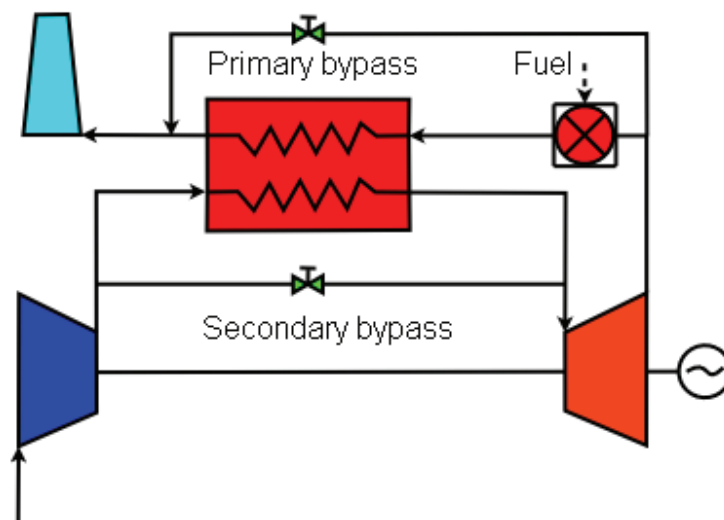
Fig. 5.9: Bypass controlling system for an EFGT plant

Figure 5.9 shows the EFGT control system proposed by Crosa (Crosa et al. 1998) from the

University of Genova, Institute for Mechanical Engineering and Energy Systems.
The power speed control of the gas turbine control system presented in Figure 5.9 is based on four parameters:

1. The fuel feed rate to the combustion chamber is parametrically controlled in relation to the turbine power demand. Due to the heat storage effects this has a very slow response and so the secondary by-pass is used for a faster process control.

2. The secondary bypass operates during transients[10]. When the power demand diminishes the secondary bypass valve opens as a function of the speed and power error reading by the gas turbine software regulated over a proportional-integral-derivative controller (PID) control loop as shown in Figure 5.10. If the power demand increases the fuel mass flow is increased and the secondary bypass closes.

3. The primary bypass is regulated to avoid thermal stress in the heat exchanger due to temperature peaks. The primary bypass is coupled with an exhaust temperature probe downstream of the combustion chamber and is also regulated over a PID control loop II as shown in Figure 5.10.

4. Varying the inlet guide vane angle (*VIGV*) of the compressor allows some control over the air mass flow and is a transient control mechanism which is not available for commercial micro gas turbines which have fixed angle compressor inlet guide vanes.
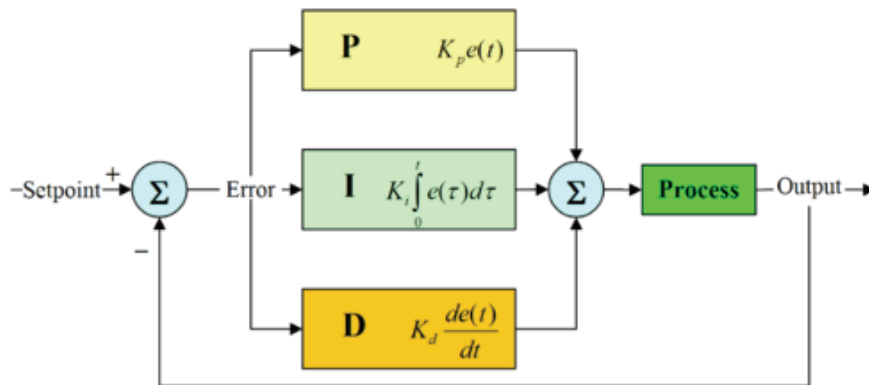
Fig. 5.10: Configuration of a proportional integral derivative controller

The proportional integral derivative controller (PID controller), is a generic feedback control loop mechanism which corrects the error between a measured process variable and the given set point as a function of three parameters:

1. Proportional value (P), which is the measured error (*e*) multiplied with the proportional gain factor (K_p).

2. Integral value (I) which is the sum of the magnitude and duration of a measured error, multiplied with the integral gain factor (K_i).

3. Derivative value (D), which is the rate of change of the process error multiplied with the derivative gain factor (K_d).

---

[10] Increase or decrease in power demand

By tuning the gain factors (K_p, K_i and K_d) to the relevant process, the PID controller enables a specific dynamic operation characteristic for the opening and closing of the respective valves. A control system, very similar to that described by Crosa et al. (1998), was employed by Traverso et al. (2003, 2005, 2006) for steady state and transient operation of their EFMGT test rig at the ARI lab in Genoa (s. Fig. 5.11).
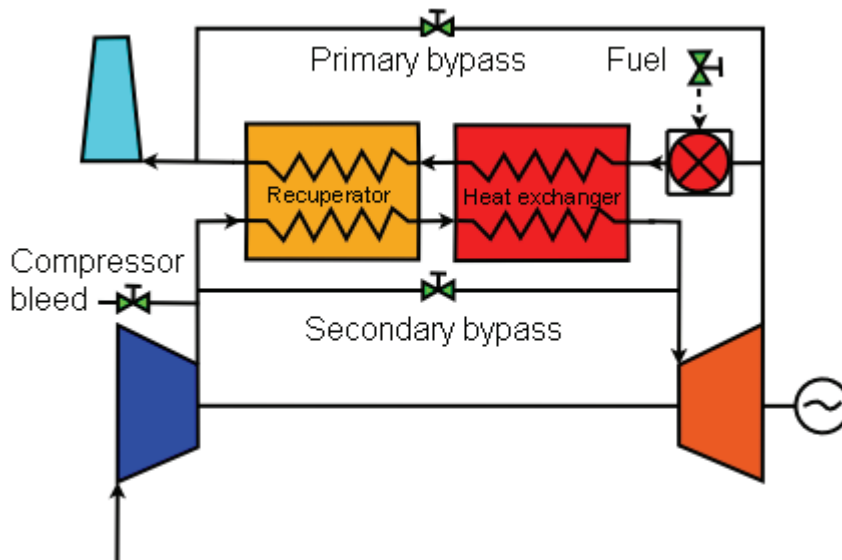
Fig. 5.11: EFMGT system with recuperator and heat exchanger

Four control strategies exist for the bypass valve system shown in Figure 5.11 (s. Tab. 5.2).

Table 5.2: EFMGT turbine control strategies (adapted from Traverso et al. 2003)

Type	Constant	Variable	secondary bypass setting
A	Turbine speed	CT*	5% open
B	CT*	Turbine speed	5% open
C	TET**	CT* and Turbine speed	5% open
D	Turbine speed and CT*	Fuel mass flow rate	Variable

*Combustion temperature **Turbine exit temperature

Normally a MGT is regulated by a constant speed control system where nominal speed can be manually set by the user (over the power demand), and the combustion temperature is regulated over a variable fuel flow rate (Type A), but with an EFMGT the thermal inertia of the system caused by the large fluid-dynamic capacitance of the heat exchanger and combustion chamber means that this will be ineffective as a fast response turbine control mechanism.
Simulation results by Travesco et al. (2003) revealed that for EFMGT systems the secondary bypass must remain fractionally (5%) open at all times to regulate fast load changes (s. Tab. 5.2). Type B and C control systems were found to be the most efficient regulation systems for EFMGTs.

The control system employed at the University of Rostock is similar to the system proposed by Crosa (1998) and employed by Traverso (2006).
The utilization of a fluidized bed reactor means that only the type B control system is possible because the fluidized bed temperature changes only very slowly and with a large time lag.

Thus a constant combustion temperature is appropriate. The turbine inlet temperature (TIT) is expected to remain relatively constant due to the constant combustion temperature.

In the EFMGT test rig configuration at the ARI lab in Genoa (s. Fig. 5.11) the opening of the secondary bypass can lead to a significant decrease in the cooling flow on the cold side of the heat exchangers. This situation is potentially dangerous for the recuperator (Traverso et al. 2005).

Placing the secondary bypass after the recuperator, as in the University of Rostock SFBC-EFMGT test bed (s. Fig. 5.12), has the advantage that the air mass flows on hot and cold sides of the recuperator are always equal, which avoids the risk of temperature peaks in the recuperator.

The basic layout of the University of Rostock SFBC-EFMGT test bed bypass system is shown in Figure 5.12.
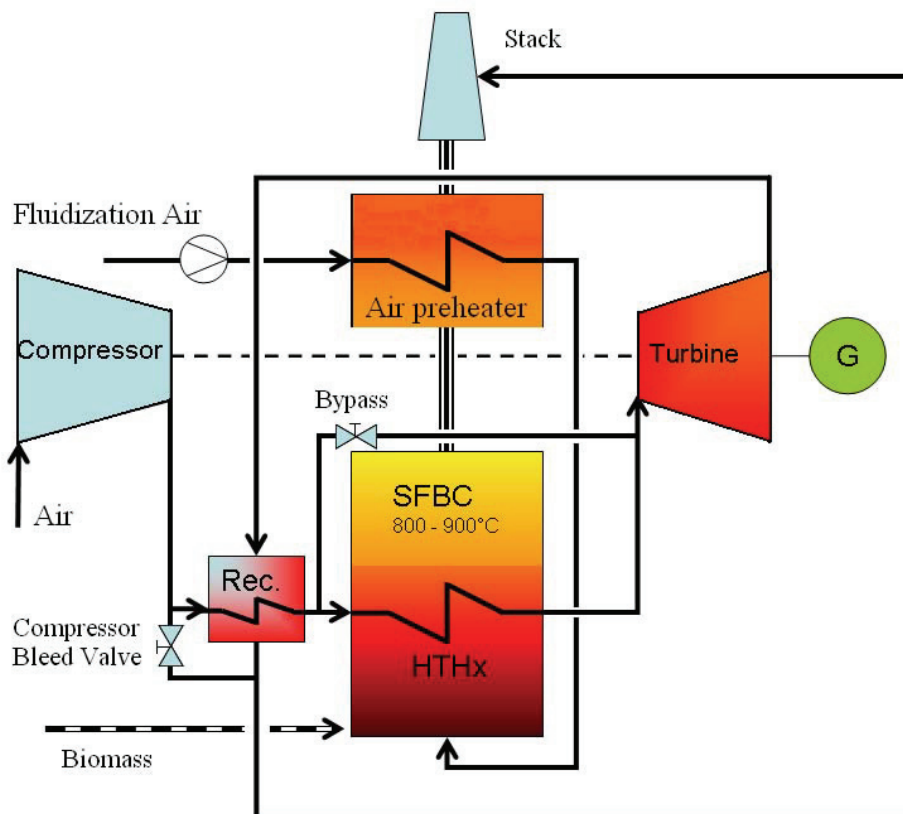
Fig. 5.12: University of Rostock SFBC-EFMGT test-bed bypass system layout

The compressor bleed valve was designed to reduce the pressure drop in the system during system start-up and shutdown and for automatic emergency shut-down in the case of turbine over speed or blackout[11].

The secondary bypass can also be used to reduce turbine inlet temperature to run at part load without altering the turbine speed. When increasing load the fuel flow rate to the SFBC reactor will also need to be increased to keep the combustion temperature constant.

The goal of the experimental operation of the SFBC-EFMGT test bed at the University of Rostock is the stable operation at one load point. Transient operation will be controlled by setting the turbine speed. The valve settings will be controlled manually.

---

[11] mains power cut

5.3   EFMGT Market Potential

In face of the global energy shortage and the aspiration to reduce greenhouse gases the general market for renewable energy is expected to increase strongly in the coming decades. Biofuelled externally fired gas turbines (BEFGTs) are recognized as a promising technology for the efficient low cost utilization of solid biomass fuels for power generation (Yan 1998). In Europe there is a growing commercial interest in the utilization of renewable biomass in small scale externally fired gas turbines for distributed rural electricity generation. The market potential is similar to biogas plants but on a smaller scale to enable the sought after "one farm[1]" energy solution.

Small scale distributed power plants can be built close to the biomass fuel source and therefore do not require the development of large transport or storage infrastructures. The market potential for biomass EFMGTs dependent on three major factors:

1   Availability and costs of biomass feedstocks;

2   Specific investment costs (€/kW) of installed electricity generation capacity;

3   Electricity feed-in tariff received by the plant operator.

5.3.1   Availability and Costs of Biomass Resources in Europe

One of the main factors defining the market potential of the EFMGT is the availability and costs of suitable biomass feedstocks (Hartmann and Strehler 1995). A detailed study of the availability of biomass in Europe has been performed by Nikolaou et al. (2003). Their results for Germany are summarized in Table 5.2.

Table 5.2: Availability and utilization of biomass resources in Germany 2000

Source	Resource	Available energy potential [PJ/year]	Current energetic utilization [PJ/year]	Unused potential [PJ/year]
Agricultural	Crop residues	130	2.5	127.5
	Livestock wastes	111.5	1.5	110
Forestry	Wood fuel	85	85	0
	Harvest residues	142	55	87
Industry	Cellulosic wastes	45.5	40	5.5
	Black liquor	16.5	16.5	0
Municipal Wastes	Organic wastes	116	59	57
	Sewage sludge	24	16	8
Total		670.5	275.5	395

Source: Nikolaou et al. (2003)

Although there is a wide variation in the market value of agricultural residues such as cereal straw, estimates can be made with reference to the data from the Ely power station (UK) which is the world's biggest straw electricity power plant (38 MWe) in operation since 2000

---

[1] refers to a small scale biomass electricity generation plant run on the biomass residues from one medium sized farm

(Edwards et al. 2006). The straw acquisition including baling, loading and transport (40 km) costs the power station operator 43.5 €/t.

Together crop residues and livestock wastes make up by far the largest proportion (60%) of the unused biomass potential in Germany. Crop residues alone account for 32% of the unused potential, followed by livestock wastes[2] with 28%. Both of these resources are specific farm based by-products which makes them very interesting for small scale distributed electricity generation in an EFMGT.

Some crop residues such as straw are already utilized in the agricultural industry, and therefore have a market value. A large proportion of the cereal straw residues must also be left on the field to maintain soil fertility.

Therefore in the study by Nikolaou et al. (2003) only 30% of the total crop residues were defined as technically available for energetic utilization. A more detailed analysis of this problematic is available in the proceedings of the expert consultation "Cereal's Straw Resources for Bioenergy in the European Union" (Dallemand 2007).

Another large potential (14%) which has merit for an externally fired cycle is the organic fraction of municipal wastes, but since this is a concentrated resource, i.e. at the landfill site, it can be assumed that due to the "economy of scale" a larger plant will be more suitable than a SFBC-EFMGT.

The utilization of a SFBC-EFGT in the MW range or a SFBC-EFGT combined cycle certainly has merit, but exceeds the confines of this dissertation and will not be further discussed here.

There is a large demand for high quality woody biomass fuels, which has created a healthy market and high prices for both wood and wood residues. The utilization of high quality woody biomass for the externally fired gas turbine cycle is therefore not likely to be cost effective even for harvest residues, although they account for 22% of the unused energy potential.

Nevertheless all primary (harvesting and sawmills) and secondary wood processing facilities have large quantities of wood-waste which could readily be utilized in an EFMGT facility, if it became economically feasible (Hansson and Nilsson 2004).

A need for such a process can be determined because the current use of steam systems in small-scale sawmills is usually not economic (Ngoma 2005).

A study was carried out by Evans and Zaradic (1996) to determine the best EFMGT system configuration for cogeneration of electricity and heat for drying lumber utilizing the wood-waste fuel generated as a by-product of the sawmilling process.

The last stage in lumber processing is usually to dry the lumber to specified moisture content in a gas fired kiln while on the other hand large amounts of wood wastes are generated during the process which must be disposed of.

Originally many sawmills designed in the first half of the 19th century did burn their waste wood to raise steam and drive the machinery in the mill, but later the steam driven machinery gave way to electric drives and natural gas and other fossil fuels were used to heat the dry-kilns. The operation of a steam plant in sawmills is not usually suitable as the small scale electrical demand of 1-2 MWe make a steam cycle inefficient and the requirement to employ a qualified steam plant operator on a 24 h per day basis is economically unattractive (Evan and Zaradic 1996). However an EFMGT could generate electricity to power the mill machinery and provide a source of heat for the lumber dry-kilns and rely on remote operation control. Generally it was found by Evans and Zaradic (1996) that it is economically feasible to satisfy sawmill process heat requirements of around 20 MW_{th} or more with cogeneration by

---

[2] also poultry wastes as described by Bianchi 2003

maximizing the quantity of heat produced and only producing enough electricity to satisfy the saw mill requirements. The utilization of a fluidized bed combustion system proved to be the most economic option for this purpose.

In Germany where the EEG guarantees a premium price for renewable electricity it may also be economically feasible to generate excess electricity for sale to the net.

The size of the EFGT plant would need to be designed to fit the fuel supply and process air requirements. Waste heat may also be utilized during the production of pellets, which are often made from the sawdust produced during milling. The main problem with most forestry applications is the scale.

An EFGT with a unit size up to 1 MW$_{th}$ would not be large enough to satisfy the needs of most sawmills or even efficiently utilize forestry harvesting wastes because these operations produce huge amounts of refuse biomass, far surpassing the input requirements for an EFMGT.

The larger plants have an increased technical and economical risk, which needs to be overcome to achieve a commercial breakthrough. Up until now just about all research in this area has been done for large coal fuelled EFGTs. This research needs to be broadened to include biomass fuelled EFGTs.

The main unused biomass potential for EFMGTs is farm based agricultural crop residues and animal wastes. Both these waste streams could be combined as fuel for an EFMGT cycle with integrated biomass dryer as suggested by Elmegaard and Qvale (2002) and Cocco et al. (2006).

5.3.2   Specific Investment Costs for an EFMGT Plant

The costs of micro turbine based generation systems are not generally competitive with other systems such as gas motors because the turbo machinery is still relatively expensive due to the low production numbers (Vincent and Strenziok 2007). It is estimated that only about 3000 micro turbines are in operation world wide (Pajusalo 2005).

Table 5.3 gives an overview of commercially manufactured micro gas turbines.

Table 5.3: Commercially manufactured microturbines

Microturbine Power [kWe]	Manufacturer
30	Capstone, USA
45	Elliot, USA
65	Capstone, USA
70	NREC, USA
70	Ingersoll Rand, USA
75	Honeywell Power Systems, USA
80	Elliot, USA
100	Turbec, Sweden
200	Capstone, USA
250	Ingersoll Rand, USA

Source: Dielmann (2001), Lymberopoulos (2004), Peters (2004)

At present in Europe only the Capstone[3] C30, C65 and recently the C200 are commercially available. The production of the Turbec[4] T100 machine is also expected to reconvene. The Elliot, Ingersoll Rand, NREC and Honeywell MGTs are only available in the USA. The market leader in both the USA and Europe is Capstone.

The investment costs for MGT technology in Germany are 10 to 15% higher than for similar sized internal combustion gas engines while the electrical efficiency is 5 to 7% lower.

The high investment costs coupled with lower efficiency makes the MGT technology unattractive in comparison to gas motors for most applications such as for biogas combustion. This has led to a slow development of the MGT market for biogas utilization in Germany (Vincent and Strenziok 2006). The prices for MGT technology available in Europe have increased in recent years as a result of the low production capacity, and increasing material costs. Nevertheless given the high reliability, unmanned operation capability and low maintenance costs, the MGT is an ideal candidate for distributed generation applications and costs are expected to fall to under 1000 €/kWe installed generation capacity (Pederson 2004). The following table gives approximate prices for the presently available MGTs in Europe.

Table 5.4: MGT investment costs

MGT Power [kWel.]	MGT costs [€][*]	Specific costs [€/kWe.]
30	46 000	1535
65	78 000	1200
200	220 000	1100

[*] Status July 2004 (C200: Status 2008)

The costs contained here are only for the delivered MGT and do not include the periphery installations or gas pressure boosters.

With the commercialization of the micro gas turbine a small gas turbine has become available which, when combined with an external biomass combustor and high temperature heat exchanger, is ideally matched to the requirements for small scale distributed electricity generation utilizing solid biomass.

The development of the EFMGT technology has the potential to create a large market for MGTs. The ability to utilize solid biofuels makes EFMGTs economically and environmentally interesting.

Table 5.5 gives estimates from several authors for the specific costs (€/kW) for EFMGT technology.

Table 5.5: Estimated specific costs for an EFMGT plant

System	Investment costs [€/kW]	Author
EFMGT target costs	500 - 650	Bram et al. 2005
200-2000 kWe	750 - 1500	ZES 2004
250 kWe	2434	Yan 1998
100 kWe	2000 - 7000	Kautz 2005
100 kWe (Talbott's)	> 4000	Walter Pehn 2006(b)

---

[3] Distributors: www.e-quad.de for natural gas applications; www.greenvironment.de for biogas applications
[4] Distributor: www.pro-2.de for natural gas, biogas, landfill gas and sewage gas

Bram et al. (2005) suggests that the key to economic feasibility lies in cogeneration based EFMGT on the scale of 100-200 kWe.

A very optimistic economic assessment by ZES (2004) defined the investment costs for a 60 kWe commercial EFMGT plant at 1500 €/kWe in the short term and 750 €/kWe in the long term giving a total cost of 90 000 €, and 45 000 € respectively.

This very low estimate is based on the assumption of a 60 kWe MGT price of 15 000 € and 20 000 € respectively, which with regard to the present prices for the standard MGT of around 78 000 € (s. Tab. 5.4) seems unlikely.

Furthermore Bram et al. (2005) suggested that a commercial EFGT could cost about 100% more than a standard gas turbine, which would give an investment cost of around 156 000 € for a 60 kWe EFMGT based on the prices in 2004 (Vincent and Strenziok 2005, Kautz 2005).

On the other hand the only commercially available EFMGT, Talbott's BG 100 (80-100 kWe), has a price tag of over 400 000 € (> 4000/€kW), which is over 300% more than the standard 100 kWe MGT.

The application of an in-bed heat exchanger as proposed in this dissertation could significantly lower the EFMGT investment costs, but the target costs of 500-650 €/kW (s. Tab. 5.5) required by Bram et al. (2005) are not achievable.

Talbott's BG 100 has shown that the EFMGT technology burning solid biomass is technically feasible, but as with nearly all new technologies, the costs are still very high.

Pajusalo (2005) suggests that the economic viability of the EFGT process will rely on an effective utilization of the turbine exhaust heat, i.e. in combined heat and power mode.

The main market area for biomass EFGTs is seen in the distributed generation of electricity from agricultural biomass. This biomass may be a mix of liquid manure, straw and other crop residues, energy maize, and/or some form of short rotation coppicing (SRC). The utilization of the wet EFGT process with integrated biomass drying would reduce the need for an extra heat sink, but some other applications such as grain drying, glasshouse heating, or even small scale food processing in the clean hot air stream could be feasible.

Its small size and possibility for unmanned operation makes the EFMGT ideal for a one-farm energy solution, with the sales of excess electricity to the grid providing an extra source of income.

The wet biomass EFMGT uses the waste heat to dry the wet biomass fuel before combustion. The increase in efficiency for this cycle is evident for fuels with a moisture content greater than 55% (Elmegaard and Qvale 2002), which makes it ideal for a mixture of solid biomass with liquid manure and sludges.

Wet biomass waste is also available as organic by-products from the food industry, such as poultry rendering plants (Bianchi et al. 2003).

A biomass dryer can also be utilized to increase the plant flexibility when operating in CHP mode as described by Cocco et al. (2006). In this case the utilization of solid residual agricultural and forestry biomass with less than 55% water content is also highly efficient.

Renewable energy subsidies, such as the EEG in Germany, and increasing energy prices will also have a strong impact on the profitability of small scale EFMGT plants for distributed electricity generation.

5.3.3   EFMGT Electricity Feed-In Tariff

Based on the present renewable energy law in Germany (EEG 2004), the feed-in tariff for up to 150 kWe can be calculated as presented in Table 5.6.

Table 5.6: German renewable electricity feed in tariff for biomass (BMU 2004)

Generation type	Feed in tariff [ct/kWh]
Regenerative biomass[*]	17
Innovative generation bonus[**]	2
Total	19

*agricultural and forestry residues and dedicated biomass crops

**fuel cells, gas turbines, steam piston engines, ORC, Kalina-Cycle and Stirling engines

The financial returns from electricity sales in Germany based on EFMGT plant availability of 90% = 7884 h/a are shown in Table 5.7.

Table 5.7: Financial return with respect to generation capacity

Electricity generation [kWe]	Financial return [€/a]
30	44 938
60	89 877
100	149 796
200	299 592

If this can lead to a profitable operation of the EFMGT plant depends on the plant investment, operation and fuel costs.

5.3.4 EFMGT Investment Costs

The following cost-breakdown is only indicative for the costs of the SFBC-EFMGT test-rig at the University of Rostock utilizing the available SFBC facilities:

Table 5.8: EFMGT indicative costs

Position	Costs €
Capstone C30 MGT	46 000
MGT adaptation to EFMGT	5 000
fluidized bed heat exchanger	3 000
hot gas lines	1 000
hot gas valves	500
measurement equipment	500
miscellaneous material	500
approximate fabrication costs	15 000
Total	71 500

Table 5.7 shows the possible investment costs with respect to the calculations by Kautz (2005) which defined investment costs of 2000 - 7000 €/kWe generation capacity as economic feasibility for a 100 kWe EFMGT plant.

Table 5.9: Feasible EFMGT investment costs with respect to power generation capacity

Electricity generation [kWe]	Investment costs [1000 €]	€/kWe
30	60 - 210	2000 - 7000
60	120 - 420	2000 - 7000
100	200 - 700	2000 - 7000
200	400 - 1 400	2000 - 7000

The wide spread results from varying economic assumptions such as fuel and operation costs and the techno-economic uncertainties when dealing with research and development projects.

5.4 EMGT Environmental Aspects

The relevant pollutant emission from biomass combustion is fine particulate emission. The abatement of solid particulate emissions requires standard equipment (Riccio et al. 2000). The formation of particulates is increased with incomplete combustion of the biomass fuel.

A reduction can be achieved by primary measures designed to limit the evolution of particulates, such as increasing the combustion efficiency, and by secondary measures designed to remove unavoidable particulates (such as fly ash) from the flue gas stream, such as implementation of cyclones and flue gas particle filters.

Fluidized bed combustion is renowned for its high combustion efficiency, which leads to low un-burnt carbon particulate emissions, and so is ideally suited to problematic solid fuels such as low grade biomass.

Moreover if the fuel contains large amounts of sulphur, an in-situ sulphur capture through addition of calcitic limestone (80 wt.% $CaCO_3$) to the SFBC reactor is able to reduce sulphur dioxide emissions to well below the environmental regulation limits.

The EFMGT itself is emission-free since the exhaust gas from the turbine is only clean hot air and the temperature level of well below 1000°C is too low for the significant formation of thermal NO_x.

The utilization of renewable biomass fuels enables a CO_2 neutral electricity generation. Furthermore if only unused residual agricultural and/or forestry biomass is utilized there is no competition with conventional agricultural crops.

5.5 Summary and Recommendations

The combination of a micro gas turbine and a fluidized bed combustion plant with integrated metallic fluidized bed heat exchanger is recommended. This will create a robust simple highly reliable system which can be constructed using conventional materials and ensures high fuel flexibility.

- The appropriate EFMGT user market is mainly rural agricultural based, especially with combined crop and animal residues.

- The investment costs for an EFMGT system should not exceed 2000-7000 €/kW, whereby under 4000 €/kW is necessary to be commercially competitive.

- The emphasis of small scale distributed generation must be clearly on efficient power generation, and should not rely on combined heat and power operation to become economically feasible.

- The SFBC low temperature robust fluidized bed combustion, is suitable for low grade heterogeneous residual biomass fuels such as, sludges, liquid manure, and forestry residues, and therefore ideal for the EFMGT process.

- The EFMGT can be adapted from conventional readily available micro gas turbine technology.

- The SFBC reactor is ideal for the realization of a wet biomass EFMGT system with biomass drying, as a small scale alternative to biogas plants for sludge utilization.

A further advantage of small scale distributed generation in general is that it supports the rural economy.

It is suggested here that the EFMGT plant must be able to exploit the whole range of biomass quality including straw and other similar agricultural residues and energy grains.
This indicates that the biomass combustion temperatures must be reduced to about 750-850°C. The compromise in this case is that lower electrical efficiencies must be accepted.
An electrical efficiency in the range of 20% is nevertheless realistic if turbine inlet temperatures around 800°C can be achieved.
To achieve such a small temperature difference ($\approx$50K) between the flue gas and compressed air stream an innovative two stage heat exchanger system consisting of the existing gas turbine recuperator and a metallic heat exchanger in the fluidized bed combustion zone has been developed as described in Chapter 7.

6   High Temperature Air Heaters

6.1   Heat Exchanger Classification

Gas turbine heat exchangers can be defined as recuperator or regenerator based on their function. In a recuperator the cold working fluid is always separated from the hot combustion gases by a wall through which the heat is transferred, there is no direct contact between the two mediums. A typical application of a recuperator is seen in most micro gas turbines.

In a regenerator the working fluid and combustion gases alternate, whereby the hot flue gases heat the wall material which in turn then heats the working fluid. This system requires at least two parallel exchangers, and a control mechanism. In a regenerator it is possible that the working fluid becomes contaminated by particulates in the flue gas.

In general heat exchangers can also be classified into three types according to the current flow-paths of the hot and cold medium as shown in Figure 6.1.

| Co- current | Counter-current | Cross-flow |
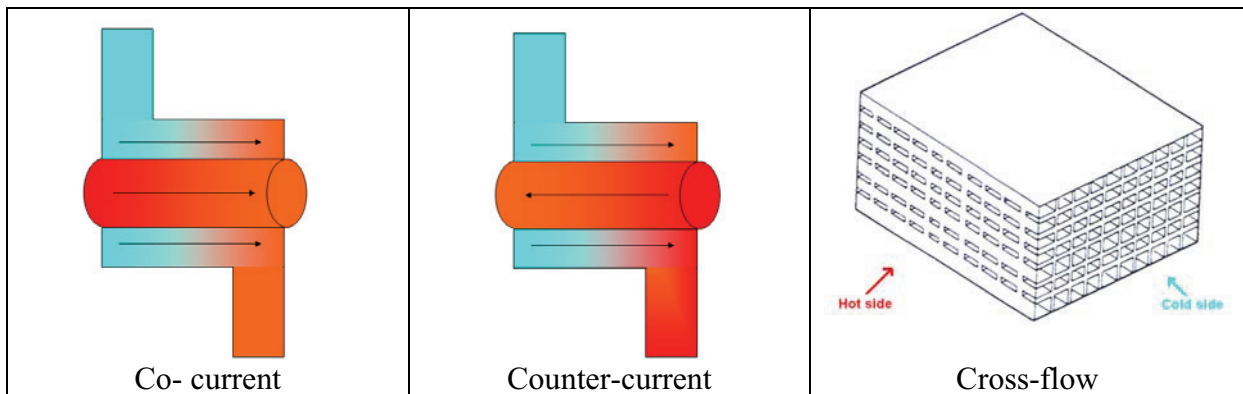
Fig. 6.1: Principle of heat exchanger classification by current flow

In co-current heat exchangers, both the hot medium and the cold medium are moving in the same direction. This design allows a good heat exchange rate for short heat exchanger tubes, but the temperature difference between the two fluids remains large.

This design limitation can be overcome by a counter-current configuration (s. Fig. 6.1) in which the hot medium flows in the opposite direction to the cold medium which means that for long tubes the temperature difference between the two fluids can be very small.

The cross-current heat exchanger configuration offers a compromise between the requirement for very long heat exchanger tubes, and high cold medium outlet temperatures.

As shown in Figure 6.1 in cross-flow heat exchangers the hot medium flows crosswise to the cold medium. This type of heat exchanger construction is particularly suitable for ceramic materials due to the strength of the compact bonded structure.

In addition to being classified according to their current flow paths heat exchangers are also classified as ceramic, metallic or composite[1] based on their construction material.

6.2   Metallic High Temperature Heat Exchangers

The only successfully operated EFGTs, the 2 MWe coal fired closed cycle plants built in the 1950's, relied on metallic heat exchangers and had maximum turbine inlet temperatures of around 700°C (Elmegaard and Qvale 2002).

---

[1] mixture of metallic and ceramic materials

In recent years many material evaluation studies have been performed by various authors to assess the suitability of metallic alloys for high temperature heat exchanger application (Wright and Stringer 1997, Yan 1998, Savolainen et al. 2005).

The development of super-alloys and heat- and corrosion-resistant cast alloys has increased the turbine inlet temperatures achievable with metallic heat exchangers from around 650°C in 1939[1] to over 1000°C in recent years.

In particular metallic heat exchangers appear the best short term option for the construction of small size EFGT units (Cocco 2006).

6.2.1 Metallic Heat Exchanger Material Properties

Metallic high temperature heat exchanger materials must exhibit good heat transfer properties, and be resistant to:

- Oxidation
- High temperature corrosion
- Sulphidation
- Erosion
- Creep
- Thermal shock and fatigue

Furthermore they must have sufficient mechanical properties such as tensile strength at high temperature and be cost-effective.

Oxidation

The formation of oxide scales acts as a diffusion barrier between the core material and the oxidative environment.

The adherence of an oxidation layer to the underlying material is dependant on the ratio of the molar volumes of the metal and its oxidation layer, known as the Pilling-Bedford ratio (PBR). A large difference in the molar volumes results in a susceptibility to spalling[2].

With a PBR higher than 1 the spalling is due to compressive stress, and with a PBR lower than 1 due to tensile stress (Savolainen et al. 2005).

The high velocity high temperature air inside the heat exchanger tubes can further oxidize the protective chromium oxide (Cr_2O_3) scale to CrO_3 which is volatile. Thus chromium is removed weakening the alloy and reducing oxidation resistance (Wright and Stringer 1997).

Resistance of the alloys to the high velocity working fluid and the building of stable oxide scales which do not produce spalled particles which pose an erosion threat to the gas turbine is an area of research interest.

A good starting point is given by the ODS alloys which build an aluminium oxide (Al_2O_3) scale which is non-volatile and thus far superior to the chromium oxide (Cr_2O_3) scale at elevated temperatures.

High Temperature Corrosion

Hot corrosion is principally caused by sodium (Na_2SO_4) and potassium sulphate (K_2SO_4) deposits on the surfaces of the heat exchanger tubes (Savolainen et al. 2005), which leads to a

---

[1] Escher Wyss, Zurich
[2] breaking off of oxide particles

chromium depletion in the underlying material. This is why chromium rich steels have a higher corrosion resistance.

In addition to their corrosive influence, accumulated fouling deposits decrease the heat transfer efficiency by decreasing thermal conductivity.

In pulverized coal fired boilers TP 310 stainless steel has been observed to loose 1.9 mm/year in wall thickness as a result of temperature driven accelerated corrosion (Wright and Stringer 1997).

The observed oxidation rates in the fluidized bed tests by Westinghouse (Datsko et al. 1991) on the other hand, were much lower, which may be because the abrasive action of the fluidized bed prevents the build up of corrosive material on the tubes.

Nevertheless due to the high potassium and sodium content in low grade biomass fuels the potential for high temperature corrosion is large.

Sulphidation

At temperatures over 600°C free SO_3 in liquid sulphate can react with the oxide layer, transforming it into metal sulphates, and thus dissolving the protective scale. This process is accelerated by the influence of sodium, potassium and chlorine in the fuel, and promotes the formation of low melting point eutectics (Savolainen et al. 2005). Increasing the chromium (ideally > 25%) content of the steel is the best protection against sulphidation, while increased nickel content decreases sulphidation resistance.

The Westinghouse fluidized bed experiments verify this finding for the fluidized bed conditions. In general the high chromium content alloys were found to be corrosion resistant, while the high nickel content alloys were corrosion susceptible.

The materials TP 314, and TP 310 are both high chromium alloys, while TP 309 has slightly lower chromium, but also lower nickel content.

All three steels are corrosion resistant, but the durability of chromium oxide (Cr_2O_3) scale against oxidizing or reducing environments in the presence of sulphur or chloride containing gases is low.

Aluminium oxide (Al_2O_3) scale is the best protection against sulphidation (Schütze 1997 in Savolainen et al. 2005).

There are techniques which could provide a protective aluminium scale-forming coating on the tubing surfaces. This could reduce metal wastage due to spallation and protect the turbine.

Erosion

Mechanical erosion accelerates the subsequent oxidation process by removing the protective metal-oxide scales. This scale exfoliation repeatedly opens up fresh base metal surfaces to oxidation, which results in metal wastage.

Exfoliation is particularly prevalent in thermal cycling situations (Yan 1998) which must therefore be avoided in the SFBC reactor.

On the other hand no significant mechanical erosion of the heat exchanger tubes in the fluidized bed due to the direct contact between the SiO_2 bed particles and the heat exchanger tubes was observed during the 2000 hour heat exchanger tube tests in the Westinghouse study. This may partly be due to the low fluidization velocity in the utilized flat fluidized bed design shown in Figure 6.5.

The impact of the fluidized bed particles on the heat exchanger tubes can be reduced by selecting a vertical as opposed to a horizontal orientation. On the other hand the reduced impact also reduces the heat flux between the fluidized bed and the heat exchanger tubes.

Creep

The slow deformation of materials at high temperature as a result of static stress is termed creep.

Creep is measured as a strain time yield limit in a tensile test. Creep increases as a function of stress and temperature and can lead to component failure (rupture). Uniform dispersion of alloying elements and fine particles, such as in oxide dispersion strengthened (ODS) alloys, improves creep resistance. Austenitic stainless steels have higher creep resistance than ferritic steels due to their face-centred cubic (FCC) structure which increases diffusion pathways.

Thermal Shock and Fatigue

Rapidly alternating temperatures induce thermal shock, which can cause material cracking by brittle fracture or thermal fatigue mechanisms.

Thermal shock results from constrained thermal expansion and/or contraction during alternate heating and cooling. This constraint leads to a build-up of stress resulting in metal fatigue leading to fatigue cracks.

This condition is intensified by simultaneous changes in stress such as can be expected within a fluidized bed and leads to thermal fatigue.

6.2.2   Metallic Heat Exchanger Material Availability

The number of alloys identified as having potential for application at high temperature decreases rapidly above approximately 815°C (Wright and Stringer 1997). The high temperature mechanical properties of steels can be improved by dispersion hardening with oxide particles such as yttrium oxide (Y_2O_3) or titanium oxide (TiO_2).

Ferritic oxide dispersion strengthened (ODS) alloys based on Fe-Cr-Al appear to be a suitable material to raise turbine inlet temperature above 900°C as they are resistant to high temperature corrosion and spallation (Bram et al. 2005).

ODS alloys provide creep strength up to around 90% of the alloy melting temperature which is superior to the modified conventionally strengthened alloys, in which the strengthening mechanisms degrade with increasing temperature (Wright and Stringer 1997).

In the second round of the EC research programme COST 501, ODS alloys for high pressure systems with temperatures up to 1100°C were assessed (Star et al. 1994).

A high temperature heat exchanger research and development project at the University of Stuttgart[1] (Germany), which was initiated in 1993 to test heat exchanger material and design a possible heat exchanger (Kussmaul et al. 1995), found that the ODS alloy PM 2000[2] has good resistance to a corrosive environment up to a temperature of 1250°C.

British Gas tested an ODS air heater with wall temperatures up to 1147°C at 3 bar in 1995 (Bram et al. 2005). The ferritic ODS alloys also have excellent resistance to gas-phase oxidation, sulfidation, and carburization attack due to the formation of a non-volatile aluminium oxide (Al_2O_3) scale (Wright and Stringer 1997).

However ODS alloys are difficult to work with because of the critical dependence of their high temperature strength on their microstructure. This results in the requirement that they must be worked hot (>300°C), and plasma cutting and welding should be avoided.

During the EC project FAIR-CT95-0291 coordinated by the Biomass Technology group in the Netherlands, candidate materials HR120, HR160, SS310 have been recommended for

---

[1] Staatliche Materialprüfanstalt (MPA) and Institut für Verfahrenstechnik und Dampfkesselwesen (IVD)
[2] 74.5% Fe, 5.5% Cr, 0.5% Ti, 0.5% Y_2O_3

construction of a conventional high temperature shell and tube heat exchanger design such as shown in Figure 6.2.
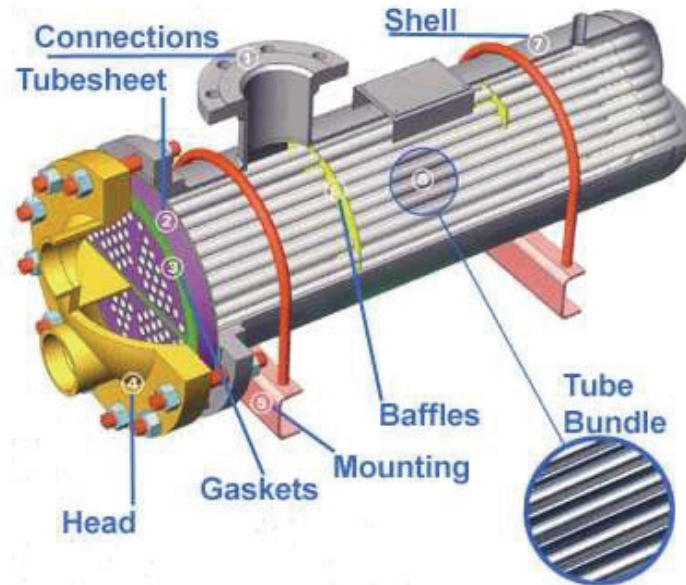
Fig. 6.2: Shell and tube heat exchanger

Austenitic heat resistant stainless steels (SS) are much more easily worked than ODS alloys, and are suitable for the lower air temperatures such as in SFBC applications (s. Tab. 6.1). They are also more readily available and less expensive. Particularly the availability of formed components such as pipe bends is important for heat exchanger construction.
Table 6.1 gives an overview of some prospective high temperature metallic heat exchanger materials discussed in the literature.

Table 6.1: High temperature metallic heat exchanger materials

Heat exchanger	Selected Materials	Air Temperature [°C]	Study
SFBC fluidized bed heat exchanger	TP-304H TP-310 Incoloy alloy 800H	816	Westinghouse in-bed air heater[a]
Pulverized coal combustion chamber tests	ODS alloy PM 2000	1250	University of Stuttgart[b]
Pressurized ODS alloy heat exchanger	Dourmetal ODM751 Dourmetal ODM331 Inconel MA 956 Plansee 2000	1100	COST 501 Round 2[c]
Shell and tube heat exchanger	HR-120 HR-160 TP-310H	850	FAIR-CT95-0291[d]

[a]Datsko et al. 1991, [b] Kussmaul et al. 1995, [c]Star et al. 1994, [d]Knoef et al. 1998

6.2.3   Westinghouse Fluidized Bed Heat Exchanger Material Tests

With respect to the material selection for an in-bed heat exchanger the results from Westinghouse's coal fired CFBC[1] in-bed air heater experiment, presented by Datsko et al. (1991), are significant. To select materials for a high temperature in-bed heat exchanger Westinghouse tested 47 heat exchanger tube materials for up to 2000 hours in a 1.8m × 1.8m bubbling atmospheric fluidized bed test facility as shown in Figure 6.3.
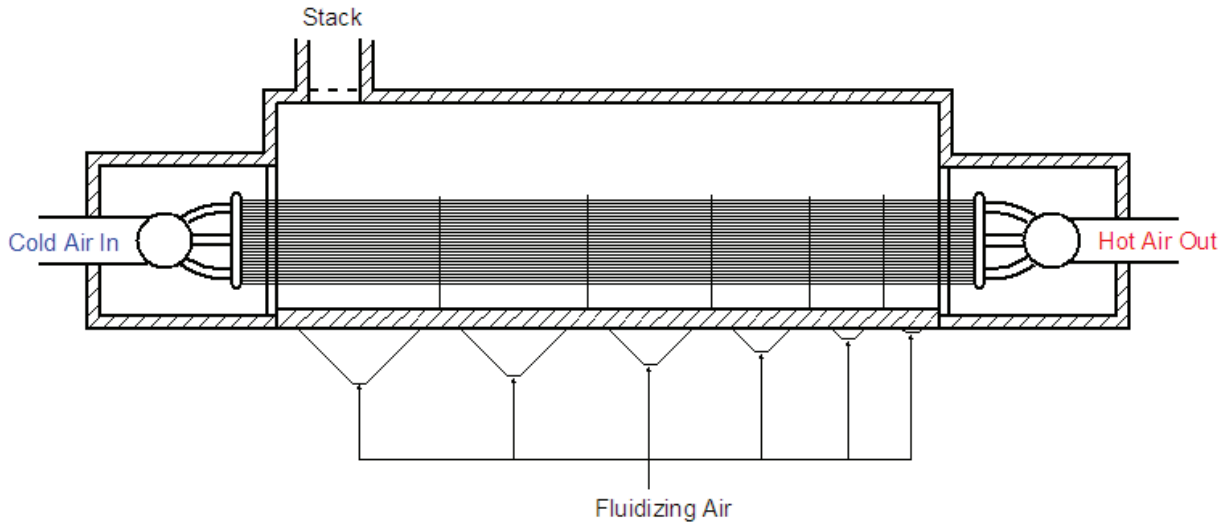
Fig. 6.3: Westinghouse CFBC in-bed heat exchanger test

The Westinghouse heat exchanger was designed to deliver air outlet temperature of 816°C. The materials tested included austenitic stainless steels, nickel base alloys, cobalt base alloys, high chromium coatings, as well as lower grade ferritic alloys.

During the Westinghouse in-bed heat exchanger tube evaluation tests it was found that in general the high chromium materials were most corrosion resistant, and high nickel materials lest resistant.

No evidence of significant erosion was observed during 2000 hours testing in the SFBC reactor (Datsko et al. 1991).

The metallurgical analysis of the tested materials by three boiler manufactures resulted in the selection of materials for the in-bed heat exchanger tube application which were considered capable of achieving a 10 year tube life-expectancy under fluidized bed conditions.

The boiler manufacturers recommended a bimetallic or coextruded combination of an outer layer of stainless steel TP 310 on the austenitic alloy tube TP 304H[2].

The inner structural layer provides the necessary mechanical properties and the TP 310 provides the corrosion resistance necessary in the fluidized bed conditions. The incoloy alloy 800H was considered conditionally acceptable, but there were concerns about rapid degradation if the TP 310 cladding is breached (Datsko et al. 1991).

For lower temperature or lower stress condition monolithic TP 310 tubes were recommended.

6.3   Ceramic Heat Exchangers

Ceramic materials offer good high temperature oxidation resistance but suffer from a lack of tensile strength and fracture toughness, which makes them unsuitable for conditions with

---

[1] circulating fluidized bed combustion
[2] The H refers to high carbon.

fluctuating mechanical stress such as under fluidized bed conditions.

The strength of a ceramic is dependant on the size and distribution of flaws, which are potential initiation points for a fracture (Wright and Stringer 1997).

Construction problems related to the mismatch in the thermal expansion of the ceramic headers and the metallic inlet line must also be accommodated for. Ceramic joints and ceramic-metallic joints still represent a challenge and require continued research (Wright and Stringer 1997).

Ceramic materials can theoretically allow much higher temperatures than metallic materials, but high pressure ceramic heat exchangers, such as required for gas turbine operation, are not commercially available and the material costs are high (Marroyen et al. 1999).

The use of ceramic materials in pressurized air heaters is hampered by its brittleness, slagging problems and high material and construction costs (Bram et al. 2005).

The main problem encountered with ceramic materials such as SiC is their susceptibility to damage by the ash and alkali or sulphur content of the coal (Savola et al. 2005).

Yan (1998) attests that ceramic heat exchangers offer good corrosion resistance but suffer from lack of tensile strength and are prone to fracture.

6.3.1   Ceramic Heat Exchangers: State of the Art

One type of ceramic heat exchanger, which solves some of these problems, is the Regenerative Pebble Heater concept developed by ATZ-EVUS in Germany (s. Fig. 6.4).

The air heater is filled with spherical ceramic pebbles that have a capacity to store heat at temperatures up to 1500°C and release it again to a compressed air stream, which is then expanded through the gas turbine.
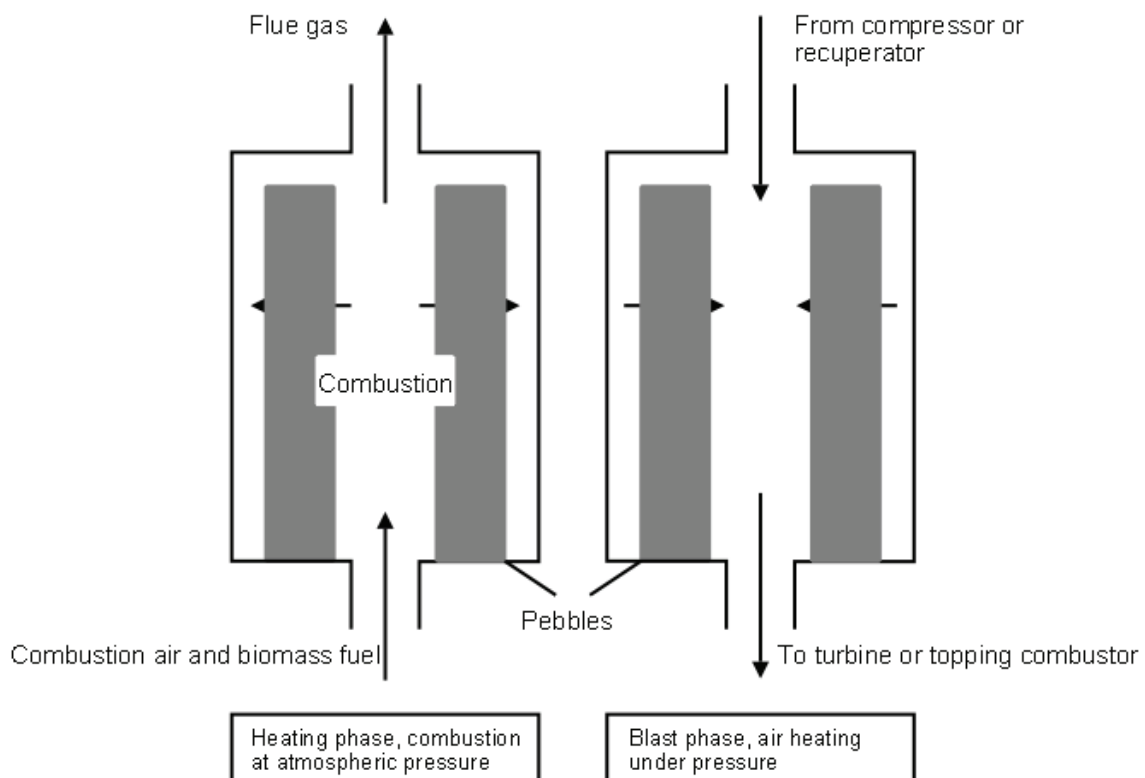
Fig. 6.4: Regenerative Pebble Heater concept (adapted from Bram et al. 2005)

Because this is a regenerative air heater at least two units must be run parallel, where the pebbles are alternately heated by the combustion gases, cleaned, pressurized, and finally cooled by returning their heat to the blast air. Temperature loss is quite low (20K) and the efficiency of the air heater is higher than 90%.

Research work in this field has been performed under the EC Exploratory Awards project ENK5-200-35003. Although in principle feasible, this technology will still need a clean fuel which does not cause slagging or fouling at the high combustion temperatures involved. Lower temperatures could be implemented, but this may cause problems due to the falling air temperatures. The very high temperatures are necessary because the blast air cools the pebbles very quickly and the minimum temperature must still be high enough to run the turbine. The turbine speed control will also be very difficult due to the strong cyclic temperature variations.
A pebble heater is not appropriate for a EFMGT concept running on biomass because the advantage of the pebble heater lies in the high combustion temperatures, and when burning biomass these are limited by the low ash melting point (molten ash would clog the pebble heater).

An economic assessment study of seven industrial cogeneration and five utility power generation applications based on ceramic heat exchangers, which was completed by McFarlin et al. (1982), indicated that only an atmospheric fluidized bed combustion (AFBC) system showed clear economic advantages in comparison to a reference pulverized coal fired system. This implies that the cost reductions attained by a smaller heat exchanger placed within the fluidization zone of an atmospheric fluidized bed combined with the efficient recuperation of the turbine exhaust as fluidization air in the fluidized bed reactor make this system economically attractive.
The problem with this type of theoretical economic study is that it assumes that a high temperature ceramic material suitable for fluidized bed conditions is available. Unfortunately more than twenty years after the completion of this study, there is still no available ceramic material for this purpose.
In actual fact ceramic heat exchangers which make up about 30% of the total system costs (Edelmann and Stuhlmüller 1997, Savola et al. 2005) present the major stumbling block for large scale EFGT systems.
This cost factor could force the development of smaller ceramic heat exchangers, but as seen in the bayonet-style heat exchangers (s. Fig. 6.5) these lead to low air-side temperatures. This is because of the low surface areas available for heat transfer and the poor atmospheric pressure heat transfer rate between the flue gas and the tubes outer surface.
On the other hand smaller fluidized bed heat exchangers can overcome this problem, but due to its brittleness ceramic materials are not suitable for fluidized bed conditions.
The most promising ceramic heat exchanger technology seems to be the bayonet tube arrangement, although inherent problems related to hot gas leakage and dispersion from radiation must still be overcome (Traverso et al. 2006).

Babcock and Wilcox (Yan 1998) performed extensive ceramic heat exchanger research in the 1990's leading to the development of a bayonet type tube in tube heat exchanger (s. Fig. 6.5).
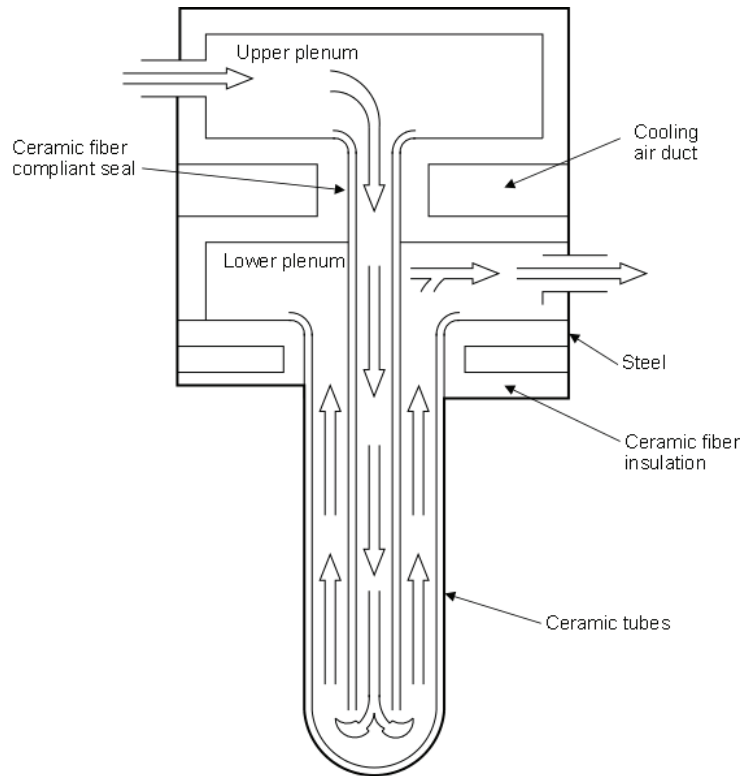
Fig. 6.5: Babcock and Wilcox bayonet tube heat exchanger from DuPont (Yan 1988)

The hot flue gas flows around the vertically hanging bayonet tubes, while air flows through the tubes. The inner tubes could also be of conventional metallic material (Hindman and DeBellis 1995). The advantage of this construction for high temperatures lies in the unhindered thermal expansion of the ceramic tubes.

The main problems experienced with high pressure ceramic tube heat exchangers were difficulties in attaching and sealing ceramic tubes, high costs and difficulties during manufacturing due to the material brittleness.

Under typical conditions the ceramic tubes attained air outlet temperatures of only 320°C with flue gas temperatures of 840°C. This low temperature is due to the low heat exchange surface area. It must be mentioned that this heat exchanger was not developed for an externally fired gas turbine. Problems were also experienced with respect to durability at elevated temperatures, air-side pressure drop and seal leakage and high costs (Yan 1998).

6.3.2   Ceramic Composite Heat Exchangers

Present research and development in high temperature ceramics[1] is focused on ceramic materials reinforced with continuous fibres or particulates to increase composite matrix strength for high-temperature, high-pressure corrosive environments.

Ceramic matrix composites (CMC) consist of a ceramic matrix reinforced with carbon fibres, which increases the material fracture toughness making them suitable for structural applications at high temperatures (1000-1500°C) in oxidizing environments. The ceramic matrix can consist of silicon carbide (SiC), silicon nitride (Si_3N_4), zirconium oxide (ZrO_2) or aluminium oxide (Al_2O_3).

---

[1] i.e. DuPont Lanxide Composites Inc. is developing continuous fiber ceramic composite (CFCC) materials

Silicon carbide (SiC) is selected as basis material for the construction of most ceramic composite heat exchangers due to its relatively high heat transfer coefficient (λ= 40W/mK at 1000°C) (Schulte-Fischedick and Zunft 2007), which is twice as high as for austenitic heat resistant stainless steels such as TP 314. Most other ceramics have very low heat transfer coefficients, which is why they are ideal for high temperature refractory fireside linings.
However SiC is not suitable for hot corrosive environments such as common for combustion gases, and may require a corrosion resistant coating such as cordierite (Schulte-Fischedick and Zunft 2007).
A prototype carbon fibre reinforced, cordierite coated finned SiC plate heat exchanger prototype for temperatures up to 1250°C has been developed at the German Aerospace Centre for a 20 MWth externally fired gas turbine process (Schulte-Fischedick and Zunft 2008).

Further experimental investigations of a finned ceramic (C/SiSiC)[1] heat exchanger for combustion gases has been performed by Schmid[2] (s. Fig. 6.6 a, b) as described in Hiller et al. (2007). The main restriction with regard to the utilization of ceramic heat exchangers is the high material costs resulting from the relatively low k_a-values (17 to 29 W/m²K for the heat exchanger shown in Figure 6.6 (b)) and the subsequent large heat exchanger area.
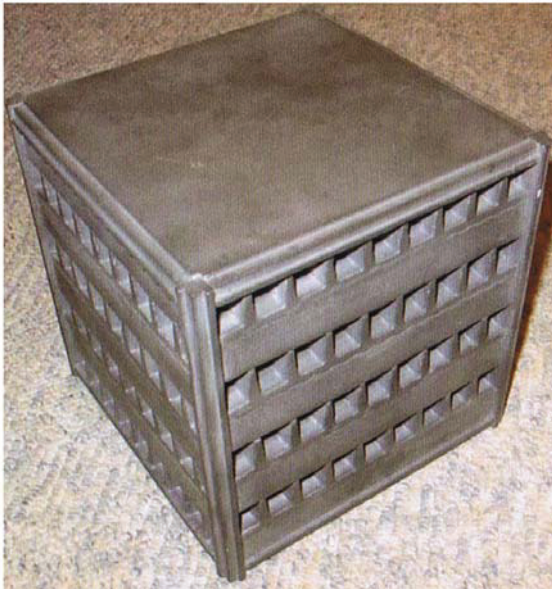
(a) Ceramic cross-flow heat exchanger   (b) Ceramic ribbed tube heat exchanger
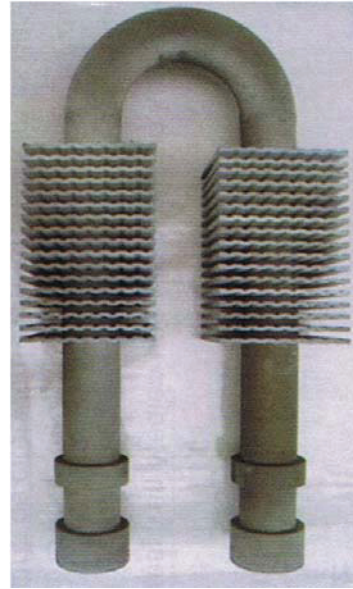
Fig. 6.6: Ceramic matrix composite heat exchanger research (Hiller et al. 2007,2008)

6.3.3   Metal Matrix Composites

Metal matrix composites (MMC) allow the combination of the tensile strength of metals with the hardness and corrosion resistance of ceramics.
Ceramic matrix composites with metals are only possible with light metals such as aluminium, magnesium or titanium. However at present their application is limited to under 800°C due to the low melting temperature of aluminium (660°C) and magnesium (650°C) and the oxidation and creep characteristics of titanium (Savolainen et al. 2005).

---

[1] carbon fibre reinforced silicon carbide composite
[2] Patent Nr. DE 199 33 426 C2 (Würfelmodul), Gebrauchsmuster, Veröffentlichungsnr. 202004018924.0 (Rippenrohr)

7   University of Rostock SFBC Heat Exchanger

The main emphasis of the research presented in this dissertation is the design, construction and testing of an in-bed heat exchanger for the biomass fuelled "Stationary Fluidized Bed Combustion-Externally Fired Micro Gas Turbine" (SFBC - EFMGT) cycle at the University of Rostock, Chair of Environmental Technology.

7.1   Approach

The heat exchanger is the key component of the SFBC-EFMGT cycle. In the EFMGT cycle the problems concerning combustion temperature, fouling, erosion and corrosion have been transferred to the heat exchanger.

The main advantage of an EFMGT cycle is that the sensitive turbo machinery runs on clean hot air. The main techno-economic hurdle for the SFBC-EFMGT cycle is the construction of a robust, efficient and cost-effective fluidized bed heat exchanger for SFBC-EFMGT as specified in Table 7.1.

Table 7.1: SFBC-EFMGT cycle specifications

1	**Combustion art**	Stationary fluidized bed combustion
2	**Combustion temperature**	750 - 850°C
3	**Heat exchanger material**	Austenitic heat resistant stainless steel
4	**Heat exchanger type**	SFBC fluidized bed heat exchanger
5	**Topping combustion**	Should if possible be avoided

The predetermination of fuel type and combustion temperature (s. Ch. 4.1) limits the availability of suitable combustion technologies severely.

The small scale SFBC reactor, which is available at the University of Rostock, Chair of Environmental Technology, is ideal for the combustion of problematic biomass fuels such as low grade residual biomass feedstocks.

The fluidized bed combustion technology has fundamental advantages for the EFMGT concept presented in this dissertation.

Specification 1:   Stationary Fluidized Bed Combustion

The decisive factor for the efficiency of the EFMGT is the turbine inlet temperature (TIT). For the externally fired micro gas turbine (EFMGT) the TIT should be as near as possible to 950°C which is the design TIT for most micro gas turbines.

The utilization of low grade biomass fuels, on the other hand, requires that the combustion temperature stays below the softening point of the biomass ash.

Low grade fuels such as straw require much lower combustion temperatures than woody biomass fuels as discussed in chapter 4.1. For the lowest grade fuels this limits the combustion temperature to under 800°C to avoid agglomeration of the fluidized bed (Steinbrecht 2006b).

The combustion temperature depends on the fuel characteristics and leads to specification 2 for agricultural residues:

Specification 2:   Combustion Temperature 750 - 850°C

The choice of heat exchanger material is a question of operating temperature and conditions within the combustion chamber. The primary issue is the choice of ceramic or metallic materials for the heat exchanger construction.

The use of ceramic heat exchanger materials allows high turbine inlet temperatures, which makes topping combustion unnecessary. This is the main advantage of ceramic heat exchangers (CerHx).

However ceramic heat exchangers are still in the development phase, with few commercially available prototypes. The necessary ceramic materials are mostly not readily commercially available, are extremely expensive and not suitable for fluidized bed conditions. The fluidization itself causes static pressure fluctuations because of the collapse of internally up-streaming gas bubbles. These actions are connected with high mass forces which are sufficient to induce mechanical failure in a brittle ceramic heat exchanger.

The main problems experienced during testing of ceramic heat exchanger prototypes are related to fouling and low durability in the abrasive, erosive and corrosive conditions within the combustion chamber (Solomon et al. 1996, Klara et al. 1997, Yan and Eidensten 2000, Savola et al. 2005).

Metallic heat exchangers, on the other hand are suitable for combustion temperatures of well over 1000°C as discussed in Chapter 6.3.

Therefore for the SFBC reactor with combustion temperatures of under 900°C an austenitic heat resistant stainless steel is suitable for the heat exchanger construction.

Furthermore austenitic heat resistant stainless steels are commercially readily available and, in comparison to ceramic materials, are relatively inexpensive.

Specification 3:   Austenitic Heat Resistant Stainless Steel Heat Exchanger

The air-side temperature achieved in the heat exchanger is dependant on the heat exchanger area and the heat transfer coefficient between the combustion chamber and the compressed air stream.

To achieve air temperatures close to the combustion temperature requires either a very large heat exchanger area or a very high heat transfer coefficient.

The size of the heat exchanger is determined by the required thermal output, available space and material costs. The heat transfer coefficient, on the other hand, is determined by a complex interaction of parameters related to the specific conditions prevailing on both sides of the heat exchanger and the heat exchanger material.

Experimental results (VDI Wärmeatlas 2002, Vincent et al. 2008) show that heat transfer coefficients achieved for a heat exchanger within the fluidization zone of a fluidized bed reactor are up to factor 10 higher than for conventional flue gas heat exchangers.

This implies that the heat exchanger area necessary to transfer the same amount of heat to the compressed air stream is a factor 10 smaller for a fluidized bed heat exchanger than for a conventional flue gas heat exchanger.

Therefore the construction of a heat exchanger integrated in the fluidized bed reactor is the logical consequence of the requirement for an efficient cost effective heat exchanger capable of delivering air temperatures close to the fuel combustion temperature.

Specification 4:   SFBC Fluidized Bed Heat Exchanger

When working with higher quality fuels the combustion temperature can be increased

substantially, in which case the required optimal turbine inlet temperatures of about 950°C should still be possible with a metallic heat exchanger (s. Chapter 6.2.7).

It is also possible to increase the turbine inlet temperature while utilizing low quality biomass and a metallic fluidized bed heat exchanger by employing natural gas supplementary firing after the heat exchanger.

Supplementary firing[1] was proposed by Bram et al. (2005) for the Vrije University of Brussels EFMGT (s. Chapter 5.1.1) and employed for the University of Genoa, EFMGT test rig (s. Chapter 5.1.2).

The combination of metallic heat exchangers with topping combustion can lead to better performance and reduce the size of the heat exchanger. However topping combustion requires a clean alternative fuel such as natural gas, which can make up to about 35% of the thermal input, and is therefore a considerable cost factor (Bram et al. 2005).

Some larger system configurations include a pyrolysis of or gasification (Marroyen et al. 1999) of the solid fuel to obtain gas for the topping combustion, but for small scale systems this would result in a large increase in the system complexity, costs and research demand.

Simulations of a biomass fuelled EFMGT by Kautz (2005) and Cocco et al. (2006) have established that electrical efficiencies of around 20-25% can be achieved for an EFMGT cycle with turbine inlet temperatures of only 800°C which are achievable with a SFBC in-bed heat exchanger (s. Chapter 6.3).

For the SFBC-EFMGT cycle for residual agricultural biomass, taking into account the compromise between turbine efficiency and fuel costs (s. Chapter 5.3.1) electrical efficiencies of 20-25% are acceptable and therefore to reduce costs topping combustion should be avoided.

Specification 5:   Topping Combustion Should be Avoided

The construction of a SFBC fluidized bed heat exchanger is the key innovation for the success of the externally fired micro gas turbine cycle.

The main advantages of this approach are

- The excellent heat transfer coefficients in the fluidized bed mean that the required heat exchanger area is very small in comparison to common flue-gas heat exchangers. This in turn has the vitally important advantage that the "dangerous" pressure drop in the heat exchanger remains very small and does not significantly influence the gas turbine efficiency.

- The stationary fluidized bed combustion (SFBC) is ideally suited for difficult residual biomass combustion and the externally fired micro gas turbine (EFMGT) has the potential to deliver substantially higher electrical efficiencies than the competing technologies for small scale distributed electricity generation (s. Chapter 1.2).

- The in-bed heat exchanger attains excellent heat transfer coefficients which allow a super compact design which reduces the heat exchanger material costs to less than 10% of a comparable flue gas heat exchanger.

---

[1] also known as topping combustion

The main research emphasis must lie on

- Designing an in-bed heat exchanger for optimal TIT and minimal pressure drop,

- adaptation of a commercially available MGT to an externally fired MGT,

- optimizing the long-term reliability of the metallic SFBC in-bed heat exchanger and

- increasing the efficiency of the SFBC-EFMGT cycle through optimal exploitation of its recuperative potential.

7.2   Fluidized Bed Heat Exchanger Design

7.2.1   Design Concept

The SFBC fluidized bed heat exchanger, as proposed in this dissertation is a special case of the counter-current flow heat exchanger described in Chapter 6.1. In the SFBC reactor the hot medium temperature (the fluidized bed material) is constant along the whole length of the heat exchanger tubes due to the intensive mixing and reheating taking place within the fluidized bed (s. Fig. 7.1). This situation is similar to a heat exchanger placed within an agitating tank as described in the literature (VDI WA 2002).
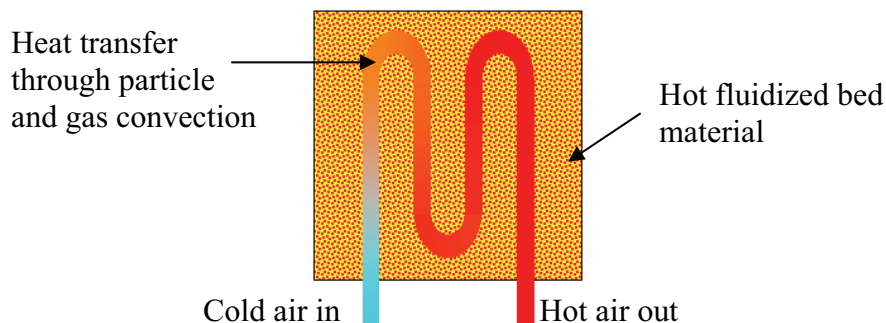
Fig. 7.1: Principle of the SFBC in-bed heat exchanger

This design configuration has the advantages of the counter-current heat exchanger, i.e. it is possible to achieve a minimal temperature difference between the heat exchanger outlet and the fluidized bed temperature.

The main mechanism responsible for the excellent heat transfer coefficient in the fluidized bed (α_{FB}) is the direct contact (particle convection) between the hot fluidized bed material and the heat exchanger walls.

Particle convection, which is unique to the fluidized bed process, can increase the heat transfer coefficient by a factor 10 in comparison to conventional flue gas heat exchangers. The heat transfer coefficient between the heat exchanger and the fluidized bed depends mainly on the fluidized bed material particle size and fluidization velocity.

Experimental results from Wunder (VDI WA 2002) have shown that under optimal conditions heat transfer coefficients of up to 750 W/m²K are possible.

7.2.2   Thermodynamic Calculation

The heat exchanger has been designed according to the methods set out below, which can be found in the Heat Atlas by the Association of German Engineers (VDI WA 2002). The heat exchanger thermal power output is calculated according to equation [7-1].

$$\dot{Q} = \widetilde{k} A \times LMTD \qquad\qquad [7\text{-}1]$$

$\widetilde{k}$ =   Average heat flux [W/m²K]
A =   Average heat exchange area [m²]
$LMTD$ =   **L**ogarithmic **M**ean **T**emperature **D**ifference [K]

$$LMTD = \frac{(\Delta T_{max}) - (\Delta T_{min})}{\ln\left(\dfrac{\Delta T_{max}}{\Delta T_{min}}\right)} \qquad\qquad [7\text{-}2]$$

The logarithmic mean temperature difference [7-2] is a function of the maximum and minimum temperature difference between the fluidized bed and the compressed air stream within the heat exchanger tubes as shown in the schematic temperature diagram in Figure 7.2.
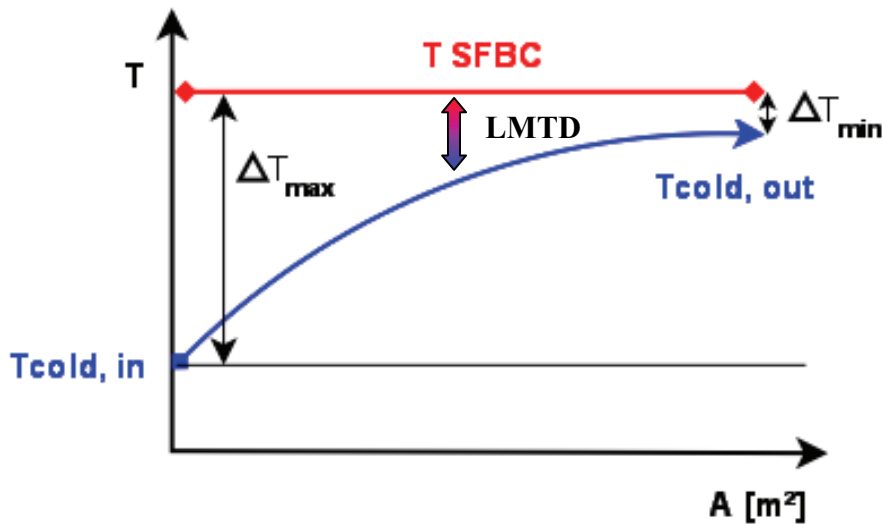
Fig. 7.2: Schematic temperature diagram of a SFBC fluidized bed heat exchanger

The average heat flux ($\widetilde{k}A$) can be determined with equation [7-3] as a function of the respective temperatures in the fluidized bed and compressed air stream.

$$\frac{1}{\widetilde{k}A} = \frac{1}{\alpha_o A_o} + \frac{\delta}{\lambda A_m} + \frac{1}{\alpha_i A_i} \qquad\qquad [7\text{-}3]$$

αA_o =   heat transfer between the fluidized bed and the outer heat exchanger wall area
$\delta/\lambda A_m$ =   heat conductance through the heat exchanger middle wall area (A_m) with the thickness (δ) and thermal conductivity (λ)

αA_i =   forced convective heat transfer from the inner heat exchanger wall area to the compressed air stream

The middle area (A_m) for cylindrical heat exchanger tubes with the inner and outer tube diameters (d_i and d_o) and the number of parallel tubes (Z_T) of the length (L) can be calculated as shown in equation [7-4].

$$A_m = \frac{A_o - A_i}{\ln \dfrac{A_o}{A_i}} = \frac{d_o - d_i}{\ln \dfrac{d_o}{d_i}} \times \pi \times L \times Z_T \qquad [7\text{-}4]$$

The heat transfer coefficient (α_o) between the fluidized bed and the outer heat exchanger wall area is assumed to be constant due to the strong mixing action within the fluidized bed.

With "Newton's Law of Cooling"[2], the total heat flux ($\dot{Q}$) between the fluidized bed and the outer heat exchanger wall (A_{Wo}) is determined with the middle temperature difference (ϑ_{FB} - ϑ_{Wo}), between the fluidized bed and outer heat exchanger wall and the fluidized bed heat transfer coefficient (α_{FB}) as shown in equation [7-5].

$$\dot{Q} = \alpha_{FB} \times A_o \times (\vartheta_{FB} - \vartheta_{Wo}) \qquad [7\text{-}5]$$

The heat conductance through the heat exchanger middle wall area (A_m) is dependant on the wall thickness (δ), the thermal conductivity of the heat exchanger tubes (λ) and the temperature gradient between the inner and outer tube surfaces (ϑ_{Wo} - ϑ_{Wi}) and can be determined with the law of heat conduction (Fourier's law[3]) as expressed in equation [7-6].

$$\dot{Q} = \frac{\lambda}{\delta} \times A_m \times (\vartheta_{W_o} - \vartheta_{W_i}) \qquad [7\text{-}6]$$

The heat flux to the compressed air stream is determined by the internal heat transfer coefficient (α_i), the inner wall heat exchanger area (A_i) and the middle temperature difference (ϑ_{Wi} - ϑ_{Air}) between the inner heat exchanger wall and the compressed air stream as shown in equation [7-7].

$$\dot{Q} = \alpha_i \times A_i \times (\vartheta_{W_i} - \vartheta_{Air}) \qquad [7\text{-}7]$$

Due to the reciprocal nature of the heat exchanger wall temperatures and the heat transfer coefficients an iterative solution is required to bring the heat flux ($\dot{Q}$) in equations [7-5 to 7-7] into equilibrium.

With the help of Fourier's law of heat conductance and Newton's law of cooling the heat transfer coefficient (α_i) for the forced convective heat flux from the inner heat exchanger wall to the compressed air stream can be defined with the dimensionless Nusselt number[4] (Nu), the thermal conductivity of the compressed air stream (λ_{Air}) and the characteristic length[5] (l) as shown in equation [7-8]. This matter is reviewed in detail in the relevant technical literature (VDI WÄ 2002, Baehr 2002, Michejew 1964).

---

[2] Sir Isaac Newton, English mathematician (1643-1727)
[3] Joseph Fourier, French mathematician and physicist (1768-1830)
[4] Wilhelm Nusselt, German physicist (1882-1957)
[5] For round heat exchanger tubes the characteristic length (l) is equal to the inner tube diameter.

$$\alpha_i = \frac{Nu \times \lambda_{Air}}{l}$$ [7-8]

As no comprehensive theory for forced convective heat transport in turbulent fluid flow exists, the only sure method to accurately determine heat transfer coefficients is their experimental verification.

For many heat exchanger constructions empirical equations for the calculation of heat transfer coefficients based on the "similarity theory"[6] are available in the literature (VDI WA 2002).

For turbulent forced convection ($Re > 10^4$) within the heat exchanger tubes and a heat exchanger length/diameter ratio > 100, the Nusselt number can be estimated empirically as a function of the Reynolds (Re) and Prandtl (Pr) numbers as shown in equation [7-9] (McAdams in VDI WA 2002).

$$Nu = 0.023 \times Re^{\frac{4}{5}} \times Pr^{\frac{1}{3}}$$ [7-9]

The Prandtl-number[7] (Pr) is a dimensionless parameter for viscosity and gives the ratio of the hydrodynamic to thermal boundary layer thickness as shown in equation [7-10],

$$Pr = \frac{v}{a}$$ [7-10]

with the kinematic viscosity (v) defined by the fluid dynamic viscosity (η) and fluid density (ρ) as show in equation (7-11)

$$v = \frac{\eta}{\rho}$$ [7-11]

and the thermal diffusivity (a) defined by the thermal conductivity of the fluid (λ), the fluid specific heat capacity (c_p) and fluid density (ρ) as shown in equation [7-12].

$$a = \frac{\lambda}{\rho \times c_p}$$ [7-12]

For the low pressure ratios of interest for the EFMGT the compressed air stream behaves as an ideal gas and therefore the thermophysical properties, λ, c_p and η can be calculated as a function of the fluid temperature as described by Steinbrecht (2006a).

The SFBC-EFMGT heat exchanger prototypes were designed to deliver the thermal input power requirement of the utilized micro gas turbine.

For the prototype SFBC-EFMGT plant at the University of Rostock an adapted C30 MGT from Capstone is utilized. The C30 MGT has a nominal power output of 30 kWe with an electrical efficiency of 30% (Capstone 2004). The required thermal input can therefore be calculated as shown in equation [7-13].

---

[6] an empirical method of finding universal relationships between variables that are made dimensionless using appropriate scaling factors
[7] named after Ludwig Prandtl, German physicist (1875-1953)

$$\dot{Q}_{Hx} = \frac{30kWe}{30\%} = 100kW_{th} \qquad\qquad [7\text{-}13]$$

The heat exchanger air outlet temperature should be as near as possible to the Capstone C30 MGT design turbine inlet temperature (TIT) of 950°C.

However with fluidized bed combustion temperatures of around 750-900°C[8] and a temperature difference (ΔT_{min}) between the fluidized bed and heat exchanger outlet, of about 50 K the maximal TIT for the SFBC-EFMGT cycle is between 700-850°C.

Another important consideration for the heat exchanger design is the fluid velocity in the heat exchanger tubes. A high fluid velocity results in high Reynolds numbers and a good heat transfer coefficient as evident from equation [7-9].

The fluid velocity (w) is a function of the air mass flow ($\dot{m}_{Air}$), density (ρ), heat exchanger tube diameter (d_i) and the number of parallel tubes (Z_T) as shown in equation [7-14].

$$w = \frac{\dot{V}}{A} = \frac{\dot{m}_{Air}}{\rho \times \left(\dfrac{\pi}{4} d_i^{\,2}\right) \times Z_T} \qquad\qquad [7\text{-}14]$$

On the other hand a high fluid velocity also causes a high pressure drop (Δp) in the heat exchanger tubes which reduces the cycle efficiency.

The heat exchanger pressure drop is a function of the friction factor (ζ), the fluid density (ρ) and velocity squared (w^2) as presented in equation [7-15] (VDI WÄ 2002).

$$\Delta p = \varsigma \times \frac{\rho\, w^2}{2} \qquad\qquad [7\text{-}15]$$

For turbulent fluid flow conditions above the laminar flow boundary ($Re > 2300$) such as expected in the in-bed tube heat exchanger, the friction factor (ζ) can be estimated empirically with equation [7-16] (Blasius in VDI WA 2002).

$$\varsigma = \frac{0,3164}{\sqrt[4]{Re}} \qquad\qquad [7\text{-}16]$$

The friction factor for the heat exchanger can be defined more accurately with equation [7-17], however this requires the experimental determination of ρ, w and Δp.

$$\varsigma = \frac{2\Delta P}{\rho w^2} \qquad\qquad [7\text{-}17]$$

The fluid density (ρ) under operating conditions can be determined with the help of the ideal gas law as shown in equation [7-18]:

$$\rho = \rho_o \frac{P_m T_o}{P_o T_r} \qquad\qquad [7\text{-}18]$$

whereby (ρ_0), (p_0) and (T_0) refer to the air density, pressure and temperature under standard conditions respectively, and (p_m) is the arithmetic middle pressure in the heat exchanger.

---

[8] With respect to biomass quality

The operation temperature should represent the real temperature in the middle of the heat exchanger, which is expected to be somewhat higher than the arithmetic middle temperature due to the asymmetrical temperature gradient (ΔT) between the fluidized bed and compressed air stream (s. Fig. 7.2). Therefore the reference temperature (T_r) as shown in equation [7-19] has been selected. This is an assumed value and must be experimentally confirmed.

$$T_r = T_{FB} + T_0 - LMTD \qquad\qquad [7\text{-}19]$$

7.2.3   Operation Characteristics

The heat transfer effectiveness (Φ) is a dimensionless operation characteristic[9] employed to assess the efficiency of a particular heat exchanger design in achieving the highest possible temperature. The heat transfer effectiveness (Φ) can be expressed as the ratio between the obtained temperature increase to the maximal possible temperature difference or as an exponential function of the heat transfer coefficient (k) with the heat capacity flux $\dot{C} = \dot{m} \times c_{pm}$ as expressed in equation [7-20].

$$\Phi = \frac{\Delta T_{Air}}{\Delta T_{\max}} = \frac{\Delta T_{Air}}{T_{FB} - T_{Air\,IN}} = 1 - e^{-k \times \frac{A}{\dot{C}}} \qquad\qquad [7\text{-}20]$$

It is important for the dimensioning of the in-bed heat exchanger that the compressed air temperature is as close as possible to the fluidized bed temperature i.e. that Φ is as close as possible to 1. For an open adiabatic system with stationary mass flow rate[10] and no work input ($\dot{W}$) the input heat flux ($\dot{Q}$) can be expressed as a function of the air mass flow ($\dot{m}_{Air}$), the middle heat capacity of the compressed air ($c_{pm\,Air}$) and the temperature difference between the heat exchanger inlet and outlet (ΔT_{Air}) as described in equation [7-21].

$$\dot{Q}_{in} = \dot{m}_{Air} \times c_{pm\,Air} \times \Delta T_{Air} \qquad\qquad [7\text{-}21]$$

The law of energy conservation (second law of thermodynamics) implies that the heat transfer through the heat exchanger wall according to equation [7-1] is equal to the change in enthalpy in the compressed air stream in equation [7-21] as described in equation [7-22].

$$\dot{Q}_{Hx} = \dot{m}_{Air} \times c_{pm\,Air} \times \Delta T_{Air} = kA \times LMTD \qquad\qquad [7\text{-}22]$$

The number of transfer units (*NTU*) can be defined by rearranging equation [7-20] to represent the ratio of temperature differences ($\Delta T_{Air} : LMTD$) as shown in equation [7-23].

$$NTU = \frac{k \times A}{\dot{m} \times c_{pm}} = \frac{\Delta T_{Air}}{LMTD} \qquad\qquad [7\text{-}23]$$

---

[9] as introduced in by F. Bosniakovic (1965)

[10] corresponds to a heat exchanger system with constant mass flow rate and no heat loss over the walls

The *NTU* method allows simplified retrospective calculation of the heat exchanger performance based alone on the measured temperature data.

7.2.4   Construction Materials

For the construction of the heat exchanger prototypes 1 and 2 at the University of Rostock monolithic austenitic heat resistant stainless steel tubes of the materials TP 314 (1.4841) and TP 309 (1.4828) were selected. These materials have similar properties to the TP 310 which was the most promising material in the Westinghouse experiment (s. Chapter 6.3.8) for a fluidized bed heat exchanger.

At the University of Rostock considerable experience with TP 314 has been gathered during previous high temperature heat exchanger tube tests (Kautz 2005). Also operation experience with the SFBC reactor, which is constructed of 5 mm TP 314 steel plate, has established the suitability of this material for fluidized bed conditions (Steinbrecht 2006b). A comparison of the stainless steel alloys TP 309, TP 310 and TP 314 is given in Table 7.2.

Table 7.2: Chemical comparison of the stainless steel alloys TP 309, TP 310 and TP 314

ASTM	Mat. No.	Fe [%]	Cr [%]	Ni [%]	P [%]	Si [%]	C [%]	Mn [%]	Max. Temp [°C]
TP 309 [a]	1.4828	Bal.	19-21	11-13	<0.045	1.5-2.5	< 0.2	2	1000
TP 310 [b]	1.4845	Bal.	24-26	19-22	<0.045	<1	<0.1	2	1050
TP 314 [c]	1.4841	Bal.	24-26	19-22	<0.045	1.5-2.5	< 0.2	2	1150

[a] heat exchanger prototype 2, University of Rostock   [b] recommended by Westinghouse
[c] heat exchanger prototype 1, University of Rostock

The alloys TP 309 and TP 314 have very similar physical and chemical characteristics to TP 310 and so can be expected to behave similarly in the SFBC reactor (s. Tab. 7.2). The mechanical and physical properties of the two selected steels are shown in Table 7.3.

Table 7.3: Mechanical and physical characteristics of the two selected steels (Thyssen 2000).

Characteristics	Unit	Mat. No.1.4841	Mat. No. 1.4828
Creep limit*; 800°C, 1000h	N/mm²	23	20
Rupture strength**; 800°C, 1000h	N/mm²	40	35
Heat conductance; 500°C	W/m K	19	21
Heat capacity; 20°C	J/kg K	500	500
Elongation at 800°C	$10^{-6}\,K^{-1}$	18	18.5
Density; 20°C	kg/dm³	7.9	7.9

*results in a permanent elongation of 1%   **total failure

One important restriction of austenitic heat resistant stainless steels is their relatively low durability in sour gas[11] environments and their tendency to become brittle when exposed to strong thermal cycling conditions (Thyssen 2000). Therefore for high sulphur fuels a in-situ desulphurisation may be necessary (i.e. with slaked lime ($Ca(OH)_2$) feedstock additive) and

---

[11] i. e. SO_2, SO_3

care must be taken to ensure an evenly distributed heat exchanger temperature profile during the SFBC start-up procedure.

7.3   SFBC-EFMGT Heat Exchanger Prototype 1

The heat exchanger prototype 1 design data is shown in Table 7.4.

Table 7.4: Heat exchanger prototype 1 design data

Design data	
Output power	100 kWth
T Air out	800°C
Dimensions	380×700 mm
Tube length	6000 mm
Tube diameter* (d_i)	12 mm
Tube number (Z_T)	9
Area (A_o)	2.5 m²

*main area

The material TP 314 was selected for the construction of in-bed heat exchanger prototype 1. TP 314 is readily available as seamless pipes for a price of between 25 €/kg and 45 €/kg[12] respective to pipe diameter (s. Tab. 7.5). The total material cost for the tubes amounted to 2166 €, which corresponds to a heat exchanger material price of approximately 22 €/kWth.

Table 7.5: Material costs: In-bed heat exchanger prototype I (seamless 1.4841 tubes)

Mat. No.	Tube diameter [mm]	Length [m]	[€/kg]	[€/m]	Total [€]
1.4841	15.0×1.5	67.1	45	22.80	1529.88
1.4841	48.3×3.2	6.7	25.46	95	636.50
Total		73.8			2166.38

The heat exchanger prototype 1 consists of a distributor and collector loop system (48.3 mm × 3.2 mm) connected by 9 tube coils (15mm × 1.5mm) with a length of six meters. The space available for the installation of the heat exchanger prototype 1 was restricted to a cylinder of 350 mm diameter and 700 mm length to fit into the SFBC reactor. This geometric restriction led to a very compact heat exchanger construction with a total area (A_o) of 2.5 m² as shown in Figure 7.3. The tight coiling was necessary to fit the required tube lengths into the limited available space. The five inner tube coils are wrapped in a helical construction of four outer tubes. To maintain an even fluid distribution the friction coefficients of the nine tube coils were tested and balanced during construction.

After extensive testing (s. Chapter. 8.1) preliminary tests with the EFMGT were performed. The purpose of these tests was to provide operation data from the turbine coupled with the heat exchanger in the fluidized bed, so that a simulation model could be developed (s. Chapter 9.1). The experimental and simulation results verified that an in-bed heat exchanger is

---

[12] ThyssenKrupp Schulte 2007

appropriate for the EFMGT cycle, but that larger tube diameters are necessary to reduce pressure drop.

The impact loss during the fluid distribution and merging was identified in the design phase as one of the main causes of the high pressure loss. Another reason for the high pressure loss (and excellent heat transfer coefficients) in the heat exchanger tubes results from the tight bends which force the repeated disintegration and renewal of the laminar boundary layers.

Based on the operation data and simulation results a larger heat exchanger was constructed, which utilizes the entire height of the fluidized bed reactor (about 2500 mm) and maintains a maximum heat exchanger pressure loss of 4% with respect to the MGT compressor pressure.

Fig. 7.3: SFBC-EFMGT fluidized bed heat exchanger prototype 1

7.4   SFBC-EFMGT Heat Exchanger Prototype 2

The design data for heat exchanger prototype 2 is shown in Table 7.6.

Table 7.6: Heat exchanger prototype 2 design data

Design data	
Output power	100 kWth
T Air out	800°C
Dimensions	380×2650 mm
Tube length*	7100 mm
Tube diameter (d_i)*	50 mm
Tube number (Z_T)	4
Area (A_o)	5 m²

*main area

The material TP 309 was selected for the SFBC in-bed heat exchanger prototype 2 construction.
The main reason for the utilization of TP 309 instead of TP 314 was the availability of standard prefabricated components such as pipe bends and the lower cost.
This material was readily available as welded pipes for a price of between 9 €/kg and 18 €/kg respective to pipe diameter (s. Tab. 7.7). The total material costs for the tubes amounted to 3120 €, which corresponds to a heat exchanger price of approximately 31 €/kWth.

Table 7.7: Material costs: Heat exchanger prototype 2

Material No.: 1.4828	Length [m]	[€/kg]	[€/m]	Quantity	Total [€]
Welded pipe 76.1 ×2	6	9.80	36	-	216
Welded pipe 54 ×2	30	18.28	47.60	-	1428
90° pipe bend 88.9 × 3	-	-	-	2	264
90° pipe bend 76.1 × 3	-	-	-	2	244
Reduction 76.1 to 54	-	-	-	4	632
Reduction 88.9 to 76.1	-	-	-	2	336
Total	36				3120

To maintain the stringent EFMGT pressure loss limitation with air mass flows of over 1000 kg/h, heat exchanger 2 has much larger tube diameters and a new concept for the fluid distribution to straight parallel tubes.
The fluid distribution concept consists of a series of 60° T-junctions in which a larger tube divides into two smaller ones, each of which further divide into smaller tubes. In this way the initial 3 ½ inch tube is divided into two 3 inch tubes which are each further divided into two 2 inch tubes to give four parallel 2 inch tubes as shown in Figure 7.4a. The four parallel 2 inch tubes with a length of 7100 mm each then build the main area of the heat exchanger. Each tube consists of four straight sections connected by 180° bends as shown in Figure 7.4b.
The increase in the heat exchanger area (A_o) to 5m² was necessary to maintain the required high heat exchanger outlet temperatures with the lower forced convective heat transfer coefficients for the larger diameter tubes.

The installation of the heat exchanger in the SFBC reactor was only possible by lifting the SFBC reactor up to the ceiling and installing the reactor in three sections with in-situ welding. This rather complicated procedure would not be necessary if the reactor was located outside and an opening was available at the top of the reactor.

Fig. 7.4a: Heat exchanger prototype 2 tube distribution system

Fig. 7.4b: Heat exchanger prototype 2 main tube system

8   Experimental Results and Discussion

After installation in the SFBC reactor and preliminary heat exchanger cold tests, hot tests were performed with an external compressor station to determine the heat exchanger 1 operation characteristics (s. Chapter 7.2.3).

Further hot tests were performed after the installation of the EFMGT. An overview of the hot operation tests performed with heat exchanger prototypes 1 and 2 (s. Figs. 7.3 and 7.2 a, b) is shown in Table 8.1. Experimental data is given in Appendix I and II.

Table 8.1: Heat exchanger tests

Date	Heat Exchanger Test Programme
06.09.07	Preliminary Heat Exchanger 1 Test
09.11.07	Straw Pellets Heat Exchanger Test
20.11.07 + 12.12.07	SFBC-EFGT External Compressor Tests
17.06.08	Preliminary Heat Exchanger 2 Test
08.07.08	SFBC-EFMGT Test 1
13.08.08	SFBC-EFMGT Test 2
11.09.08	SFBC-EFMGT Test 3

The results obtained during the heat exchanger tests with the external compressor station were utilized to generate a simulation model of the SFBC-EFGT cycle as described in Chapter 9.1. Following the reconstruction of the EFMGT and the design and construction of heat exchanger prototype 2 a new test series was initiated.

After installation in the SFBC reactor a preliminary hot test with the existing SFBC compressor system was performed to determine the heat exchanger 2 operation characteristics (s. Chapter 7.2.3). Further tests of the complete SFBC-EFMGT system followed.

8.1   Heat Exchanger 1 Tests

8.1.1   Preliminary Heat Exchanger 1 Test

A schematic illustration of the preliminary SFBC prototype 1 heat exchanger test bed configuration showing the relevant temperature (T), pressure (p) and mass flow (m) measurement points is presented in Figure 8.1.

Fig. 8.1: Heat exchanger 1 preliminary test configuration

The SFBC reactor was fired with natural gas and light fuel oil. The measurement data is presented in Appendix I, Table 1. The measurement instrumentation is further described in Appendix III. The purpose of the preliminary tests was to asses the operation characteristics of the heat exchanger with an external compressor system[1] prior to the installation of the EFMGT.

The results of the preliminary heat exchanger test demonstrated that during stationary operation with an air mass flow of 121 kg/h and a pressure of 0.49 bar a heat exchanger output of 29.53 kW (s. App. I, Tab. 2) with an average air temperature of 826°C can be achieved.
The average fluidized bed temperature was 854°C which gives a temperature difference between the fluidized bed and heat exchanger outlet of only 28K (s. Fig. 8.2).

---

[1] compressor station consisting of one CompAir Compressor (V07G) and two membrane compressors (Hyko) in parallel operation

Fig. 8.2: Temperature diagram preliminary heat exchanger test

The energy balance of the SFBC reactor with heat extraction in the in-bed heat exchanger during the preliminary test (s. Fig. 8.1) is shown in Table 8.2.

Table 8.2: Heat exchanger preliminary test* energy balance

Attribute	Formula	kWth
Input SFBC	$\dot{Q}_{FG} = \dot{m}_{Fuel} \times LCV_{Fuel} + \dot{m}_{Fl.Air} \times c_{p\,m\,Fl.Air} \times T_{Fl.Air}$	109.64
Output heat exchanger	$\dot{Q}_{Hx} = \dot{m}_{Air} \times c_{p\,mAir} \times \Delta T_{Air}$	29.53
Flue gas	$\dot{Q}_{FG} = \dot{m}_{FG} \times c_{p\,m\,FG} \times T_{FG}$	
Energy loss**	$\dot{Q}_{loss} = \dot{Q}_{FB} - \dot{Q}_{Hx} - \dot{Q}_{FG}$	80.12
Balance	$\dot{Q}_{FB} = \dot{Q}_{Hx} + \dot{Q}_{FG} + \dot{Q}_{loss}$	109.64

*Test data from 06.09.07 **over reactor walls and liquid fuel lance cooling

The heat exchanger prototype 1 operation characteristics (s. App. I, Tab. 3) were calculated as described in Chapters 7.2.2 and 7.2.3.

Table 8.3: Heat exchanger prototype 1 operation characteristics*

Heat exchanger efficiency (η)	0.27	[-]
Fuel efficiency (η_{Fuel})	0.37	[-]
Heat transfer effectiveness (Φ)	0.97	[-]
Number of transfer units (*NTU*)	3.38	[-]
Heat transfer coefficient (*k*)	55.00	[W/m²K]
Friction factor (ζ)	52.42	[-]

*s. App. I, Tabs. 2 and 3

Due to the low air mass flow (121 kg/h) only 37% of the fuel energy content (LCV) could be transferred to the compressed air stream.

The air mass flow was limited by the compressor system and pressure drop (Δp) over the heat exchanger (36.76 kPa). The friction factor (ζ) for the whole heat exchanger (s. Tab. 8.3) was determined with the measured heat exchanger pressure drop as described in equation [7-17].

The heat exchanger operation characteristics, effectiveness (Φ), number of transfer units (*NTU*) and heat transfer coefficient (*k*) were determined from the experimental data with equations [7-20], [7-23] and [7-1] respectively (s. App. I, Tab. 3).

The very high heat transfer effectiveness ($\Phi = 0.97$) and high temperature (826°C) indicated that with an increasing air mass flow much higher heat exchanger efficiencies can be achieved.

The heat exchanger prototype 1 is visible in the SFBC reactor during start-up operation in Figure 8.3.

Fig. 8.3: Heat exchanger 1 in the SFBC reactor during start-up operation

8.1.2   Straw Pellets Heat Exchanger Test

Table 8.4: Straw pellets heat exchanger test

Fig 8.4: Straw pellets feedstock

Heat exchanger operation data		
$T_{air\ in}$	29	[°C]
$T_{air\ out}$	762	[°C]
m_{air}	109	[kg/h]
T_{SFBC}	800	[°C]
Hx output	24	[kW]

The heat exchanger was tested with straw pellets combustion to assess the heat exchanger behaviour with residual biomass fuels (s. Fig. 8.4).

The temperature of the SFBC reactor was kept at under 800°C to ensure that no fuel ash sintering occurred. This led to lower heat exchanger air temperatures. The air volume flow was measured with an orifice gauge as described in Appendix III.

In this test the SFBC compressor (induced draught fan) was utilized as the air source for the heat exchanger and the fluidized bed simultaneously, which limited the air mass flow to 109 kg/h and the heat exchanger inlet pressure to 0.55 bar. The lower temperature and air mass flow corresponds to a drop in the heat exchanger output from 29 to 24 kW (s. Tab. 8.4).

8.1.4   SFBC-EFGT External Compressor Tests

To assess the operation characteristics of the heat exchanger with a higher pressure and air mass flow further tests with a larger external compressor system[2] were performed.

The main purpose of the external compressor tests was to gather data for the development of a theoretical model of the SFBC-EFMGT system able to simulate the process with increased compressor inlet pressure and volume flow. The simulation study was completed within the framework of an undergraduate syllabus project as described in Chapter 9.1.

The external compressor EFGT-SFBC tests were performed with a fuel mix of convention light fuel oil and natural gas or solid biomass pellets[3]. Figure 8.5 shows the EFMGT adapted from a Capstone C30 MGT.

Fig. 8.5: Packaged EFMGT

---

[2] 2 CompAir diesel compressors in parallel operation to give a maximal air mass flow of 440 kg/h at up to 8 bar
[3] with extracted colza cake, a residue from the rapeseed oil production process
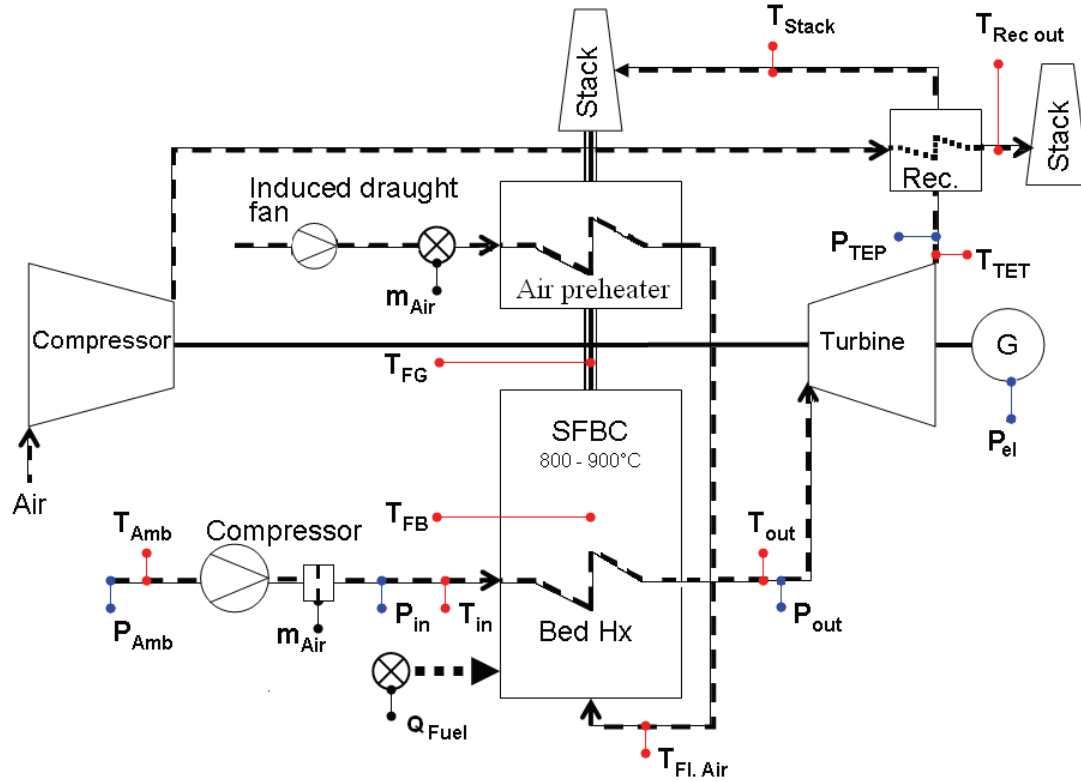
Fig. 8.6: SFBC-EFMGT test configuration with external compressor station

Table 8.5: SFBC-EFMG external compressor measurement programme[*]

Parameter		Unit
Ambient temperature	T_{Amb}	°C
Temperature before heat exchanger	T_{in}	°C
Temperature after heat exchanger	T_{out}	°C
Turbine exit temperature	T_{TET}	°C
Stack temperature	T_{Stack}	°C
Ambient pressure	P_{Amb}	Pa
Pressure before heat exchanger	P_{in}	Pa
Pressure after heat exchanger	P_{out}	Pa
Turbine exit pressure	P_{TEP}	Pa
Fluidizing air temperature	$T_{Fl.Air}$	°C
Fluidized bed temperature	T_{FB}	°C
Temperature flue gas	T_{FG}	°C
Recuperator exit temperature	$T_{Rec\ out}$	°C
Fuel input**	Q_{fuel}	kW
Mass flow heat exchanger air	$m_{Air\ Hx}$	kg/h
Mass flow fluidization air	$m_{Air\ FB}$	kg/h
Electricity to grid	P_{el}	kW

*measurement data is presented in Appendix I, Tab. 4
**calculated from the measured fuel mass flow and known LCV
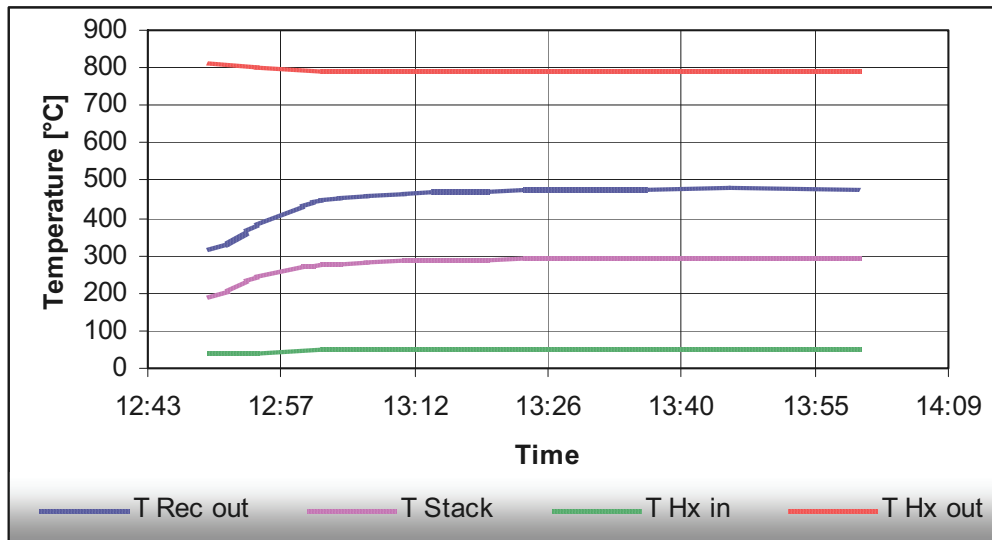
Fig. 8.7: SFBC-EFMGT temperature diagram

The temperature diagram as shown in Figure 8.7 verifies that the design turbine inlet temperature of over 800°C is realistic for the whole operation range up to 100 kW$_{th}$ (s. Fig. 8.8). The temperature difference between the fluidized bed and heat exchanger outlet decreases with increasing air mass flow. This can be explained by the increased turbulence and therefore improved convective heat transfer from the inner heat exchanger walls to the compressed air stream. The measured recuperator outlet temperature of around 480°C is available as heat exchanger inlet temperature. In the tests however, the EFMGT compressor air after the recuperator was vented to the stack to insure that the compressor pump limit was not reached. The heat exchanger was therefore fed by the external compressor system.

The heat exchanger prototype 1 operation characteristics (s. Chapter 7.2.3) were calculated from the experimental data for the steady state operation points measured during the external compressor operation tests (s. App. I, Tab. 4).
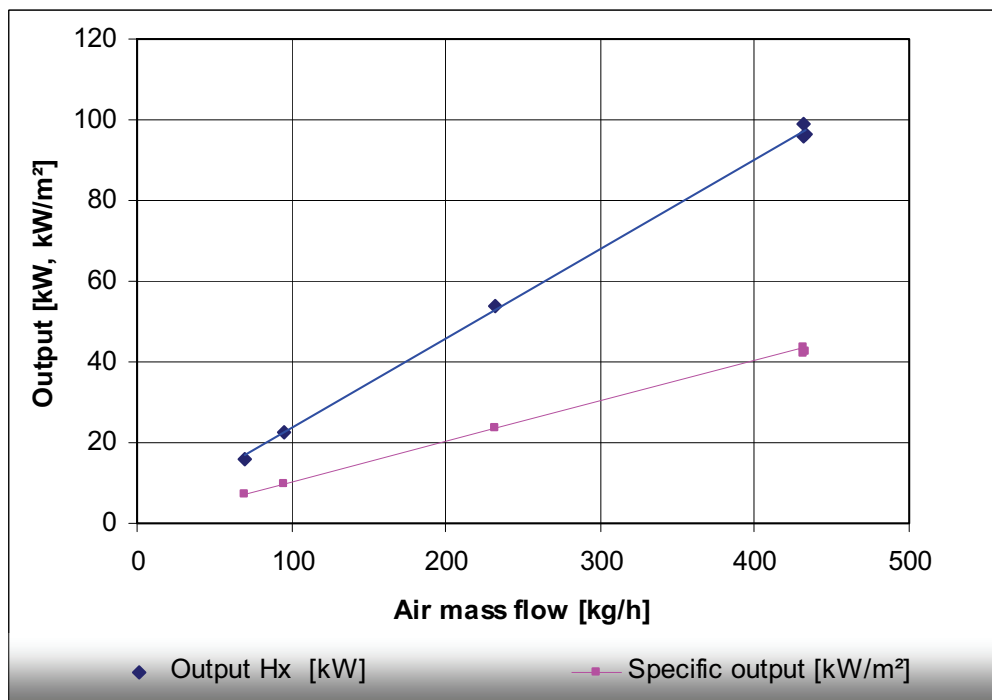
Fig. 8.8: Heat exchanger 1 output with respect to air mass flow

The results presented in Figure 8.8 clearly demonstrate that the heat exchanger is capable of delivering the design thermal output (100 kW$_{th}$) for the SFBC-EFMGT cycle. The achieved heat exchanger output was > 40 kW/m² with an air mass flow of around 440 kg/h. This correlates to a heat transfer coefficient (k_a) of up to 218 W/m²K as shown in Figure 8.9.
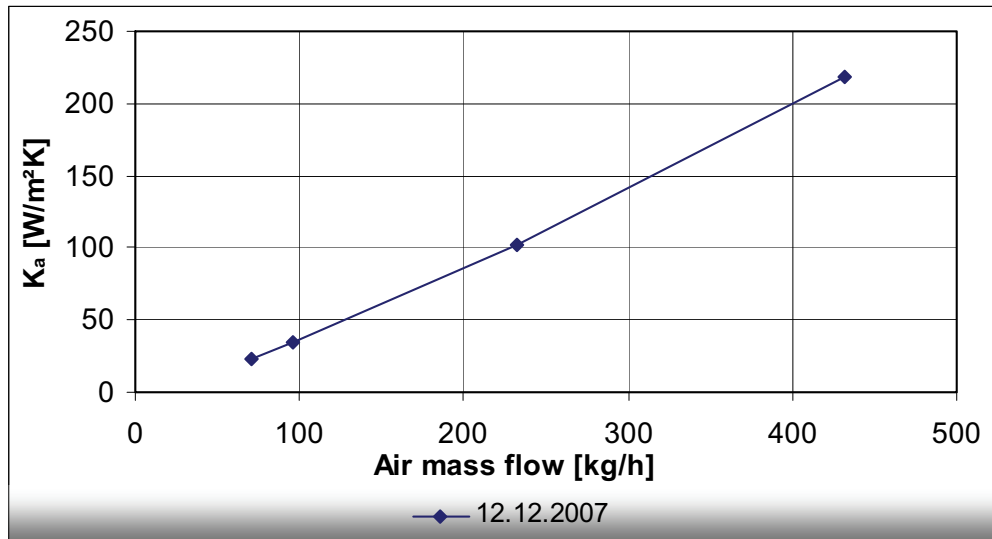
Fig. 8.9: Heat transfer coefficient with respect to air mass flow

Both the heat exchanger thermal output (s. Fig. 8.8) and the heat transfer coefficient (k_a) presented in Figure 8.9 show a near linear increase with increasing air mass flow, which clearly indicates the potential for a much higher heat flux capacity. This can be explained by the increasing turbulence and therefore better forced convective heat transfer coefficients within the heat exchanger tubes with increasing air mass flow.
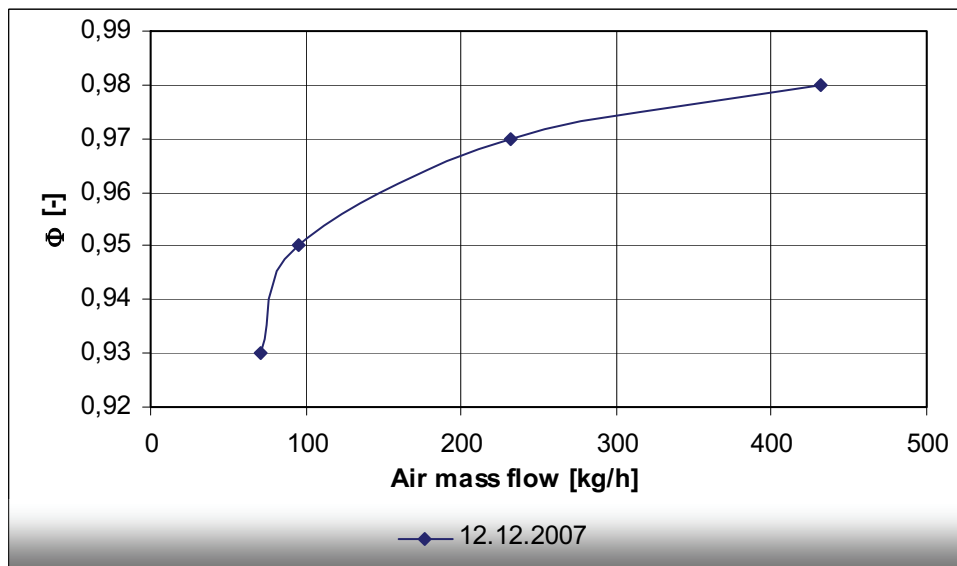
Fig. 8.10: Heat transfer effectiveness with respect to air mass flow

The heat exchanger displays an excellent effectiveness (Φ) which increases with air mass flow. The heat exchanger effectiveness (Φ) can be determined as a function of the air mass flow with the Gauss-Jordan-Elimination[4] method. The measurement data can be approximated

---

[4] expansion of the Gaussian elimination algorithm by the German mathematician Wilhelm Jordan (1842-1899)

by an exponential function of the type:

$$f(x) = (a_1 \times (1 - e^{-a_2 x})$$

with $a_1 = 0.975681$ and $a_2 = 0.034835$ and a standard deviation of $R^2 = 0.97$. The number of transfer units (NTU) also increases with air mass flow as shown in Figure 8.11. The logarithmic function

$$y = 0.8059 \times \ln(x) - 0.767$$

gives an excellent correlation ($R^2 = 0,999$) of the measured data. This allows an accurate extrapolation of NTU for an increased air mass flow in the heat exchanger. The increasing NTU is a further indication that better heat exchanger operation characteristics can be achieved with further increased air mass flow.
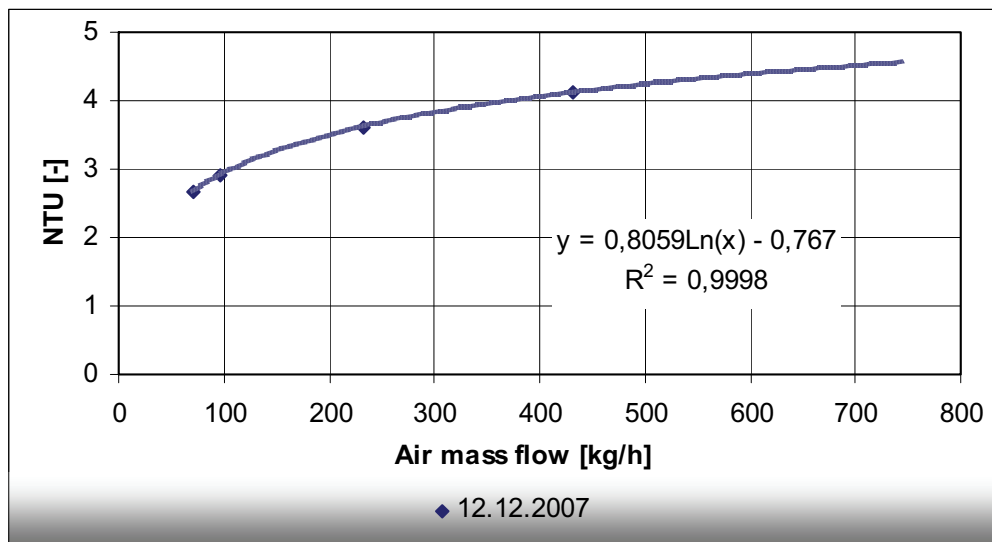
Fig. 8.11: Number of transfer units with respect to air mass flow

The heat exchanger pressure drop increases with air mass flow and temperature as a result of the increased fluid velocity. Figure 8.12 shows the pressure drop in heat exchanger 1.
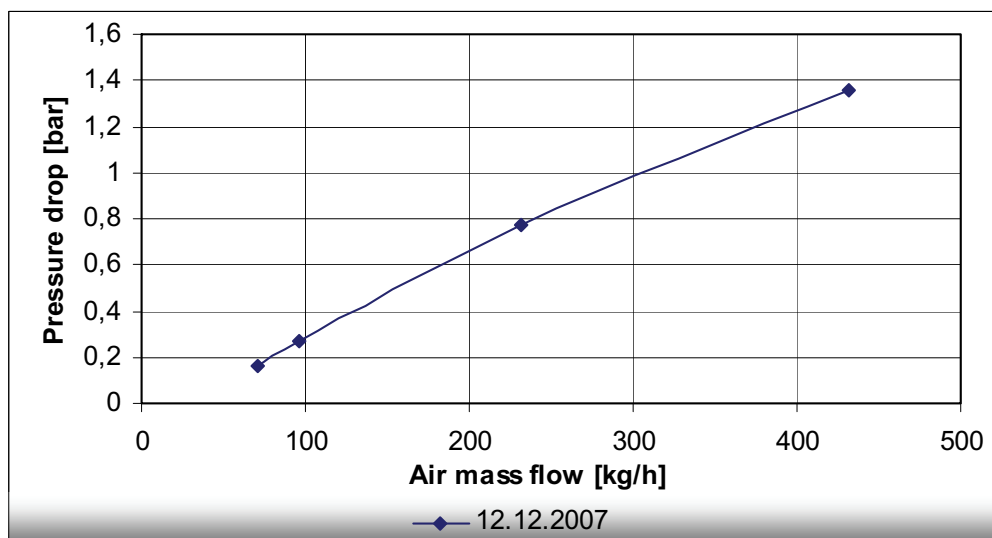
Fig. 8.12: Heat exchanger 1 pressure drop with respect to air mass flow

The friction factor (ζ) has been calculated (s. Equation 7-17) for the heat exchanger with respect to increasing air mass flow as shown in Figure 8.13.
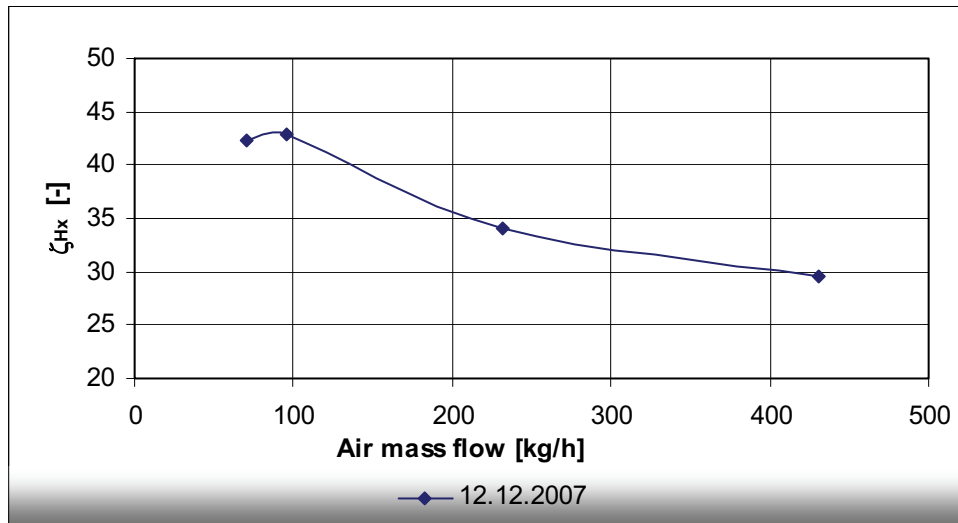
Fig. 8.13: Heat exchanger 1 friction factor with respect to air mass flow

Under full turbulent conditions ($Re > 10^5$) the heat exchanger fiction factor (ζ_{Hx}) is ideally independent of the fluid pressure, temperature and air mass flow. The decreasing friction factor with increasing air mass flow is probably due to the increased turbulence; a decrease in friction with increasing turbulence is known from the literature (VDI 2002). If only the higher air mass flow is taken into consideration, a friction factor of around 30 can be assumed.

The determination of the heat exchanger friction factor allows the theoretical calculation of the heat exchanger operation characteristics for an increased air mass flow with higher compressor ratios as described in Chapter 9.1.

Figure 8.14 presents a strip chart of the turbine operation during the external compressor test.
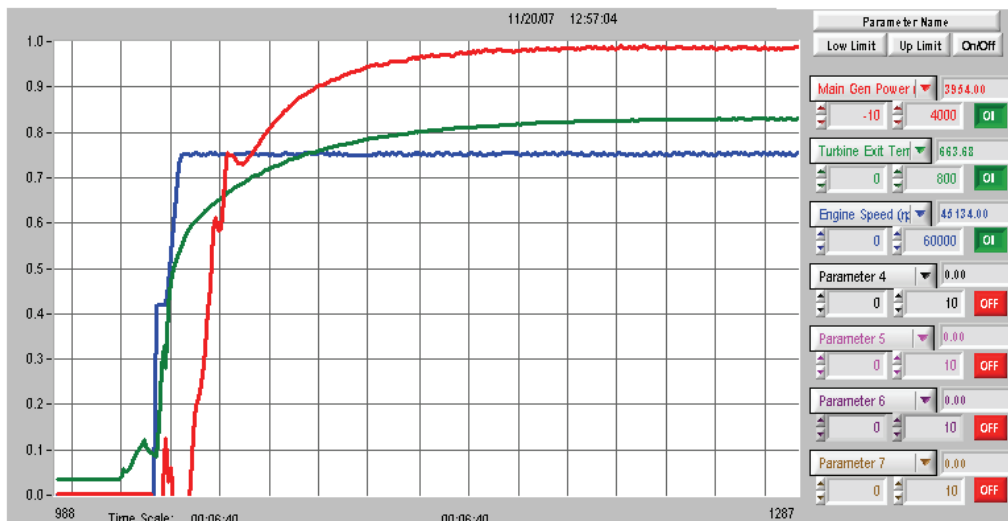
Fig. 8.14: EFMGT external compressor operation

A turbine software was utilized which kept the turbine speed at a constant set point. This control regime is equivalent to type B as described in Chapter 5.2.

For the steady state operation conditions described in Appendix I, Table 4 an electrical input to the grid of 3.1 kWe was achieved. The maximal generator output was 3,954 kW with an engine speed of 45 134 rpm as shown in Figure 8.14.

The difference between the generation power and the input to the grid is due to the electrical consumption of the MGT.

The low generation capacity could not be sufficiently thermodynamically explained. Therefore a relatively severe internal air flow leakage was suspected in the turbine. The relatively high turbine outlet temperature (661°C) was a cause of concern, and is a further indication of internal air leakage.

8.1.5   Heat Exchanger 1: Summary and Conclusions

- A cost-effective (30 €/kWe) metallic in-bed heat exchanger can be constructed for the fluidized bed reactor.

- The design air temperatures of over 800°C can be obtained in the metallic in-bed heat exchanger.

- A temperature difference between the heat exchanger outlet and fluidized bed of less than 50K is realistic.

- The design heat exchanger output of 100 kW can be achieved.

- An excellent heat flux between the fluidized bed and the compressed air stream was determined.

- Two options exist to reduce the heat exchanger pressure drop. Firstly the compressor pressure ratio could be increased; however, this would require the replacement of the MGT compressor, which was deemed not feasible within the context of the present research work.
  The second option is to increase the heat exchanger tube diameters or number of parallel tubes. The heat exchanger prototype 1 design however was the result of the geometric restrictions within the fluidized bed reactor, which limited the number of parallel tubes to a maximum of 9.

- Based on a detailed analysis of the extensive heat exchanger data, gathered over 52 hours of operation, and assessment of the simulated SFBC-EFMGT behaviour (s. Chapter 9.1) under a range of operation conditions, a full scale heat exchanger for up to 1100 kg/h air mass flow was designed.

- The utilization of the entire height (about 2500mm) of the fluidization zone of the SFBC reactor was necessary to enable a heat exchanger design for a maximum air side pressure loss of 4% with respect to the nominal MGT compressor pressure.

8.2   Heat Exchanger 2 Tests

The full size heat exchanger prototype was constructed as described in Chapter 7.4 (s. Figs. 7.4a, b).

8.2.1   Preliminary Heat Exchanger 2 Test

A schematic illustration of the preliminary heat exchanger 2 test configuration showing the relevant temperature (T), pressure (p) and mass flow (m) measurement points is presented in Figure 8.15.
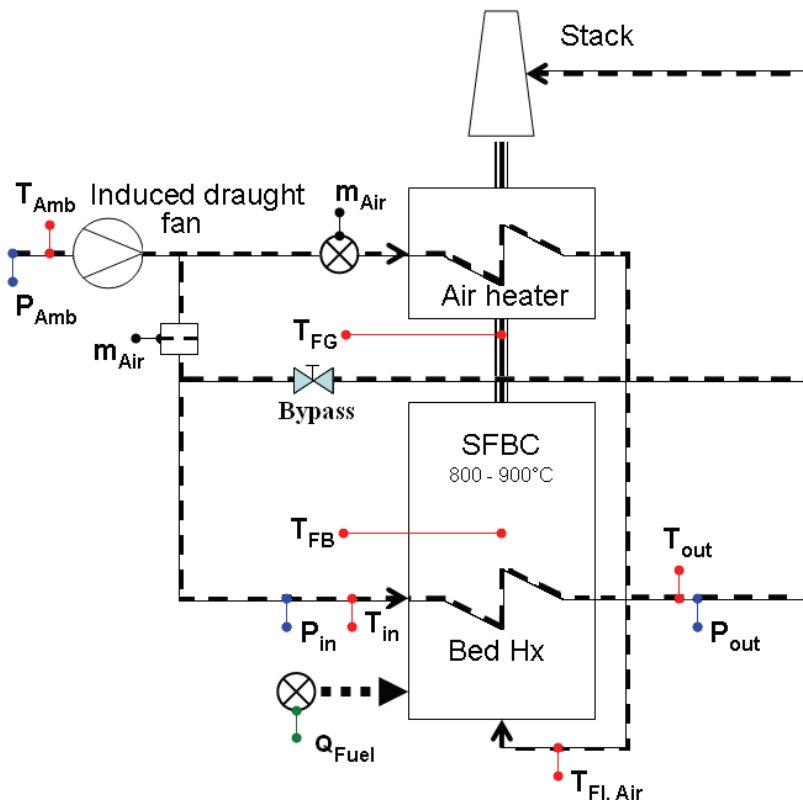
Fig. 8.15: Heat exchanger 2 preliminary test configuration

For the preliminary test a heat exchanger air mass flow of up to 445 kg/h was supplied by the existing SFBC induced draught fan.
The SFBC reactor was fired with natural gas and light fuel oil and the combustion temperature was held nearly constant at 850°C for the whole test.
During the preliminary heat exchanger test it was possible to accurately calculate the air volume flow entering the heat exchanger with an orifice gauge and then determine the air mass flow and heat exchanger output (s. App. II, Tab. 1). The measurement instrumentation is further described in Appendix III.
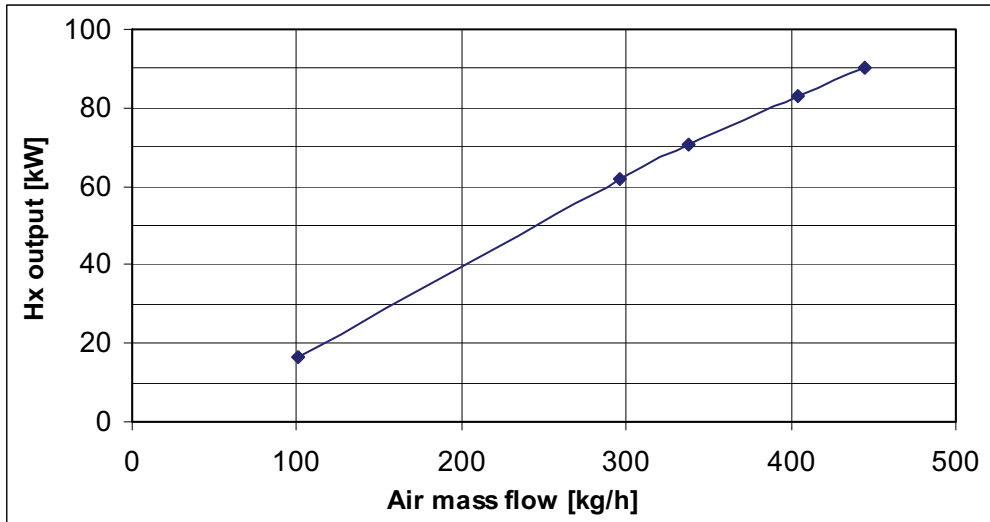
Fig. 8.16: Measured heat exchanger output with respect to air mass flow

The low heat exchanger air inlet temperatures (around 25°C) and the fluidized bed temperature of 850°C resulted in a large temperature gradient in the heat exchanger leading to a heat extraction of up to 90 kW from the fluidized bed with an air mass flow of 445 kg/h as shown in Figure 8.16.

To overcome the severe pressure drop criterion (< 4% of the compressor pressure) a bypass system was designed (s. Chapter 5.2) to reduce the heat exchanger pressure drop to below 4% of the nominal EFMGT compressor pressure during the low pressure start-up operation phase.
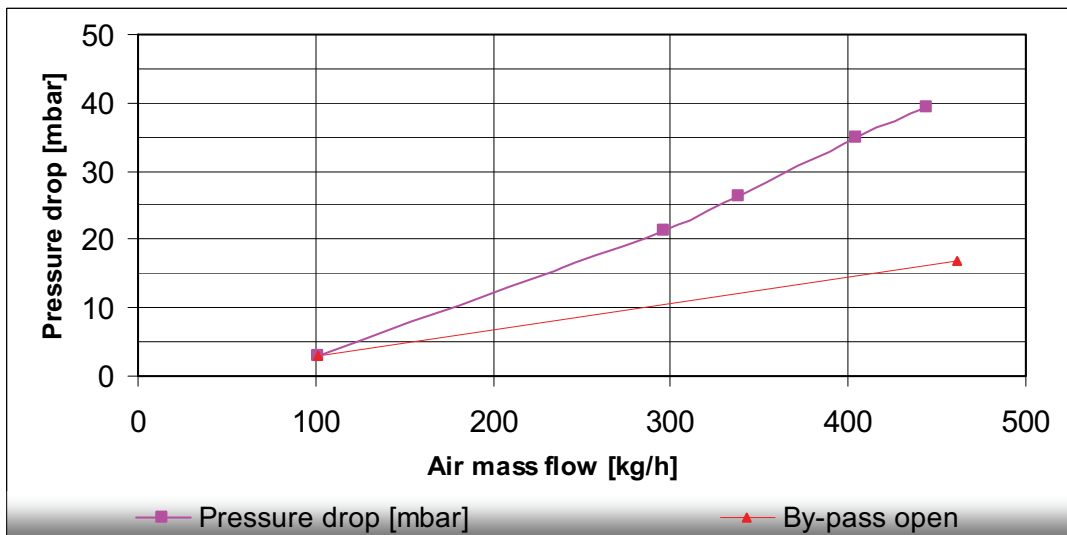
Fig. 8.17: Heat exchanger 2 pressure drop with respect to air mass flow

Figure 8.17 shows that the pressure drop in the heat exchanger is decreased by over 50% (from 39 to 17 mbar) when the bypass is fully opened.
Opening the bypass between the heat exchanger inlet and outlet reduces the air mass flow through the heat exchanger, thus reducing the pressure drop. The test results were employed to calculate the heat exchanger friction coefficient (ζ_{Hx}) presented in Figure 8.18 (s. Equation 7-17) for the SFBC steady state operation (s. App. II, Tab. 2).
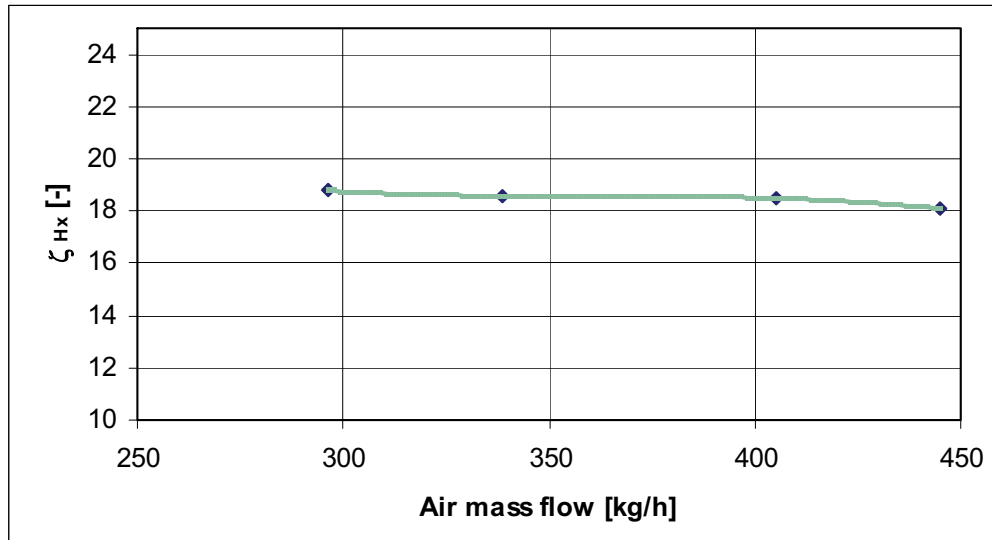
Fig. 8.18: Heat exchanger 2 friction factor with respect to air mass flow

The friction coefficient ($\zeta_{Hx} \approx 18.5$) was nearly constant as expected for full turbulent conditions. This allows the utilization of the friction coefficient to predict the pressure drop over the heat exchanger for the conditions expected in the SFBC-EFMGT cycle.

Figure 8.19 presents the predicted heat exchanger pressure drop[5], the 4% pressure drop limit and pressure drop with the bypass open when the air mass flow is increased to over 900 kg/h.
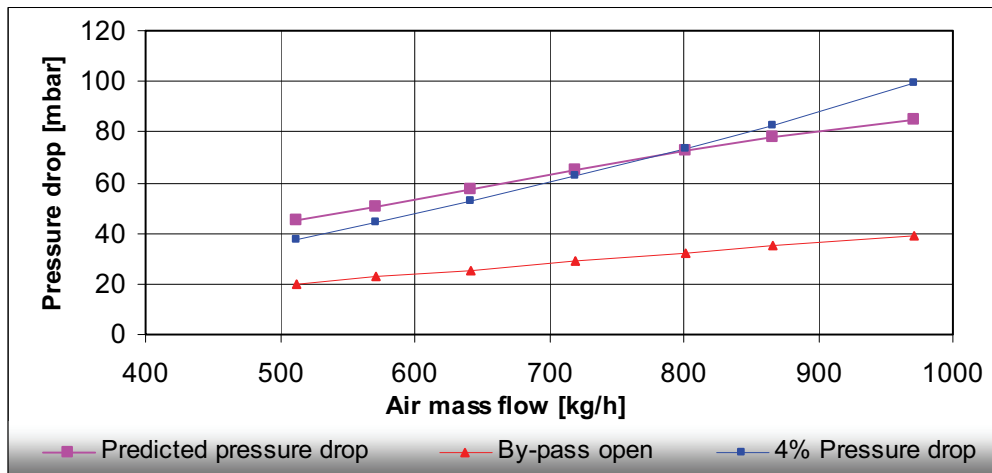
Fig. 8.19: Predicted heat exchanger pressure drop with respect to air mass flow

As seen in Figure 8.19 the predicted heat exchanger pressure drop lies above the 4% limit for the lower air mass flow. This is due to the lower air pressure build up in the compressor for the lower rotational speed. In the case that the turbine compressor reaches the pump-limit (when blocking occurs) the bypass can be opened to reduce the heat exchanger pressure drop. The opening of the bypass also lowers the air temperature after the heat exchanger, reducing the turbine power. By solving equation [7-20] iteratively (s. Chapter 9.2) for a given air mass flow (m_{Air}), fluidized bed temperature (T_{FB})[6], heat exchanger inlet temperature ($T_{Hx\ in}$) and fluidized bed heat transfer coefficient (α_{FB})[7], the heat exchanger outlet temperature ($T_{Hx\ out}$) and enthalpy (Q_{Hx}) can be calculated as shown in Figures 8.20 and 8.21.

---

[5] with a friction coefficient $\zeta = 18.5$
[6] A fluidized bed temperature of 850°C was selected.
[7] A fluidized bed heat transfer coefficient of 200 W/m²K was selected.
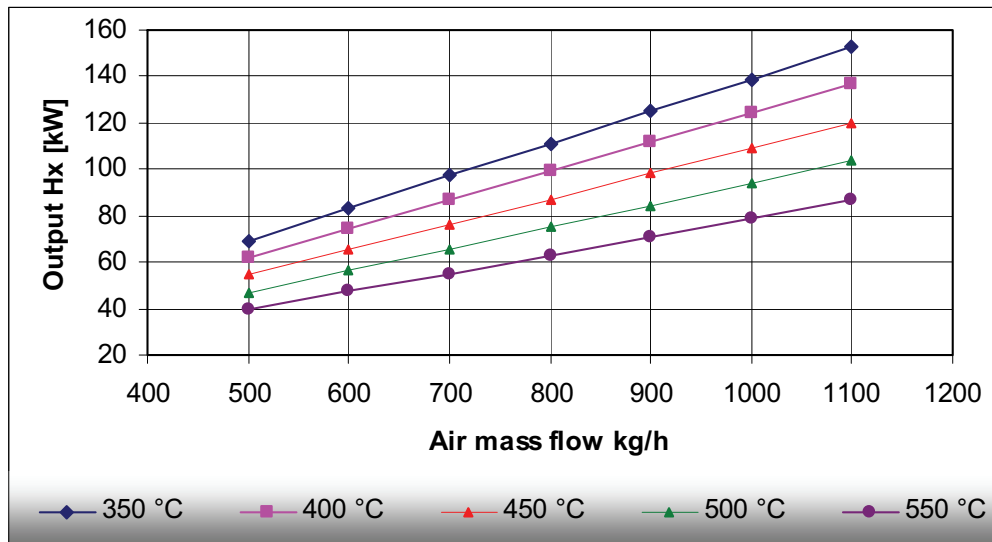
Fig. 8.20: Predicted heat exchanger output respective to inlet temperature and air mass flow

With increasing heat exchanger inlet temperature the heat flux from the fluidized bed to the compressed air stream decreases. The results presented in Figure 8.20 imply that the design heat exchanger output criterion of 100 kW$_{th}$ can be achieved with a heat exchanger inlet temperature of up to 500°C.

Figure 8.21 presents the simulated heat exchanger outlet temperatures with regard to heat exchanger inlet temperature and air mass flow. The heat exchanger input temperature depends on the output temperature of the recuperator. The air mass flow is a function of the EFMGT speed.
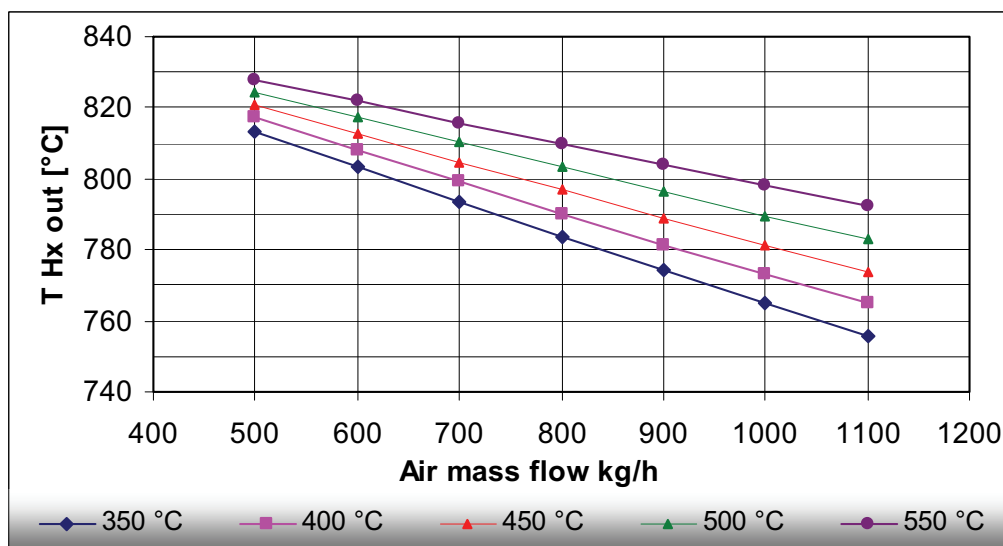
Fig. 8.21: Predicted outlet temperature with respect to inlet temperature and air mass flow

The simulation results imply that to maintain the design heat exchanger output criterion of 800°C at 1000 kg/h air mass flow, a heat exchanger inlet temperature of 550°C is necessary. The ideal heat exchanger inlet temperature therefore lies between of 500°C and 550°C (s. Fig. 8.20 and 8.21).

8.2.2   SFBC-EFMGT Test Series

After the reinstallation of the EFMGT the three SFBC-EFMGT tests shown in Table 8.2 were performed with the test bed configuration as shown in Figure 8.22.
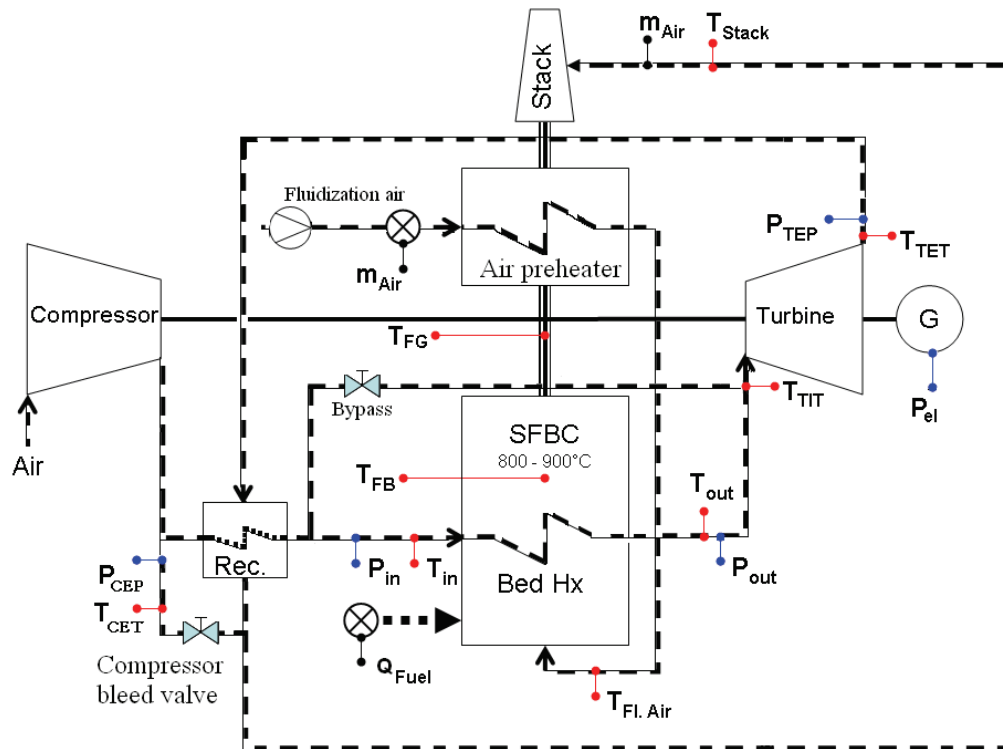
Fig. 8.22: Heat exchanger 2 SFBC-EFMGT test-bed configuration
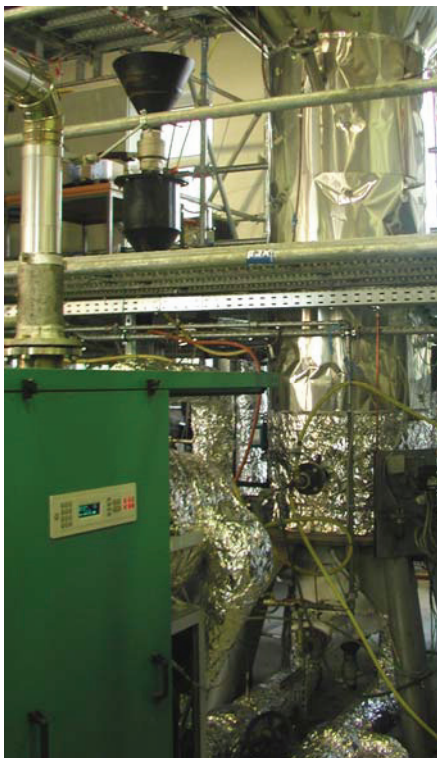
Fig. 8.23: a) EFMGT and SFBC reactor   b) SFBC fluidized bed heat exchanger 2

The schematic illustration of the heat exchanger 2 SFBC-EFMGT test-bed configuration presented in Figure 8.22 shows the relevant temperature (T), pressure (p) and mass flow (m) measurement points and the electrical output P_e. The measurement instrumentation is further described in Appendix III. The measurement data is given in Appendix II.

Figures 8.23 a, b show the coupling of the EFMGT with the SFBC reactor and the integration of heat exchanger 2 in the SFBC reactor respectively.

8.2.2.1 SFBC-EFMGT Test 1
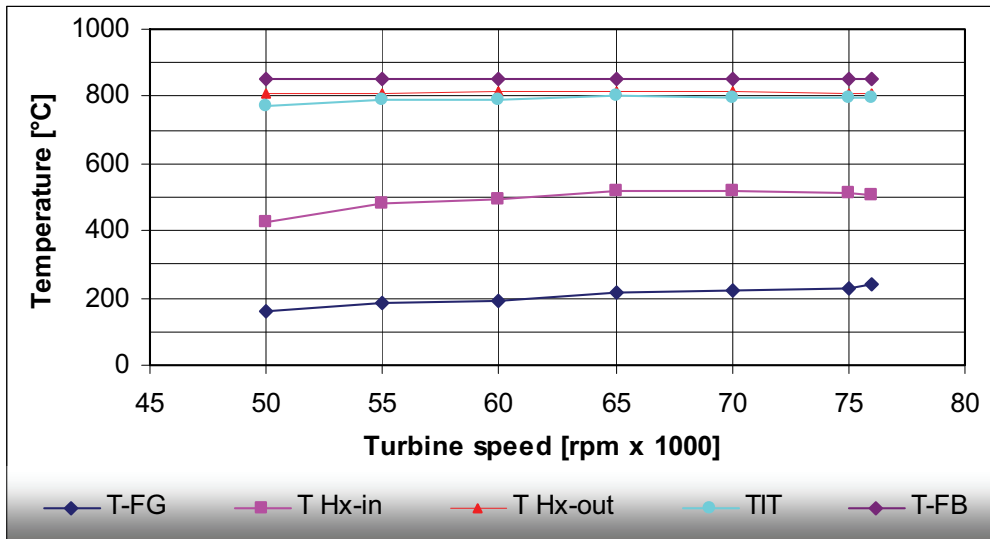
Fig. 8.24: SFBC-EFMGT temperature distribution with respect to turbine speed, test 1

A temperature after the heat exchanger (T Hx-out) of slightly over 800°C was achieved for the measured turbine operation range from 50 000 to 75 000 rpm with a heat exchanger inlet temperature range from 428°C to 519°C and a fluidized bed temperature of around 850°C as shown in Figure 8.24 (s. App. II, Tab. 3).

Figure 8.25 shows the measured compressor pressure in comparison to the standard MGT compressor pressure.
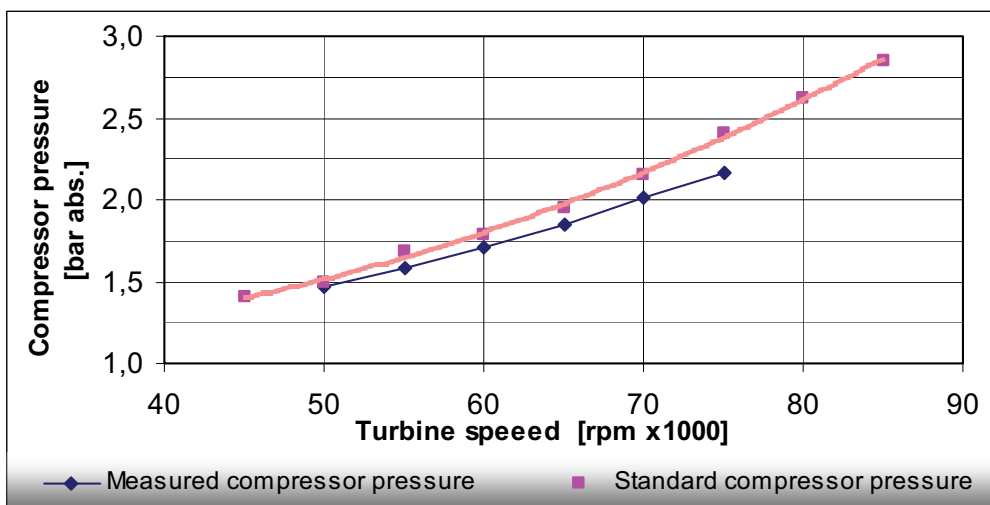
Fig. 8.25: Heat exchanger compressor pressure with respect to turbine speed, test 1

The lower pressure build-up by the compressor indicates that part of the compressor air is bypassing the turbine and escaping directly to the stack.
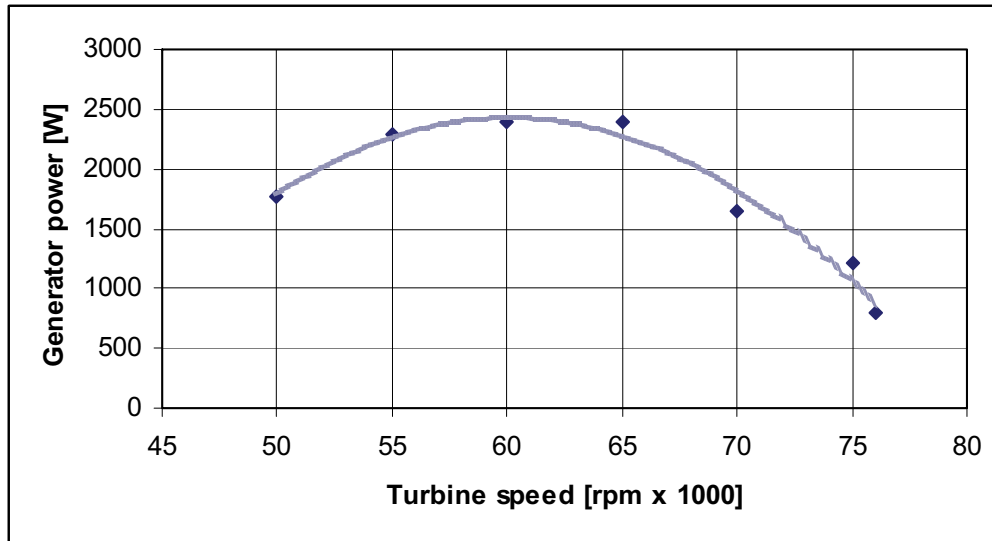
Fig. 8.26: EFMGT generator power output with respect to turbine speed, test 1

The maximal generator power output of 2.4 kWe was achieved at a turbine speed of 60 000 rpm as shown in Figure 8.26 (s. App. II, Tab. 4). The decreasing power generation with further increasing turbine speed is a further indication for internal air leakage problems. After the replacing a turbine seal with a welded connection further SFBC-EFMGT tests were performed.

8.2.2.2   SFBC-EFMGT Test 2
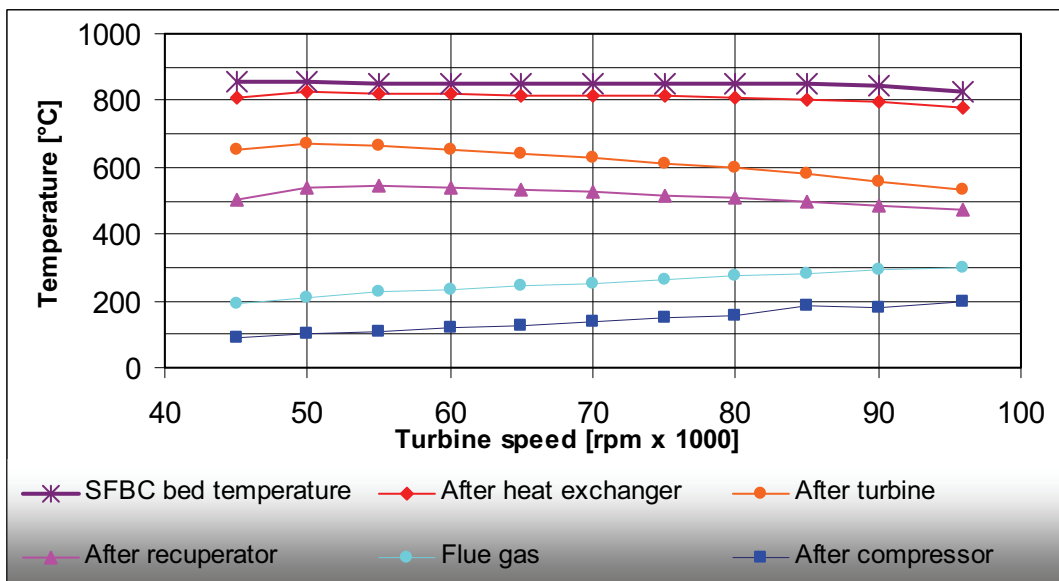
Fig. 8.27: SFBC-EFGT temperature distribution with respect to turbine speed, test 2

The temperature distribution shown in Figure 8.27 validates the ability of the heat exchanger to maintain the required temperature of around 800°C for practically the whole turbine operation range except for at the maximal turbine speed of 96 000 rpm. At 96 000 rpm the

SFBC reactor combustion temperature decreased to 829°C, which resulted in a comparative reduction in air temperature after the heat exchanger to 781°C.

This is because a further increase in SFBC fuel input was not possible due to increasing temperatures in the SFBC reactor freeboard. Usually the complete fuel combustion is maintained within the fluidization zone, but when the oxygen content is depleted to less than 4%[8] the combustion process continues in the freeboard leading to an increase in freeboard temperatures. The installation of the heat exchanger required the closing of the fluidizing air nozzles directly adjacent to the inlet and outlet tube to avoid sandblasting the tube surfaces. This resulted in a reduction in the maximal fluidization air flow.

Constructive measures such as additional fluidization air nozzles could be taken to allow for a higher fuel flow without increasing the freeboard temperature. Another possibility to alleviate this problem would be the installation of a "freeboard cooler" to pre-heat the fluidized bed combustion air as described in Chapter 5.1.3. (Gallmetzer et al. 2008).

The measured heat exchanger outlet temperature of over 800°C for nearly the whole turbine operation range (s. App. II, Tab. 5) suggests that the fluidized bed heat transfer coefficient (α_{FB}) for the simulation results presented in 8.20 and 8.21 was underestimated. Figure 8.28 presents the simulated fluidized bed heat transfer coefficient (α_{FB}) for the measured heat exchanger outlet temperature with respect to turbine speed.
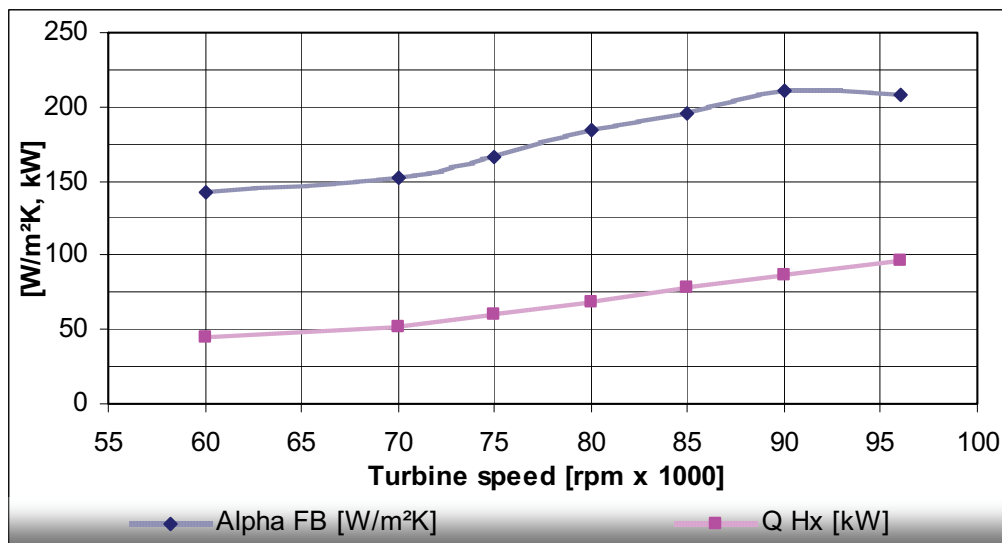
Fig. 8.28: SFBC heat transfer coefficient with respect to air mass flow, heat exchanger 2

The fluidized bed heat transfer coefficient (α_{FB}) increases with respect to increasing turbine speed i.e. air mass flow in the heat exchanger. This is due to the increased convective heat transfer from the inner heat exchanger wall to the compressed air stream within the heat exchanger tubes. The forced convective heat transfer within the heat exchanger tubes is the "pinch point" which limits the heat flux in the SFBC in-bed heat exchanger.

The heat exchanger thermal output reached 96 kW at a turbine speed of 96 000 rpm. Figure 8.29 presents the corresponding electrical output of the turbine.

---

[8] measured in the flue gas
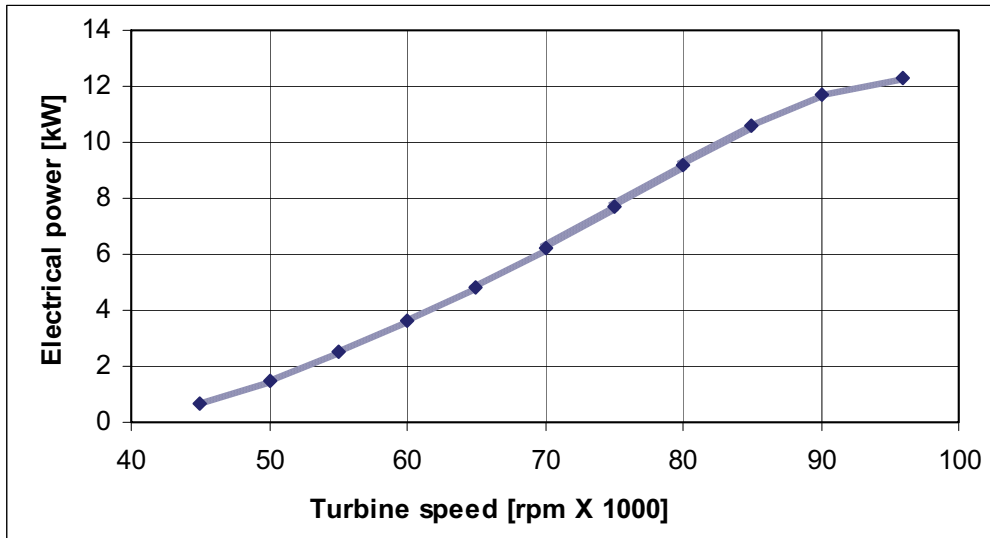
Fig. 8.29: EFMGT electricity generation with respect to turbine speed

The electricity generated by the EFMGT was fed into the University electrical grid. The electrical power generation during the test on 13.08.08 is shown in Figure 8.29. A maximum power output of 12.3 kW was measured at a turbine speed of 96 000 rpm (s. App. II, Tab. 6). The maximal electrical efficiency of the EFMGT calculated as the ratio of electrical output (P_e) to the heat exchanger thermal input[9] is thus:

$$\frac{P_e}{\dot{Q}\,Hx_{in}} = \frac{12.4}{96} = 0.13 \ [-] \qquad\qquad [8\text{-}2]$$

The achieved electrical efficiency of 13% is around half of the nominal electrical efficiency of the original Capstone C30 MGT. An electrical efficiency of around 15% could have been achieved if the SFBC bed temperature of over 850°C could have been held for the turbine operation speed of 96 000 rpm.
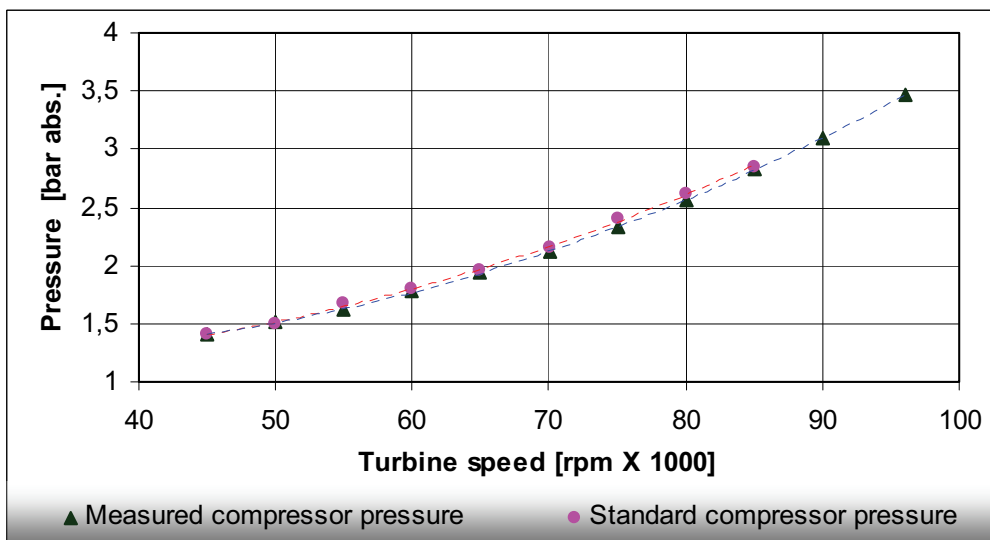
Fig. 8.30: EFMGT compressor pressure with respect to turbine speed

The compressor pressure shown in Figure 8.30 is only slightly lower than the standard Capstone C30 MGT compressor characteristic, which is a large improvement in comparison

---

[9] Based on the heat exchanger output calculated with the friction factor ζ =18.5

94

to the previous test (s. Fig. 8.25). An increase in electrical efficiency could be achieved by further decreasing the pressure drop in the heat exchanger and air lines, increasing the quality of the turbine seals to avoid internal air leakage, and decreasing the internal heat transport in the turbine.
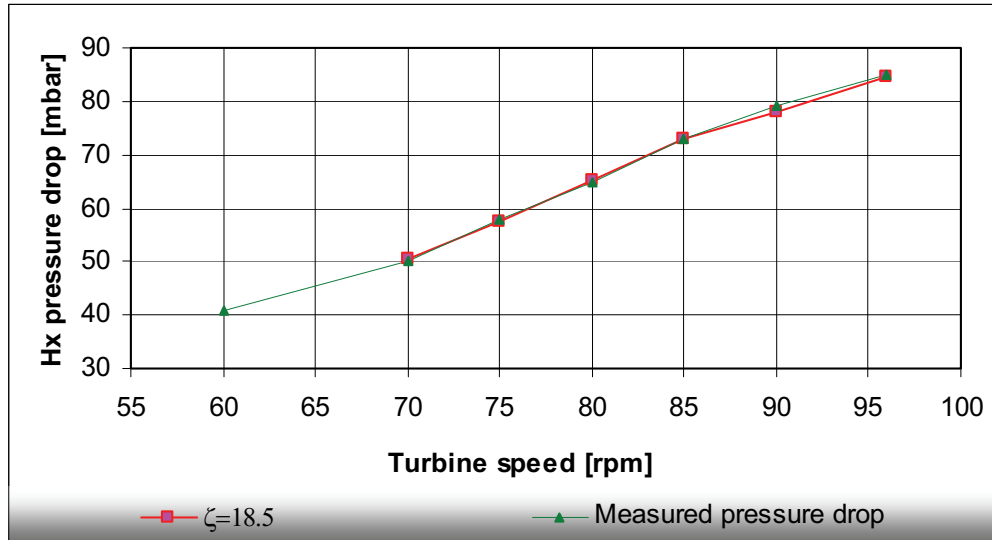
Fig. 8.31: Heat exchanger pressure drop with respect to turbine speed

The measured pressure drop in the heat exchanger as shown in Figure 8.31 is in excellent accord with the pressure drop calculated with the heat exchanger friction coefficient (ζ=18.5). Figure 8.32 presents the heat exchanger output calculated assuming that the total air mass flow measured in the stack passes through the heat exchanger, in comparison to the output calculated based on the determined friction coefficient.
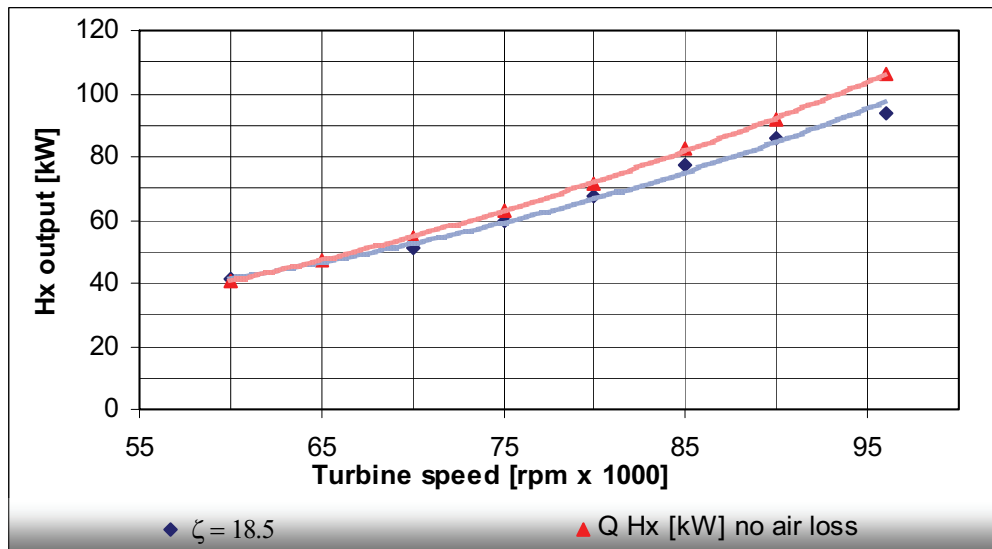
Fig. 8.32: Heat exchanger output with respect to turbine speed

The discrepancy between the estimated heat exchanger output determined with the friction coefficient (ζ) and the heat exchanger output calculated based on the air mass flow measured in the stack increases with turbine speeds above 60 000 rpm. At 96 000 rpm the difference amounts to around 10 kW.
To clarify this situation in the SFBC-EFMGT test 3 the heat extracted from the fluidized bed was also determined with the SFBC energy balance (s. Fig. 8.40).

The heat exchanger operation characteristics: number of transfer units (*NTU*), heat exchanger effectiveness (Φ) and heat transfer coefficient (k_a) were determined based on the air mass flow determined with the friction coefficient as described in Appendix II, Tab. 2.
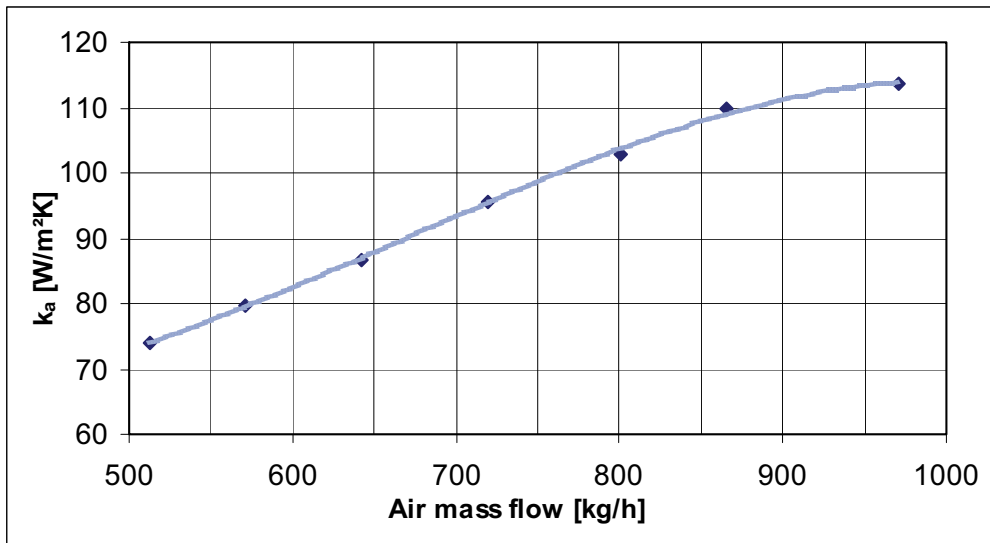
Fig. 8.33: Heat exchanger heat transfer coefficient with respect to turbine speed

An increase in the heat transfer coefficient (k_a) from 73 W/m²K at 60 000 rpm, to 113 W/m²K at 96 000 rpm was determined (s. Fig. 8.33).
This behaviour can be explained by the increasing convective heat transfer from the inner heat exchanger wall to the compressed air stream as a result of increasing air velocity and turbulence.
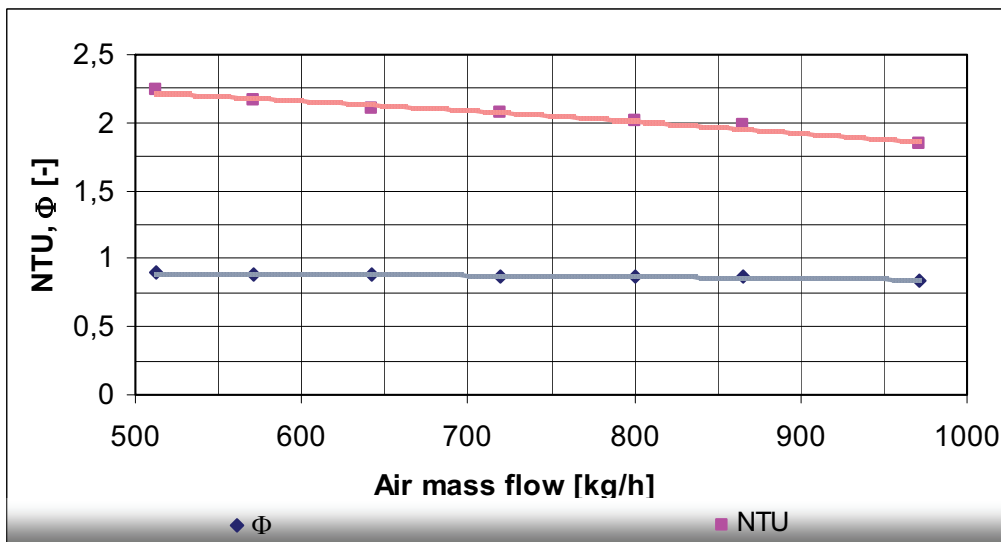
Fig. 8.34: Number of transfer units (*NTU*) and heat exchanger effectiveness (Φ)

The heat exchanger effectiveness (Φ) remained relatively constant (0.87 to 0.84), however the number of transfer units (*NTU*) dropped (from 2.35 to 1.83) with increasing air mass flow in the heat exchanger as shown in Figure 8.34.
This can be explained by the increasing temperature difference between fluidized bed temperature and heat exchanger outlet temperature as shown in Figure 8.35.
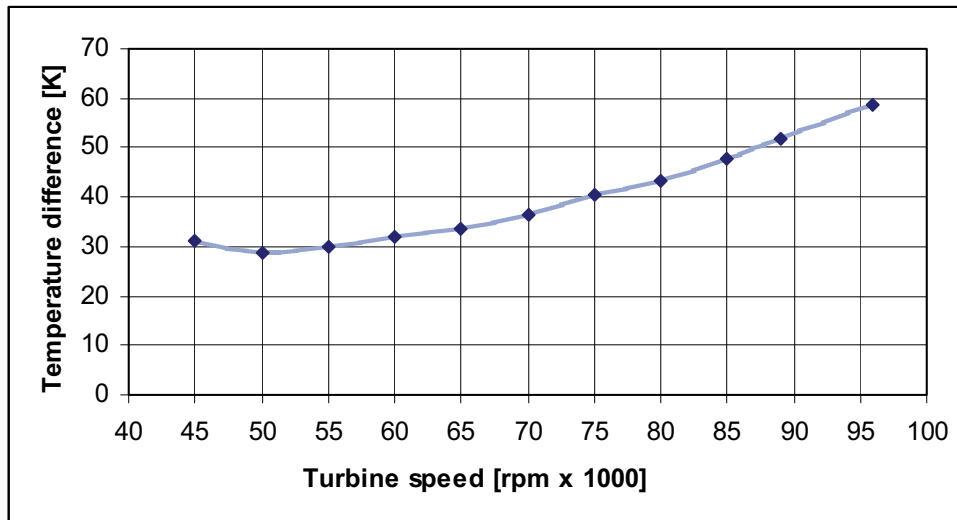
Fig. 8.35: Temperature difference between fluidized bed and heat exchanger outlet

The increase in temperature difference between the fluidized bed and the heat exchanger air outlet temperature runs parallel to a decrease in heat exchanger inlet temperature (from 494°C to 465°C, s. App. II, Tab. 5) i.e. temperature after the recuperator (s. Fig. 8.27).
A further test was performed to assess the SFBC-EFMGT operation with extracted colza cake, a biomass residue from the rapeseed oil production process.

8.2.2.3   SFBC-EFMGT Test 3

Concerning the heat exchanger and turbine operation the results obtained in tests 2 and 3 were practically identical.
The SFBC feedstock does not influence the EFMGT operation when the biomass combustion temperature is over 850°C such as is the case for rapeseed residues.
The SFBC reactor was fired with natural gas and light fuel oil and then rapeseed residues to enable a direct comparison of SFBC-EFMGT operation with biomass and conventional fuel.
The operation characteristics with conventional fuel and biomass were identical, and show only minimal difference to the results achieved in test 2.

The maximal electrical output was 12.4 kW at 96 000 rpm; the heat exchanger outlet temperature difference (T_{SFBC} - $T_{Hx\ out}$) rose from 31.1K at 45 000 rpm to 58.8K at 96 000 rpm and the heat exchanger exit temperature fell from 822°C to 781°C respectively [s. App II, Tab. 7]

Figure 8.36 shows a LabView temperature strip chart of the EFMGT and heat exchanger. The temperature before the turbine (yellow) is slightly lower than the temperature after the heat exchanger (blue) due to heat dissipation in the air lines. The temperature before the heat exchanger (green) sinks with increasing air mass flow due to decreasing recuperator outlet temperature. The increase in air mass flow is reflected in the increasing temperature after the compressor (white) and in the stack (red).
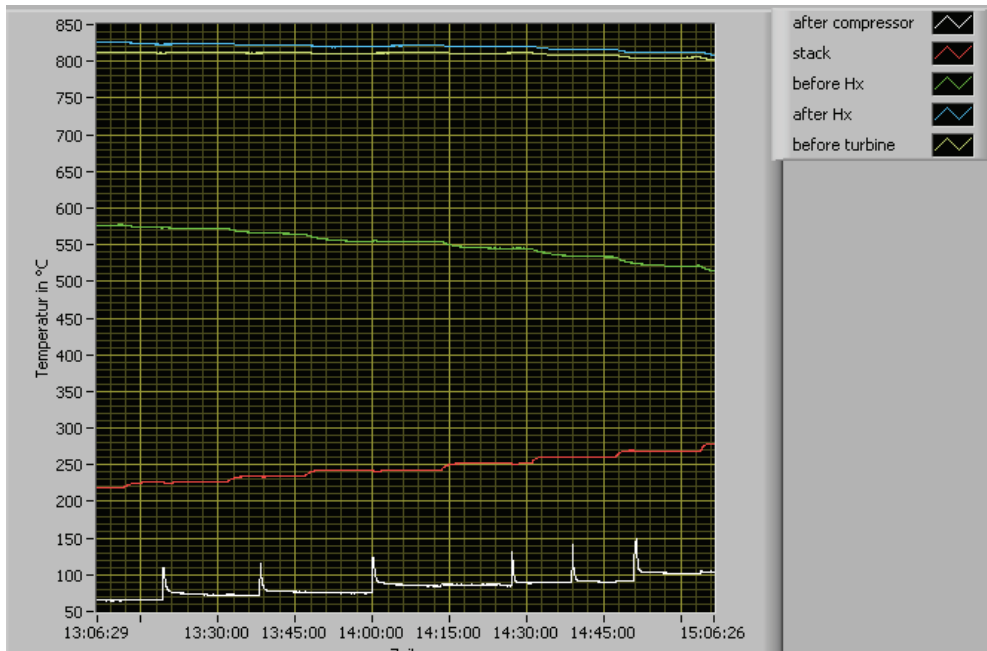
Fig. 8.36: Temperature strip chart of the EFMGT-SFBC test 3

The temperature after the compressor was measured in the compressor bleed valve air stream (s. Fig. 8.22). As during normal operation this valve is closed, the measured temperature is the static air temperature. To measure the correct air temperature the valve was opened (white peaks in Figure 8.36). The maximum peak temperature is an estimate of the temperature after the compressor. The "real" temperature after the compressor is somewhat higher because the opening of the bleed valve caused a slight system pressure drop and therefore lower compressor outlet temperatures.
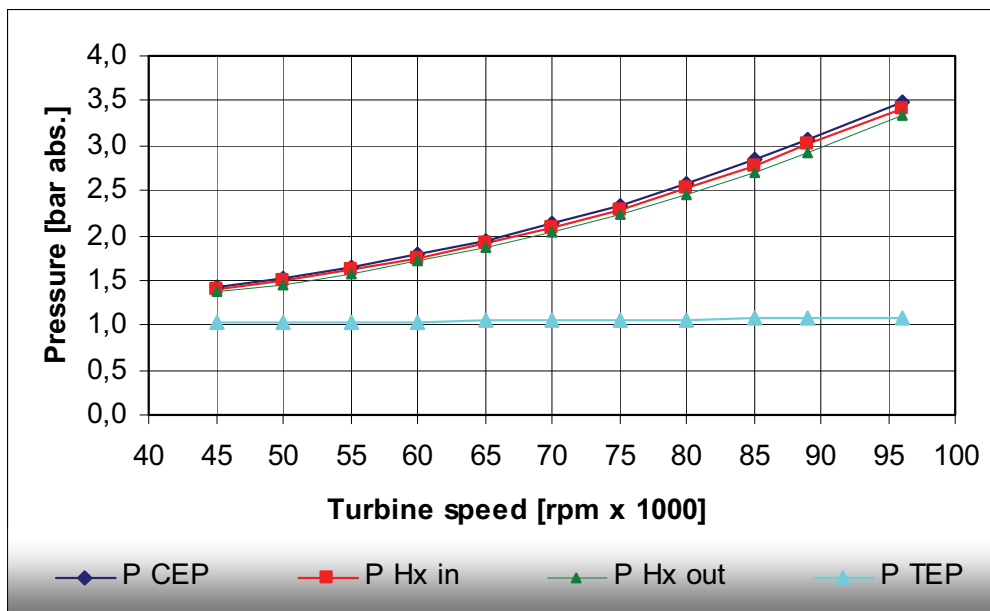
Fig. 8.37: EFMGT system pressure distribution with respect to turbine speed

Figure 8.37 shows the air pressure distribution within the EFMGT and heat exchanger (s. App. II, Tab. 7). At a turbine speed of 96 000 rpm a maximal compressor pressure of 3.493 bar (absolute pressure) was measured. The pressure loss in the recuperator resulted in a heat exchanger inlet pressure of 3.422 bar (Δp = 71 mbar). The pressure drop in the heat exchanger

(Δp = 87 mbar) resulted in a pressure of 3.335 bar before the turbine. This amounts to a total pressure drop of 158 mbar as shown in Figure 8.38.
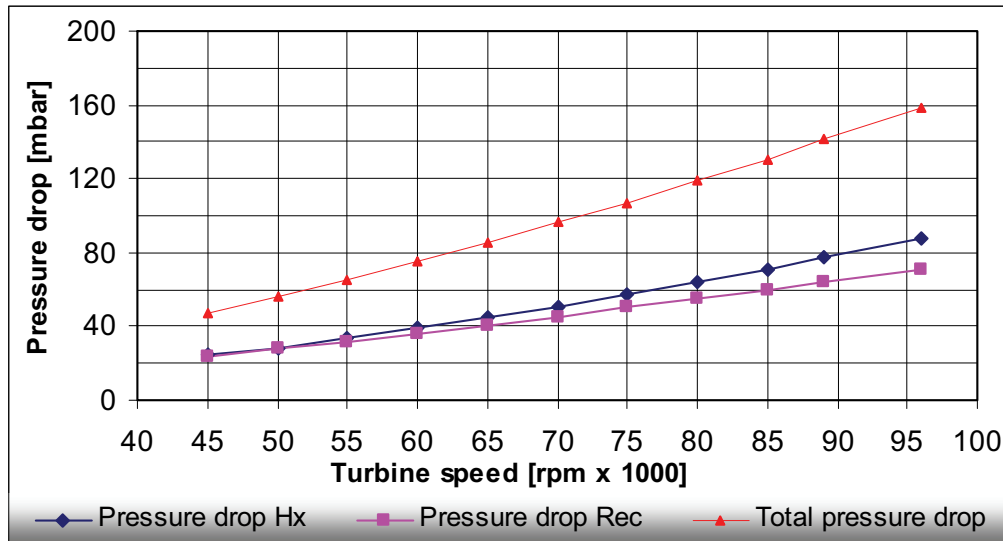
Fig. 8.38: EFMGT system pressure drop with respect to turbine speed

The measurement of the air mass flow in the stack after the turbine with a Prandtl probe (s. App. II, Tab. 8) was an important aspect of the SFBC-EFMGT test 3. The results were in very good accord with earlier measurements and validated that the EFMGT compressor is able to generate the nominal MGT air mass flow of 0.31 kg/s at full load (s. Fig. 8.39).
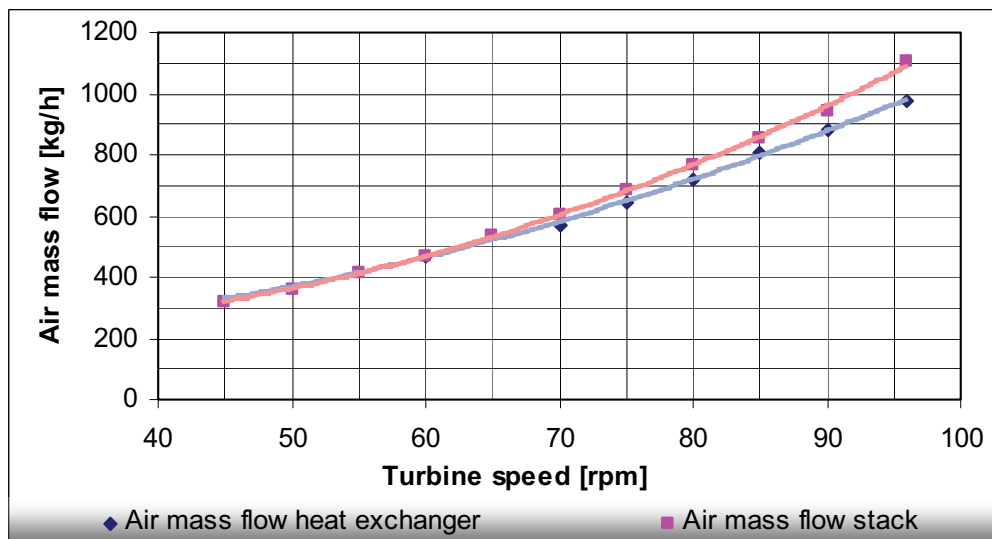
Fig. 8.39: EFMGT air mass flow with respect to turbine speed

However, the air mass flow in the heat exchanger calculated with the friction coefficient (ζ) is significantly lower than measured in the stack for turbine speeds above 70 000 rpm as seen in Figure 8.39. The lower air mass flow corresponds to the lower than expected heat exchanger output.

To confirm the heat exchanger thermal output the heat extracted from the SFBC reactor in steady state condition (s. App. II, Tab. 9) was determined based on the SFBC energy balance (s. Fig. 8.40).
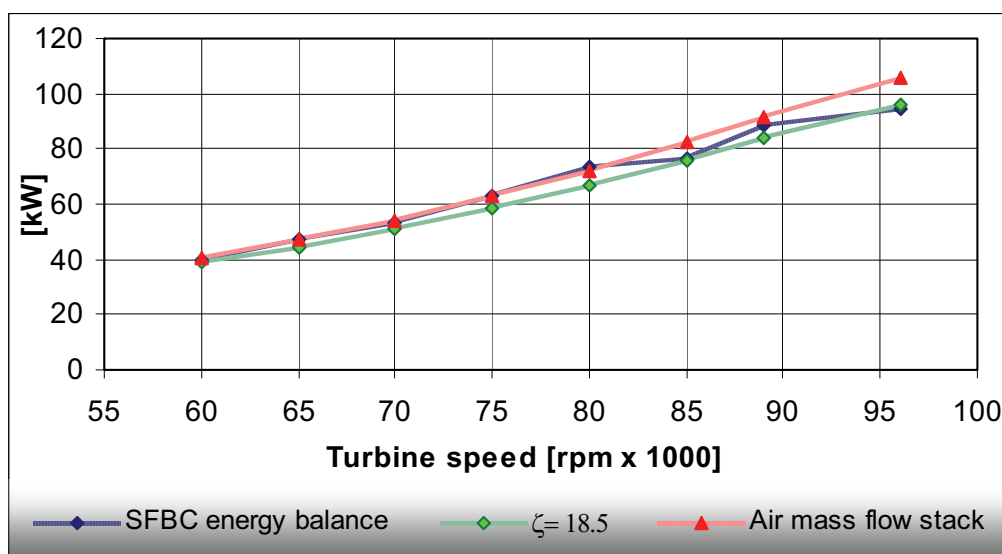
Fig. 8.40: Heat exchanger output from SFBC energy balance

Figure 8.40 shows the heat exchanger output calculated with three methods. The red line describes the heat exchanger output when the total air mass flow measured in the stack passes through the heat exchanger, i.e. the maximum heat exchanger output.
The green line shows the heat exchanger output when only the air mass flow calculated with friction coefficient (ζ) passes through the heat exchanger. The blue line represents the heat exchanger output determined with the SFBC energy balance.
The energy balance calculations must, however be treated with caution because the requirement of absolutely stable SFBC operating conditions was very difficult to maintain especially with respect to the freeboard temperature.

The heat exchanger output calculated from the SFBC energy balance suggests that the possible air leakage is not as severe as expected from the friction coefficient calculations, but nevertheless could be significant for turbine speeds > 85 000 rpm, although there is some evidence that the lower output for the turbine speeds 85 000 and 96 000 rpm could be due to not stationary conditions in the fluidized bed at the time of measurement. There is also some uncertainty with respect to the accuracy of the temperature measurement after the heat exchanger due to the high viscosity of the fluid and the possibility of a laminar temperature gradient within the air lines. Although this should not be significant, at least for the higher turbine speeds due to the high velocities (25-50 m/s) and therefore high Reynolds numbers (4×10^4 to 9×10^4) at the measurement point.
Also a slight air leakage which increases with increasing pressure would explain why the increase in electricity generation as shown in Figure 8.29 begins to flatten out at turbine speeds over 85 00 rpm.

The only sure method to test this hypothesis would be to reopen the turbine and replace the relevant seal with a welded seal, and perform further tests. In this case the SFBC reactor would also need to be adapted to allow for a greater fluidization air mass flow, thus reducing the freeboard temperature and enabling a higher enthalpy extraction from the bed. This course of action is recommended for further research but unfortunately can not be covered in this dissertation.

9   SFBC-EFMGT Theoretical Modelling

The theoretical modelling of the SFBC-EFMGT system enables the assessment of the plant efficiency and prediction of the plant behaviour under variable conditions.

The test bed configurations described in Chapter 8 (s. Fig. 8.22) represent by no means the optimal plant configuration, but allowed the measurement and assessment of the plant behaviour, on which well grounded simulation models have been developed.

9.1   SFBC-EFMGT Heat Exchanger 1 Simulation

The heat exchanger 1 test data (s. App. I) was utilized, within the framework of an undergraduate syllabus project, to develop a theoretical model of the SFBC-EFMGT cycle conforming to the relevant technical guidelines (VDI 4670) for the calculation of thermodynamic properties of humid air and combustion gases.

Figure 9.1 shows the schematic diagram of the SFBC-EFMGT test-bed process with the simulation key points 1-6.
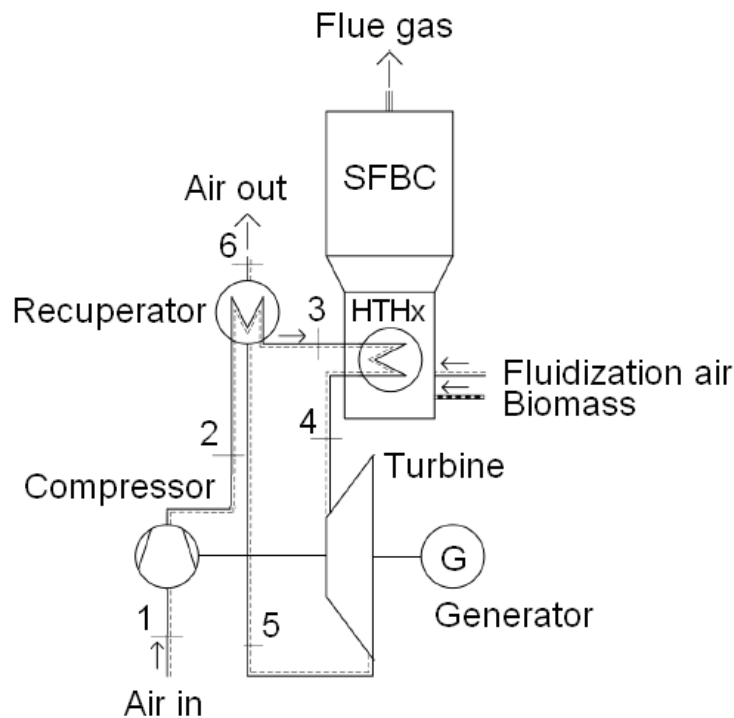
Fig. 9.1: SFBC-EFMGT test-bed simulation diagram

The main purpose of the study was to simulate the operation characteristics of the heat exchanger and EFMGT with a higher compressor ratio to assess the potential of the process with a different compressor design.

The specific enthalpy and entropy (h-s) diagram shown in Figure 9.2 was calculated with the theoretical model for a compressor ratio of $\pi = 5$ and an air mass flow $\dot{m}_{Air} = 400$ kg/h. The heat exchanger pressure drop, which is evident in the difference in isobars p_2 and p_4 (s. Fig. 9.2), was determined with the heat exchanger friction factor calculated as described in equation [7-17].
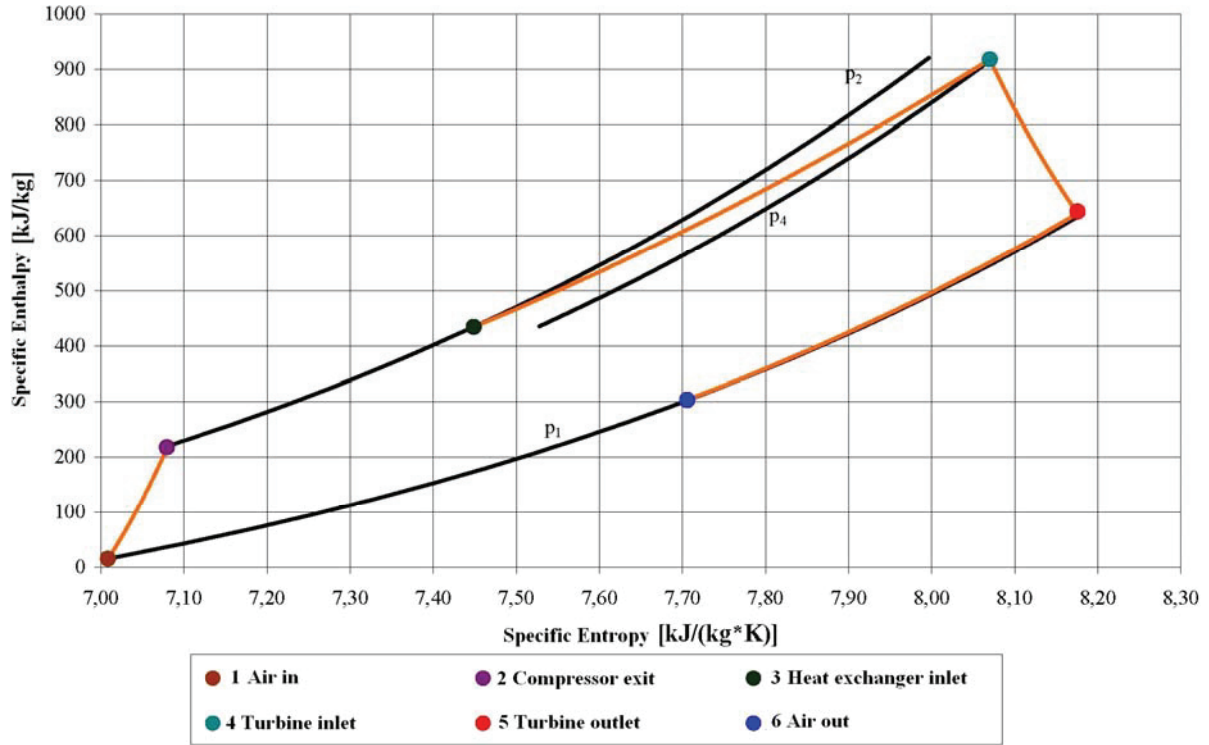
Fig. 9.2: SFBC-EFMGT test-bed simulation h-s diagram

The air mass flow was increased from 50 kg/h to 550 kg/h in steps of 50 kg/h with a compressor ratio compressor ratio π= 5 and a fluidized bed temperature of 850°C.

$$\eta_{th} = \frac{P_T - P_C}{\dot{Q}_{in}} = \frac{(h_4 - h_5) - (h_2 - h_1)}{(h_4 - h_3)} \tag{9-1}$$

$$Pe = (P_T - P_C)\eta_m\eta_e \tag{9-2}$$

The thermal efficiency (s. Eq. 9-1) decreases with increasing air mass flow from around 21% at 50 kg/h to around 5% at 550 kg/h as shown in Figure 9.3.
The main reason for the reduction in efficiency with increasing air mass flow is the increasing pressure drop in the heat exchanger. The pressure drop increases with respect to the squared air velocity in the heat exchanger tubes (s. Equation 7-15) and the velocity increases linearly with the air mass flow, i.e. the pressure drop increases quadratically with regard to the increase in air mass flow. Due to the increasing pressure drop the enthalpy difference in the turbine decreases and the turbine efficiency sinks.
The electrical output[1] (s. Equation 9-2) on the other hand increases initially from around 4 kW to around 7.5 kW due to the beneficial effect of the increased air mass flow.
However, after reaching the optimal air mass flow of 375 kg/h the detrimental effect of the increased heat exchanger pressure drop prevails and the electrical output sinks rapidly as shown in Figure 9.3.

---

[1] Calculated with $\eta_m = 0{,}97$ and $\eta_{el} = 0{,}96$
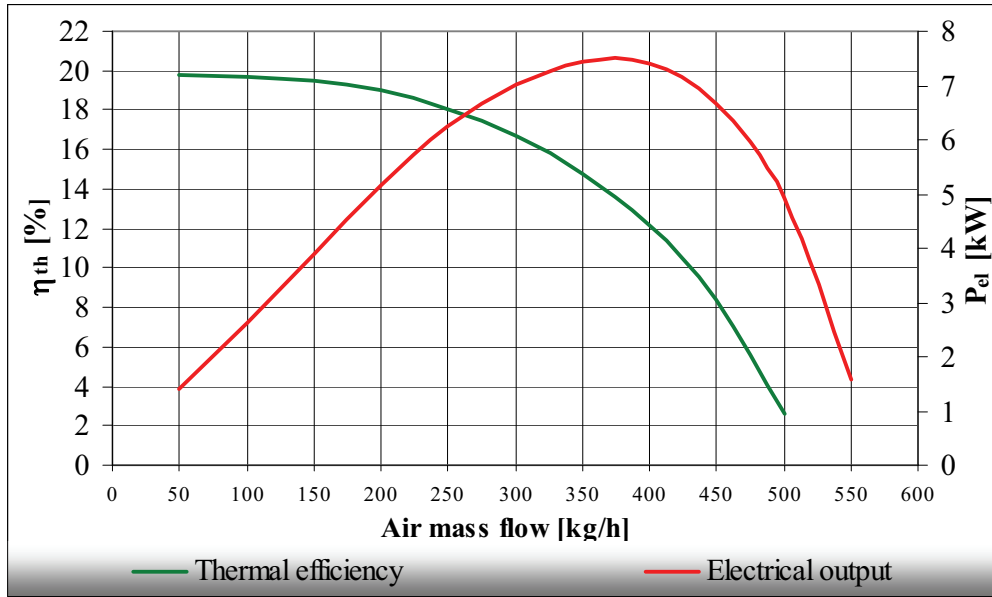
Fig. 9.3: SFBC-EFMGT test-bed simulation: Thermal efficiency and electrical output

9.2   SFBC-EFMGT Heat Exchanger 2 Simulation

9.2.1   Heat Exchanger 2 Preliminary Test Model

Based on the preliminary heat exchanger 2 test results (s. App. II Tab. 1) a steady state iterative model was developed for the prediction of the SFBC heat exchanger operation with the EFMGT based on the thermodynamic principles described in Chapter 7.2.2 and 7.2.3. The simulation model results are shown in Chapter 8.2.1 Figures 8.20 and 8.21.
The model is also employed to iteratively determine the fluidized bed heat transfer coefficient when the heat exchanger exit temperature is known. The iterative model balances equation [9-3 see also 7-20] shown below.

$$\dot{Q}_{Hx} = \dot{m}_{Air} \times Cp_{m\,Air} \times \Delta T_{Air} = kA \times LMTD \qquad [9\text{-}3]$$

However, the matter is complicated by the uncertainty of the exact air mass flow in the heat exchanger due to the possibility of internal air leakage in the turbine.
The simulation model accurately reproduced the measured heat exchanger outlet temperature and thermal output with the air mass flow[2] calculated with the friction coefficient (ζ)[3] and the iteratively determined (s. Fig. 8.28) fluidized bed heat transfer coefficients (α_{FB}) as shown in Figure 9.4. The results verified that the heat exchanger design is suitable to deliver the required heat flux to the turbine with the required temperature, and underlines the effect of falling heat exchanger inlet temperatures. A further increase in heat exchanger inlet temperature, for example with an air pre-heater in the SFBC flue gas, would also have a beneficial effect.

---

[2] s. App. II Tab. 8
[3] s. App. II Tab. 2
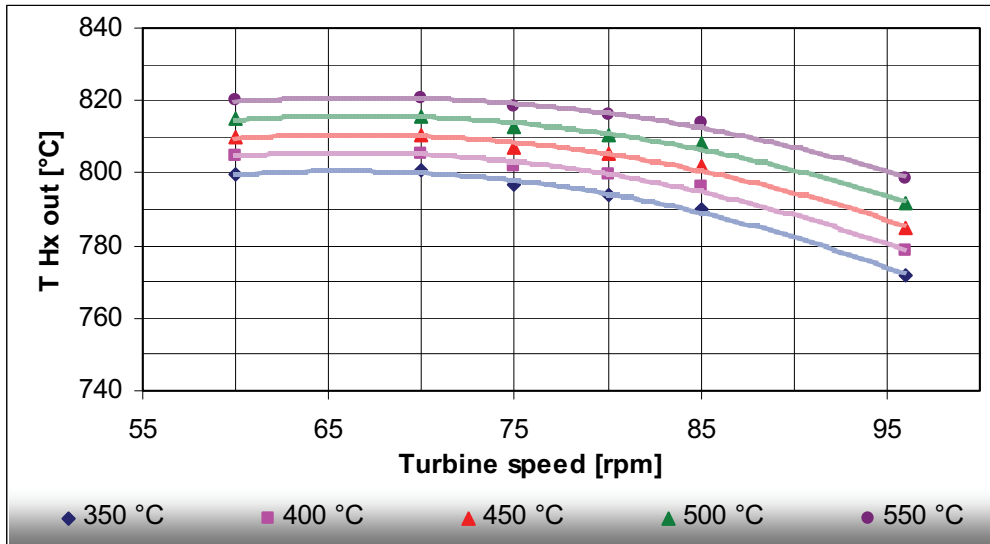
Fig. 9.4: Heat exchanger outlet temperature with respect to inlet temperature and air flow

9.2.2   SFBC-EFMGT Ebsilon Process Simulation

Within the context of a diploma thesis at the University of Rostock, Chair of Energy Systems and Turbo Machinery, the commercial process simulation software Ebsilon professional 7.0 (s. App. III, e) was employed to develop a SFBC-EFMGT model based on the heat exchanger prototype 2 operation data (s. App II, Tabs. 6 to 10).

The data was recorded for steady state turbine operation at speeds of 45 000 rpm to 90 000 rpm in steps of 5 000 rpm and also the operation speeds 89 000 rpm and 96 000 rpm. The significant process data (s. Fig. 8.22) was automatically recorded every 3 seconds with the respective measurement and automation software (s. App. III). The data gives a quasi transient map of the SFBC-EFMGT plant operation over the entire turbine speed range.

By describing the operation data points with the Gauss-Siedel method a continuous curve is created from which the whole process can be accurately replicated for any turbine speed. For a given turbine speed the software calculates the air mass flow (m) temperature (T), pressure (p) and enthalpy ($\dot{Q}$) of the working fluid for the process key points.

Table 9.1: Ebsilon process simulation key points

1	Compressor inlet
2	Compressor exit
3	Heat exchanger inlet
4	Heat exchanger outlet
5	Turbine inlet
6	Turbine exit
7	Stack

1   Compressor inlet

The first step involves the determination of the compressor inlet air state and the calculation of entropy with respect to the standard state values.

Table 9.2: Ebsilon process simulation standard state values

Standard pressure (p_0)	101.325	[kPa]
Standard temperature (T_0)	273.15	[K]
Relative humidity (rh)[4]	60	[%]

Humid air is a mixture of water vapour and the gases Nitrogen (N_2), Oxygen (O_2) with traces of Argon (Ar), carbon dioxide (CO_2) and Neon (Ne) which within the temperature range 200 to 3300K and near atmospheric pressure behaves as an ideal gas (VDI 4670).
The humid air molar enthalpy $h^0_{M,mix}$ with respect to the gas temperature (T) can therefore be determined as the sum of the enthalpy of each individual component $h^0_{M,k}(T)$ multiplied with their respective volumetric content (x_k) as shown in equation [9-6][5] and [9-7].

$$h^0_{M,k}(T) = c_{k,0} + \sum_{i=1}^{K} c_{k,i}\left(\frac{T}{T_0}\right)^{b_i+1} \qquad [9\text{-}6]$$

$$h^0_{M,mix}(T,\bar{x}) = \sum_{i=1}^{K} h^o_{M,k}(T)x_k \qquad [9\text{-}7]$$

The specific enthalpy h^0_{mix} is the ratio of the molar enthalpy to the molar mass of air.
The specific entropy is determined in a similar manner. First the molar entropies of the individual components $s^0_{M,k}$ with respect to the gas temperature (T) and pressure (p) are determined [9-8][6], and subsequently the molar entropy of the gas mixture $s^0_{M,mix}(T,p,\bar{x})$ is calculated [9-10]. The specific entropy is calculated by division of the molar entropy of the gas mixture with the molar mass of air.

$$s^0_{M,k}(T,p) = d_{k,0} + d_{k,1}In\left(\frac{T}{T_0}\right) - R_M In\left(\frac{p}{p_0}\right) + \sum_{i=2}^{10} d_{k,i}\left(\frac{T}{T_0}\right)^{b_1} \qquad [9\text{-}8]$$

$$s^0_{M,mix}(T,p,\bar{x}) = \sum_{K=1}^{K} x_k s^0_{M,k}(T,p) - R_M \sum_{K=1}^{K} x_k In(x_{k)} \qquad [9\text{-}9]$$

Thus for a given temperature and pressure the enthalpy (h) and entropy (s) of the working fluid can be explicitly defined from which all relevant thermodynamic properties can be derived.

---

[4] Ratio of the water vapour partial pressure to the saturation pressure
[5] c_{ko}, c_{ki} are material specific constants (j*mol^{-1}), b_i is the polynomial equation temperature exponent (VDI 4670)
[6] $d_{k,0}$, $d_{k,1}$, $d_{k,i}$ are material specific constants, R_M ideal gas constant (VDI 4670)

2   *Compressor exit*

To calculate the fluid entropy and enthalpy after the compressor, as shown in equations [9-6] to [9-9] above, the temperature and pressure after the compressor must be determined.
The pressure after the compressor with respect to the turbine speed was measured (s. App II, Tab. 6).
By generating characteristic functions which fit the measured data Ebsilon is able to accurately determine the pressure after the compressor for any turbine speed.
The second degree polynomial equation [9-10] for example reproduces the measured compressor pressure (y) as a function of the turbine speed (x) with a correlation of $R^2 > 0.999$.

$$y = 0.0004648x^2 - 0.0248299x + 1.5935987 \qquad [9-10]$$

The temperature after the compressor was measured in the compressor bleed valve. To obtain a more accurate temperature value the compressor bleed valve was opened very slightly (so that the compressor outlet pressure remained unchanged) until a constant temperature was achieved.
The ideal isentropic compression temperature (T_{2s}) can be calculated with the compressor ratio (π) as shown in equation [9-11 s. also 2-16].

$$T_{2,s} = T_1 (\pi)^{\frac{x-1}{x}} \qquad [9-11]$$

With equations [9-6] and [9-7] the enthalpy (h_{2s}) can be calculated for the temperature (T_{2s}). With the enthalpy h_2 and h_{2s} the compressor inner efficiency (η_{iC}) can be calculated as shown in equation [9-12, s. also 2-13].

$$\eta_{iC} = \frac{h_{2s} - h_1}{h_2 - h_1} \qquad [9-12]$$

3   *Heat exchanger inlet*

The heat exchanger inlet temperature and pressure is dependant on the temperature increase and pressure drop in recuperator respectively.
The pressure drop ($1 \Rightarrow 2$) in the recuperator was measured (s. App. II, Tab. 6) and can, for example, be described with respect to turbine speed as a polynomial function [9-13] with a correlation of $R^2 > 0.999$.

$$y = 0.0004623x^2 - 0.0254208x + 1.6021971 \qquad [9-13]$$

The pressure in the stack was assumed to be equal to the ambient pressure so that the pressure loss in the recuperator ($5 \Rightarrow 6$) can be calculated from equation [9-14]:

$$p_{loss} = p_3 - p_{ambient} \qquad [9-14]$$

The temperature increase in the recuperator, on the other hand, corresponds to the turbine exit temperature (*TET*) and is calculated iteratively until the system enthalpy steams are in balance as shown in Figure 9.5.

Heat given to primary flow	Q21	90.2036406885	kW
Transferred heat	QT	90.203639043	kW
Heat delivered from sec. flow	Q34	90.2036406884	kW
Heat transfer coefficient	KA	0.7154097537	kW/K
Mean log temperature diff.	DTM	126.0866776992	K
Lower terminal temperature diff.	DTLO	129.8534237403	K
Upper terminal temperature diff.	DTUP	122.393488708	K
KA calculated from characteristic line	KACL	0.7154097537	-

Fig. 9.5: Heat transfer in the recuperator with respect to a turbine speed of 96 000 rpm

4   *Heat exchanger outlet*

Both the pressure drop and temperature increase in the heat exchanger were measured (s. App. II, Tab. 6) and can be described as a function of the turbine speed with a high degree of accuracy ($R^2 > 0.99$ respectively).
The fluidised bed temperature can be assumed to be constant (s. App II, Tab. 8), up to a turbine speed of 90 000 rpm as discussed in Chapter 8.2.2.2.
For the Ebsilon model a constant fluidized bed temperature of 850°C was selected irrespective of the turbine speed. The heat transfer in the heat exchanger is shown in Figure 9.6 for a turbine speed of 89 000 rpm.

Heat given to primary flow	Q21	95.2744019615	kW
Transferred heat	QT	95.2743984816	kW
Heat delivered from sec. flow	Q34	95.2744021416	kW
Heat transfer coefficient	KA	0.5668561548	kW/K
Mean log temperature diff.	DTM	168.0750886799	K
Lower terminal temperature diff.	DTLO	375.8840178356	K
Upper terminal temperature diff.	DTUP	56.0595114759	K
KA calculated from characteristic line	KACL	0.5668561548	-

Fig. 9.6: Heat transfer in the heat exchanger with respect to a turbine speed of 89 000 rpm

5   *Turbine inlet*

The measured turbine inlet temperature (s. App. II, Tab. 6) is a function of the heat exchanger outlet temperature minus the loss in the air lines to the turbine. The temperature difference declines with the increase in turbine speed (i.e. air mass flow). The pressure loss in the air lines is assumed negligible so that the heat exchanger outlet pressure is equal to the turbine inlet pressure.

6   Turbine exit

The turbine exit temperature (T_5) and pressure (p_5) were measured (s. App. II, Tabs. 6 and 7) and, for a given constant fluidized bed temperature, can be described as a function of the turbine speed with a very high degree of accuracy ($R^2 > 0.999$ respectively).

The ideal isentropic temperature ($T_{6,s}$) can be calculated from T_5 with the turbine pressure ratio (π_T) as shown in equation [9-15 s. also 2-11].

$$T_{6,s} = T_5 \left(\frac{1}{\pi} \right)^{\frac{x-1}{x}}$$ [9-15]

With equations [9-6] and [9-7] the enthalpy (h_{6s}) is derived from the temperature (T_{6s}) and the turbine inner efficiency (η_{iT}) can be calculated as shown in equation [9-16, s. also 2-14].

$$\eta_{iT} = \frac{h_5 - h_6}{h_5 - h_{6,s}}$$ [9-16]

7   Stack

The temperature in the stack was measures and the pressure in the stack was assumed to be atmospheric pressure. The pressure loss in the recuperator was calculated as shown in equation [9-14].
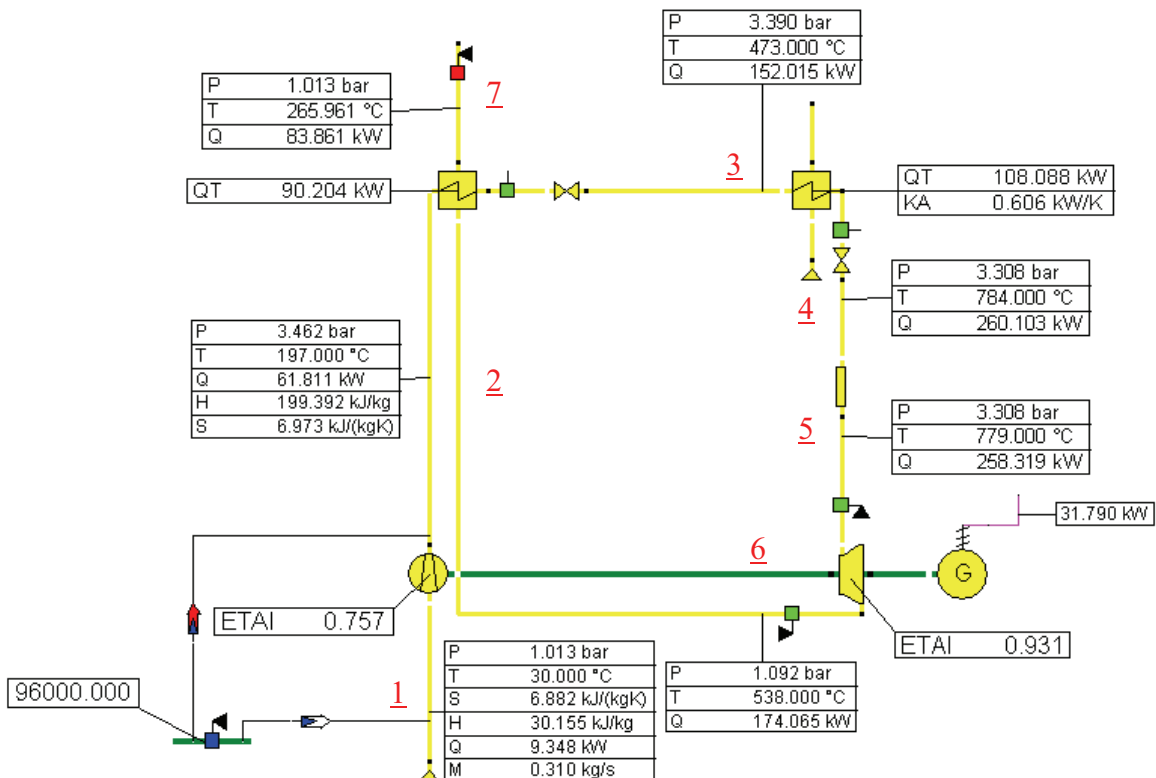
Fig. 9.7: Ebsilon SFBC-EFMGT spreadsheet 1 with respect to turbine speed 96 000 rpm

From the given input data (s. App. II, Tabs. 6 and 7) the program calculates the enthalpy flux in the heat exchangers[7] (QT) and the internal efficiencies (ETAI) of the compressor and turbine. Figure 9.7 and 9.8 show the Ebsilon SFBC-EFMGT spreadsheet and T-s diagram calculated for a turbine speed of 96 000 rpm.
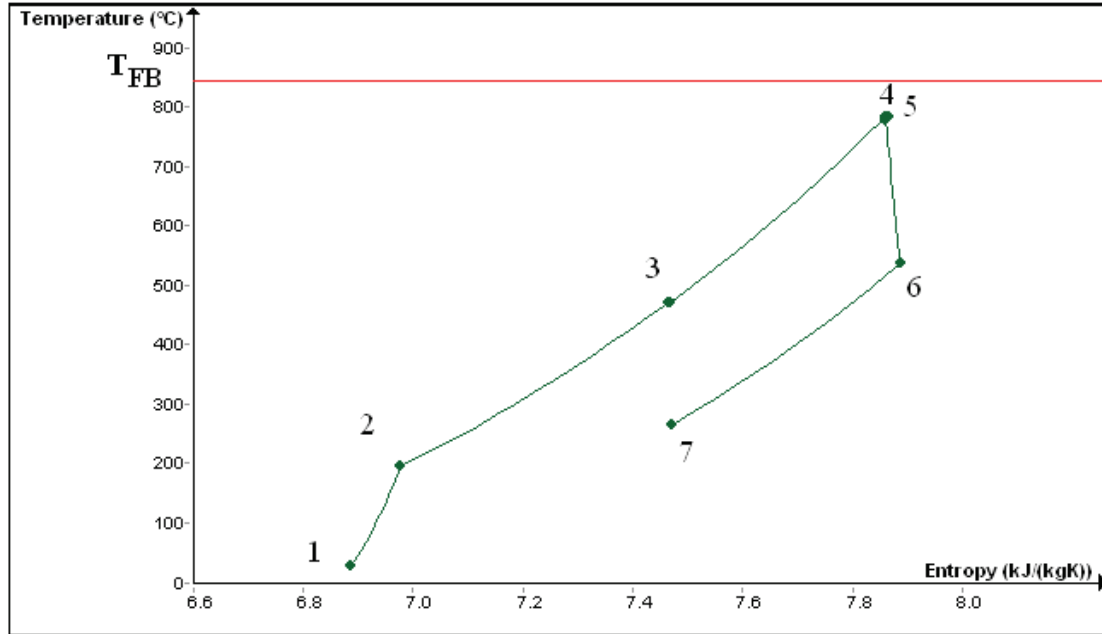
Fig. 9.8: Ebsilon T-s diagram with respect to a turbine speed of 96 000 rpm

Initially the Ebsilon model was fed the measured temperature and pressure data and the electricity generation in the turbine was calculated as shown in Figure 9.7. For the turbine speed of 96 000 rpm the model calculated an electricity generation of 31.79 kW.

An assessed of the Ebsilon model results shown in Figure 9.7 reveals that the turbine efficiency is very high (93%), and increases with decreasing turbine speed! This unusual behaviour suggests that the temperature after the turbine is too low[8]. One possible explanation is that an internal turbine air leakage between the recuperator outlet (position 3 in Figure 9.8) and the turbine inlet (position 5 in Figure 9.8) occurs, thus cooling the turbine inlet and reducing electricity generation.
In a second simulation the Ebsilon model was fed the measured electricity generation data with respect to turbine speed (s. App. II, Tab. 7) and the temperature after the turbine was calculated (Fig. 9.9).

---

[7] recuperator and fluidized bed heat exchanger
[8] The inspection of the temperature probe (TET) revealed no serious deviance from a second probe installed on 30.09.08.
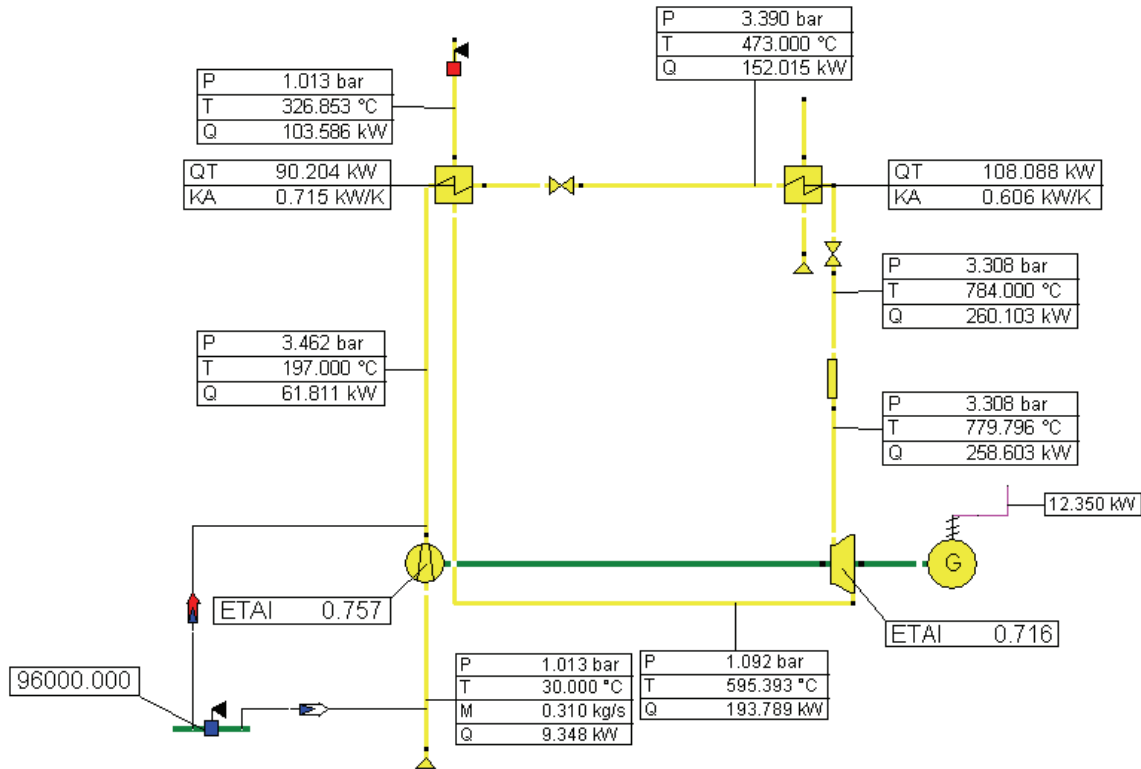
Fig. 9.9: Ebsilon SFBC-EFMGT spreadsheet 2 with respect to turbine speed 96 000 rpm

The comparison of the temperature after the turbine in Ebsilon SFBC-EFMGT spreadsheet 1 (Fig. 9.7) and spreadsheet 2 (Fig. 9.9) reveals that a temperature difference of only 57K is necessary to account for the observed difference in electrical generation capacity.

The next question which was investigated with the Ebsilon model was:

How large an air leakage would be necessary to account for the measured low turbine exit temperature and low generation capacity?

To help answer this question the Ebsilon model was fed with the measured turbine exit temperatures and achieved electrical generation data, and a bypass between the recuperator exit and turbine inlet was inserted. The model delivers an iterative solution for the necessary air mass flow in the bypass with respect to turbine speed to account for the measured electrical generation and temperature after the turbine (s. Fig. 9.10).
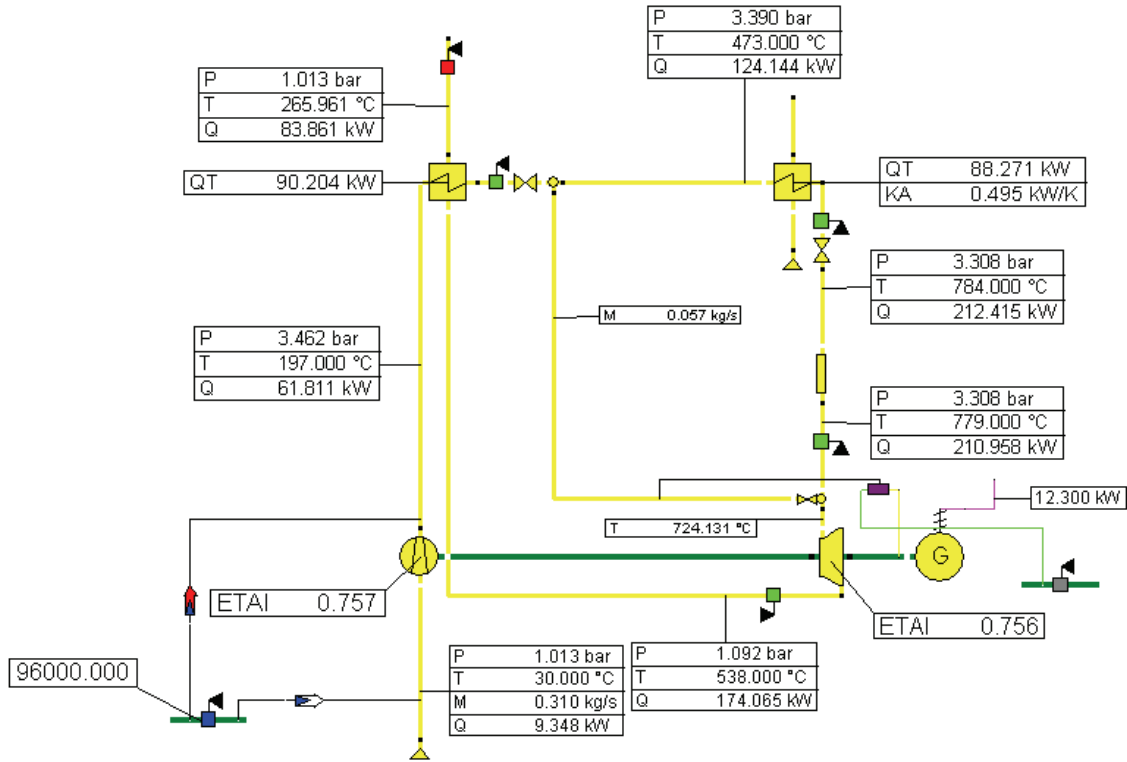
Fig. 9.10: Ebsilon SFBC-EFMGT spreadsheet 3 with respect to turbine speed 96 000 rpm

As seen in Figure 9.11 for the maximum generation speed of 96 000 rpm an air leakage between the recuperator and turbine inlet of 205 kg/h (corresponds to 18% of the total air mass flow) would be necessary.
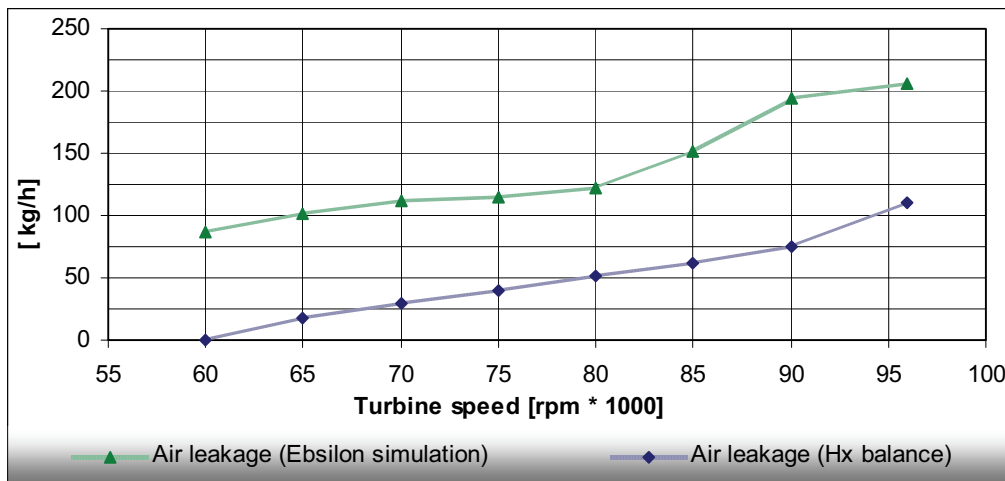
Fig. 9.11: Potential air leakage with respect to turbine speed

If such a leakage really exists is unclear but is technically possible because these two air streams are only separated by a high temperature compression seal, which may become permeable as a result of the thermal expansion of the metallic turbine casing and increasing compressor pressure. However, the difference in the air mass flow measured in the stack and the calculated air mass flow in the heat exchanger with the friction coefficient (ζ), was maximal 110 kg/h.

Although these findings support the hypothesis of an air leakage in the turbine they must be treated with caution because the lower temperature measured after the turbine could also be

the result of the cooling of the working fluid through internal heat exchange processes within the turbine. It is probable that both these mechanisms play a role leading to the reduction in turbine inlet temperature and therefore generated electricity.

There is sufficient evidence that the optimisation of the turbine with respect to air leakage and internal heat exchange will increase the electrical output to over 20 kWe.

9.2.3   SFBC-EFMGT Plant Integration and Cycle Efficiency

With a stationary steady state model the overall efficiency of the SFBC-EFMGT test-bed configuration (s. Fig. 9.12) can be calculated.
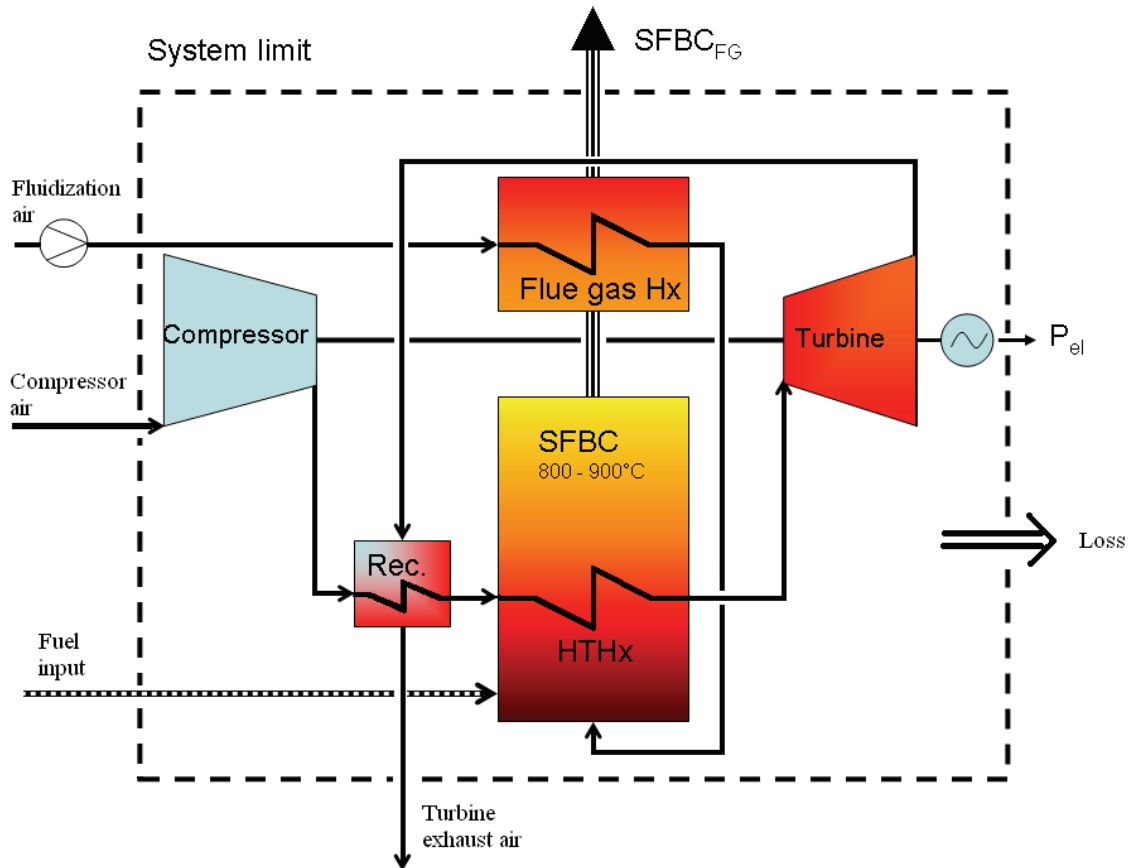
Fig. 9.12: SFBC-EFMGT test-bed model

When the fluidization air ($\dot{Q}_{FL.\ Air}$) and fuel input ($\dot{Q}_{fuel}$) streams are known and the output streams are accurately measured this model allows an assessment of the overall electrical efficiency of the test bed as exemplarily shown in equation [9-4] for a turbine speed of 96 000 rpm (s. App. II, Tab. 10) with an estimated electrical output of 20 kW.

$$\eta_{el} = \frac{P_e}{\dot{Q}_{feul}} = \frac{20}{175} = 0.114\ [-] \qquad\qquad [9\text{-}17]$$

The overall electrical efficiency of 11.4% is relatively low, however the large enthalpy flux remaining in the turbine exhaust air after the recuperator, and SFBC flue gas after the air preheater is available for further recuperative utilization in the SFBC-EFMGT process as shown in Figure 9.13.

To increase the SFBC-EFMGT cycle efficiency the turbine exhaust air should be further utilized, for example to dry wet biomass as shown in Figure 9.13 or to preheat the fluidization air for the SFBC reactor as shown in Figure 9.14. Also rest heat utilization in a hot water cycle for municipal heating should be included. Furthermore particle cleanup such as a bag house fabric filter and primary emission reduction measures such as addition of slaked lime (Ca(OH)$_2$) to the SFBC reactor are proposed to ensure that environmental regulation are met.
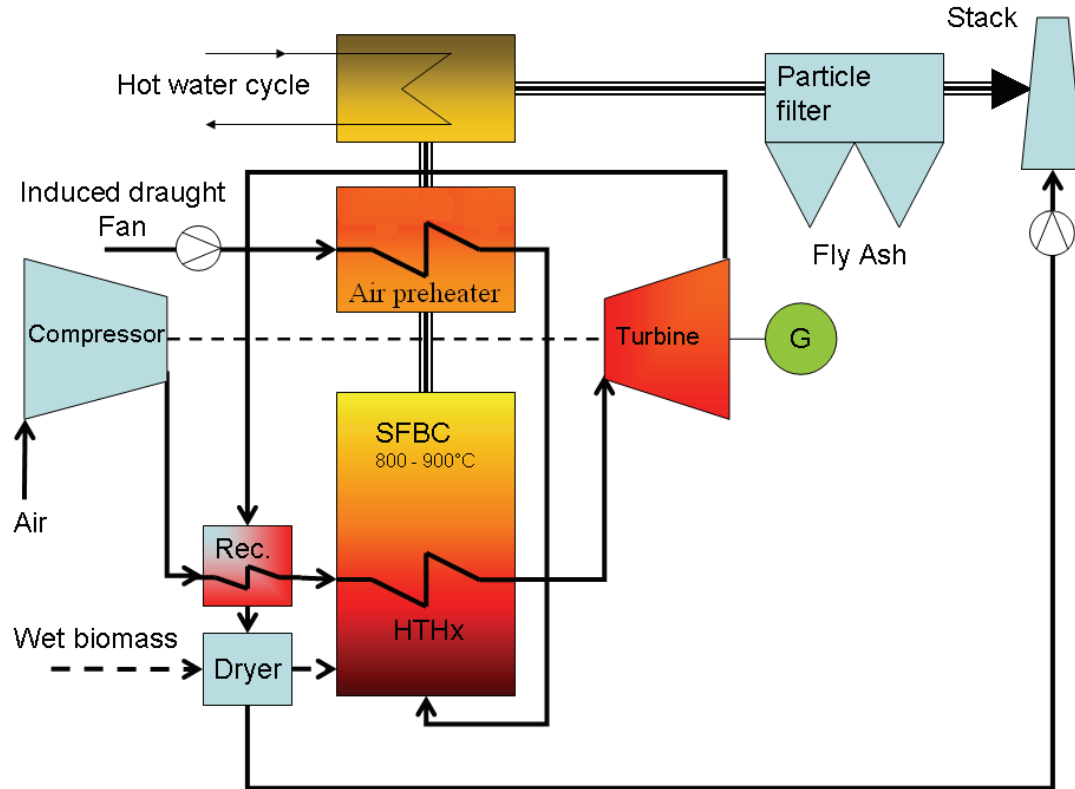
Fig. 9.13: SFBC-EFMGT plant concept with wet biomass dryer

If the EFMGT exhaust air at a temperature[9] of 334-369°C is cooled to 120°C in a biomass dryer a nominal[10] thermal input of up to 65 kW is achievable, and the necessary fuel input is therefore reduced by 65 kW. The drying and preheating of wet fuels such as sludges in the turbine exhaust air before their combustion in the SFBC reactor leads to a direct increase in their calorific value (LCV) and thus plant electrical efficiency by reducing fuel consumption. Thus an electrical efficiency of 18.2% [9-18] can be attained.

$$\eta_e = \frac{P_e}{\dot{Q}_{fuel,DRY}} = \frac{20}{110} = 0.182 \; [-] \qquad\qquad [9\text{-}18]$$

The efficiency of the heat exchanger in this case increases to:

$$\eta_{Hx} = \frac{\dot{Q}_{Hx}}{\dot{Q}_{fuel,DRY}} = \frac{100}{110} = 0.90 \; [-] \qquad\qquad [9\text{-}19]$$

---

[9] The EFMGT exhaust air temperature falls with increasing turbine speed due to the increasing turbine efficiency.

[10] at the turbine design speed of 96 000 rpm

The thermal efficiency of the SFBC-EFMGT cycle can also be much improved if, as shown in Figure 9.13, the SFBC flue gas after the air preheater is further utilized to heat water for municipal purposes.

With an assumed reduction in the flue gas temperature from 450°C to 120°C in the flue gas/water heat exchanger around 30 kW$_{th}$ can be extracted. Thus a theoretical total plant thermal efficiency of 45.5% [9-20] can be attained.

$$\eta_{th} = \frac{\dot{Q}_{out}}{\dot{Q}_{in}} = \frac{\dot{Q}_e + \dot{Q}_{th}}{\dot{Q}_{fuel,DRY}} = \frac{20+30}{110} = 0.455 \; [-] \qquad\qquad [9\text{-}20]$$

The direct coupling of the turbine exhaust air into the SFBC reactor would seem to be a more efficient recuperation method but can lead to fundamental turbine operation problems such as surging, due to the instable operation characteristic of the fluidized bed process. Micro gas turbines are very sensitive to pressure changes due to their very high speed and fast response times. Pressure variations in the air lines down stream of the turbine can cause a self amplifying high frequency turbine speed variation leading to unstable compressor surging behaviour.

Another difficulty, as seen in Figure 9.15, is that the Capstone C30 MGT exhaust air mass flow is much higher than the air mass flow required by the SFBC reactor.

At 45 000 rpm 72% and at 96 000 rpm only 24% of the compressor air mass flow is required for the SFBC reactor, which makes a direct recuperation as fluidization air problematic.
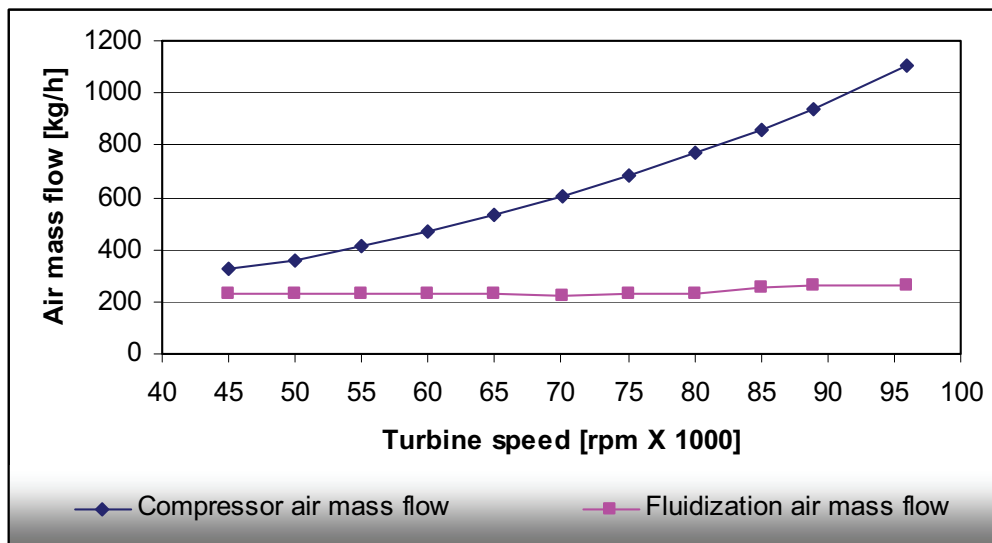
Fig. 9.14: Compressor and fluidization air mass flow with respect to turbine speed

To avoid the problems associated with the discontinuous fluidized bed pressure regime and differences in air mass flow between the SFBC and EFMGT, the SFBC fluidization air could be preheated by the SFBC exhaust air in a ribbed[11] heat exchanger as shown in Figure 9.15.

The advantage of this configuration is that an increase in electrical efficiency can also be achieved with much dyer fuels such as forestry residues, which can be combusted at higher temperatures, which will further increase the electrical efficiency of the turbine.

---

[11] continuous tube, heat exchanger with ribbing on the fluidization air side
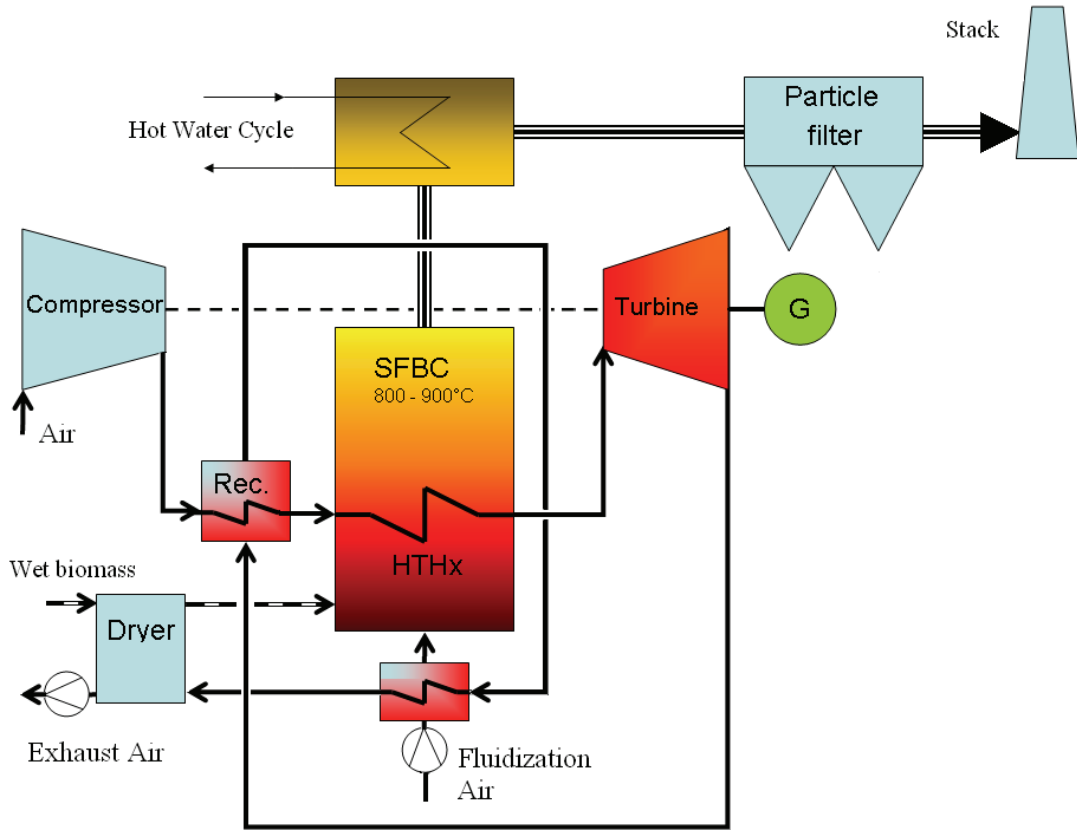
Fig. 9.15: SFBC-EFMGT plant concept with wet biomass dryer
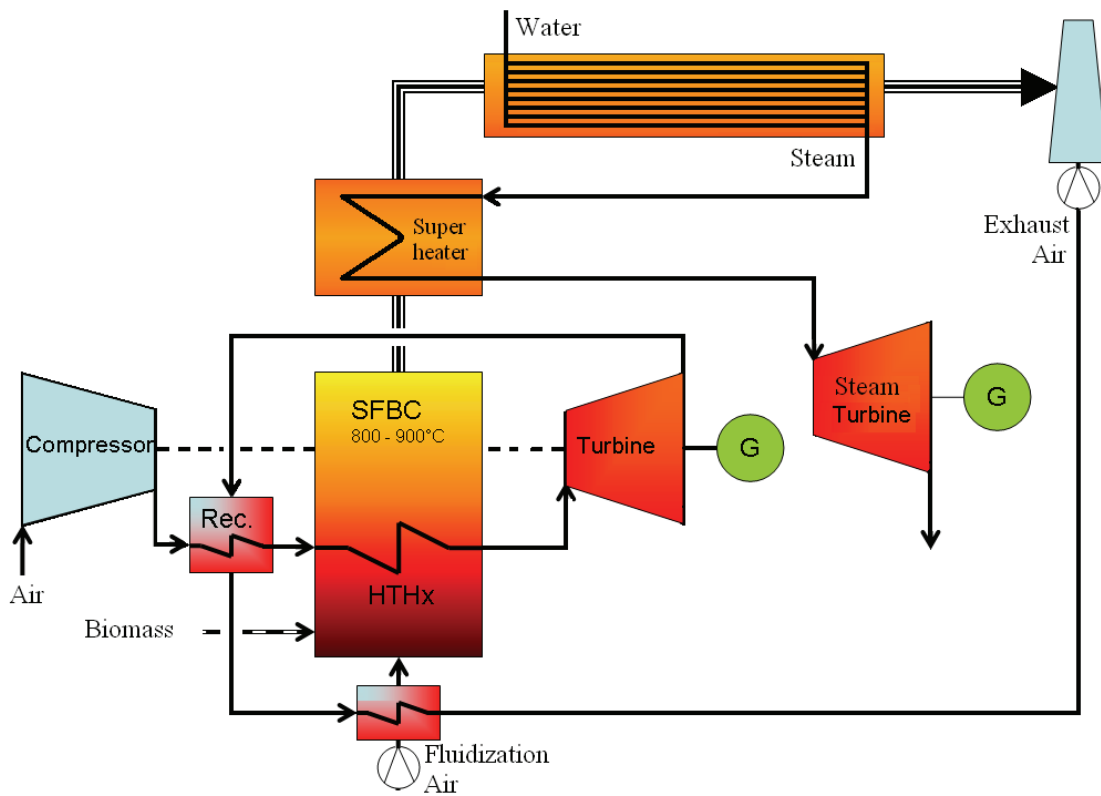
Fig. 9.16: SFBC-EFMGT-CC concept

115

A logical extension of this process is the combined cycle concept (s. Fig. 9.16) in which the SFBC flue gas is utilized to raise steam for a bottoming steam cycle.

The combined cycle concept allows a higher electrical efficiency, but also requires higher investment costs, which means that a larger scale is necessary for the cycle to become economically viable.
The following fundamental conclusions for the SFBC-EFMGT cycle can be formulated:

- A recuperative utilization of the turbine exhaust air and SFBC flue gas is critical to increase the plant efficiency i.e. as SFBC fluidization air or for fuel drying or for domestic heating purposes, or for a bottoming steam cycle if the SFBC is of large enough scale. Other high value utilizations for the clean hot exhaust air stream such as foodstuff or timber drying are also viable.

- A further requirement is that the SFBC temperature remains stable at the optimal combustion temperature. This requires that the feedstock theoretical combustion temperature is high enough to sustain the SFBC process with heat extraction, i.e.100 kW$_{th}$ for the C30 EFMGT cycle.

- The limits for the system heat extraction are determined by the heat exchanger geometry (space requirement), SFBC feedstock calorific value and metering to the fluidized bed and the fluidization air mass flow. The physical limit for the SFBC reactor lies by around 1 MW$_{th}$ /m² reactor tube lateral cross section.

- The combination of a SFBC reactor with in-bed heat exchanger, for the operation of an externally fired micro gas turbine, with a biomass fuel dryer is a very promising concept, which when operated with the right combination of wet fuels (85% moisture content) such as municipal sludges, residual agricultural biomass and forestry residues, has the potential to deliver high efficiencies (> 45%) with low fuel costs.

Fig. 9.17: EFMGT coupled with SFBC reactor, University of Rostock test-bed

10   Summary and Perspectives

Based on a comprehensive evaluation of small scale biomass electricity generation systems it was established that there is notable lack of commercially available technologies utilizing solid biomass feedstocks in the electricity generation range of 100-400 kWe.

On the other hand this is the ideal generation capacity for small scale distributed electricity generation from residual agricultural biomass. Most commercial technologies are either not suitable for solid biomass, or not available in the selected power range.

The large majority of research work has been performed on large scale coal fuelled EFCC[1] and EFHAT[2] cycles, but due mainly to problems with the high temperature heat exchanger, these cycles are not techno-economically viable.

Historically the only successful EFGT plants utilized high temperature metallic heat exchangers, but due to low turbine inlet temperatures the efficiency of these plants was too low to be competitive with conventional gas turbines.

Higher efficiencies are theoretically achievable with complex combined cycles or humidification of the turbine air (STIG[3]-cycle, EFHAT cycle) but the costs are prohibitive. Ceramic heat exchangers and supplementary firing after the heat exchanger can also increase the cycle efficiency, but due to high construction and operation costs and low reliability of the heat exchangers, this is at present not commercially attractive.

An assessment of the literature on externally fired gas turbine cycles in general and externally fired micro gas turbines (EFMGTs) in particular, revealed that the development of an efficient, reliable and cost-effective high temperature heat exchanger is the major techno-economic hurdle for the EFGT technology.

Therefore the main challenge within the context of this dissertation was the development of a suitable robust high temperature metallic heat exchanger for the for the SFBC-EFMGT plant.

An assessment of the SFBC-EFMGT cycle utilizing residual biomass fuels revealed that all residual feedstocks are appropriate which have a high enough calorific value and density to sustain the fluidized bed combustion process with simultaneous heat extraction from the bed. Pelleting of very light feedstocks may in some cases be necessary.

An assessment of heat exchanger designs, materials and costs revealed that metallic heat exchangers are suitable for the air temperatures and erosive environment expected in SFBC applications.

It was determined that the linking of an externally fired micro gas turbine (EFMGT) with a metallic fluidized bed heat exchanger in a SFBC reactor has major advantages with respect to existing small scale biomass electricity generation systems.

Firstly the excellent heat transfer coefficients in the fluidized bed can reduce the required size of a metallic in-bed heat exchanger heat exchanger by up to a factor of 10. The fluidized bed heat exchanger has a surface area of only 5 square meters and is thus more than a factor 10 smaller and cheaper than similar air/flue gas heat exchangers and around a factor 50 cheaper than a similar ceramic heat exchanger. Also the excellent combustion characteristics of the stationary fluidized bed at moderate temperatures (800-900°C) make it ideal for problematic low grade biomass fuels such as agricultural and forestry residues.

The recuperated gas turbine combined with a SFBC in-bed heat exchanger offers an elegant optimization between high TIT[4] and limited[5] biomass combustion temperatures by delivering air temperatures close to the fluidized bed combustion temperature.

---

[1] externally fired combined cycles
[2] externally fired humid air cycles
[3] steam injected gas turbine
[4] turbine inlet temperature
[5] The combustion temperature is limited by the ash sintering temperature.

Based on these findings a metallic heat exchanger was designed to transfer 100 kW_{th} from the fluidized bed to the EFMGT compressed air stream at a temperature of over 800°C and an air mass flow of up to 1100 kg/h.

The material costs for the fluidized bed heat exchanger (100 kW_{th}) constructed from readily available cost effective austenitic heat resistant stainless steels, amounted to around 3000 €. Commercial construction costs of a similar heat exchanger of around 30 €/kW_{th} should therefore be realistically achievable.

The successfully SFBC-EFMGT cycle tests at the University of Rostock, Chair of Environmental Technology, validated the feasibility of coupling a MGT with a SFBC reactor via a metallic in-bed heat exchanger. This is the first time that a SFBC-EFMGT cycle has been successfully tested, and a patent for the cycle is under consideration.

The heat exchanger delivered excellent results with regard to the ability to extract the required heat flux of 100 kW_{th} from the SFBC reactor, and maintain a temperature of over 800°C for nearly the whole turbine operation range[6].

A very good heat transfer capacity from the fluidized bed to the compressed air stream (k_a up to 113 W/m²K) was achieved in the heat exchanger with a very low heat exchanger pressure drop (maximum 87 mbar) which is well below the required limit of 4%[7] of the compressor pressure, and under the 100 mbar[8] recommended by Kautz and Hansen (2007).

A very good heat exchanger effectiveness ($\Phi \approx 87\%$) was determined which corresponds to a temperature difference between the fluidized bed and the heat exchanger outlet of less than 60 K for the entire turbine operating range.

The EFMGT in the test-bed configuration achieved an electrical output of 12.4 kW. The efficiency of the heat exchanger in the test-bed configuration reached 54%. There is substantial evidence that internal air leakage and heat transfer between processes in the turbine are responsible for the lower generation capacity.

A theoretical heat exchanger efficiency of up to 90% is possible if the hot turbine exhaust air is utilized to dry wet biomass fuels before combustion in the SFBC reactor.

A conservative theoretical output of 20 kWe is considered realistic if the EFMGT is further optimized. If a fuel dryer is utilized as suggested by Cocco et al. (2007), then higher electrical efficiencies can be attained.

To increase the overall cycle efficiency a further recuperative utilization of the turbine exhaust air and SFBC flue gas is absolutely critical, i.e. as SFBC fluidization air in combination with fuel drying and for domestic heating purposes.

The SFBC-EFMGT cycle with a fuel dryer has a theoretical electrical efficiency of over 18%, which is higher than other small scale electricity generation technologies utilizing solid biomass.

The SFBC-EFMGT cycle with a fuel dryer has a theoretical thermal efficiency of over 45%. The clean hot turbine exhaust air is also suitable for applications such as foodstuffs or timber drying.

By upgrading to a SFBC-EFMGT combined-cycle electrical efficiencies of over 30% can be expected, but due to the higher investment costs and the "economy of scale" this system must be of a larger dimension.

Suggested further research and development work includes the optimization of the heat exchanger to further reduce pressure drop, optimization of the EFMGT to reduce internal air leakage and heat transfer, and also optimization of SFBC reactor to increase the fluidization air mass flow.

---

[6] At 96 000 rpm the temperature fell below 800°C due to the decrease in fluidized bed temperature.
[7] necessary to avoid reaching the compressor pump limit
[8] necessary to avoid unacceptable loss in cycle efficiency

Furthermore long term continuous operation tests (>10 000h) are necessary to verify the durability of the heat exchanger in the erosive fluidized bed environment, and the long term stability of the other system components. These tests should be performed in cooperation with an industrial partner interested in the commercialization of the SFBC-EFMGT cycle.

As summed up by Yan (1998) the main features of the EFGT technology are fuel flexibility, incorporation of conventional technology, absence of particle cleanup for the turbine path, and potential for high efficiency; and the primary obstacle which must be overcome is the development of a reliable low cost high temperature heat exchanger.
The assessment of the heat exchanger operation and simulation data has shown that placing a reliable cost-effective metallic heat exchanger within the fluidization zone of the SFBC reactor is the key to the success of the EFMGT cycle.

Bibliography

Agarwal, P. and Frey, C. H. (1995): Performance Model of the Externally Fired Combined Cycle (EFCC) System. Proc. of the 88th Annual Meeting Air and Waste Management Association, Paper No. 95-7.02, June 18-23, 1995, San Antonio, TX, USA

Agren, N. D., Westermark, M. O., Bartlett, M. A. and Linquist, T. (2002): First Experiments on an Evaporative Gas Turbine Pilot Power Plant: Water Circuit Chemistry and Humidification Evaluation, Transactions of the ASME. Journal of Engineering for Gas Turbines and Power Vol. 124, January 2002, pp. 96-102

Anheden, M., Ahlroth, M., Martin, A. R. and Svedberg, G. (1999): Externally Fired Gas Turbine Cycles for Small Scale Biomass Cogeneration. International Joint Power Generation Conference, Burlingame, CA, USA, 1999, Proceedings, Vol. 1, pp. 129-137

Ashworth, R. C., Keener, H. M. and Hall, A. W. (1994): Small-Scale AFBC Hot Air Gas Turbine Power Cycle. Proc. of the 13th International Fluidized-bed Combustion Conference, May, 7-10, 1994, Orlando, FL, USA

Baehr, H. D. (2002): Thermodynamik. Grundlagen und technische Anwendungen. 11., korr. und erg. Aufl., Berlin, Springer-Verlag, 2002

Berliner Zeitung (2008): Tagesthema Biosprit, No. 78, 03. April 2008

Bianchi, M., Cherubini, F., De Pascale, A. and Peretto, A. (2003): Cogeneration from Poultry Industry Wastes – Part I: Indirectly Fired Gas Turbine Application. Proc. of the 16th International Conference on Efficiency, June 30- July 3, 2003, Copenhagen, Denmark

BIZ (2002): Pellet-Zentralheizungen. Marktübersicht 2, Biomasse Info-Zentrum, Universität Stuttgart, www.holzpellets-boerse.de/marktuebersicht_pellets_zentralheizung

BMU (2004): Mindestvergütungssätze nach dem neuen Erneuerbare-Energien-Gesetz (EEG) vom 21. Juli 2004, Bundestagsdrucksache 15/2864. www.bmu.de

BMU (2007): Monitoring zur Wirkung des novellierten Erneuerbare-Energien-Gesetzes (EEG) auf die Entwicklung der Stromerzeugung aus Biomasse. Leipzig, 23. Februar 2007, Institut für Energetik und Umwelt GmbH im Auftrag des Bundesministeriums für Umwelt, Naturschutz und Reaktorsicherheit (BMU), www.bmu.de

BMWi (2007): Energiedaten, Tabelle 22, letzte Änderung: 02.10.2007, http://www.bmwi.de/BMWi/Navigation/Energie

Bosniakovic, F. (1965): Technische Thermodynamik I und II, 1965 Theodor Steinkopff, Dresden

Bram, S., De Ruyck, J. and Novak-Zdravkovic, A. (2005): Status of External Firing of Biomass in Gas Turbines. Proc. IMechE Vol. 219 Part A: J. Power Energy 2005, pp 137-145

Capstone (2004): C30 Instruction Manual. Capstone Turbine Corporation. www.microturbine.com

Cocco, D., Deiana, P. and Cau, G. (2006): Performance Evaluation of Small Size Externally Fired Gas Turbine (EFGT) Power Plants Integrated with Direct Biomass Dryers. Energy: The International Journal, Vol. 31, 2006, pp. 1459-1471

Crosa, G., Fantini, L., Ferrari, G., Pizzimenti, L. and Trucco, A. (1998): Steady State and Dynamic Performance Prediction of an Indirect Fired Gas Turbine Plant. IGTI ASME Paper 98-GT-167

Dallemand, J.-F. (2007): Cereals Straw Resources for Bioenergy in the European Union. Proc. of the Expert Consultation, October 14-15, 2006, Pamplona, Spain

Datsko, S. C., Domian, H. A. and Mohammed, S. (1991): Atmospheric Fluid Bed Cogeneration Air Heater Experiment. Materials Evaluation for an In-bed Heat Exchanger to Heat Air to 1500 Degrees F, 816 Degrees C. Task 8, Observe, Reduce and Review Test Data. Executive Summary, 1991, 188 pp, Babcock and WilcoxCo., Alliance, OH, USA

Dielmann, K. (2001): Micro-Gasturbinen - Technik und Anwendung. Brennstoff, Wärme, Kraft. Bd. 53 No. 6, 2001, pp. 6-11, Springer Verlag

Duvia, A. and Gaia, M. (2002): ORC Plants for Power Production from Biomass from 0.4 MWe to 1.5 MWe: Technology, Efficiency, Practical Experiences and Economy. Paper 02A00361 at the 7th Holzenergie-Symposium, October 18, 2002, ETH Zürich

ECN (2004): Mid Term Project Report. EU-Project TDT-3R Multi Fuel (NNE5-2001-00363), Energy Research Centre of The Netherlands, Feb. 2004

Edelmann, H. and Stuhlmüller, F. (1997): EFCC - Ein zukünftiges Konzept für Kohle-Kombi-Kraftwerke. VGB Kraftwerkstechnik, Vol. 77, No. 7, 1997, pp.573–543

Edwards, R., Suri, M., Huld, T. and Dallemand, J. (2006): GIS-Based Assessment of Cereal Straw Energy in the European Union. In Proceedings of the Expert Consultation: Cereals Straw Resources for Bioenergy in the European Union, October 14-15, 2006, Pamplona, Spain

EEG (2004): Gesetz für den Vorrang Erneuerbarer Energien. BGBl. I Nr. 13, 2000, S. 305 und BGBl I 2004, p.1918

Eidensten, L., Yan, J. and Svedberg, G. (1996): Biomass Externally Fired Gas Turbine Cogeneration. Transactions of the ASME, J. of Engineering for Gas Turbines and Power, Vol. 118, 1996, pp. 604-609

Elmegaard, B., Henriksen, U. and Qvale, B. (2003): Thermodynamic Analysis of Supplementary-fired Gas Turbine Cycles. Int. Journal of Applied Thermodynamics, Vol. 6, 2003, p. 2

Elmegaard, B. and Qvale, B. (2002): Analysis of Indirectly Fired Gas Turbine for Wet Biomass Fuels Based on Commercial Micro Gas Turbine Data. Proceedings of the ASME Turbo Expo, June 3-6, 2002, Amsterdam, The Netherlands, Paper GT-2002-30016

Elmegaard, B., Qvale, B., Carapelli, G. and Tron, F. P. (2001): Open-Cycle Indirectly Fired Gas Turbine for Wet Biomass Fuels. Proceedings of ECOS, July 4-6, 2001, Istanbul, Turkey, pp. 361-368

Evans, R. L. and Zaradic, A. M. (1996): Optimisation of a Wood-Waste-Fuelled Indirectly Fired Gas Turbine Cogeneration Plant. Bioresource Technology 57, 1996, pp. 117-126

Farina, F. and Avanzini, P. G. (1993): Problems Related to the Design of an IFGT Test Facility. ASME Cogen Turbo, Vol. 8, 1993, pp. 55-64

Ferreira, S. B. and Pilidis, P. (2001): Comparison of Externally Fired and Internal Combustion Gas Turbines Using Biomass Fuel. J. of Energy Resources Technology, Vol. 123, No 4, 2001, pp. 291-296

Ferreira, S. B., Pilidis, P. and Nascimento, M. A. R. (2003): The Use of Biomass Fuels in Gas Turbine Combined Cycles: Gasification vs. Externally Fired Cycle. RIO 3 - World Climate & Energy Event, December 1-5, 2003, Rio de Janeiro, Brazil

Ferreira, S. B., Pilidis, P.and Widell, H. (2002): Optimisation of Biomass Fuelled Gas Turbines Using Genetic Algorithms. Proc. of the ASME Turbo Expo 2002, Paper GT-2002-30131

FNR [Fachagentur für Nachwachsende Rohstoffe] (2005): Handreichung Biogasgewinnung und -nutzung. www.fnr.de

Foster-Pegg, R. W. (1990): A Small Air Turbine Power Plant Fired with Coal in an Atmospheric Fluid Bed. J. of Engineering for Gas Turbines and Power, Vol. 112, No. 1, 1990, pp. 21-27

Foster-Pegg, R. W. (1993): A Method for Assessing and Comparing the Potential Efficiencies of Advanced Fossil Fuelled Combined Cycles, 7th ASME Cogen-Turbo Power Congress and Exhibition, 21-23 September 1993, Bournemouth, England, pp. 11-17

Frey, H. C. and Agarwal, P. (1996): Probabilistic Modelling and Optimisation of Clean Coal Technologies. Case Studies of the Externally-Fired Combined Cycle (EFCC) System. Proc., 89th Annual Meeting Air and Waste Management Association, June 23-28, 1996, Pittsburgh, PA, USA

Gallmetzer, G., Gaderer, M., Volz, F., Scheffler, F. and Spliethoff, H. (2008): Biomass Fired Hot Air Gas Turbine with Fluidized Bed Combustion. Proc. of the 9th International Conference on Circulating Fluidized Beds, May 13-16, 2008, Hamburg, Germany

Garvin, J. (2001): Estimate Heat Transfer and Friction in Dimple Jackets. J. of Chemical Eng. Progress, Vol. 101, No 8, 2001, p. 73

GE-Energy (2008): Jenbacher Gas Motors. www.ge-energy.com

Gomez, C. (2005): Die wichtigsten Änderungen in der EEG-Novelle vom August 2004 und ihre Umsetzung in der Praxis. Tagungsband zur 14. Jahrestagung des Fachverbandes Biogas e.V., 11.-14. Januar 2005, Nürnberg, Germany

Greenenvironment (2007): Greenvironment GmbH Brochure 2007
www.greenenvironment.de

Hansen U. and Kautz M. (2004): Simulation von extern gefeuerten Gasturbinen (EFGT-Cycle).
Universität Rostock, Institut für Energie- und Umwelttechnik, IEUT
www.fms.uni-rostock.de/ieut/EFGT

Hansson, F. and Nilsson, A. (2004): Hot Air Gas Turbine Mg2 for Electricity Production.
Division of Thermal Power Engineering, Department of Heat and Power Engineering,
Lund Institute of Technology, 2004 Sweden
www.m.lth.se/programmet/examensarbete/exartiklar/Hansson,%20Nilsson

Hartmann, H. und Strehler, A. (1995): Die Stellung der Biomasse im Vergleich zu anderen
erneuerbaren Energieträgern aus ökologischer, ökonomischer und technischer Sicht.
Schriftenreihe Nachwachsende Rohstoffe, Band 3, 1995. Landwirtschaftsverlag GmbH
Münster

Hassel, E., Kornev, N., Herwig, H. und Stephan, P. (2008): Erhöhung des Wärmeüberganges
durch Wirbelinduktion in Oberflächendellen - Die Physik des komplexen
Transportvorganges und ihre Bewertung. Stand der Forschung. Internal paper
University Rostock, Fakultät für Maschinenbau und Schiffstechnik, Lehrstuhl für
Technische Thermodynamik, 2008

Hiller, A., Löser, J., Schmid, C., Hennef, S. und Nauditt, G. (2007): Neue Möglichkeiten zum
Einsatz von keramischen Wärmeübertägern bei Prozessen mit hohen Temperaturen
und schwierigen Atmosphären. Tagungsband. Verfahren und Anlagen der
Hochtemperaturenergietechnik: Stand und Entwicklungsperspektiven. 39.
Kraftwerkstechnisches Kolloquium, 11 - 12. Oktober 2007, Dresden

Hiller, A., Löser, J., Schmid, C., Hennef, S. and Nauditt, G. (2008): New Possibilities for the
Application of Ceramic Heat Exchangers in Processes with High-temperatures and
Difficult Atmospheres. Int. J. of Electricity and Heat Generation, Vol. 7, 2008,
pp. 48-51, Publication of VGB PowerTech e.V.

Hindman, D. L. and DeBellis, C. L. (1995): Performance of an Advanced Heat Exchanger
Using Ceramic Composite Tubes in a Hazardous Waste Incinerator. HDT, Vol. 33,
1995, pp. 3-13

Huang, F. F. and Naumowicz, T. (1992): Overall Performance Evaluation of an Externally-
fired Air-turbine Combined Cycle Power Plant Based on First Law as well as Second
Law Analysis. Proc. of the International Symposium on Efficiency, Cost, Optimisation
and Simulation, Zaragoza, Spain, 15-18 June 1992, pp. 399-406

Hurley, J. P., Seery, D. J., Robson, F. L. (2003): Experience with ODS High-Temperature Heat
Exchanger in a Pilot-Scale HIPPS Plant. Science Reviews, Materials at High
Temperatures. Vol. 20 No. 1, 2003, pp. 39-44

IPCC (2007) Intergovernmental Panel on Climate Change Fourth Assessment Report (AR4),
2007 www.ipcc.ch

Jahraus, B. und Dieckmann, R. (1995): Der Kombiprozeß mit indirekt kohlebefeuerter Gasturbine. VDI Bericht Nr. 1182, 1995, pp. 287-301

Janssen, R. (2004): Biofuel-Burning Microturbines. Opportunities for Biofuel-Burning Microturbines in the European Decentralised-Generation Market. Presentation in Workshop: Biofuelled Micro Gas Turbines in Europe – Market Opportunities and R & D Requirements. Brussels, September 24, 2004

Jonsson, M. and Yan, J. (2005): Humidified Gas Turbines – A Review of Proposed and Implemented Cycles. Energy, Vol. 30, 2005, pp. 1013-1078

Karl, J. (2006): Dezentrale Energiesysteme. Neue Technologien im liberalisierten Energiemarkt. 2., verbesserte Auflage, 2006, Oldenburg Wissenschaftsverlag

Karl, J. and Hein, D. (2002): Performance Characteristics of the Biomass Heatpipe Reformer. Proc. of the 12th European Conf. on Biomass for Energy, 17-21 June, 2002 Amsterdam, The Netherlands

Karl, J., Karellas, S., Kuhn, S., Metz und T. (2004): Erzeugung von Synthesegas mit dem Biomass Heatpipe Reformer – Betriebserfahrungen und Leistungsgrenzen. Energetische Nutzung von Biomasse, DGMK-Fachtagung 19.-21 April 2004, Velen, Westfalen, Tagungsbericht, pp. 55-64

Karl, J., Schmitz, W., Hein, D. (2000): Allotherme Wirbelschichtvergasung - Möglichkeiten zur Realisierung des Wärmeeintrags in Wirbelschichten. Tagungsband 4, DGMK-Fachtagung, Energetische und baustoffliche Nutzung von Abfällen und Biomassen, 10-12 April 2000, Velen/Westfallen, Deutschland

Kautz, M. (2005): Auslegung von extern gefeuerten Gasturbinen für dezentrale Energieanlagen im kleinen Leistungsbereich. Dissertation an der Fakultät für Maschinenbau und Schiffstechnik der Universität Rostock, 2005

Kautz, M. and Hansen, U. (2004): The Externally Fired Gas Turbine (EFGT-Cycle) and Simulation of the Key Components. Third European Congress Economics and Management of Energy in Industry, 6-9 April 2004, Estoril-Lisbon, Portugal

Kautz, M. and Hansen, U. (2007): The Externally-Fired Gas-turbine (EFGT-Cycle) for Decentralized Use of Biomass. Applied Energy 84, 2007, pp. 795-805

Kautz, M., Hansen, U. u. Karl, J. (2004): Die extern gefeuerte Gasturbine. Universität Rostock, Institut für Energie- und Umwelttechnik, www.fms.uni-rostock.de/ieut/Velen_Kautz

Klara, J. M., Wherley, M. R., Ward, J. H., VanBibber, L. and Figueroa, J. D. (1997): Advanced HIPPS for the 21st Century. Proceedings of the Advanced Coal-Based Power and Environmental Systems Conference, July 22-24, 1997, Pittsburgh, Pennsylvania, USA

Knoef, H. A. M., Wagennar, B. M., Penumerman, P. and Stassen, H. E. M. (1998): Indirectly Fired Gas Turbine for Rural Electricity Production from Biomass. Biomass for Energy and Industry, 10th European Conference and Technology Exhibition, June 8-11, 1998, Würzburg, Germany

Korobitsyn, M. A. (1998): New and Advanced Energy Conversion Technologies. Analysis of Cogeneration, Combined and Integrated Cycles. Chapter 5: Externally Fired Combined Cycle. PhD Thesis, University Twente, printed by Febodruck BV, Enschede, 1998

Kussmaul, K., Maile, K. and Hein, K. R. G. (1995): Development of Heat Exchangers Operating in the Very High Temperature Regime. Composite and Energy Proc. ACM, 8-10 May, 1995

Kyoto Protocol (1997): Kyoto Protocol to the United Nations' Framework Convention on Climate Change. Kyoto, December 11, 1997

Lazzaretto, A. and Segato, F. (2001a): Thermodynamic Optimization of the HAT Cycle Plant Structure - Part I: Optimization of the "Basic Plant Configuration". Journal of Engineering for Gas Turbines and Power, January 2001, Vol. 123, pp. 1-7

Lazzaretto, A. and Segato, F. (2001b): Thermodynamic Optimization of the HAT Cycle Plant Structure - Part II: Structure of the Heat Exchanger Network. Journal of Engineering for Gas Turbines and Power, January 2001, Vol. 123, pp. 8-16

Lenk, U. (2006): Entwicklungsperspektive der Kraftwerkstechnik unter Berücksichtigung individueller Unternehmenskompetenzen. Vortrag am Lehrstuhl für Energiesysteme und Strömungsmaschinen, Universität Rostock, 4. Dezember 2006. Uwe Lenk, Siemens Power Generation, Erlangen, Germany

Lymberopoulos, N. (2004): Microturbines and their Application in Bio-Energy. Centre for Renewable Energy Sources European Commission DG-TREN EESD Contract No: NNE5-PTA-2002-003/1

Marroyen, D., Bram, S. and De Ruyck, J. (1999): Progress of an Externally Fired Evaporative Gas Turbine Cycle for Small Scale Biomass Gasification. Paper 99-GT-322

Maunsbach, K., Isaksson, A., Yan, J., Svedberg, G. (2001): Integration of Advanced Gas Turbines in Pulp and Paper Mills for Increased Power Generation. Journal of Engineering for Gas Turbines and Power, October 2001, Vol. 123, pp. 734-740

McFarlin, D. J., Sgamboti, C. T. and Lessard, R. D. (1982): Ceramic Heat-Exchanger Applications Study. Technical Report No ORNL/SUB-81-92352/1, United Technologies Research Center, 1982, East Hartford, CT, USA

Metz, T., Kuhn, S., Karellas, S. Stocker, R., Karl, J. and Hein, D. (2004): Experimental Results of the Biomass Heatpipe Reformer: 2nd World Conf. on Biomass for Energy, May 10-14 2004, Rome, Italy

Michejew, M. A. (1964): Grundlagen der Wärmeübertragung. Verlag Technik, Berlin, 1964

Ngoma, G. D. (2005): Comparative Numerical Investigations of a Wood Residue Indirectly Fired Gas Turbine. Proc. of the 5th IASTED International Conference on Power and Energy Systems, Benalmádena 05, 2005, Acta Press, Anaheim

Nikolaou, A., Remrova, M., Jeliazkov, M. (2003): Biomass Availability in Europe. Lot 5: Bioenergy's Role in the EU Energy Market. Biomatnet Report, BTG Czech Republic, Centre for Renewable Energy Sources and ESD Bulgaria Ltd., 2003 www.biomatnet.org

Obernberger, I., Carlsen H., Biedermann, F. (2003): State of the Art and Future Developments Regarding Small Scale Biomass CHP Systems with Special Focus on ORC and Stirling Engine Technologies. International Nordic Bioenergy Conference 2-5 September, Jyväskylä, Finnland 2003

Pajusalo, L. (2005): The Market Potential for a Bio-IFGT. Identification of Opportunities in Finland and Sweden, Hanken, Pajusalo 2005 www.eny.hut.fi/research/process_integration/bioifgt_Jan2004Dec2005

Pedersen, A. H. (2004): Microturbine Energy Systems. The OMES Project, EU Project No NNE5-1999-20128, Public Report, June 2004

Pehn, W. (2006a): Kraft-Wärme-Kopplung mit 100 kWel aus fester Biomasse. Proceedings of the 15th Symposium Bioenergy, 23-24 November 2006, Kloster Banz, Bad Staffelstein, pp. 88-91

Pehn, W. (2006b): Personal Comment November 2006 (Tabott's BG100 sales agent in central Europe)

Peters, B. (2004): Business Trends for Micro Turbines. Presentation in Workshop: Bio-Fuelled Micro Gas Turbines in Europe - Market Opportunities and R & D Requirements. September 24, 2004, Brussels

Pritchard, D. (2002): Biomass Combustion Gas Turbine CHP. Report: ETSU B/U1/00679/00/REP, DTI Pub. URN No 02/1345. Talbott's Heating Ltd. Stafford, GB, 2002

Riccio, G., Martelli, F. and Maltagliati, S. (2000): Study of an External Fired Gas Turbine Power Plant Fed by Solid Fuel. ASME-0015-GT-2000, Proc. of the 45th ASME Gas Turbine and Aeroengine Technical Congress, Exposition and Users Symposium, May 8-11, 2000, Munich, Germany

Savola, T., Tveit, T.-M. and Laukkanen, T. (2005): Biofuel Indirectly Fired Microturbine – State of the Art. Energy Engineering and Environmental Protection. Helsinki University of Technology, www.eny.hut.fi/research/process_integration/bioifgt_Jan2004Dec2005/bioifgt_index.html

Savolainen, K., Mononen, J., Ilola, R. and Hänninen, H. (2005): Materials Selection for High Temperature Application. TKK, Laboratory of Engineering Materials Publications, Espoo, 2005

Schmid, M. R. and Gaegauf, C. K. (2008): Biomass Combined Cycle: Efficient Solution for Decentralized Biomass Power. Proc. of the 16th European Biomass Conference, June 2-6, 2008, Valencia, Spain

Schulte-Fischedick, J. und Zunft, S. (2007): Entwicklung keramischer Plattenwärmeüberträger für Einsatztemperaturen bis 1250°C. Tagungsband. Verfahren und Anlagen der Hochtemperaturenergietechnik: Stand und Entwicklungsperspektiven. 39. Kraftwerkstechnisches Kolloquium, 11. - 12. Oktober 2007, Dresden

Schulte-Fischedick, J. und Zunft, S. (2008): Keramische Plattenwärmeüberträger für die Anwendung in Hochtemperaturprozessen. Int. J. of Electricity and Heat Generation, Vol. 7, 2008, pp. 43-47, Publication of VGB PowerTech e.V.

Sörgel, G. (1996): Dampf- und Gasturbinen. Lehrheft 3 [Manuskript]. Technische Universität Dresden, Institut für Energiemaschinen und Maschinenlabor

Solomon, P. R., Serio, M. A., Cosgrove, J. E., Pines, D. S., Zhao, Y., Buggeln, R. C. and Shamroth, S. J. (1996): A Coal-fired Heat Exchanger for an Externally Fired Gas Turbine. Journal of Engineering for Gas Turbines and Power, Vol. 118, 1996, pp. 22

Spilling (2008): Spilling Energie Systeme GmbH, PowerTherme Combined Heat and Power Unit, www.spilling.de

SRU (2007): Klimaschutz durch Biomasse. Special Report on Biomass by the German Commission of Experts for Environmental Questions, Juli 2007, www.SRU.de

Star, F., White, A. R. and Kazimierzak, B. (1994): Pressurized Heat Exchanger for 1000°C Operation Using ODS Alloys. Materials for Advanced Power Engineering, Part II, 1994, pp. 1393-1411

Steinbrecht, D. (2006a): [Vorlesungsskript], Abschnitt 1. Technische Verbrennung, Emissionen, Verfahrenstechnische Berechnungen mit Verbrennungsgasen. Universität Rostock, Fakultät für Maschinenbau und Schiffstechnik, Lehrstuhl Umwelttechnik, 15.03.2006

Steinbrecht, D. (2006b): [Vorlesungsscript], Abschnitt 2. Wirbelschichtfeuerungen, Schwerpunkt Stationäre Wirbelschichtfeuerungen. Universität Rostock, Fakultät für Maschinenbau und Schiffstechnik, Lehrstuhl Umwelttechnik, 10.07.2006

Stirling (2007): Kraft-Wärme-Kopplung mit Stirlingmotoren, www.stirling-engine.de

Talbott's Biomass Generators [Flyer] (2006), www.talbotts.co.uk

Talbott, R., Talbott, E., Benjamin, C. and Pritchard, D. L. (2004): Patent EP 1 350 016 B1 and DE 601 06 976 T2 2005.12.01.Talbott's Heating Ltd., Stafford, GB

Thyssen (2000): Werkstoffblatt TS 1.4841 and TS 1.4828, from 10/2000

Traverso, A., Calzolari, F. and Massardo, A. 2005: Transient Analysis of and Control System for Advanced Cycles Based on Micro Gas Turbine Technology. Transactions of the ASME, Journal of Engineering for Gas Turbines and Power, Vol. 127, pp. 340-347

Traverso, A., Magistri, L., Scarpellini, R. and Massardo, A. F. (2003): Demonstration Plant

Expected Performance of an Externally Fired Micro Gas Turbine for Distributed Power Generation. Proc. ASME Turbo Expo, June 16-19, 2003 Atlanta, Georgia, USA

Traverso, A., Massardo, A. F. and Scarpellini, R. (2006): Externally Fired Micro Gas Turbine: Modelling and Experimental Performance. Applied Thermal Engineering: Design, Processes, Equipment, Economics, Vol. 26, No 16, 2006, pp. 1935-1941

Turboden (2008): Turboden Srl, Brescia, Italy. www.turboden.it

VDI 4670 (2000): Thermodynamische Stoffwerte von feuchter Luft und Verbrennungsgasen. VDI Richtlinie - VDI-Handbuch Energietechnik, Beuth-Verlag, Berlin 2000

VDI-Wärmeatlas (2002): Berechnungsblätter für den Wärmeübergang. Hrsg. Verein Deutscher Ingenieure, VDI-Gesellschaft Verfahrenstechnik und Chemieingenieurwesen. Springer Verlag, 9. Aufl., 2002

Vincent, T. S. and Strenziok, R. (2005): Multi Fuel Operated Clean Energy Process: Clean Coal End Products Combustion and Emissions Characterisation. International Symposium Moving Towards Zero-Emission Plants, June 20-22, 2005, Leptokarya Pieria, Greece

Vincent, T. S. and Strenziok, R. (2007): The Micro Gas Turbine in Field Trials with Fermenter Biogas. Proc. of the 15th European Biomass Conf., May 7-11, 2007, Berlin, Germany

Vincent, T. S. Strenziok, R. and Steinbrecht, D. (2008): Cogeneration of Electricity and Heat from Biogenous Solid Fuels in a Stationary Fluidised Bed Reactor Linked with an Externally Fired Micro Gas Turbine. Proc. of the 16th European Biomass Conference, June 2-6, 2008, Valencia, Spain

Wilen, C., Moilanen, A. and Kurkela, E. (1996): Biomass Feedstock Analyses. VTT Publication 282, Technical Research Centre of Finland, 1996, Espoo

Wingelhofer, F. (2006): Die direkt holzstaubgefeuerte Gasturbine als innovatives Konzept zur Nutzung regenerativer Energien. Proc. of the 15th Symposium Bioenergy, 23.-24. November 2006, Kloster Banz, Bad Staffelstein, pp. 92-97

Wolf, J., Barone, F. and Yan, J. (2002): Performance Analysis of Evaporative Biomass Air Turbine Cycle with Gasification for Topping Combustion. Journal of Engineering for Gas Turbines and Power, October 2002, Vol. 124, pp. 757-761

Wright, I. G. and Stringer, J. (1997): Materials Issues for High-temperature Components in Indirectly-fired Cycles. International Gas Turbine & Aeroengine Congress & Exhibition: 2-5 June, 1997, ASME 11 pp. Orlando, Florida, USA

Yan, J. (1998): Externally fired Gas Turbines. The State-of-the-Art of Research and Engineering Development. Technical Report, Stockholm, Dep. of Chemical Engineering and Technology, Royal Institute of Technology, 1998, Stockholm

Yan, J. and Eidensten, L. (2000): Status and Perspective of Externally Fired Gas Turbines. J. of Propulsion and Power, Vol. 16, No 4, 2000, pp. 572-576

Yan, J., Eidensten, L., Svedberg, G. (1994): Performance Evaluation of Biomass Externally Fired Evaporative Gas Turbine System. 8th Congress & Exposition on Gas Turbines in Cogeneration and Utility, OR, USA, October 25-27 1994, pp. 663-671

ZES [Zentrum für Energieforschung Stuttgart] (2004): [Abschlussbericht] Extern gefeuerter Gasturbinen-Prozess zur Kraft-Wärme-Kopplung mit biogenen Festbrennstoffen. 2004, www.zes.uni-stuttgart.de/deutsch/downloads/ZES_2004_0005_EFCC

Appendix I: Heat Exchanger Prototype 1 Test Data

Table 1: Measured data heat exchanger test (06.09.07)

Time	P_{in}[kPa]	P_{out}[kPa]	ΔP[kPa]	T_{in} [°C]	T_{out} [°C]	ΔT [K]	$\dot{V}_{Air}$ [m³/h]
14:30	49.03	12.26	36.77	30.3	828	797.7	70.4
14:35	49.03	12.26	36.77	30.7	827	796.3	70.4
14:40	49.03	12.26	36.77	30.9	826	795.1	70.3
14:45	49.03	12.26	36.77	31.0	826	795.0	70.4
14:50	49.03	12.26	36.77	30.8	826	795.2	70.4
14:55	49.03	12.26	36.77	30.5	826	795.5	70.4
15.00	49.03	12.26	36.77	30.7	825	794.3	70.4
Average	**49.03**	**12.26**	**36.77**	**30.7**	**826.3**	**795.5**	**70.4**

Table 2: Calculated data heat exchanger test (06.09.07)

Fluid	Air	
Standard density (ρ_0)	1.293	[kg/m³]
Standard pressure (p_0)	101.325	[kPa]
Standard temperature (T_0)	273.15	[K]
Fluidized bed temperature (T_{FB})	854.4	[°C]
Ambient pressure (p_{amb})	101.3	[kPa]
Middle heat exchanger temperature $$T_m = \frac{T_{out} - T_{in}}{2}$$	397.8	[°C]
Lateral cross section area $$A_{lat} = \frac{\pi}{4} d^2 \times Z_T$$	0.0010179	[m²]
Standard volume flow $$\dot{V}_0 = \dot{V}_{Air} \times \frac{p}{p_0} \times \frac{T_0}{T}$$	93.9	[m³/h]
Air density after compressor $$\rho_{Air} = \rho_0 \times \frac{p}{p_0} \times \frac{T_0}{T}$$	1.725	[kg/m³]
Air mass flow $$\dot{m}_{Air} = \dot{V}_N \times \rho_0$$	121.4	[kg/h]
Middle air velocity in heat exchanger $$w_m = \frac{\dot{V}_{m\,Air}}{A_{lat}}$$	42.38	[m/s]
Heat exchanger output $$\dot{Q}_{Hx} = \dot{m}_{Air} \times c_{p\,mAir} \times \Delta T_{Air}$$	29.53	[kW]

Table 3: Heat exchanger operation characteristics heat exchanger test (06.09.07)

Friction coefficient

$$\varsigma_{Hx} = \frac{2\Delta p}{\rho\, w_m^2}$$

52.42   [-]

Heat exchanger efficiency

$$\eta_{Hx} = \frac{\dot{Q}_{Hx}}{\dot{Q}_{FB}}$$

0.27   [-]

Heat exchanger (fuel) efficiency

$$\eta_{Hx} = \frac{\dot{Q}_{Hx}}{\dot{Q}_{Fuel}}$$

0.37   [-]

Heat transfer effectiveness

$$\Phi = \frac{\Delta T_{Air}}{\Delta T_{max}} = \frac{\Delta T_{Air}}{T_{FB} - T_{Air\,IN}}$$

0.96   [-]

Number of transfer units

$$NTU = \frac{k \times A}{\dot{m} \times c_{p_m}} = \frac{\Delta T_{Air}}{LMTD}$$

3.38   [-]

Heat flux

$$k = \frac{\dot{Q}}{LMTD \times A}$$

55.03   [Wm²/K]

Logarithmic mean temperature difference

$$LMTD = \frac{(\Delta T_{max}) - (\Delta T_{min})}{\ln\left(\dfrac{\Delta T_{max}}{\Delta T_{min}}\right)}$$

235.37   [K]

Heat exchanger output

$$\dot{Q}_{Hx} = kA \times LMTD$$

29.53   [kW]

Table 4: SFBC-EFMGT external compressor tests steady state operation data

Heat exchanger air source: SFBC induced draught fan

OP1-OP2 (20.11.07) Fuel: Natural gas and light fuel oil

OP3-OP5 (12.12.07) Fuel: Extracted colza cake pellets, natural gas and light fuel oil

Characteristic	Unit	OP1	OP2	OP3*	OP4	OP5	OP6
Q_{Fuel}	kW	161.7	155.1	125.6	165.5	193.8	85.3
$Q_{Fl.Air}$	kW	2.7	28.3	2.4	2.0	32.5	2.5
Q_{comb}	kW	187.4	183.4	131.2	128.0	167.5	226.3
T_{FB}	°C	808.0	808.0	843.9	844.9	847.9	830.8
$T_{Freeboard}$	°C	837.0	849.0	790.0	804.4	861.9	873.6
$O_{2\,(Dry)}$	%	2.7	3.9	9.0	8.3	4.3	3.6
CO_2	%	11.9	11.0	9.9	10.4	14.5	15.4
CO	ppm	34.0	6.0	63.0	59.0	34.0	50
NOx	ppm	-	-	163.0	141.0	78.0	48
SO_2	ppm	-	-	357.0	385.0	619.0	627
m_{HxAir}	kg/h	433.2	431.9	25.0	95.8	231.7	431.3
$T_{Hx\,in}$	°C	50.0	51.0	19.4	20.2	45.7	50.3
$T_{Hx\,out\;balance}$	°C	790.0	789.5	786.9	800.1	826.2	818.3
$p_{Hx\,in}$	bar	2.940	2.940	0.256	0.430	1.657	3.653
$p_{Hx\,out}$	bar	1.02	1.04	0.098	0.167	0.927	2.366
T_{TET}	°C	661.0	660.0	-	-	-	-
P_e	kW	3.1	3.1	-	-	-	-
T_{Stack}	°C	289.0	291.0	-	-	-	-

* not in steady state

Appendix II: SFBC-EFMGT Heat Exchanger 2 Test Data

Table 1: SFBC steady state operation data preliminary test (17.06.08)

Heat exchanger air source: SFBC Induced draught fan
Fuel: Natural gas, light fuel oil

Characteristic	Unit	OP1	OP2	OP3	OP4
Q_{Fuel}	kW	136.7	160.6	163.5	134.3
$Q_{Fl.Air}$	kW	24.8	26.4	27.8	28.4
Q_{comb}	kW	160.9	162.6	188.4	191.9
T_{FB}	°C	851.8	850.8	851.5	848.4
$T_{Freeboard}$	°C	803.4	821.6	840.1	849.8
O_2 (Dry)	%	7	7.2	5	4.1
CO_2	%	9.5	9.4	10.8	11.4
CO	ppm	12	8	13	27
NO_x	ppm	25	25	27	27
SO_2	ppm	32	30	36	38
$m_{Hx\,Air}$	kg/h	276.7	316.8	381.4	417.6
$T_{Hx\,in}$	°C	44	48	52	55
$T_{Hx\,out}$	°C	794	789	784	777
$p_{Hx\,in}$	bar abs	0.147	0.200	0.273	0.333
$p_{Hx\,out}$	bar abs	0.126	0.173	0.239	0.294
Q_{Hx}	kW	62	70	83	90

Table 2: Heat exchanger friction coefficient calculation from preliminary test (17.06.08)

	$m_{Hx\,Air}$ [kg/s]	Δp_{Hx} [Pa]	ΔT_m [K]	T_r* [K]	ρ_r** [kg/m³]	ζ_{HX} [-]
OP1	0.082	2120.69	293.85	831.10	0.49	18.80
OP2	0.094	2647.80	287.79	836.16	0.50	18.59
OP3	0.113	3497.71	298.32	826.33	0.54	18.50
OP4	0.124	3922.66	299.42	822.13	0.57	18.08
Average						18.49
SFBC heat exchanger 2						$\zeta \approx$ **18.50**

* T_{FB} - ΔT_m **Air density at reference temperature (T_r)

Table 3: LabView data average values SFBC-EFMGT test 1 (08.07.08)

Turbine speed [rpm]	T_{CET} [°C]	T_{Stack} [°C]	$T_{Hx\,in}$ [°C]	$T_{Hx\,out}$ [°C]	T_{TIT} [°C]	p_{CEP} [bar abs.]	$p_{Hx\,in}$ [bar abs.]	$p_{Hx\,out}$ [bar abs.]	p_{TEP} [bar abs.]
50 000	68	159	428	809	774	1.471	1.444	1.418	1.021
55 000	59	183	480	812	788	1.584	1.552	1.520	1.023
60 000	56	193	496	812	792	1.710	1.673	1.636	1.026
65 000	53	214	519	816	800	1.854	1.811	1.769	1.031
70 000	58	222	519	812	799	2.008	1.960	1.913	1.036
75 000	67	229	514	810	798	2.169	2.116	2.064	1.042
76 000	68	238	509	807	796	2.348	2.289	2.233	1.049

Table 4: Capstone data average values SFBC-EFMGT test 1 (08.07.08)

Turbine speed [rpm]	Main gen. power [W]	Turbine exit temp. [°C]	Compressor inlet temp. [°C]	Ambient pressure [kPa]	Output power [W]
50 000	1765	632	27	98	808
55 000	2293	633	26	99	1243
60 000	2399	622	26	98	1256
65 000	2395	622	26	99	1256
70 000	1643	608	26	99	454
75 000	1654	610	26	99	470
76 000	805	596	27	99	-429

Table 5: LabView data average values SFBC-EFMGT test 2 (13.08.08)

Turbine speed [rpm]	T_{CET}^{*} [°C]	T_{Stack} [°C]	$T_{Hx\,in}$ [°C]	$T_{Hx\,out}$ [°C]	T_{TIT} [°C]	p_{CEP} [bar abs.]	$p_{Hx\,in}$ [bar abs.]	$p_{Hx\,out}$ [bar abs.]	p_{TEP} [bar abs.]
45000	94	186.12	494.42	810.38	785.95	1.404	1.382	1.358	1.019
50000	109	211.35	539.11	824.27	808.71	1.505	1.479	1.450	1.022
55000	114	223.14	543.95	822.38	809.53	1.628	1.598	1.564	1.025
60000	123	236.57	540.73	819.35	808.69	1.770	1.735	1.696	1.030
65000	126	244.52	535.74	817.30	807.70	1.934	1.895	1.850	1.034
70000	129	255.94	524.07	813.89	805.62	2.117	2.073	2.022	1.039
75000	136	264.71	515.10	811.24	803.86	2.325	2.276	2.219	1.045
80000	154	274.48	502.47	806.71	799.99	2.556	2.502	2.439	1.052
85000	162	283.86	492.30	802.09	795.99	2.813	2.754	2.684	1.060
90000	183	291.77	483.49	794.76	789.28	3.097	3.031	2.954	1.071
96000	196	299.32	465.81	775.52	770.83	3.458	3.386	3.300	1.084

*Corrected values from 11.09.08

Table 6: Capstone data average values SFBC-EFMGT test 2 (13.08.08)

Turbine Speed [rpm]	Compressor inlet temp. [°C]	Turbine exit temp. [°C]	Output power [kW]
45000	29	629	0.70
50000	30	672	1.49
55000	29	666	2.47
60000	29	655	3.56
65000	29	643	4.75
70000	29	628	6.15
75000	29	612	7.65
80000	30	597	9.17
85000	31	579	10.60
90000	31	558	11.54
96000	31	539	12.35

Table 7: LabView data average values SFBC-EFMGT test 3 (11.09.08)

Turbine speed [rpm]	T_{CIT} [°C]	T_{CET} [°C]	T_{stack} [°C]	$T_{Hx\ in}$ °C]	$T_{Hx\ out}$ [°C]	T_{TIT} [°C]	T_{TET} [°C]	T_{FB} [°C]
45000	34	94	219	576	822	811		852
50000	34	109	226	572	824	812	684	852
55000	33	114	234	565	822	812	675	853
60000	32	123	243	555	821	811	660	854
65000	32	126	252	545	820	811	648	853
70000	33	129	261	534	816	808	633	853
75000	31	136	269	521	812	805	618	852
80000	31	154	278	509	809	801	600	852
85000	31	162	286	498	804	798	579	851
89000	30	183	292	488	799	793	565	839
96000	30	196	302	470	781	775	538	854

Table 7 Continued: LabView data average values SFBC-EFMGT test 3 (11.09.08)

Turbine speed [rpm]	p_{CEP} [bar abs.]	$p_{Hx\ in}$ [bar abs.]	$p_{Hx\ out}$ [bar abs.]	p_{TEP} [bar abs.]	$\dot{m}_{Stack}$ [kg/h]	P_e [kW]	Δp_{Hx} [mbar]	Δp_{Rec} [mbar]
45000	1.412	1.389	1.365	1.031	321	0.80	24.23	23.18
50000	1.516	1.488	1.460	1.033	360	1.50	28.39	27.56
55000	1.639	1.607	1.574	1.036	414	2.40	33.86	31.24
60000	1.782	1.747	1.707	1.040	466	3.60	39.28	35.82
65000	1.945	1.905	1.860	1.044	534	4.90	45.03	40.32
70000	2.130	2.085	2.034	1.049	607	6.10	50.78	45.36
75000	2.340	2.290	2.233	1.054	682	7.90	57.24	50.04
80000	2.579	2.524	2.460	1.061	768	9.40	64.00	55.05
85000	2.838	2.779	2.708	1.069	857	10.80	71.04	59.67
89000	3.074	3.009	2.932	1.077	941	11.80	77.09	64.50
96000	3.493	3.422	3.335	1.092	1102	12.40	87.15	71.22

Table 8: Prandtl probe measurement of the air mass flow in the stack (11.09.08)

Turbine speed [rpm]	T [K]	p_{dyn} [Pa]	w [m/s]	$\dot{V}$ [m³/s]	ρ [kg/m³]	$\dot{m}$ [kg/h]	$\dot{m}$ [kg/s]	p_{Stack} [bar abs.]
45000	470	44	10.82	0.12	0.75	321.34	0.089	1.017
50000	478	56	12.32	0.13	0.74	359.65	0.100	1.017
55000	484	75	14.35	0.16	0.73	413.81	0.115	1.017
60000	496	97	16.56	0.18	0.71	465.98	0.129	1.017
65000	503	129	19.24	0.21	0.70	533.90	0.148	1.017
70000	512	170	22.27	0.24	0.69	606.61	0.169	1.017
75000	521	219	25.46	0.28	0.68	682.15	0.189	1.017
80000	530	282	29.15	0.32	0.67	767.83	0.213	1.017
85000	539	357	33.08	0.36	0.66	856.68	0.238	1.017
89000	545	436	36.74	0.40	0.65	940.97	0.261	1.017
96000	555	608	43.80	0.48	0.64	1101.75	0.306	1.017

$$w = 1.2931 \sqrt{\frac{1000}{B} \times \frac{T}{289.15} \times P_{dyn}}$$

B	1017	mbar
$ρ_0$	1.293	kg/m³
T_0	273.15	K
p_0	1.013	bar
A_{lat}	0.01093588	m²

Table 9: SFBC energy balance (11.09.08)

Turbine speed [rpm x 1000]		45	50	55	60	65	70	75	80	85	89	96
SFBC fuel input	[kW]	94	96	102	108	115	122	134	145	154	168	175
Input fluidization air	[kW]	214	22	22	23	23	23	24	24	28	28	29
Σ Input SFBC	[kW]	115	118	124	130	139	146	157	170	182	196	204
Enthalpy FG	[kW]	59	59	60	60	62	62	64	66	75	77	79
Energy loss*	[kW]	30	30	30	30	30	30	30	30	31	29	31
Output Hx	[kW]	26	29	34	40	47	53	63	73	76	89	94
EFMGT stack	[kW]	36	37	45	52	58	65	72	84	90	92	104
SFBC FG out	[kW]	38	37	37	38	38	39	40	41	47	49	50

*includes 7.5 kW for the water cooled liquid fuel injection lance

Appendix III: SFBC-EFMGT Measurement Instrumentation and Simulation

The measurement positions are shown in the test configuration diagrams 8.1, 8.6 and 8.22 respectively.

Position	Description
Compressor inlet temperature	Capstone CIT probe
Ambient temperature	Thermocouple type K
Ambient pressure	Piezo-resistive transmitter type S-10 / Capstone intern
Compressor exit pressure	Piezo-resistive transmitter type S-10 / Bourdon gauge
Compressor exit temperature	Thermocouple type K
Hx inlet pressure	Piezo-resistive transmitter type S-10 / Bourdon gauge
Hx inlet temperature	Thermocouple type K
Hx exit pressure	Piezo-resistive transmitter type S-10 / Bourdon gauge
Hx exit temperature	Thermocouple type K
Turbine inlet temperature	Thermocouple type K
Turbine exit temperature	Capstone TET probe
Turbine exit pressure	Piezo-resistive transmitter type S-10 / Bourdon gauge
Stack temperature	Thermocouple type K
Fluidized bed temperature	Thermocouple type K
Freeboard temperature	Thermocouple type K
Flue gas temperature	Thermocouple type K
Mass flow fluidization air	Vortex flowmeter
Mass flow heat exchanger air	Standard orifice gauge
Mass flow fuel	Variable frequency drive fuel screw conveyor/ Natural gas fuel flow meter… Liquid fuel injection

a)   Temperature Measurement

For the SFBC reactor, heat exchanger and EFMGT air lines thermocouples of the type K (DIN IEC 584) were utilized.

For the heat exchanger 1 tests and the preliminary heat exchanger 2 test on 17.06.08 the temperatures were read from a multimeter (TypeVC303 from Voltcraft) or thermocouple (Voltcraft K204 Digital 4-Channel Thermometer) and manually registered. For all other heat exchanger 2 tests the temperatures were manually registered, and automatically recorded every 3 seconds with National Instruments Measurement & Automation programme LabVIEW version 8.0 run under Microsoft Windows® XP Professional. The manual registration and automatically generated measurement data were in good accord.

The compressor inlet temperature and turbine outlet temperature were measured with the original Capstone temperature probes with data registration in 3 second intervals over the entire test with the Capstone remote software.

The fluidized bed, freeboard, and flue gas temperature were automatically measured and registered by the SFBC system software. A more detailed description of the SFBC plant at the University of Rostock, Chair of Environmental Technology, is given by Steinbrecht (2006b).

b)   Pressure Measurement

The air pressure measurements for the heat exchanger prototype 1 and on 17.06.08 for heat exchanger prototype 2 were performed with the help of Bourdon gauges and registered manually.

In all later tests the pressure measurements were performed with Bourdon gauges with manual registration, and also automatically registered by piezo-resistive pressure transmitters (type S-10[1] WIKA Alexander Wiegand GmbH & Co., Germany) in combination with National Instruments Measurement & Automation Programme LabVIEW version 8.0 run under Microsoft Window® XP Professional as shown below.
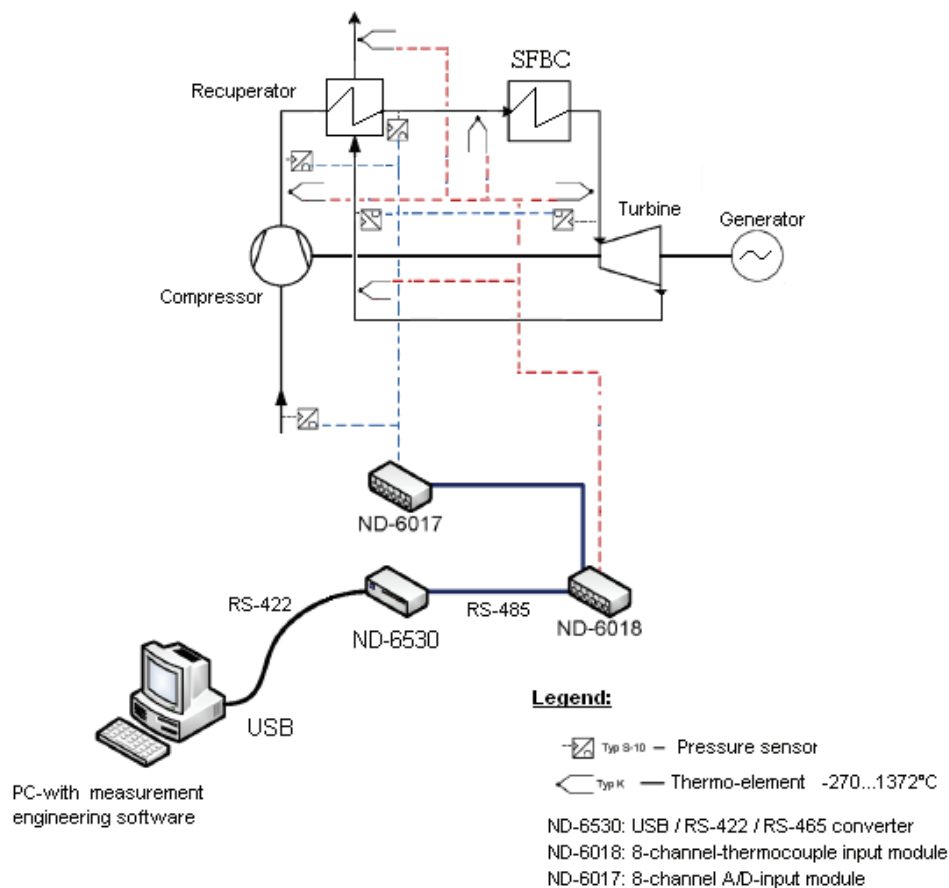
Nudam mess system configuration

The pressure sensors (Type S-10 from WIKA) induce a pressure dependant signal from 0…10 V. This value is then digitalized in the Analog-Digital Convertor (NuDam 6017), and relayed to the 8 channel thermocouple input module (NuDam 6018).

The NuDam ND-6018 is an 8 channel thermocouple module which converts the measured digital temperature signal into a value in °C.

The NuDam ND-6018 communicates with the PC USB Com-port (RS-422 interface) via the RS-422/RS-485-interface converter module (NuDam 6530).

Measurements were made over the entire test in 3 second intervals. The values shown in App. II Tabs. 3, 5 and 7 are the average values for the respective constant turbine operation speeds.

---

[1] with a measurement error of 0.1%

NuDam 6017, NuDam 6018 and NuDam 6530
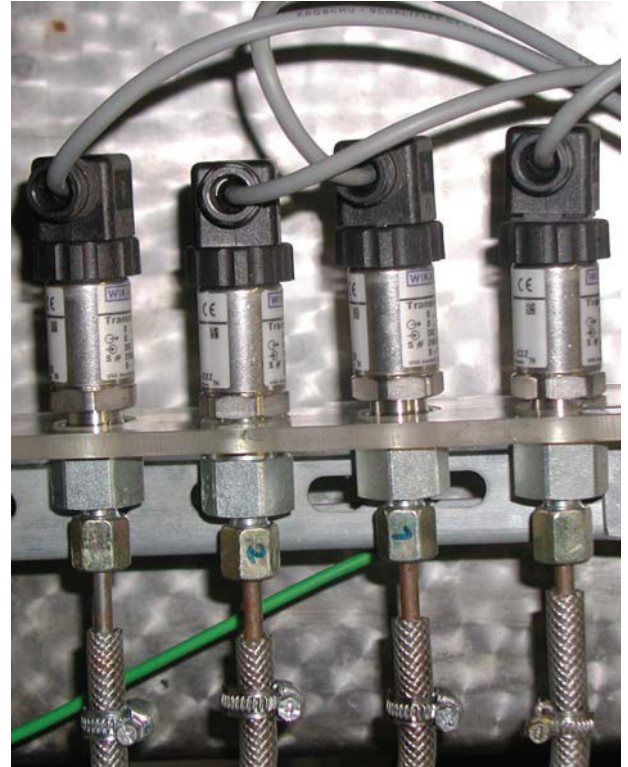
WIKA piezo-resistive pressure transmitters

c)   Air Mass Flow

The fluidization air mass flow was measured and registered by a Vortex flowmeter for all tests. The air mass flow in the heat exchanger was measured with the help of an orifice gauge for all heat exchanger 1 tests and the preliminary heat exchanger 2 test on 17.06.08.

For all other heat exchanger 2 tests the air mass flow in the heat exchanger was calculated with the help of the heat exchanger friction coefficient, determined in the preliminary test, and calculated from the SFBC energy balance. The air mass flow in the stack after the turbine was measured with the help of a Prandtl probe and inclined tube manometer as shown below.
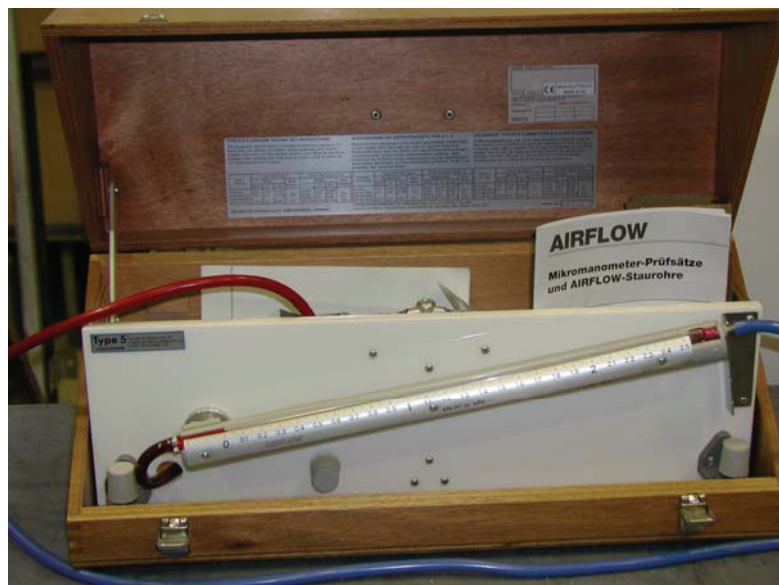

Airflow inclined tube manometer

d)   Fuel Mass Flow

The SFBC has three fuel systems:

1) A metered natural gas fuel flow is injected over nozzles in the SFBC floor.

2) Liquid fuel is injected into the lower SFBC fluidization zone with a calibrated fuel pump.

3) Solid (biomass) fuel is charged to the lower SFBC fluidization zone with a calibrated variable frequency drive fuel screw conveyor system (prior calibration necessary).

A more detailed description of the small scale SFBC plant at the University of Rostock, Chair of Environmental Technology shown below is given by Steinbrecht (2006 b).
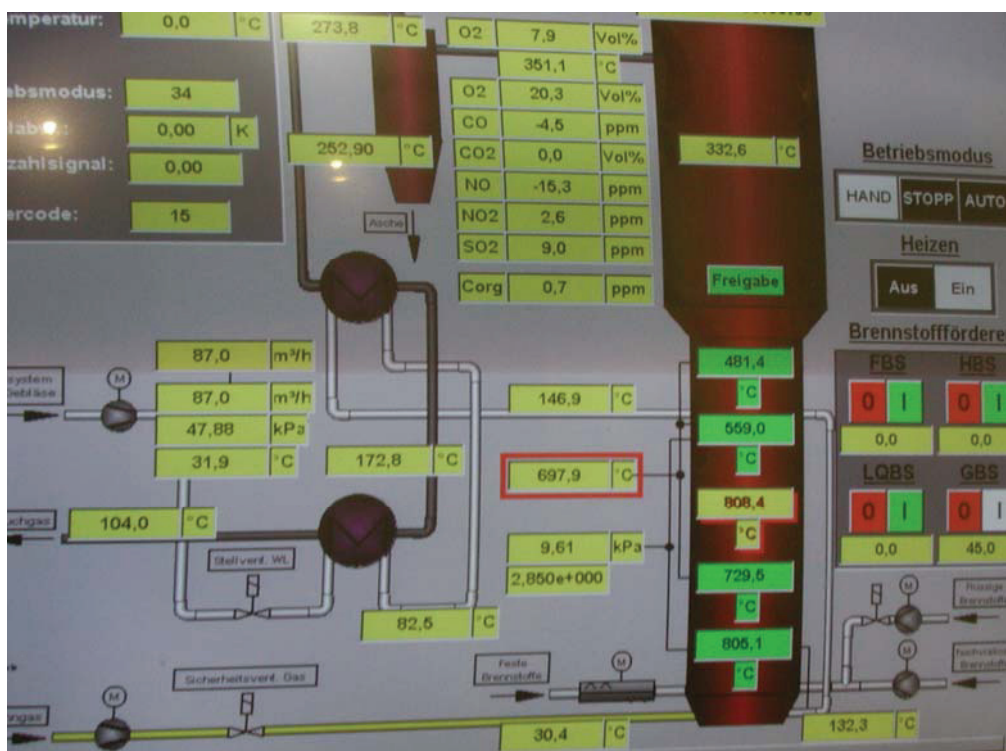
SFBC reactor mess system configuration

e)   Capstone Remote (CRMS Ver 4.25 User Edition)

The internal Capstone measurement system in combination with the software package Capstone Remote (CRMS Ver 4.25 User Edition) which was run under Microsoft Window® XP Professional, was utilized to assess the Capstone data given in App. II Tabs. 4 and 6. A more detailed description of the Capstone measurement and instrumentation system is given in the Capstone C30 Users Manual (www.microturbine.com.). The Capstone remote data registration chart is shown below.

No	Parameter (Units)	Value	Record	No	Parameter (Units)	Value	Record
1	Control Date		ON	28	System Prime Status	0	OFF
2	Control Time		ON	29	LFC Prime	0	OFF
3	Engine Speed (rpm)	0	ON	30	Boost Pump	0	OFF
4	Turbine Exit Temp (°C)	0	ON	31	LFC Prime state	0	OFF
5	Compressor In Temp (°C)	0.0	ON	32	Boost Pump Status	0	OFF
6	Ambient Pressure (kPa)	0.0	ON	33	Drain Pump Status	0	OFF
7	Incident Record	0	ON	34	Prime Sol. Status	0	OFF
8	Starts	0	ON	35	RFC DC Bus (V)	0	OFF
9	Hours		ON	36	Output Frequency (Hz)	0	ON
10	System Severity Level	0	ON	37	Output Current Phase A (A)	0.0	ON
11	System State		ON	38	Output Current Phase B (A)	0.0	ON
12	Power Enable	0	ON	39	Output Current Phase C (A)	0.0	ON
13	Power Demand (W)	0	ON	40	Output Current Neutral (A)	0.0	ON
14	Power Supply Voltage (V)	0.0	ON	41	Output Voltage Phase A (V)	0	ON
15	Start Command (0/1)	0	ON	42	Output Voltage Phase B (V)	0	ON
16	Fuel Inlet P LP (kPa)	0.0	OFF	43	Output Voltage Phase C (V)	0	ON
17	Fuel Outlet P LP (kPa)	0.0	OFF	44	Output Power Phase A (W)	0	ON
18	Fuel Inlet P HP (kPa)	0.0	OFF	45	Output Power Phase B (W)	0	ON
19	SPV Fuel Ex P (kPa)	0.0	OFF	46	Output Power Phase C (W)	0	ON
20	Bat Therm.Temp (°C)	0.0	OFF	47	Output Power (W)	0	ON
21	Bat SOC (%)	0.0	OFF	48	Bat No. Eq. Charges	0	OFF
22	Bat Volts (Vdc)	0	OFF	49	Meter Watts In (W)	0.0	OFF
23	BC DC Bus (V)	0	OFF	50	Meter Watts Out (W)	0.0	OFF
24	Inv DC Bus Volts (Vdc)	0	OFF	51	Meter VAR In (VAR)	0.0	OFF
25	LFC Injector State	0.0	OFF	52	Meter VAR Out (VAR)	0.0	OFF
26	LFC Pressure Command (kF	0	OFF	53	Turbine number	0	OFF
27	LFC Pressure Feedback (kF	0	OFF	54	MultiPac Enable	0	OFF

System: Unit_1   MicroTurbine Data 1

Capstone remote data acquisition with CRMS Ver 4.25 User Edition

f) Ebsilon Professional (Version 7.0)

The commercial process simulation software EBSILON® is the abbreviation for "**e**nergy **b**alance and **si**mulation of the **lo**ad response of power generating or process controlling **n**etwork structures".
Ebsilon Professional is a calculation programme for energy and mass flow balancing of power plant processes.
Ebsilon Professional permits the balancing of
- individual components
- component groups
- sub-systems
- complete systems
without taking into account, whether these components or systems build a closed or an open model.

Ebsilon Professional has an uninterrupted model structure with
- a standard component, which is used for modelling the usual power plant model,
- an additional component for modelling complex power plant processes.

In this way, Ebsilon Professional is also capable of balancing,
- water/steam processes,
- gas turbine processes and
- combination processes

with heat extraction.

Ebsilon Professional uses the
- IAPWS-IF97 of the IFC-76 steam table and
- cp-polynomial for air/flue gas

as the data basis.

Ebsilon Professional is a variable programme system with which you can balance all the power plant models with the help of a closed solution system (based on a sequential solution method). Controllers are necessary for a versatile use of this system. They are used as iteration controllers of how the components and their characteristics must be specified by the user. The iteration run is optimized by the "self-learning" properties of the controller.

Based on this philosophy Ebsilon Professional proves to be a very flexible system. Thanks to the experiences all the possible power plant systems can be balanced with the help of this system.

The cycle is modelled as a non-linear equations system solved by a series of linear equation systems. The variable coefficients and the right-hand sides are formed by using the values of the preceding iteration step. The iteration ends when the basis variable no longer changes.

To accelerate the convergence the variable right-hand sides and the coefficients are developed through the Taylor series during the entire preceding iteration step. In this way, the non-linear equations system is solved with the Newton method.

To solve a series of linear equation systems an iteration method is used, since the matrix is filled only slightly. A Gauss-Seidel method is selected after extensive comparisons of computing time and convergence.

The user must do this essential work before he can start with the calculation: The user must model the cycle as exactly as possible by using the available components. The rules for modelling are as follows:

Rule 1: Check whether the selected component really has the physical properties, in order to be simulated.

Rule 2: Connect the components reasonably under absolute consideration of the meaning of each connection.

Rule 3: In case none of the available components possess the properties of the process components it must be checked, whether another corresponding menu component can be used in place of this component.